Study of the Tropospheric Trace Gases over the Indian Subcontinent

Thesis Submitted for the Degree of

Doctor of Philosophy

In

Physics

To

Kumaun University, Nainital (India)

By

Piyush Bhardwaj

Aryabhatta Research Institute of Observational Sciences (ARIES)

Manora Peak, Nainital, 263002, Uttarakhand, India

July 2016

DECLARATION

I hereby declare that the work presented in this thesis is a result of investigations carried out by me at the Aryabhatta Research Institute of observational sciences (ARIES), Nainital, under the joint supervision of Dr. Manish Naja (ARIES, Nainital) and Prof. H. C. Chandola (Department of Physics, D.S.B. Campus, Kumaun University, Nainital). This thesis work has not been submitted for the award of any degree, diploma, associateship or fellowship of any University or Institute.

Place: Nainital

Date: July 2016 (Piyush Bhardwaj)

CERTIFICATE FROM THE

SUPERVISORS

This is to certify that

1. The synopsis of the present thesis entitled **"Study of the tropospheric trace gases over the Indian subcontinent"** for award of the degree of Doctor of Philosophy in Physics has duly been approved by the Kumaun University, Nainital (Letter no.-Shodh/Physics/43/2013, dated 27/12/2013).
2. The thesis embodies the work of Mr. Piyush Bhardwaj himself.
3. Mr. Piyush Bhardwaj worked under our joint supervisions for this thesis as a Research Fellow at the Aryabhatta Research Institute of Observational Sciences (ARIES), Nainital. He has put in more than 200 days of attendance at ARIES, Nainital during this period.
4. The thesis has not been submitted before for the award of any degree, diploma, associateship or fellowship of any University or Institute.

Dr. Manish Naja
ARIES, Manora Peak,
Nainital

Prof. H. C. Chandola,
Department of Physics,
D.S.B Campus,
Kumaun University, Nainital

Dedicated to

my

Family

Acknowledgements

It is a great pleasure to thank those who made this thesis possible and who helped me increase my potential in the PhD program. Since the very outset to the accomplishment of my research during PhD, I must begin by expressing my profound gratitude to Dr. Manish Naja, my thesis supervisor who introduced me to the world of atmospheric science. His vast experience and knowledge have helped me immensely in learning the subject. His hard-working nature and simplicity taught me to deal with tough situations. I would also like to thank to my co-supervisor Prof. H.C. Chandola, Physics Dept. D.S.B. Campus Nainital, Kumaun University for helping me out in registration and University matters. I was also equally supported by Prof. M.C. Durgapal, Prof. O.P.S. Negi from Physics Dept. S.S.J. campus Almora, in the Kumaun University.

My sincere thanks is extended to our collaborator Dr. Rajesh Kumar presently working at NCAR, USA. I cannot forget to show my humble thanks to Prof. Shyam Lal (PhD supervisor of my supervisor) and Mr. S. Venkataramani from PRL for their fruitful discussions. I am grateful to the Director ARIES, Dr. Wahab Uddin for being kind to help in all academic and administrative issues. I am also thankful to the ex-director of the institute, Prof. Ram Sagar for his special motivation to do a better science.

I had been given a chance to be a part of SusKat campaign. I would love to thank Dr. Maheswar Rupakheti, Dr. Arnico Panday and Prof Mark Lawrence for their guidance to conduct fruitful experiments in Kathmandu valley. I am also thankful to the other team members Dipesh, Bhogendra and Khadak. During the field campaign I learned a lot of things and had great company with my friends Chinmoy, Amit and Kim Ji Hyoung. I express my gratitude to Drs. Sasha Madronich, Gabriele Pfister and Mary Barth from NCAR for helping me during my NCAR visit. I also thank Paula Fisher and Shonna Montoya for helping in logistics during this trip. I give my special thanks to Dr. Rajesh, Pinki Bhabhi, Dr. Vineet, Dimple Bhabhi and Carlos J. Valle Díaz who made this trip memorable

and provided homely environment. I also thank ICIMOD, IASS for providing me funds to make several trips to Nepal and to attend EGU meeting in Vienna during my PhD. I am also thankful to Prof. K. K. Moorthy from ISRO headquarters, and Prof. S. K. Satheesh from IISc Bengaluru. Further, I am thankful to various online portals and archival teams for satellite datasets which are used in this thesis. I am also thankful to ISRO-ATCTM project for supporting different observations.

I acknowledge the technical staff Mr. Nitin and Mr. Deepak for helping in continuous operation of our instruments in the atmospheric lab at ARIES. I am thankful to the ARIES Academic Committee, all faculties and staff. I would love to thank Er. Samresh and Moumita bhabhi for giving me a family like environment in ARIES. I thank the ARIES library staff Mr. Prashant, Mr. Arjun, librarian Mr. Satish, computer center staff Ers. Deep Pant, Sanjit Sahu, Mohit Joshi, Hemant Kumar for helping me during my PhD. I will not forget to thank the canteen staff, security staff and gardeners at ARIES who made my stay at Hostel pleasant. I am thankful to my seniors Drs. Manash, Jessy, Neelam, Rupak, Eshwar, Pankaj, Akash, Sumana, Narendra, Ram Kesh, Brajesh, Haritma, Devesh, Ravi, Hema, Tapaswini, KK, Rajiv, Sumit, Bharat, Prashanth, Alka and Srabanti. I thank my friend and a brother Dr. Arun Awasthi who motivated me to work harder. I cannot forget to thank my friend Vivek who always helped me in ARIES and Haldwani. I am also thankful to my friends Yahspal and Naveen from PRL. Special thanks to my batchmate Subhash along with all nice juniors Neha, Suvendu, Subhajeet, Abhishek, Parveen, Aditi, Arti, Aabha Mridweeka, Ekta, Vineet, Anjasha, Raya, Piyali, Sapna, Priyanka, Gaurav, Bharti, Surender, Shilpa, Tirthendu, Rakesh, Jaianand and special thanks to my friend circle including Vijay Bhatt, Mukesh, Kuldeep, Ashwani & Pankaj for making my stay at hostel enjoyable and helping me in tough situations. Special thanks to Anurag for helping me during thesis writing and completion.

My achievements won’t be possible without the support of my family and I always admired my mother who always struggled for me and taught me to face all the harsh situations of my life. She has always been a constant source of support and inspiration for me. A big thanks to my father who also worked extremely hard to fulfill our needs, he also supported me in all situations and taught me to do hard work. I am thankful to my siblings Shikha and Aayush for

their care and wonderful company at home. I am thankful to my father-in-law and mother-in-law who also helped me in many situations and special thanks to my in-laws Maj. S P Singh and Madhu. I extend my thanks to my brother and a close friend Dr. Vashi. This thesis wouldn't be possible if I would not get support from my loving wife Dr. Archana, she was the backbone during this thesis and her constant encouragement pushed me to do right things at right time. Her mere presence provided me positivity and her care during my hard times was commendable. At the end I would like to say a big thanks to the Creator of the World, the almighty God.

Preface

The present thesis entitled “Study of the Tropospheric Trace Gases over the Indian Subcontinent” deals with investigations carried out by the author under the joint supervision of Dr. Manish Naja (ARIES, Nainital) and Prof. H. C. Chandola (Kumaun University, Nainital). In view of the vital role played by ozone and its precursor gases over highly polluted, densely populated Indian subcontinent, the present work deals with the study of these trace gases to understand the underlying processes and fill the observational gaps over this region. This thesis comprises of results from two extensive field campaigns viz., SusKat and RAWEX-GVAX conducted in the Himalayan region for the first time. Present thesis also includes satellite based long-term study of biomass burning over the Indian subcontinent and balloon borne measurements of ozone and meteorological parameters over Manora Peak, Nainital. The thesis is divided into seven chapters.

The **Chapter-1** deals with the brief introduction and importance of trace gases in the troposphere. This is followed by their impacts and processes controlling their tropospheric budgets. Further, the present scenario of observations and modeling studies performed over this region and role of biomass burning is discussed. In the last, the objectives and the brief outlines of other chapters are provided.

In **Chapter 2** the various measurement techniques for the detection of surface ozone, CO and meteorological parameters are described. These measurements were conducted at ARIES, Manora Peak, Nainital (79.45^{o}E, 29.36^{o}N, 1958 m

amsl), Nainital; a high altitude site located on a mountain top and Pantnagar (79.5^{o}E, 29.0^{o}N, 231 m amsl) and Bode (27.59N, 85.39E, 1326 amsl) in Kathmandu valley. The vertical observations of ozone and meteorological parameters are made using ozonesondes and radiosondes at Nainital. The detection principle of these instruments, brief description about their setup and their specifications are discussed here. The retrieval techniques of various satellites based and emission inventory datasets used in this thesis are presented in this chapter. In the last sections, the different models and their setup used during this work are also briefly discussed in this chapter.

The seasonal, interannual and long term influences of biomass burning over the Indian subcontinent using satellite data and different emission inventories is presented in **chapter-3.** Active fire location retrievals from the Moderate Resolution Imaging Spectroradiometer (MODIS), the retrievals of aerosol optical depth (AOD) from MODIS Terra and tropospheric column NO2 from Ozone Monitoring Instrument (OMI) are used to understand the effects of biomass burning on the tropospheric pollution loadings over South Asia during 2003-2013. Biomass burning emission estimates from Global Fire Emission Database (GFED) and Global Fire Assimilation System (GFAS) are used to quantify uncertainties and regional discrepancies in the emissions of CO, NO_x and BC due to biomass burning over Indian subcontinent. In Asia, the frequency of fire activity is highest over Southeast Asia, followed by South Asia and East Asia. The biomass burning activity over Indian subcontinent shows a distinct seasonal cycle that peaks during February-May with some differences among four (north, central, northeast and south) regions. The annual biomass burning activity in north, central and south

regions shows an increasing tendency, particularly after 2008, while a decrease is seen in northeast region during 2003-2013.The increase in fire counts over the north and central regions contributes 24% of the net enhancement in fire counts over South Asia. MODIS AOD and OMI tropospheric column NO_2 retrievals are classified into high and low fire activity periods and show that biomass burning leads to significant enhancement in tropospheric pollution loading over both the cropland and forest regions. The enhancement is much higher (110-176 %) over the forest region compared to the cropland (34-62%) region.

The results from the simultaneous measurements of ozone, CO and meteorological parameters made at Bode, Pantnagar and Nainital during SusKat field campaign are presented in **chapter-4**. The diurnal variations at Bode are typical of a polluted site with the sharp day time build-up in ozone and CO having higher levels during morning and evening hours. The average early morning CO levels were higher during winter than spring. However, daytime ozone levels were slightly higher during spring when compared with those during winter. It is seen that CO levels are higher at Bode as compared to those at Pantnagar. These higher levels at Bode are suggested to be due to local sources during winter season with some contributions from regional pollution during spring season. Simultaneous higher levels (2-fold increase) of ozone and CO are observed at Bode, Pantnagar and Nainital during a regional pollution event in the first week of May 2013. WRF-Chem simulations showed large nighttime variations in meteorological parameters at Bode. The daytime differences in temperature and RH between model and observations are ~1^{o}C and 10% respectively. Model was able to capture winds well over the valley and < 10% differences were observed. Daytime

differences, between observations and model are lesser in CO when compared with ozone.

Chapter 5 includes the five year long (2011-2015) observations of vertical profiling of ozone and meteorological parameters using balloon borne sensors. The near surface temperature was highest during the month of June (16.5 ± 1.9 C) and February being the coldest (4.5 ± 3.2 C), however maximum variations are also observed during winter months. The high wind speed indicated the presence of subtropical jet stream around 10-14 km. Maximum wind speed reached by these jets are about 94 m/s. Ozone levels in the lower troposphere showed prominent seasonality with highest levels during May and lowest during summer-monsoon period. These seasonal variations are also consistent with the previous studies performed over this region. The springtime enhancement in lower tropospheric ozone levels was observed due to northern Indian biomass burning. It is found that biomass burning could induce enhancement in ozone from 15 ppbv to 31 ppbv. Five events of downward ozone transport are identified when enhancement in ozone and PV while reduction in CO and RH are observed. Out of these events, increase in ozone is estimated to be as high as 191% during year 2015.

Chapter 6 describes the results from high resolution balloon borne observations of meteorological parameters made during Regional Aerosol Warming Experiment - Ganges Valley Aerosol Experiment (RAWEX-GVAX) field campaign. The winds from reanalysis datasets and radiosonde are shown to be in

better agreement at 250 hPa (altitude of subtropical jet) than those at 100 hPa or 500 hPa. These observations indicated that Atmospheric Infrared Sounder (AIRS) temperature profiles are negatively biased in the lower altitude region, while they are positively biased near tropopause. WRF simulated results are able to capture variations in temperature, humidity and wind speed profile reasonable well. WRF and AIRS derived tropopause height, tropopause pressure, tropopause temperature also show agreement with radiosonde observations. The summary of this thesis work along with future prospectives are presented in **Chapter 7.**

List of Publications

1. Ojha, N., Naja, M., Sarangi, T., Kumar, R., Bhardwaj**, P.,** Lal, S., Venkataramani, S., Sagar, R., Kumar, A., Chandola, H. C., *On the Processes Influencing the Vertical Distribution of Ozone over the Central Himalayas: Analysis of Yearlong Ozonesonde Observations* Atmos. Environ. 2014, doi:10.1016/j.atmosenv.2014.01.031.
2. Joshi H., Naja M., Singh K.P., Kumar R., **Bhardwaj P.,** Babu S.S., Satheesh S.K., Moorthy K.K., Chandola H.C., *Investigations of aerosol black carbon from a semi-urban site in the Indo-Gangetic Plain region,* Atmos. Environ. 2015, doi:10.1016/j.atmosenv.2015.04.007.
3. Sarangi T., Naja M., Lal S., Venkataramani S., **Bhardwaj P.,** Ojha N., Kumar R., Chandola H.C., *First observations of light non-methane hydrocarbons (C2-C5) over a high altitude site in the central Himalayas,* Atmos. Environ. 2015, doi: 10.1016/j.atmosenv.2015.10.024.
4. **Piyush Bhardwaj,** Naja M., Kumar R., Chandola H. C., *Seasonal, interannual and long term variabilities in biomass burning activity over South Asia,* Environ. Science and Pollution research 2015, doi:10.1007/s11356-015-5629-6.
5. Manish Naja, **Bhardwaj P.,** Singh N., Kumar D.V., Kumar R., Ojha N., Sagar R., Satheesh S. K., Moorthy K. K., Kotamarthi V. R., *High frequency vertical profiling of meteorological parameters using AMF1 facility during RAWEX-GVAX at ARIES, Nainital*, Current Science, Vol. 111, No. 1, 10 July 2016.
6. **Piyush Bhardwaj**, M. Naja, M. Rupakheti, A. K. Pandey, M. G. Lawrence, S. Lal, R. Kumar, H.C. Chandola, *Ozone and some of the precursors at an urban*

site in the Kathmandu Valley, Nepal during SusKat-ABC international field campaign, [to be submitted in Atmos. Chem. Phys.].

7. **Piyush Bhardwaj**, M. Naja, R. Kumar, G G. Pfister, S. Madronich, M. G. Barth, A.K. Panday, M. Rupakheti, H.C. Chandola, M.G. Lawrence, *Evaluation of WRF-Chem model for the SusKat-ABC international field campaign: Gas-phase species,* [to be submitted in Atmos. Chem. Phys.].
8. **Piyush Bhardwaj**, M. Naja, R. Kumar, G G. Pfister, S. Madronich, M. G. Barth, C. Wiedinmyer, A.K. Panday, M. Rupakheti, M.G. Lawrence, *Processes controlling surface ozone and related species during the SusKat-ABC international air pollution field campaign: WRF-Chem model simulations,* [to be submitted in Atmos. Chem. Phys.].
9. Manish Naja and **P. Bhardwaj,** *Ozone variations at and around a high altitude site in the central Himalayas*, **[**in preparation].
10. **Piyush Bhardwaj**, et al., *Influences of northern Indian biomass burning, down ward transport and other processes on vertical ozone over central Himalayas*, [in preparation].

List of Acronyms and Abbreviations

AATSR	Advanced Along Track Scanning Radiometer
AGL	Above Ground Level
AIRS	Atmospheric Infrared Sounder
AOD	Aerosol Optical Depth
AOT40	Accumulated threshold of ozone over 40ppb
ARM	Atmospheric Radiation Measurement
ARW	Advance Research WRF
AVHRR	Advanced Very High Resolution Radiometer
BC	Black Carbon
CFCs	Chlorofluorocarbon compounds
CMAQ	Community Multi-scale Air Quality
CPCB	Central Pollution Control Board
CRDS	Cavity Ring Down Spectroscopy
DOE	Department of Energy
DU	Dobson Unit
EC	Elemental Carbon
ECC	Electrochemical Concentration Cell
ECMWF	European Center for Medium-Range Weather Forecast
EDGAR-HTAP	Emission Database for Global Atmospheric Research - Hemispheric Transport of Air Pollution
EEA	European Environment Agency
EOS	Earth Observing System
FINN	Fire Inventory from NCAR
GAW	Global Atmospheric Watch
GDAS	Global Data Assimilation System
GFAS	Global Fire Assimilation System
GFED	Global Fire Emission Database
GFS	Global Forecasting System
GOCART	Goddard Chemistry Aerosol Radiation and Transport

GPS	Global Positioning System
GRIB	Gridded Binary
GVAX	Ganges Valley Aerosol Experiment
HFAP	High Fire Activity Period
HYSPLIT	Hybrid Single Particle Integrated Trajectory Model
IGP	Indo-Gangetic Plain
IGY	International Geophysical Year
IMD	Indian Meteorological Department
INDOEX	Indian Ocean Experiment
IR	Infra-Red
LFAP	Low Fire Activity Period
LIDAR	Light Detection and Ranging
LIF	Laser Induced Fluorescence
MATCH	Multi-scale Atmospheric Transport and Chemistry
MEGAN	Model of Emissions of Gases and Aerosols from Nature
MM5	Mesoscale Model version 5
MODIS	Moderate Resolution Imaging Spectroradiometer
MOZART	Model for Ozone and Related chemical Tracers
NAAQS	National Ambient Air Quality Standards
NCAR	National Center for Atmospheric Research
NCEP	National Centre for Environmental Prediction
NDIR	Non Dispersive Infrared
NH	Northern Hemisphere
NMHCs	Non-Methane Hydrocarbons
NMM	Nonhydrostatic Mesoscale Model
NOAA	National Oceanic and Atmospheric Administration
OC	Organic Carbon
OMI	Ozone Monitoring Instrument
PNNL	Pacific Northwest National Laboratory
PV	Potential Vorticity
RAWEX	Regional Aerosol Warming Experiment
RH	Relative Humidity

STE	Stratosphere-Troposphere exchange
TRMM	Tropical Rainfall Measuring Mission
US-EPA	United States Environment Protection Agency
USGS	United States Geological Survey
UTLS	Upper troposphere and lower stratosphere
UV	Ultra Violet
VOCs	Volatile Organic Compounds
WHO	World Health Organization
WMO	World Meteorological Organization
WPS	WRF Pre-processing System
WRF	Weather Research and Forecast
WRF-Chem	Weather Research and Forecast with Chemistry

Contents

Chapter 1

Introduction

Earth's atmosphere is a thin gaseous envelope that is essential for the survival of living beings. Atmosphere contains gases and aerosols as its constituents with later confined mostly in the lower troposphere. Three gases namely Nitrogen (~78.1 %), Oxygen (~20.9 %) and Argon (~0.9%) constitute 99.9% of the atmospheric mass. The remaining minor fraction (less than about 0.01 %) of the gases are known as trace gases and are most sensitive to the perturbations caused due to various atmospheric and human induced processes. Increasing levels of these trace gases are responsible for different issues pertaining to global climate and air pollution. There are hundreds of trace gases in the Earth's atmosphere and they can be broadly classified based on their atmospheric lifetime time. The long-lived trace gases like carbon dioxide (CO_2), methane (CH_4), nitrous oxide (N_2O), chlorofluorocarbons (CFCs), etc. have nearly homogeneous distributions in both hemispheres mainly due to their longer lifetime of few tens of years to few hundreds and thousands years. The short-lived species however are highly variable in space and time and thus their global distribution show hotspots near their emission sources and have very low concentrations at remote places. Examples of such gases are ozone (O_3), carbon monoxide (CO), different nitrogen compounds (NO, NO_2, N_2O_5, HNO_3,

NO_3, PAN, etc.), volatile organic compounds (VOCs) which have lifetime of few minutes to hours, days and months. Lifetimes of these gases are also highly dependent on their placement in the altitude. In addition to these trace gases, there are several radicals having lifetimes of less than a second to few minutes and those are formed during several photochemical reactions that takes place in the troposphere. Some of the examples of these radicals are hydroxyl radical (OH), nitrate radical (NO_3) and hydroperoxy radical (HO_2).

These trace gases although being low in concentration can have significant impact on air quality, atmospheric chemistry and climate change. These gases are emitted naturally by various processes such as growth of plants over land or in the sea, volcanic eruptions and by anthropogenic activities which includes the combustion of fossil fuels in industrial, transportation and household activities, biomass burning including post-harvest burning of crop residues in agricultural fields, burning of biofuels etc. In principle, both the natural processes and human activities can affect the atmospheric composition and climate of our planet, but the contribution of human activities in the global climate change has been estimated to be significantly larger than the natural influences [*IPCC AR5,* 2013]. Many of the trace gases like CO, nitrogen oxides (NO_x), CH_4, VOCs which are of largely anthropogenic origin, leads to the formation of secondary air pollutants like ozone, in presence of sunlight. Tropospheric ozone is a key atmospheric constituent that (1) controls the oxidizing capacity of the troposphere, (2) have harmful effect on living beings and plants if available in higher concentrations, (3) is a greenhouse gas that can influence the radiative balance of Earth's atmosphere, (4) is also a pollutant which if combined with some other pollutants in presence of sunlight can form photochemical smog

over the urban centers and thus deteriorate the air quality.

This chapter begins with a brief description of ozone and its precursor gases in the troposphere followed by their impacts and tropospheric budgets. Different processes controlling the global budgets of these trace gases are described in section 1.2. The present scenario of observations and modeling studies over this region and role of biomass burning is presented in section 1.3. The outline of other chapters comprising this thesis is provided in section 1.4.

1.1 Ozone and precursor gases in the troposphere

1.1.1 Tropospheric ozone

Tropospheric ozone is produced by oxidation of CO, CH_4 and VOCs also known as precursor gases, in the presence of NO_x and sunlight. Since pre-industrial time, the emissions of these precursors and tropospheric ozone have been observed to be increasing over the last few decades [*Volz and Kley,* 1988; *Marenco et al.,* 1994; *Naja and Lal,* 1996; *Parrish et al.,* 2009; *Tanimoto et al.,* 2009; *Cooper et al.,* 2010; *Logan et al.,* 2012]. The detailed roles of the tropospheric ozone in the atmosphere are described below.

Role in OH formation: Ozone is a major precursor of the hydroxyl (OH) radical which plays an important role in the tropospheric chemistry. The photolysis of ozone molecules at the wavelengths shorter than 319 nm [*Levy,* 1971] produces electronically excited O (^1D) atoms, which in turn react with the water vapor (H_2O) molecules to produce the hydroxyl radical as shown below:

$$O_3 + h\nu\ (\lambda < 319\ nm) \rightarrow O_2 + O\ (^1D) \qquad (R1.1)$$

$$O(^1D) + H_2O \rightarrow 2\ OH \qquad (R1.2)$$

In above reaction only a small fraction of O (^{1}D) atoms produced in reaction (R1.1) generates the OH radicals via reaction (R1.2). The remaining O (^{1}D) atoms are quenched to the ground state O (^{3}P) by O_2 or N_2 molecules and combine with O_2 to reform O_3. For instance, only 10% of the O (^{1}D) atoms generate OH radical at 50% relative humidity and 300 K temperature [*Pitts and Pitts,* 2000].

The OH radical acts as a "detergent" in the troposphere since it removes many reactive and toxic gases which are emitted or produced by wide range of natural and anthropogenic processes in the troposphere. The OH radical is reported to destroy about 3.7 Gt of trace gases every year, including ozone precursor gases such as CH_4, CO and VOCs [*Ehhalt,* 1999]. For example, OH radical initiates the removal of CO, CH_4 and isoprene (C_5H_8) from the atmosphere through the following reactions

$$CH_4 + OH \rightarrow CH_3 + H_2O \qquad (R1.3)$$

$$CO + OH + O_2 \rightarrow CO_2 + H_2O \qquad (R1.4)$$

$$C_5H_8 + OH \rightarrow C_5H_7 + H_2O \qquad (R1.5)$$

Since OH radicals are recognized to play a very significant role in limiting the radiative forcing of long-lived greenhouse gases [*Forster et al.,* 2007], therefore many efforts have been made to understand the budget and long-term trends of OH radicals in the troposphere [e.g. *Miller et al.*, 1998; *Prinn et al.,* 2001; *O'Doherty* et al., 2004; *Bousquet et al.,* 2005]. The concentrations of OH radicals are highest in the tropics due to higher solar insolation and larger amount of water vapor (see reactions R1.1 and R1.2). The globally weighted average tropospheric OH concentrations are estimated to be about 10^6 radicals per cm^3 [*Prinn et al.,* 2001;

Krol and Lelieveld, 2003]. However, increase in the emissions of CH_4, CO and VOCs are expected to decrease the global OH levels. For instance, large enhancements in CO concentrations during 1997 Indonesian wild fires lowered the OH levels by about 6% [*Duncan et al.*, 2003].

Air quality and impacts on human health and vegetation:

Tropospheric ozone is a criteria pollutant indicated by different environmental agencies such as United States Environment Protection Agency (US-EPA), European Environment Agency (EEA), Central Pollution Control Board, India (CPCB) etc., and its higher levels have been identified to have potential health and environmental impacts. The different agencies have different guidelines (Table 1.1) above which ozone levels are considered harmful. Several epidemiological studies show that ozone, if inhaled by the humans can be taken-up subsequently by the cells in the lung and thereby interfering with their proper functioning [*Just et al., 2002*], further it can also cause other respiratory problems including increase in asthma attacks [e.g. *Thruston et al., 2001*; *Desqueyroux et al.*, 2002; *Kennedy*, 2007] and in worst cases can lead to death. They can also penetrate into the circulatory system and lodge in organs such as liver and heart. They generate reactive oxygen species such as the OH radicals which can cause inflammation which in turn exacerbates the pre-existing ailments. The prolonged exposure to ozone can also develop lung cancer. Recent modeling studies also suggests that O_3 along with $PM_{2.5}$ is also found to be responsible for premature mortality and years of human life lost [*Lelieveld et al., 2013*].

Table 1.1: *Ambient air ozone guidelines issued by some of the agencies worldwide [Reid, 2007; National ambient air quality standards (NAAQS), 2009]. Ozone levels, higher than the below listed levels for the mentioned time period are indicated to be harmful.*

Country/Region	Value (ppbv)	Averaging period(hr)	Remark
Australia	80	4	
Canada	65	8	Fourth highest annual value averaged over 3 years.
China	60	1	This limit is for Class I (residential) areas. Higher limits are set for Class II and Class III (industrial) areas.
European Union	60	8	Not to be exceeded more than 25 times per calendar year, averaged over three years.
India	50 90	8 1	8 hourly or 1 hourly values shall be compiled with 98% of the time in a year.
Japan	60	1	
Mexico	110	1	Daily Maximum
United States	80	8	Fourth highest annual value averaged over three years.

The deposition of ozone, can damage the natural ecosystems. Ozone when enters the plant's leaves along with other trace gases through its pores known as "stomata" can dissolve in the water within the plant and there can react with the other chemicals. These chemical reactions lead to cellular damage inside leaves that adversely affects the plant growth, decreases photosynthesis rate [*Ashmore,* 2005]. Different ozone metrics are used to assess the effects of surface ozone, on the vegetation across the globe, the major ones are W126 [*Wang and Mauzerall,* 2004], accumulated threshold of ozone over 40ppb (AOT40), seasonal mean ozone

concentrations for 7 and 12 hours (M7, M12). Several groups have studied the ozone induced damages in crops on global scale [*Avnery et al., 2011a, 2011b; Hollaway et al., 2012; Chuwah et al., 2015*] to regional scales e.g. over East Asia [*Wang and Mauzerall,* 2004], over Europe [*Holland et al.,* 2006], the USA [*Adams et al.,* 1998] and over India [*Engardt,* 2008; *Roy et al.,* 2009; *Ghude et al.,* 2014; *Sinha et al.,* 2015]. All of the above studies estimated ozone related losses in agricultural crops e.g., wheat, corn, maize, rice etc. and their respective economic losses.

Influence on Earth's radiation budget and global warming: The solar radiation is the primary driver of global mean radiation budget of the Earth's atmosphere. About 30% of the incident solar radiation is reflected back to space by the clouds and Earth's surface; about 47% is absorbed by the Earth's surface (most of the radiation in shortwave range) and about 23% is absorbed by the atmosphere [*Trenberth et al.,* 2009]. To conserve the incoming energy, the Earth's surface and atmosphere radiates nearly same amount of energy in the form of longwave radiation. The longwave radiation emitted by the Earth's surface is absorbed and reradiated by the greenhouse gases. Thus, any changes in the concentrations of greenhouse gases can perturb the Earth's radiation budget and this change in the radiation budget is also quantified as "radiative forcing". The radiative forcing metric is also used by IPCC to assess the individual contribution of different trace species to the global climate change [*IPCC AR5,* 2013]. Ozone is an effective greenhouse gas since it strongly absorbs the outgoing terrestrial radiation at around 9.6 μm. The radiative forcing of tropospheric ozone is generally estimated using the model simulations. Gauss et al., [2006] showed the change in annual mean

tropospheric column ozone amounts due to increase in anthropogenic emissions is about 9.8 ± 1.6 DU between the years 1850-2000. Several studies estimated the radiative forcing due to increase in concentrations of tropospheric ozone since the preindustrial times [*Bojkov,* 1988; *Marenco et al.,* 1994; *Brentsen et al.,* 1996; *Oltmans et al.,* 1998; *Lamarque et al.,* 2005; *Gauss et al.,* 2006]. Recent IPCC assessment report [2013] has indicated that net radiative forcing of tropospheric ozone is 0.40 ± 0.20 W/m^2 and it has been ranked third after CO_2 and CH_4 in the list of climate forcing agents. Here, it is also important to note that the warming effect of one ozone molecule in the atmosphere is higher by about 1200-2000 times than that of one CO_2 molecule and is also higher than that of CH_4 (22) and N_2O (217) [*Ramanathan et al.,* 1985; *Schwarzkopf and Ramaswamy,* 1993; *Marenco et al.,* 1994].

Tropospheric ozone budget: Numerous efforts have been made to estimate the individual contributions of above mentioned processes to the global budget of tropospheric ozone [for e.g., *Stevenson et al.,* 2006]. The individual contributions of the photochemical production and loss, stratospheric input and dry deposition processes to the global ozone budget in twenty-one global 3-D atmospheric chemistry models are shown in Figure 1.1. The average±1sigma contributions of photochemical production and the stratospheric input to the global ozone production, from these models, are estimated to be 5072±614 and 570±183 Tg $year^{-1}$, respectively while those of photochemical loss and dry deposition to the global ozone loss are estimated to be 4652±713 and 600±195 Tg $year^{-1}$, respectively. In general, the global ozone production and loss budgets are dominated by the photochemistry. However, large uncertainties among these model estimates reflect

the substantial gaps in our understanding of the various processes controlling the tropospheric ozone.

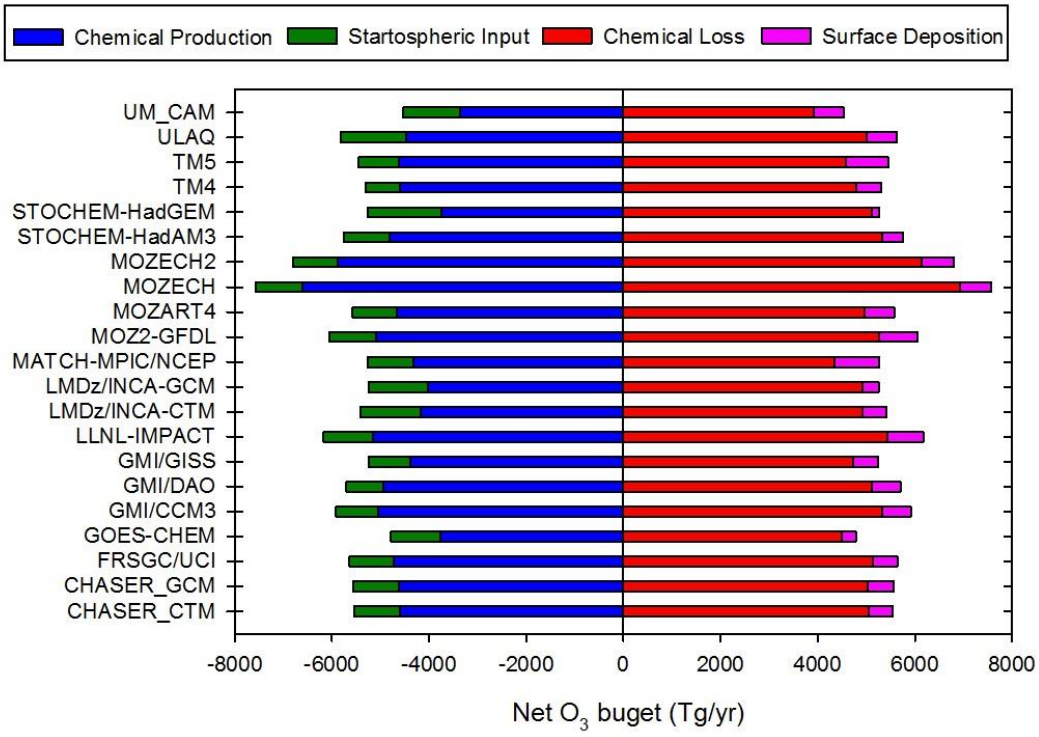

Figure 1.1: *The figure shows present day global production and loss processes of tropospheric ozone simulated by 21 global 3-D chemistry transport models for the year 2000. Refer Stevenson et al. [2006] for description of these models.*

1.1.2 Carbon monoxide:

Carbon monoxide (CO) is a colorless, odorless and poisonous gas, which is produced by the incomplete combustion of fuels (e.g. coal, wood, charcoal, oil, kerosene, gasoline, natural gas, etc.). It is a criteria pollutant and can lead to ozone production in presence of NO_x and sunlight [e.g., *Levy*, 1971; *Crutzen*, 1973; *Logan et al.*, 1981]. It also plays an important role in the troposphere by controlling the OH radical concentration [*Logan et al.*, 1981] as about 70% of total OH loss is due

to CO. The changes in CO concentrations can influence the climate by affecting greenhouse gases such as CH_4 that are generally removed by OH, and also can affect tropospheric ozone [e.g., *Daniel and Solomon*, 1988; *Mickley et al.,* 1999]. The lifetime of CO is about 2 months. CO is toxic gas, which, if inhaled can cause harmful health effects depending upon its concentration. At lower levels of poisoning (>35-few hundred ppmv) it can cause lightheadedness, confusion, headache, vertigo, memory loss etc., which at even higher levels often leads to toxicity of the central nervous system and heart, and even death. It can react with hemoglobin (in blood) to form carboxyhemoglobin (HbCO) and thereby inhibiting its ability to carry oxygen to various body parts, leading to hypoxia.

Several studies in past have estimated the global tropospheric CO budgets with large uncertainties, however all of these indicated that major sources being oxidation of hydrocarbons (including methane), fossil fuel burning and biomass burning and sink being reaction with OH radical and stratospheric uptake [*Logan et al.,* 1981, *Seiler and Conrad,* 1987, *Khalil and Ramussen,* 1990, *Pacyna and Graedel,* 1995, *Holloway et al.,* 2000, *Duncan et al.,* 2007]. Duncan et al., [2007] used GOES-Chem 3-D model to calculate annual CO budgets and is shown below in the Table 1.2.

Table 1.2: *Estimated global budget of carbon monoxide in the troposphere. (Compiled from Duncan et al., 2007).*

Types of Sources and Sinks	**Budget (Tg/yr)**
Fossil fuel combustion	464-487
Biomass burning	451-573
Biofuels	189
Oxidation of NMHCs	354-379
Oxidation of methane	778-861
Sources – Total	2236-2489
Sinks (reaction with OH, Consumption by soil, flux into stratosphere) – Total	2231-2366

1.1.3 Nitrogen oxides ($NO_x = NO + NO_2$)

Nitrogen oxides often known as NO_x is a sum of nitric oxide (NO) and nitrogen dioxide (NO_2). NO_x is largely produced in the form of NO from reaction between nitrogen and oxygen (inert at ambient temperature) during combustion at high temperatures and largely converts in NO_2. Such high temperatures can be found inside a vehicle engine, industrial boilers, kilns, lightning flashes etc. NO_x play a key role in ozone production and loss processes in the presence of other precursor gases and sunlight. It also contributes in the formation of smog and acid rain in the atmosphere. Tropospheric NO_2 is also a criteria pollutant indicated by several environmental agencies worldwide. The exposure to nitrogen oxides can cause irritation of the eyes, nose, throat and lungs, further it can aggravate existing respiratory problems such as asthma and heart disease.

Tropospheric budget of NO_x is quantified with large variations in the past [*Ehhalt and Drummond*, 1982; *Logan*, 1983; *Lee at al.*, 1997; *Muller and Stravrakou*, 2005; *Denmen et al.*, 2007; *IPCC AR5* 2013]. IPCC's latest assessment report suggests that total global sources of NO_x contribute about 51.9 TgN/yr in which major contribution is from anthropogenic sources (total 43.1 TgN/yr, ~83% of the total) like fossil fuel combustion and industrial processes (33 TgN/yr), biomass and biofuel burning (7.1 TgN/yr), agriculture (2.3 TgN/yr) and aircraft (0.7 TgN/yr). Natural sources contribute less than 20% with 8.8TgN/yr, this includes lightening emissions (5 TgN/yr), soils emissions (3.3 tgN/yr) and some from chemical reactions in the troposphere (< 05 TgN/yr). Major sink for NO_x is wet/dry deposition in form of nitric acid. Several studies indicated that the emissions of NO_x are increasing and it would result in net increase in N-deposition over land [*Lamarque et al.*, 2005b, *Denetener et al.*, 2006].

1.1.4 Methane and volatile organic compounds:

Methane is second most abundant greenhouse gas after CO_2 in our atmosphere. It is relatively well mixed with a residence time of ~10-12 years [*Prather et al.*, 2012; *IPCC AR5*, 2013; *Voulgarakis et al.*,2013]. Although being shorter in lifetime (compare to CO_2) its global warming potential, which is a measure of effectiveness of trapping radiation, is about 34 times greater than that of CO_2 over a 100-year period [*IPCC AR5*, 2013]. Methane is produced naturally from wetlands or decomposition of organic matter and emitted anthropogenically via fossil fuel emissions, waste management, from fermentation in cattle, biomass burning and rice paddies. The anthropogenic part dominates in the global estimates of methane in the troposphere. The oxidation of CH_4 via OH radical produces ozone,

formaldehyde and CO, making methane a precursor of ozone. Several studies in the past have estimated the tropospheric budgets for methane [*Khalil et al.,* 1993; *Wuebbles and Hayhoe,* 2002; *Wang et al.,* 2004; *Mikaloff-Fletcher et al.,* 2004a; *Chen and Prinn,* 2006]. *Mikaloff-Fletcher et al.,* [2004a] estimated CH_4 budgets for the year 1999 and found total source contribution to be 610 Tg(CH_4)/yr which includes 350 Tg(CH_4)/yr from anthropogenic sources like ruminants (91), biomass burning (88), rice agriculture (54), gas oil industry (52), landfills and waste (35) and coal mining (30). Natural sources (260 Tg(CH_4)/yr) of methane are like wetlands (231) and termites (29). The dominant loss process for atmospheric methane is via its reaction with hydroxyl radical (OH) which contributes 507 Tg(CH_4)/yr (~88% of the total sink), other sinks being uptake by stratosphere (40) and soils (30).

There are hundreds of thousands of organic compounds in the troposphere with mixing ratios from pptv to ppbv levels and lifetimes from minutes to months. VOCs, as defined by World Health Organization (WHO), are the organic compounds that have saturation vapour pressure greater than 1020 hPa at 25^{o}C. Majority of VOC emissions are from biogenic sources [*Muller,* 1992] with minor contribution from anthropogenic sources (about a factor of 10). The major biogenic VOCs are isoprene (~40%), terpenes and monoterpenes (~12%). The anthropogenic emissions include fossil fuel combustion, biomass burning, natural gas emissions, industrial processing of chemicals etc. and majority of compounds emitted are alkanes (~41%), alkenes (~36%) and aromatics (~23%). VOCs in the troposphere are primarily removed by their reaction with OH radical, to form ozone and other oxygenated compounds, other sinks being reaction with ozone, nitrate radical and

halogen radicals [*Jenkin et al.,* 2003; *Saunders et al.,* 2003]. These species have much higher potential of ozone formation than methane or CO and this generally increases with increases in number of carbon atoms. In addition to their role in photochemical cycle, some of the species also impact climate, directly as a greenhouse gas or by conversion to aerosols on oxidation. Many of the VOCs can impact human health adversely, their short term exposures can cause eyes, nose and throat irritation, headaches, nausea, dizziness, worsening of asthma symptoms etc., while long exposure can cause cancer, damage liver, kidney and failure of central nervous system etc. Despite their higher ozone formation potential, role in photochemistry and adverse health effects these are very poorly quantified by observations as well as modeling studies. Global emission budgets of the tropospheric VOCs also show very large uncertainties (Table 1.3).

Table 1.3*: Global annual emission rates for selected groups of VOCs in Tg/yr. Table is adapted for Koppmann [2007].*

Source	Annual emissions (uncertainty)
Anthropogenic - total	100
Fossil fuel burning	60 (30-115)
Biomass burning	40 (19-70)
Natural – total	1187
Ocean	7 (3-14)
Terrestrial Plants	1180 (400-4600)
Total	**1287**

1.2 Processes controlling the budgets of trace gases

The trace gases in the atmosphere undergo a variety of processes like chemical transformations, horizontal and vertical transport, deposition etc. those control their budgets. In general, the gases are emitted from ground and water bodies, gets transformed (chemically, physically) and transported (dynamics) to the atmosphere, and at some point of time are removed from atmosphere by variety of ways e.g., deposition (wet or dry). In following section above mentioned processes will be discussed.

1.2.1 Emissions:

Trace gases those are emitted directly into the atmosphere are called primary trace gases (e.g. CO, CH_4, NMHCs, NO etc.). The sources emitting trace gases can be of anthropogenic origin and/or natural origin. The natural sources include volcanic eruptions, soil, vegetation, natural forest and grassland fires, wetlands, termites, lightning, oceans, etc. while the anthropogenic emission sources include the industrial processes, fossil fuel combustion, domestic cooking, crop residue burning, deforestation, agricultural practices, mining and transport etc. In general, the global total emissions of CO and NO_x are dominated by anthropogenic emissions while biogenic emissions dominate in case of VOCs and have been discussed in previous sections.

1.2.2 Chemical production and loss:

Production: The chemical production and transformations of trace gases are

another major source of them in the troposphere. The gases produced by the chemical reactions among primary trace gases are known as secondary trace gases (e.g. ozone). These reactions play an important role in the tropospheric budgets of different gases e.g. ozone, CO, hydrocarbons etc. It has been described in section 1.1.1 that ozone plays a key role in the troposphere via OH radical and here we discuss its chemical production and loss mechanism. The ozone production in atmosphere takes place only when an oxygen atom, $O(^3P)$ reacts with an oxygen molecule (O_2) in presence of third molecule (R1.6).

$$O(^3P) + O_2 + M \rightarrow O_3 + M \qquad \text{(R1.6)}$$

In the stratosphere, the oxygen atoms are produced from photodissociation of oxygen molecules in presence of ultraviolet (UV) radiation shorter than 240 nm (R1.7).

$$O_2 + h\nu\ (\lambda < 240\ \text{nm}) \rightarrow O + O \qquad \text{(R1.7)}$$

However, this reaction (R1.7) is not dominant in the troposphere due to screening of shortwave UV radiation in the stratosphere and its non-availability in the troposphere. In fact, the stratosphere was thought to be the only source of tropospheric ozone during pre-1970s [e.g. *Regener,* 1949; *Junge,* 1962]. However, the role of photochemical ozone production mechanism was recognized only during early 1970s [*Chameides and Walker*, 1973; *Crutzen*, 1973]. It was shown that the photodissociation of NO_2 leads to production of atomic oxygen in the troposphere that is used for the production of the ozone in the troposphere. A highly complex set of reactions known as the "photochemical smog mechanism" [*Haagen-Smit,* 1952] proposed during the "Los-Angeles" smog event [*Middleton et al.,* 1950] for the chemical production of ozone in the troposphere. Although this mechanism is very complex and involves hundreds of reactions but it can be presented in a

simplified form as shown below:

$$OH + RH \rightarrow R + H_2O \quad \text{(R1.8)}$$

$$R + O_2 + M \rightarrow RO_2 + M \quad \text{(R1.9)}$$

$$RO_2 + NO \rightarrow RO + NO_2 \quad \text{(R1.10)}$$

$$RO + O_2 \rightarrow HO_2 + R'CHO \quad \text{(R1.11)}$$

$$HO_2 + NO \rightarrow OH + NO_2 \quad \text{(R1.12)}$$

$$NO_2 + h\nu\ (\lambda < 410\ nm) \rightarrow NO + O \quad \text{(R1.13)}$$

$$O + O_2 + M \rightarrow O_3 + M \quad \text{(R1.7)}$$

$$\text{Net:}\quad RH + 2O_2 + h\nu\ (\lambda < 410\ nm) \rightarrow R'CHO + H_2O + O_3 \quad \text{(R1.14)}$$

In the above reaction set, RH represents the hydrocarbons (CH_4 and NMHCs), R′CHO represents the carbonyl compounds (aldehyde or ketone) and RO_2 represent the peroxy radicals such as CH_3O_2, $C_2H_5O_2$ etc. From this simplified mechanism, it is clear that the oxidation of hydrocarbons by the OH radicals followed by the NO_2 photolysis leads to the production of ozone in the troposphere. Apart from hydrocarbons, CO is also a precursor gas to ozone which also forms hydroperoxy radicals when react with hydroxyl radical (OH) and leads ozone production via a similar set of chemical reaction.

Apart from the above chemical reactions for ozone production, the chemical reactions also play an important role in the global budget of precursor gases, like the oxidation of CH_4 by OH radical is the major chemical source of CO in the troposphere. The reaction of methane with OH radicals produces methyl radical (CH_3) which in turn reacts rapidly with O_2 to form methyl peroxy (CH_3O_2) radical. The CH_3O_2 radical then produce formaldehyde (CH_2O) through a set of reactions

involving NO and HO_2 and OH radicals. The formaldehyde molecules undergo photolysis reaction to produce CO molecules. The NMHCs also oxidizes to give formaldehyde which further contributes to production of CO.

Loss: The chemical reactions play an important role in removing the trace gases from the atmosphere. For example, the photolysis of ozone molecules at the wavelength less than 310 nm followed by the reaction of O (^1D) atoms with water vapor (see reactions R1.1 and R1.2) is a major chemical loss processes of the tropospheric ozone on the global scale. Further, the chemical reactions of ozone with HO_x (OH and HO_2) are another major loss of ozone at the global scale:

$$OH + O_3 \rightarrow HO_2 + O_2 \qquad (R1.15)$$

$$HO_2 + O_3 \rightarrow OH + 2O_2 \qquad (R1.16)$$

However, the reactions (R1.15) and (R1.16) are important only in the remote areas characterized by low NO_x levels. In the urban regions those are characterized by high NO_x levels, the titration of ozone by NO_x is the dominant loss process for ozone during nighttime as shown below:

$$NO + O_3 \rightarrow NO_2 + O_2 \qquad (R1.17)$$

$$NO_2 + O_3 \rightarrow NO_3 + O_2 \qquad (R1.18)$$

In addition to these reactions, some other reactions such as the radical recombination reactions, HO_x-NO_x reactions also contribute indirectly to the ozone loss. However, the contribution of such reactions to the ozone budget is significant only at the urban scales.

The aqueous phase chemistry involving aerosol particles and the halogen chemistry in the marine boundary layer are other important ozone loss process in the

atmosphere. The major removal processes of CO in the troposphere are the oxidation by OH radical, soil uptake and transport to the stratosphere. The principle sink of NO_x in the troposphere is oxidation to nitric acid (HNO_3) that is scavenged by the precipitation due to its high solubility in water. The primary sink of volatile organic compounds is also the oxidation by hydroxyl radical. More details about these loss processes can be seen elsewhere [e.g. *Brasseur et al.,* 1999; *Pitts and Pitts,* 2000; *Seinfeld and Pandis,* 2006].

1.2.3 Deposition:

The deposition at the Earth's surface or in rain drops, soil uptake and washout during rain are few of the processes that remove trace gases from the atmosphere. The dry deposition of any gas at an air-surface interface (e.g. surface of a tree, a building, a window, glass, soil etc.) removes it from the atmosphere and the processes occurs when it impacts and sticks to the surface [*Sehmel,* 1980]. The dry deposition flux (F) of a gas can be defined as the product of its ambient concentration (C) and the deposition velocity (V_d):

$$F = -V_d\, C \qquad (1.1)$$

where V_d is generally defined as the inverse of the sum of three resistances (the aerodynamic resistance R_a, the quasi-laminar boundary layer resistance R_b and the surface or canopy resistance, i.e. R_c) connected in series [e.g., *Wesley and Hicks,* 1977; *Walcek et al.,* 1986; *Russell et al.,* 1993]. The dry deposition velocities of ozone at a flat grass field in Portugal show a distinct diurnal variation with lowest values of about 0.1 cm/s during the night to the maximum values of 0.2-0.5 cm/s during the day [*Pio et al.,* 2000]. Similar diurnal pattern in ozone deposition

velocity with median deposition velocities of 0.04 cm/s during the nighttime and 0.32 cm s during the daytime has also been reported from a tropical forest area in northern Thailand [*Matsuda et al.,* 2005]. NO_x forms nitric acid (HNO_3) in moist atmosphere, which is a component of acid rain and can be deposited back to surface.

1.2.4 Dynamical and meteorological processes

In addition to the major sources and sinks of trace gases discussed above, the concentrations of trace gases in the atmosphere are also affected significantly by the dynamical and meteorological processes such as stratosphere-troposphere exchange (STE), advection, convection etc.

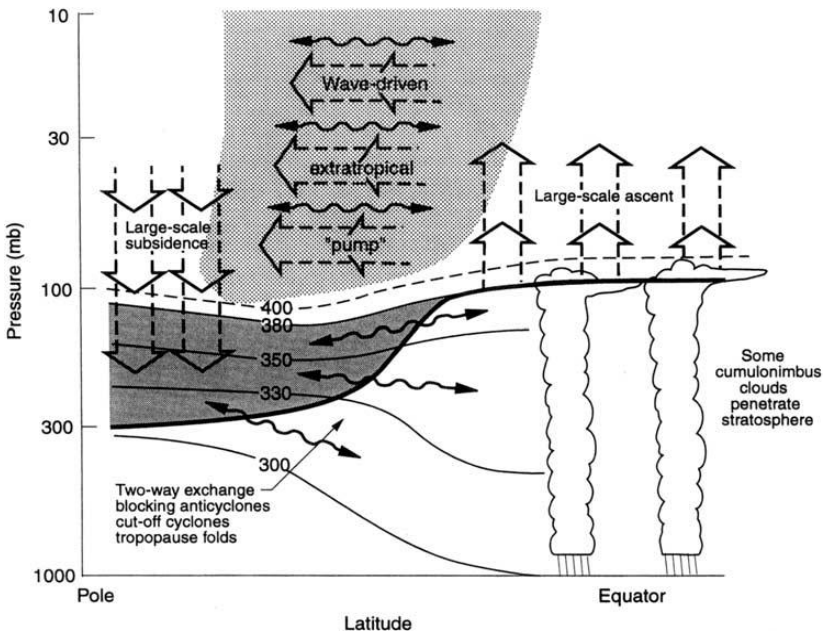

Figure 1.2: *Dynamical aspects of stratosphere-troposphere exchange (taken from Holton et al. [1995]; their Figure 3).*

Stratosphere-Troposphere Exchange: The dynamics of the troposphere and the stratosphere cannot be separated in principle [*Hoskins et al.,* 1985] and the downward transport from the stratosphere represents a significant input of trace gases, in particular of ozone, into the tropospheric chemical system [*Holton et al.,* 1995; *Mandal et al.,* 1998]. The stratosphere-troposphere exchange mechanism has been discussed in many review papers [e.g. *Vaughan,* 1988; *Davies and Schuepbach,* 1994; *Holton et al.,* 1995]. STE process is shown in Figure 1.2 and has been suggested as one of the major contributing factor to the springtime maximum of surface ozone observed at a number of sites across the globe [e.g. *Oltmans,* 1981; *Levy et al.,* 1985; *Logan,* 1985]. The contribution of stratospheric sources to the surface ozone has been found to be small in some observations studies [e.g. *Dibb et al.,* 1994; *Derwent et al.,* 1998] while it has been shown to be substantial at some locations, particularly at the higher-altitude mountain sites [e.g. *Tsutsumi et al.,* 1998; *Langford et al.,* 2009; *Cristofanelli et al.,* 2010]. The flux of ozone from the stratosphere to the troposphere in the northern hemisphere (NH) has been estimated to be 3-8 x 10^{10} molecules cm^{-2} s^{-1} [*Crutzen*, 1995], however, the flux in the southern hemisphere is about half of that over the NH. The total ozone production in the stratosphere is estimated to be about 5 x 10^{13} molecules cm^{-2} s^{-1} and only 0.1% of total stratospheric ozone in transported to the troposphere [*Crutzen*, 1995]. Further, the global ozone loss from the photolysis ($14x10^{10}$ molecules cm^{-2} s^{-1}) in the troposphere is estimated to be greater than the stratospheric input of ozone to the troposphere.

Advection and convection: In addition to stratosphere-troposphere exchange, the trace gases can also be transported over large distances and altitudes through

advection, convection and frontal lifting. The horizontal transport of air masses due to winds is called advection while the vertical mixing of trace species resulting from heating at the surface is called convection. The vertical lifting of air mass from the boundary layer to free troposphere in the warm air ahead of the cold fronts is known as frontal lifting. Frontal activity has been shown to play an important role in exporting the Asian air-mass to western Pacific [e.g. *Bey et al.,* 2001] and also in transporting from Northern America [*Milne et al.,* 2000]. Advection has been shown to transport the air-mass on regional [e.g. *Prospero et al.,* 1981; *Diouri et al.,* 1998; *Pochanart et al.,* 2001; *Naja et al.,* 2003a; *Moorthy et al.,* 2003; *Hegde et al.,* 2007] and intercontinental scales [e.g. *Jacob et al.,* 1999; *Heald et al.,* 2003; *Liu et al.,* 2003; *Zhang et al.,* 2008; *Pfister et al.,* 2010, *Lawrence et al.,* 2010]. However, the spatial extent to which trace gases can be transported depends upon the lifetime of that gas in the atmosphere. The trace gas with shorter lifetime are subjected to depletion due to photochemical and other removal processes and exhibits lower mixing ratios in the air masses transported away from the sources while rest of the other gases may have similar levels or higher levels due to chemical reactions [*Gregory et al.,* 1996]. Different other trace gases and radicals may also form and deplete during enroute transport of air-mass. Convection redistributes the trace gases vertically and can inject them into upper troposphere from where they can be transported to large distances through advection. For instance, *Park et al.* [2007] showed that deep convection during Asian summer monsoon can transport CO up to an altitude of about 12 km and much of the CO is then advected in the upper troposphere northeastwards across the Pacific Ocean and southeastwards with the cross-equatorial Hadley flow.

1.3 Present scenario over the Indian subcontinent

The Indian subcontinent is among the most populated and highly polluted regions in the world. This region has widely-varying landscapes including the Himalayas on the northern side, semi-arid and desert land masses in the west, tropical rainforests in the east and south, sea-shores in south and the Indo-Gangetic plain stretched from north to east (see Figure 1.3).

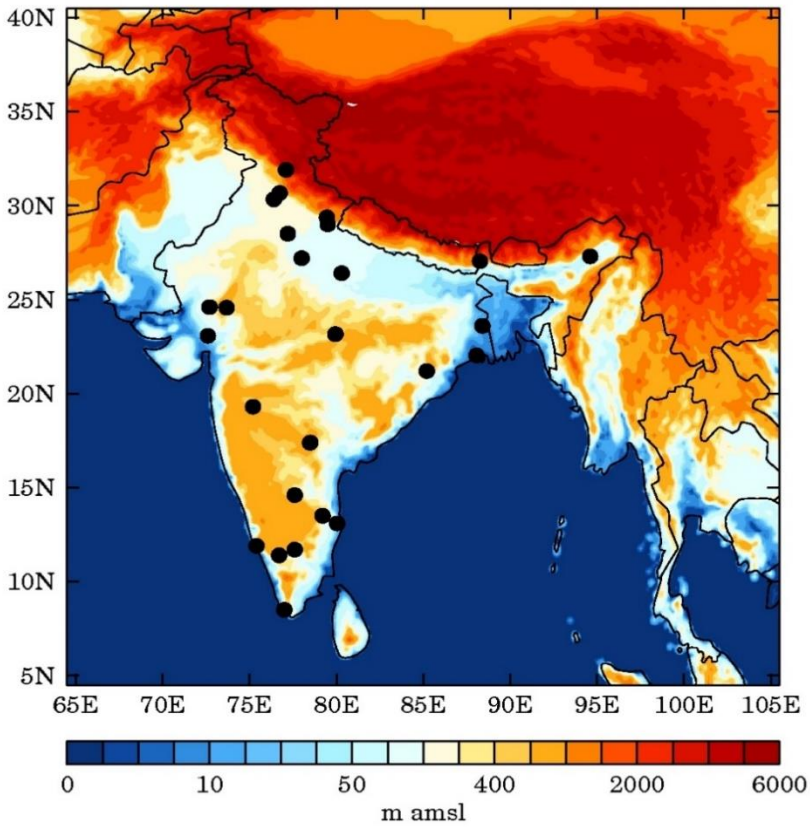

Figure 1.3: *Topography of the Indian subcontinent and the locations of some surface ozone observation sites over Indian region.*

The economic liberalization of India in 1991 led to a rapid growth in the industries, transportation, urbanization, agricultural activities and consequently significant increase in the anthropogenic emissions over this region are observed [e.g. *Streets*

and Waldhoff, 2000; *Akimoto*, 2003; *Ohara et al.*, 2007]. The increasing emissions have strong implications not only for the large population residing in this region but also for the people living in other parts of the world as these pollutants can be transported to wide regions [*Lawrence and Lelieveld,* 2010].

Additionally, the widespread use of biofuels and crop residues in domestic cooking activities and collocation of biomass burning sources with fossil fuel burning sources allows spontaneous mixing of trace gases and aerosols emitted by these sources. This might lead to the chemical processes that may differ from those occurring in the other parts of the world where the emissions are dominated either by the fossil fuel burning sources (e.g. North America and Europe) or by the biomass burning sources (e.g. Africa) [*Lelieveld et al.,* 2001; *Reiner et al.,* 2001]. Few studies in the past have focused on estimating the emissions of trace species from biomass burning and understanding their impact on the air quality and radiation budget of the downwind regions over the Indian subcontinent [*Venkatraman et al.,* 2006; *Kharol and Badrinath,* 2006, *Kumar et al.,* 2011; *Ghude et al.,* 2013; *Jena et al.,* 2014; *Sinha et al.,* 2015], however these studies have provided short-term information about the role of biomass burning in context of the Indian region and a detailed investigation of long-term changes including the seasonal and interannual variability of the biomass burning activity over the Indian subcontinent was lacking. In light of the above conditions, the long-term observations (both surface and vertical) of trace gases and chemistry transport modeling are highly needed over this region. The next section will provide an overview of the studies based on ground-based observations including land and ocean based campaigns, balloon borne observations, satellite observations and

chemical transport models that are previously carried out over the Indian subcontinent.

1.3.1 Observations

Ground-based observations: The first measurements of surface ozone were made during mid 1950s over the Indian region using an Ehmert instrument [*Ramanathan*, 1956; *Dave*, 1957; *Naja and Lal*, 1996]. However, continuous measurements of surface ozone were only started during 1960-70s when Indian meteorological department initiated the measurements at the six stations namely Trivandrum, Kodaikanal, Pune, Nagpur, Delhi and Srinagar [*Sreedharan and Tiwari*, 1971]. These observations provided important information about the surface ozone levels nearly over the entire latitudinal extent of India but were based on observations using chemical methods. The more accurate measurements of surface ozone based on the ultraviolet photometry technique were started at a number of sites including Pune [*Khemani et al.*, 1995], Ahmedabad [*Naja*, 1997; *Lal et al.*, 2000], Gadanki [*Naja and Lal;* 2002], Trivandrum [*Nair et al.*, 2002], Mt Abu [*Naja et al.*, 2003b] and Delhi [*Jain et al.*, 2005] during the 1990s. Later, surface ozone measurements were also started at Darjeeling [*Lal*, 2007], Anantapur [*Reddy et al.*, 2008, 2012], Kolkata, Haldia [*Purkait et al.*, 2009], Hyderabad [*Badrinath et al.*, 2009] and Kannur [*Nishanth et al.*, 2011]. The initial network of surface ozone observations was limited to western and southern parts of India with very limited measurement sites over northern India including the IGP region. Later several other sites in IGP and nearby regions also reported ozone and precursor measurements [*Singla at al.*, 2011., *Ojha et al.*, 2012, *Bhuyan et al.*, 2014, *Gaur et al.*, 2014, *Sarangi et al.*,

2014]. Apart from the ozone measurements, surface measurements of CO, NO_x, CH_4 and non-methane hydrocarbons have been reported from Ahmedabad [*Lal et al.,* 2000; *Sahu and Lal,* 2006], Mt Abu [*Naja et al.,* 2003b; *Sahu,* 2004], Gadanki [*Naja and Lal,* 2002], Manora Peak [*Sarangi et al.,* 2016] and the Arabian Sea, Indian Ocean and Bay of Bengal [*Lal et al.,* 1998; *Chand et al.,* 2001; *Naja et al.,* 2004; *Srivastava et al.,* 2012; *Sahu et al.,* 2006, 2011]. Many of these observation sites are initiated under different observation networks like ISRO-ATCTM and MAPAN.

Apart from Indian region, limited and discontinuous surface measurements of ozone and precursor gases were made at Nepal, Pakistan and Bangladesh. Few measurements of ozone and some of precursor gases were performed in Kathmandu valley using passive air sampling, online analyzers etc. [*Sharma et al.,* 2000, *Pudasainee et al.,* 2006, 2010, *Panday and Prinn,* 2009, *Panday et al.,* 2009]. Other than Kathmandu valley, ozone and precursor gas measurements were also performed at Nepal Climate Observatory - Pyramid near Everest basecamp [*Bonasoni et al.,* 2010]. Four-year continuous measurement of ozone, CO and NO at Dhaka, Bangladesh indicated highest levels of these pollutants in winter season with lowest values during monsoon months [*Sikder et al.,* 2013]. Such studies are limited over Pakistan [*Ahmed and Aziz,* 2013, *Rasheed et al.,* 2014]. Overall, apart from Indian region very limited measurements elsewhere in the subcontinent has led to poor understanding of spatial and temporal distribution of ozone and precursors.

Vertical distribution measurements: The vertical distributions of ozone over the

Indian region have also been measured using the balloon-borne sensors. The vertical distribution of ozone is measured regularly by the Indian Meteorological Department (IMD) at Delhi, Trivandrum and Pune using the balloon-borne instrument. These measurements have been used to examine long-term changes in the vertical distribution of tropospheric ozone during 1972-2001 [*Saraf and Beig,* 2004] and to study the impact of Pinatubo volcanic eruption on the distribution of ozone the Indian region [*Beig et al.,* 2002]. Balloon-borne measurements made over the oceanic region during the Indian Ocean Experiment (INDOEX) [*Mandal et al.,* 1999] have been used in conjunction with Model of Ozone and Related Tracers -2 (MOZART-2) model to analyze the tropospheric distribution of ozone and precursors over the tropical Indian Ocean [*Saraf et al.,* 2003]. The balloon-borne ozone measurements have also been used to study the seasonal variability of ozone in the boundary layer and middle troposphere at Ahmedabad [*Lal,* 2007; *Srivastava et al.,* 2012,] and to understand transport effects on the vertical distribution of ozone over marine regions [*Lal et al.,* 2013] and over an urban site in western India [*Lal et al.,* 2014]. Later ozonesonde measurements were also initiated over Nainital [*Ojha et al.,* 2014]. Additionally, some campaign based observations were made over Kanpur [*Gupta et al.,* 2007] and in marine regions surrounding India [*Srivastava et al.,* 2011]. The long term vertical measurements are still limited to western and southern parts of India and very limited (only for a year) were done over the Himalayan and IGP region. No such measurements are reported outside India and within the subcontinent.

Land and ocean campaigns: Apart from the surface and balloon-borne observations, several campaigns have also been conducted over the inland and

adjoining marine regions (the Arabian Sea, the Bay of Bengal and the Indian Ocean) of India to investigate the spatial and temporal evolution of pollutants from this region and to assess their impact on radiation budget. These campaigns are important although for a shorter time but diverse measurements at very high resolution can be made to understand various aspects of atmospheric chemistry over a desired region. The major campaigns conducted in this region are the Indian Ocean Experiment (INDOEX) during 1996, 1997, 1998 and 1999 winter [e.g. *Lal et al.,* 1998; *Mitra,* 1999; *Naja et al.,* 1999; *Satheesh et al.,* 2000; *Chand et al.,* 2001; *Lal and Lawrence,* 2001; *Ramanathan et al.,* 2001; *Lelieveld et al.,* 2001; *Chand et al.,* 2003; *Naja et al.,* 2004], ISRO-GBP land campaign during February-March 2004 over the Central/peninsular India [e.g. *Moorthy et al.,* 2004; *Jayaraman et al.,* 2006; *Gadhavi and Jayaraman,* 2006] and during December 2004 over the Indo-Gangetic Plain region [e.g. *Tripathi et al.,* 2006; *Dumka et al.,* 2006; *Ganguly and Jayaraman,* 2006; *Ramachandran et al.,* 2006] and Integrated Campaign for Aerosols, Gases and Radiation Budget (ICARB) during February-May 2006 over the Indian mainland, the Arabian Sea, the Bay of Bengal and the tropical Indian Ocean [e.g., *Moorthy et al.,* 2006]. All these campaigns provided important information on the processes controlling the surface ozone and the optical, physical and chemical properties of aerosols. Recently an international field campaign Sustainable atmosphere for Kathmandu valley (SusKat) was carried out in Kathmandu valley and results from this campaign are being presented in chapter 4.

1.3.2 Satellite data analysis

In addition to the ground-based, balloon borne and ship-borne observations, several studies have also utilized satellite retrievals of both trace gases to study their spatial and temporal distribution over the Indian region. *Fishman et al.,* [2003] used coincident observations of total ozone from the Total Ozone Mapping Spectrometer (TOMS) and stratospheric ozone profiles from Solar Backscattered Ultraviolet (SBUV) instrument to derive global maps of tropospheric ozone column and showed that total tropospheric ozone values over the Indo-Gangetic Plain (IGP) region are significantly higher than those over other Indian regions. *Ghude et al.,* [2008b] used tropospheric NO_2 concentrations derived from Global Ozone Monitoring Experiment (GOME) and Scanning Imaging Absorption Spectrometer for Atmospheric Cartography (SCIAMACHY) for the period of 1996-2006 and estimated an increasing trend in NO_2 values over Delhi and Mumbai. They also showed that seasonal cycle of NO_2 show higher levels during winter-spring (March-May) and a minimum during the summer/monsoon (June-September). *Ghude et al.,* [2010] utilized tropospheric NO_2 column from Ozone Monitoring Instrument (OMI) to investigate the rain-induced soil NO_x emissions over the Indian region and estimated an average emission flux of ~23-28 ng N m^{-1} s^{-1} during the onset of rainy season in India. *Kar et al.,* [2010] used CO retrievals from Measurements of pollution in the Troposphere (MOPITT), aerosol data from Cloud-Aerosol Lidar and Infrared Pathfinder Satellite Observations (CALIPSO) and tropospheric column ozone from Ozone Monitoring Instrument/ Microwave Limb Sounder (OMI/MLS) to show that higher levels of pollutants over the IGP region during wintertime are associated with large scale subsidence over this region. *Girach et al.,* [2014] used MOPITT retrievals to show seasonal variations in lower

tropospheric and upper tropospheric CO peaks in winter and summer respectively with a decreasing trend during last 14 years in lower tropospheric and columnar CO. Apart from Indian region, positive trends of tropospheric column NO_2 were found using OMI and SCIAMACHY data over Pakistan [*Haq et al.,* 2014].

1.3.3 Modeling

The chemical transport models, both on global and regional scales can be used to simulate the spatial and temporal distribution of trace gases, these also provide in-depth information on different processes over a region. The initial Model for Atmospheric Transport and Chemistry (MATCH) modeling results over Indian region couldn't reproduce maxima and minima in the seasonal cycle of ozone at Ahmedabad and Mt. Abu [*Naja et al.,* 1997]. The model showed some biases at some of the sites however it also performed reasonably well at other sites. Later, another global mode,l Model of Ozone and Related Tracers-2 (MOZART-2) was used to analyze the observations of ozone and precursors made over the Indian Ocean during INDOEX, over the Indo-Gangetic Plain region and to assess the changes in anthropogenic emissions between 1991 and 2001 [*Saraf et al.,* 2003, *Beig and Ali,* 2006, *Beig and Brasseur,* 2006].

Surendran et al., [2015] used MOZART-4 model to show positive bias of about 1-30 ppbv in surface ozone at 13 different stations over Indian region. Apart from these, few other global model studies [*Roy et al.,* 2008; *Engardt,* 2008; *Mittal et al.,* 2007; *Kumar et al.,* 2010; *Ojha et al.,* 2012] were also performed and all of these qualitatively capture the observed seasonal cycle of surface ozone, however, large

biases were also observed at different sites across the Indian subcontinent. Over the Kathmandu valley mesoscale meteorological model MM5 at 1 km resolution was used to investigate the dynamical factors contributing to the diurnal variations in air pollutants [*Panday et al.,* 2009].

The first regional model setup (WRF-Chem) with a complete seasonal cycle over South Asian region was done by *Kumar et al.,* [2012a, 2012b] for the year 2008 and showed that the biases in meteorological fields can introduce errors up to ± (10-25%) in ozone, CO and NO_x simulations. WRF-Chem model captured the seasonal variations of ozone and CO over few sites however differences were observed in NO_x [*Kumar et al.,* 2012b]. Further, the vertical distribution of TES ozone, MOPITT CO are well represented by the model, however it underestimated some of the other satellite retrievals, with highest differences were during spring. Further model also indicated region to be NO_x limited [*Kumar et al.,* 2012b]. WRF-Chem was also used with 11 CO tracers to assess source contributions from different region [*Kumar et al.,* 2013]. This study indicated that the wintertime high CO in boundary layer and free troposphere was primarily due to anthropogenic emissions and CO inflow respectively [*Kumar et al.,* 2013]. It was shown that the CO from the IGP can reach cleaner marine environments of Arabian sea and Bay of Bengal with contribution of about 42 and 76% respectively [*Kumar et al.,* 2013].

1.4 Objectives and organization of the thesis

The Indian subcontinent, particularly northern region that includes two contrasting regions (pristine Himalaya and one of the most polluted IGP) is one of the least

studied parts of the world. Surface and vertical measurements are very limited and information on different emission sources, like biomass burning has significant uncertainty. The satellite retrievals indicate high levels of pollution across IGP and this pollution under favorable meteorological conditions can be transported to other regions as well, including the pristine Himalayas. In light of above facts, the broad objectives of this Thesis are the following:

- To assess the seasonal and interannual distribution of biomass burning and its contribution in budgets of various trace species over the Indian subcontinent using satellite data.
- To study the variability in surface ozone and precursor gases in the Himalayan region and assessing the role of IGP and Kathmandu valley.
- To investigate the variability and long term changes in the vertical distribution of ozone and contribution of biomass burning over this region by conducting balloon-borne measurements from ARIES Nainital in the central Himalayas.
- To investigate the meteorological characteristics of the central Himalayan region by using the high frequency balloon-borne measurements of meteorological parameters.

The outlines of this thesis which is composed of seven chapters is described here. In **chapter 2,** the operating principles of different instruments for surface and vertical measurements of ozone and precursor gases along with a brief description of the measurement techniques, retrieval procedures employed by different space-borne sensors and description of two models used for this study are discussed. **Chapter 3** describes the seasonal, interannual and long term

changes in biomass burning those inferred from satellite retrieved data and different emission inventories. **Chapter 4** describes the observation made during an international field campaign (SusKat) and associated modeling results during December 2012 to June 2013. The five year long (2011-2015) vertical measurements of ozone using balloon borne sensors are presented in **Chapter 5**. The results from high frequency balloon borne measurements of meteorological parameters made during Regional Aerosol Warming Experiment - Ganges Valley Aerosol Experiment (RAWEX-GVAX) campaign are discussed in **Chapter 6**. The important findings from the work presented in this thesis are summarized in **Chapter 7** along with the future research plans in this area**.**

Chapter 2

Methodology

Accurate and precise observations of trace gases have always been in need to better understand their spatial and temporal variations and other associated processes in the atmosphere. There have been significant improvements in different techniques related with surface based, balloon borne, space borne observations and modeling skills during past few decades. However, this is a challenging task because atmospheric lifetimes of these species have large variability with some (e.g. OH radical) living for less than a second to some residing for hundreds of years (e.g. CFCs) depending upon their reactivity. This enormous range in their lifetimes, and the different physio-chemical properties of trace species, no single instrument is able to detect these species and hence, several different types of instruments have been developed in the recent decades for the measurement of these species. The accuracy of many of these instruments has been reported to be less than 10% [*Heard, 2006*]. These instruments have been deployed on a number of platforms like ship borne, balloon borne, aircraft borne and space borne apart from the ground.

These multi-platform measurements have contributed significantly to our understanding of various processes controlling these trace species in the Earth's atmosphere.

In past few decades, significant improvements have been made in ground based measurement techniques of ozone and CO. Surface ozone can be measured by electrochemical [*Komhyr, 1969*], chemiluminescence and ultra-violet (UV) absorption methods, however UV absorption method is preferred for continuous long term measurements. CO can be measured by Non-Dispersive Infra-Red technique (NDIR); Cavity ring down spectroscopy (CRDS) or Laser Induced Fluorescence (LIF). Vertical observations of ozone are generally done by electrochemical sensors and it is among the most accurate technique that can provide ozone profiles up to the middle stratosphere. Unlike other methods such as LIDAR and satellite observing systems, ozonesondes are not affected by clouds and are capable of resolving strong ozone gradients in the upper troposphere and lower stratosphere (UTLS) [e.g. *Thompson et al.*, 2011]. The vertical measurements of meteorological parameters are done using a radiosonde which has sensors for pressure, temperature and relative humidity and its in-built GPS is used to calculate winds and position. The measurement techniques discussed above are either point observations or represent a very small region, so to have a better understanding of a broader region some of the satellite retrieved data-sets and emission inventories are also used in this work.

Present chapter includes a discussion of the different instruments employed for in situ measurements of trace gas, various satellite derived products, different

emission inventories and models used in this study. The chapter is divided into five sections which include ground based instruments, balloon borne observation, satellite observations, emission inventories and different models used in this work. The operating principles of various instruments used to measure ozone and CO are discussed in section 2.1. The balloon borne observations of ozone and meteorological parameters are discussed in section 2.2. The information about various space-borne sensors, their retrieval algorithm is provided in section 2.3. The various emission inventories and models used in this thesis are discussed in sections 2.4 and 2.5 respectively.

2.1. Trace gas detection in atmosphere

In this section different techniques available for the detection of ozone and CO are discussed. Ozone was discovered by Schönbein in 1939 and its measurement was done using a chemical test paper named after him. Later some other methods for ozone detection were also developed but no stable method was available till 1950s. During International Geophysical Year, electrochemical method for ozone detection were developed and later patented by *Komhyr et al.,* [1969]. In this method the amount of ozone in ambient medium is proportional to the current generated by its reaction with KI solution. Later another method for ozone detection was developed which was based on absorption of UV radiation by ozone molecules at about 254 nm. This method is more extensively used for continuous measurement of ambient ozone across the globe.

CO measurements started in late 1940's using spectroscopic techniques but were of

less scientific importance during those years. The interest in CO measurements was regained during 1960's when importance of CO in oxidizing capacity of troposphere was discovered. During the same period, gas chromatographic techniques were also developed and global concentrations of CO were measured. Overall, the CO measurement techniques are primarily based on either spectroscopy or gas chromatography. In the present work, CO measurements are done using absorption spectroscopic techniques that rely on absorption of infrared (IR) radiation by CO molecules.

2.1.1 Surface measurements of ozone

Present work includes ozone measurements using two different online analyzers *viz*., Teledyne M400E and Thermo Model-49i. The response time for these analyzers is about 20 seconds and have minimum detection limit of about one ppbv (Table 2.1). The accuracy of these instruments is reported to be about 5% [*Kleinman et al*., 1994]. For this thesis work, ozone datasets at different temporal resolutions (5 minutes to 60 minutes) are stored and analyzed. Both the analyzers detect ozone through its absorption in UV wavelength (254 nm). The Schematic diagram of a Thermo ozone analyzer is shown in Figure 2.1. Air from the inlet is passed through a teflon filter to remove aerosol particles before entering the instrument where it is divided into two air streams. One of the air streams is sent directly to the absorption cell and the other one is passed through an ozone scrubber (MnO_2). These two air streams (represents air with and without ozone) reaching two different absorption cells alternatively are controlled by 3-way solenoid valves. The both air streams are exposed to UV radiation (254 nm) for 5-10 seconds through an UV lamp to produce measurement (I) and reference (I_0) signals.

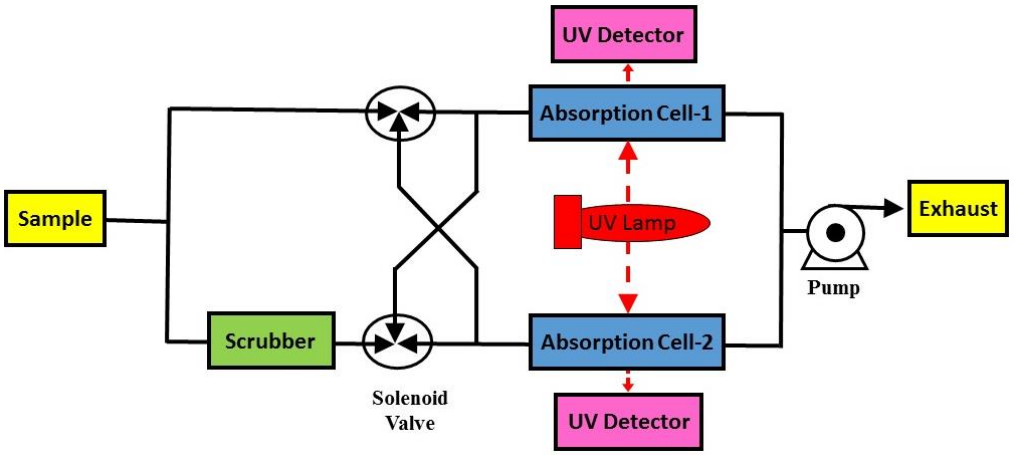

Figure 2.1: *Schematic diagram of a Thermo ozone instrument.*

The difference in intensities is caused by attenuation of UV light by ozone and its amount can be estimated using the following relation known as Beer-Lambert's Law:

$$I = I_0 \, e^{-\sigma \, n_{o3} \, L} \qquad \textbf{[2.1]}$$

Where I_0 is the attenuated UV light intensity due to air (excluding ozone - reference signal) and I is the attenuated UV light intensity due to air (including ozone - measurement signal) σ is the molecular absorption cross-section of ozone (cm^2), L is the effective length of the absorption cell (cm), and n_{o3} is the number density of ozone (number/cm^3).

Since we use mixing ratios to represent amount of ozone present in the troposphere so the relation 2.1 becomes,

$$I = I_0 \, e^{-Ko_3 \, Co_3 \, L} \qquad \textbf{[2.2]}$$

Where,

$Ko_3 = \sigma\, n_{air}$ is the molecular absorption coefficient for ozone at 254 nm (308 cm^{-1}),

n_{air} is the number density (concentration) of dry air (number/cm^3).

$C_{o3} = n_{o3} / n_{air}$ is the ozone mixing ratio in air.

The attenuation caused by other trace species including aerosols is compensated in the above relation because of its differential nature since I and I_0 both includes those contributions. Further to compensate for the variations in temperature and pressure inside absorption cell, instruments have the respective sensors which are used to apply necessary corrections. The UV lamp used in these analyzers is a low pressure, cold cathode mercury vapor lamp which provides 254 nm UV radiation. The attenuated signals are detected by a photodiode with built in interference filters centered at about 254 nm.

Table 2.1*: Intercomparision between Teledyne M400E and Thermo Model-49i ozone measurement instruments.*

	Thermo 49i	**Teledyne M400E**
LDL	1.0 ppbv	0.6 ppbv
Zero Drift	≤ 1 ppbv (24 hours)	≤ 1 ppbv (24 hours)
	≤ 2 ppbv (7 days)	≤ 1 ppbv (7 days)
Span Drift	< 1% per month	≤ 1% of FS (24 hours)
		≤ 1% of FS (7 days)
Response time	20 sec (10 sec lag time)	20 sec (10 sec lag time)
Linearity	±1% of Full Scale (FS)	< 1% of FS

Zero and span checks are done regularly using an internal ozonator and a zero air

generator (Thermo model 1160). In addition to the zero and span tests, ozone observations from both instruments are also inter-compared by running them side by side and using a common inlet and good positive correlations (r^2 = 0.99) were observed. Further details of such inter-comparisons from the two makers are reported in *Sarangi et al*. [2014].

2.1.2 Surface measurements of CO

Two instruments, Thermo Model-48i and Horiba APMA-370 were employed for the measurement of CO during this thesis work. Basic observation principle of these instruments is same (IR absorption by CO at 4.6 μm) nevertheless there are few methodological differences. In Thermo instrument, ambient air is drawn to the instrument where it is passed through optical bench and is subjected to radiation from an IR source which is chopped by a set of filter wheel rotated by a motor. The alternating rotating wheel having CO and N_2 produces a reference and measurement beams respectively whose differential amplitude is proportional to the CO concentration. Therefore, this setup is also called gas filter correlation (GFC) based method (Figure 2.2). The interferences from other gases are compensated since they absorb reference and measurement beams equally. The IR source is a wire wound resistor operating at high temperatures to create IR radiation (heat).

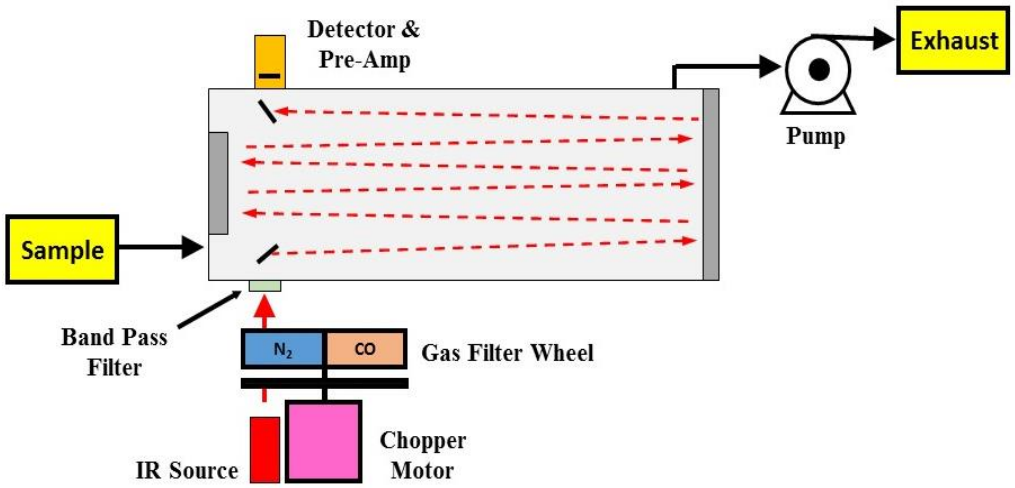

Figure 2.2 *Schematic diagram representing Thermo Model 48i CO instrument.*

The detection principle of Horiba APMA-370 analyzer is also based on IR absorption technique but it uses slightly different method. In this instrument a solenoid valve is used rather than a conventional optical chopper. The sample and reference beams are sent alternatively every second. The modulation signal would only be generated when there is a change in concentration of sample gas and thus no zero drift is observed in this instrument. The reference signal is generated by purging the sample through an oxidation process, where an oxidizing catalyst burns CO to CO_2. Other interfering components are present in both zero and sample gases. A single optical cell is used in cross flow modulation to remove (1) zero drift problems as the instrument is constantly zeroed and (2) problems associated with moving components in the optical bench that can cause optical misalignments due to vibrations. A schematic diagram representing a Horiba APMA-370 CO monitor is shown in Figure 2.3 and it consists of a light source (IR), a measurement cell, a detector assembly, an optical filter and a flow modulator.

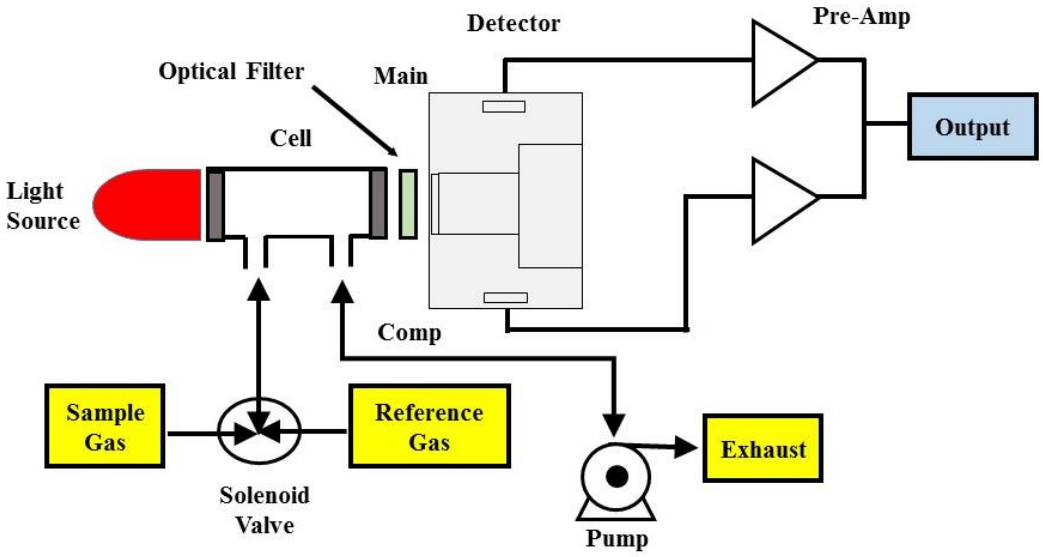

Figure 2.3: *Schematic diagram representing Horiba APMA-370 CO instrument.*

Regular zero check and span check for CO instruments are done using primary gas cylinders from Linde UK and secondary gases from Ultra-Pure Gases and Chemotron Science Laboratories. Multipoint calibrations are carried out in different observational ranges using a zero air generator (Thermo model 1160) and a dynamic gas calibrator (Thermo model 146i).

2.2 Balloon borne measurements of ozone and meteorological parameters

Vertical measurements of ozone and meteorological parameters such as air temperature, pressure, relative humidity, wind speed and wind direction are made using balloons carrying an ozonesonde (for ozone detection) and a radiosonde (having meteorological sensors, GPS and transmitter).

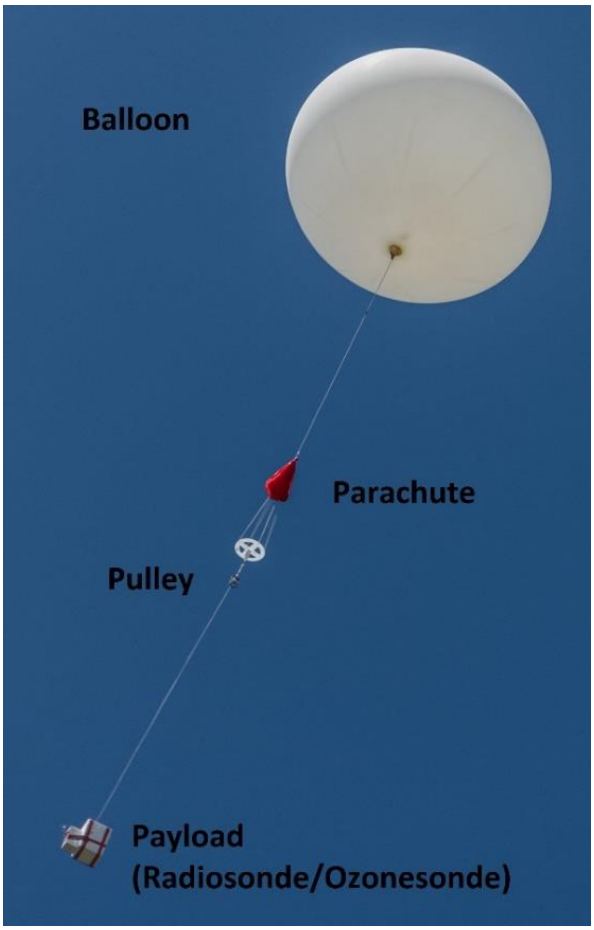

Figure 2.4: *Balloon with ozonesonde and radiosonde during the ascent from ARIES, Nainital.*

For the present work two different vertical datasets using balloon based measurements are used, viz., ARIES balloon borne measurements including ozone and meteorological data for a period of 5 years and meteorological data using radiosonde only during GVAX field campaign. Figure 2.4 shows balloon in flight carrying an ozonesonde and a radiosonde as payload.

2.2.1 ARIES balloon borne measurements

Ozonesondes have a long developmental history and regular measurements were

initiated during late 1960s. An ozonesonde is a compact and lightweight instrument that can measure ozone up to 30-35kms, with high resolution. There are three major types of ozonesondes which are used across the globe, (1) Brewer-Mast after *Brewer and Milford*, [1960], (2) electrochemical concentration cell (ECC) after *W. D. Komhyr* [1969] and carbon iodine cell (KC96) after *Kobayashi and Toyama*, [1966]. Each of the above have similar detection principle but different designs [*Smit et al.,* 2007] and during past few decades several inter-comparison studies have been done [*Attmannspacher and Dutch*, 1970; *Barnes et al*., 1985; *Kerr et al*., 1994; *Komhyr et al*., 1995; *Boyd et al*., 1998; *Smit et al*., 2007; *Deshler et al*., 2008]. ECC ozonesondes developed by *Komhyr* [1969] are most widely used and more than 80% of measurement stations (GAW/WMO) across the globe use it for ozone vertical profiling. ECC ozonesondes that is used in present work will be discussed in subsequent sections, however detailed principle and design of other types of ozonesondes can be seen elsewhere [e.g. *Brewer and Malford*, 1960; *Kobayashi and Toyama*, 1966; *Claude et al*., 1987; *Fujimoto et al*., 2004].

The balloon sounding setup consists of ground receiving unit, ozonesonde preparation setup, payload (including sensors) and balloon setup. The ground receiving unit consists of an antenna (including a pre-amp), modem, receiving unit and a computer. Ozonesonde preparation unit consists of an ozonizer/testing unit, chemicals (for preparation of sensing solutions), flow testing meter, pressure/vacuum gauge etc. Payload consists of a radiosonde and an ozonesonde (contained in a Styrofoam box). Balloon setup consists of a rubber balloon (1200 g), a parachute, helium/hydrogen filling setup, a pulley etc. Figure 2.5 shows the photographs of these units and Figure 2.6 shows an overview of the balloon

sounding setup.

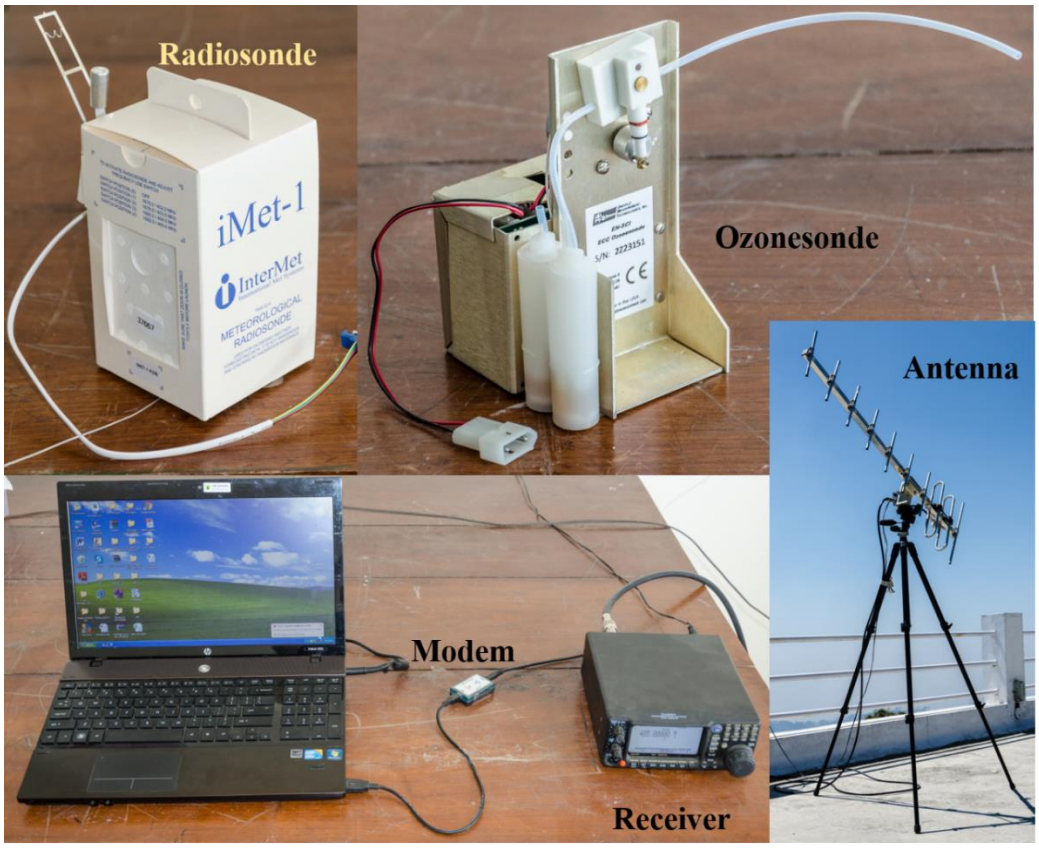

Figure 2.5: *Ozonesonde, radiosonde, antenna and receiver coupled with the laptop via MODEM as used during the observations.*

The rubber balloon is inflated with helium/hydrogen gas such that it can attain a constant ascent rate of about 5m/sec and can go up to 20-7 hPa (30-35 km) in altitude. The payload is attached to balloon via a parachute and a pulley to avoid free fall (after balloon bursts) and to avoid any jerks. Ozonesonde is attached to radiosonde via V7 interface electronics and radiosonde transmits the meteorological data (pressure, temperature and relative humidity sensors), location (GPS) and ozone data to the ground station. The transmitted signal is received at ground

through a yagi antenna mounted on a tripod (with built in pre-amp) coupled with a 403Mhz receiver and 1200 baud rate modem which is further processed by data acquisition software in a personal computer.

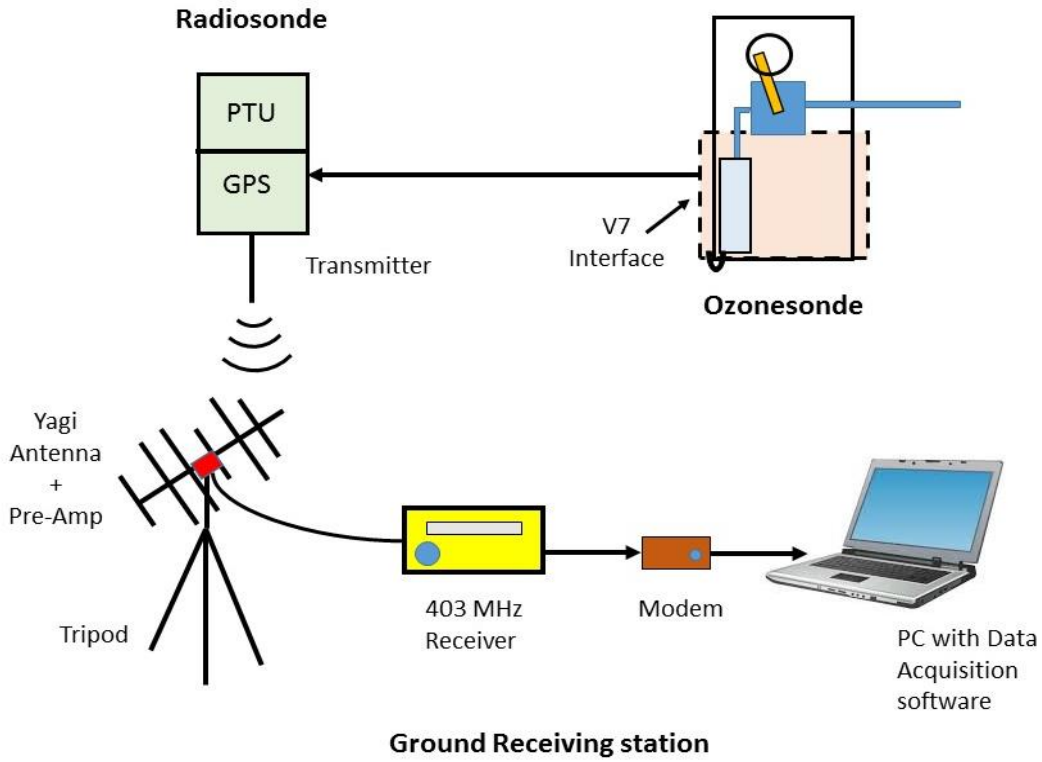

Figure 2.6: *Layout of the balloon sounding experiments showing the measurement, data transmission and receiving system.*

These balloon flights were conducted every Wednesday with some exceptions/extra flights done on other days. The duration of a complete flight, including ascent and descent is 2-3 hours. For this study only ascent data is used since descent data have considerable time lag between measurement and its data recording due to fasted descent rate.

2.2.1.1 Radiosonde

InterMet model iMet-1-RSB 403 MHz GPS, radiosondes were used for this study. It has sensors for temperature, relative humidity (RH), pressure and a GPS. The temperature and RH sensors are placed on a boom which is outside of the sonde. The temperature sensor is a small glass bead thermistor coated with aluminum to minimize the effects of solar and infrared heating. As the balloon ascends the changes in ambient temperature changes the resistance of the thermistor. RH detector is a variable capacitor which has a water sensitive dielectric polymer inside it. The amount of water vapor in atmosphere changes the permittivity of the dielectric material and thus capacitance, which is converted to RH reading. The pressure detector is placed inside radiosonde box; it is a silicon piezo-resistive sensor. Small variation in pressure causes the micro-mechanical changes inside the sensor which is converted to an electrical signal. The accuracies of pressure, temperature and humidity measurements are shown below in Table 2.2. This radiosonde also has a 12-channel GPS receiver and a 403 MHz data transmitter. The transmitter is a crystal-controlled oscillator that controls the opted channel frequency. It has a linearly polarized dipole antenna, which transmits FM modulated signal containing digital data for meteorological parameters (PTU) and GPS.

***Table 2.2**: Specifications of InterMet 403 MHz iMet-1 radiosonde's PTU sensors.*

	Pressure	**Temperature**	**Relative Humidity**
Range	2 to 1070 hPa	-95 to 95 ^{o}C	0 % to Saturation
Resolution	0.01 hPa	0.01 ^{o}C	0.1 %
Response time	1 sec	3.6 sec (1013 hPa, -80 to 40 ^{o}C)	2 sec (1013 hPa, +25 ^{o}C) 60 sec (1013hPa, -35 ^{o}C)
Accuracy	± 1.8 hPa (>400 hPa) ± 0.5 hPa (<400 hPa)	± 0.3 ^{o}C (-80 to +40 ^{o}C)	± 5 % (-60 to +50 ^{o}C) ± 2% change near saturation

The radiosonde is coupled to an ozonesonde via a V7 electronic interface. The inbuilt GPS is used to track the position of the sensors and to calculate wind speed and wind direction. The weight of radiosonde with battery is about 260 g.

2.2.1.2 Ozonesonde

Ozone detection principle of an ECC ozonesonde (EN-SCI model 2ZV7) [*Komhyr et al*., 1969; *Komhyr et al*., 1995] is based on the titration of ozone molecules in potassium iodide (KI) solution. An ECC ozonesonde consists of a pump, two teflon half cells which have platinum meshes as electrodes and are connected via ion bridge to a V7 electronic interface. KI solutions at different concentrations are used as electrolyte solutions. The presence of different KI concentrations in the cathode (0.5% KI) and anode (Saturated with KI) chambers causes a spontaneous internal cell emf of approximately 0.13 V at 25^{o}C. When air containing ozone is bubbled via inert teflon tubes into cathode cell, it reacts with KI to give iodine molecule,

$$2KI + O_3 + H_2O \rightarrow 2KOH + O_2 + I_2 \qquad \textbf{[2.5]}$$

This iodine molecule makes contact with the platinum electrode where it is reduced back to iodide ions by uptake of 2 electrons,

$$I_2 + 2e \text{ (Cathode)} \rightarrow 2I^- \qquad \textbf{[2.6]}$$

thereby generating a current (I_m) in the external circuit. This current when corrected for background value (I_b) is directly proportional to the uptake of ozone in the cathode cell (or amount of I_2). By knowing the flow rate of air sampling pump (t) which is time (seconds) taken by sonde pump to force 100 ml of air through the sensor, pump temperature (T_p) and conversion efficiency (η_c) of ozone sensor, ozone partial pressure (P_{O3}) can be deduced using the following relation,

$$P_{O3} = 4.307 \times 10^{-3} * T_p * (I_m - I_b) / \eta_c * t \quad \text{(mb)} \qquad \textbf{[2.7]}$$

where the constant 4.307×10^{-3} is the ratio of gas constant to faraday's constant and above relation is valid if no ozone is destroyed in the air sampling system. This relation can be further converted to obtain mixing ratio of ozone,

$$C_{O3} = P_{O3} * 1000/P = 4.307 * T_p * (I_m - I_b) / \eta_c * t * P \quad \text{(ppbv)} \qquad \textbf{[2.8]}$$

Where, P is the ambient pressure at measurement altitude. The conversion efficiency (η_c) of the ozone sensor is equal to 1 at neutral pH. To attain neutral pH, sodium hydrogen phosphate (Na_2HPO_3) is added as a buffer with potassium bromide (KBr) as a stabilizer that controls the conversion of O_3 to I_2. This method is preferred for balloon flights due to its faster response time (1-2 seconds) and compact design. Table 2.3 and 2.4 below provides the general and performance specifications of an ECC ozonesonde.

***Table 2.3**: General specifications for an ECC ozonesonde.*

Operating Pressure	1050 – 4 hPa
Operating Temperature	0 – 40 ^{o}C Inside flight box Ambient temperatures to -90 ^{o}C
Power requirements	12-18 VDC, 120 mA
Weight	480g - including battery (240g for flight box)

***Table 2.4**: Performance specifications of an ECC ozonesonde.*

Pressure (hPa)	1000	200	100	10	4
Accuracy (%)	±5	± 12	±5	±5	±10
Precision (%)	±4	±12	±3	±3	±10
Resolution (km)	0.3	0.3	0.3	0.4	0.4

As the balloon ascends and it reaches higher altitude the pump efficiency decreases that draws the ambient air for ozone observation. This decrease in pump efficiency can be corrected by multiplying appropriate pump correction factor (P.C.F) which is a function of ambient atmospheric pressure. The Table 2.5 below provides the pump correction factor for various altitudes. In general, it is smaller than 1% up to first 20 kms and is ~2-3% up to 30 kms [*Komhyr et al.,* 1985, 1986, *Torres,* 1981].

***Table 2.5**: Pump efficiency (η_c) of an ECC ozonesonde.*

Pressure (hPa)	Pump Correction Factor
1000-200	1
150-70	1.01
50	1.02
30	1.03
20	1.04
15	1.05
10	1.07
7	1.08
5	1.13

2.2.1.3 Preparation of the ozonesonde

The ozonesonde is tested prior to launch, once 3-7 days before launch and then on the flight day. The main objective for advance preparation is to check the overall performance of the instrument, to charge it with the sensing solutions and to attain low sensor background current. This preparation should be done in clean and controlled environment. The main steps performed during advance preparation are shown as a flow chart (Figure 2.7).

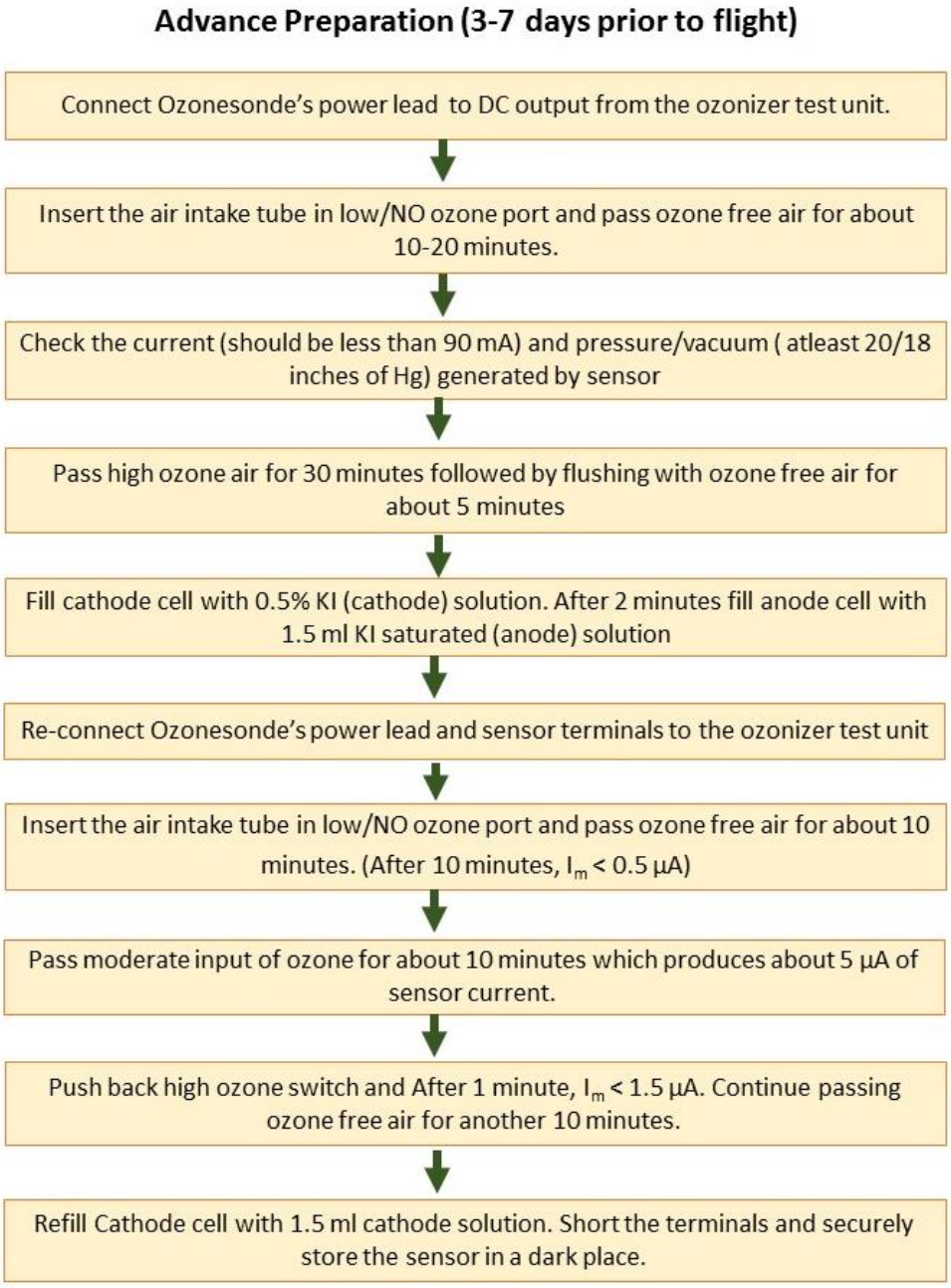

Figure 2.7: *The flow-chart explains the advance preparation method for an ozonesonde.*

If the sensor draws more than 90 mA of current or is developing less pressure or vacuum, then some preventive measures have to be taken which includes rubbing of pump piston to decrease the friction inside and addition of few ml of acetone into

the pump inlet. If the performance is still not improved, then sensor is discarded. Once all the steps shown in Figure 2.7 are performed the sonde sensor leads are shorted by a shorting plug or ordinary copper wire and is kept securely in the dark and clean environment till flight day. On the day of flight, the sonde is again checked for its performance (following the steps given in Figure 2.8). The response time of any sensor is defined as,

$$R = 100 \times (i_{t = 0\ min} - i_{t=1\ min})/i_{t = 0\ min} \geq 80\% \quad \textbf{[2.9]}$$

If this is greater than 80% then the sensor can be used for the flight.

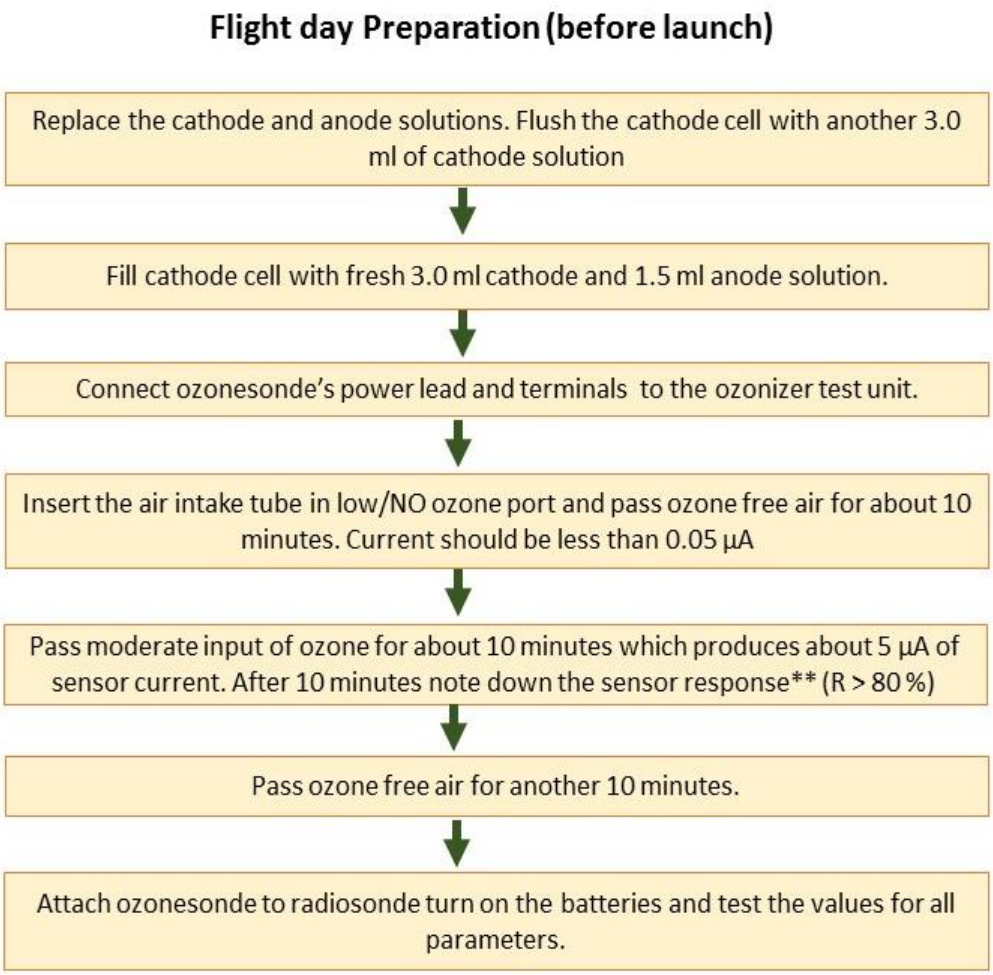

Figure 2.8: *The flight day preparation method for an ozonesonde.*

Once all these tests are done ozonesonde and radiosonde are packed together as a payload, and is tied with balloon, parachute and reel-pulley (as shown in the Figure 2.4) and launched. The data acquisition software on the PC collects the raw data and is stored for further processing using PV7 software (provided by Droplet measurement technologies) and then is used for further analysis.

2.2.2 Balloon-borne sounding system – RAWEX-GVAX campaign

Apart from weekly balloon soundings (including an ozonesonde and a radiosonde) from ARIES radiosonde observations were also made during GVAX-RAWEX field campaign for about 10 months. This campaign was jointly conducted by United States of America's Department of Energy and ARIES, ISRO and IISc. During this campaign weather balloons were launched four times (0000, 0600, 1200 and 1800 GMT or 0530, 1130, 1730, and 2330 IST) every day which led to a total of 1069 flights during June 2011-March 2012. The balloon-borne sounding system of Atmospheric Radiation Measurement (ARM) Mobile Facility - 1 (AMF-1) is a Vaisala DigiCORA III sounding system (shown in Figure 2.9) that comprises Vaisala RS92-SGP radiosonde, Vaisala GC25 ground check set, GPS omnidirectional antenna and UHF antenna.

Figure 2.9: *The above figure depicts the experimental setup of balloon borne sounding system which comprises of Vaisala DigiCORA III sounding system during GVAX campaign.*

The RS92-SGP radiosonde has sensors for measurements of pressure, temperature and relative humidity. The humidity sensor (H-HUMICAP) is a thin film capacitor, and its capacitance between electrodes (dielectric medium) is sensitive to amount of water vapor present in atmosphere. The temperature sensor (F-THERMOCAP) consists of two platinum wires separated by a glass–ceramic dielectric, whose permittivity is a strong function of temperature. The pressure sensor (BAROCAP) is a micromechanical sensor that is based on changes in dimensions of silicon membrane. When pressure is applied, the silicon membrane bends and the vacuum gap between electrodes changes, thus changing the capacitance, which is converted to get pressure. The specifications of pressure temperature and RH sensors are given in Table 2.6.

***Table 2.6**: Specifications of Vaisala RS-92SGP radiosonde's PTU sensors.*

	Pressure	**Temperature**	**Relative Humidity**
Range	3 to 1080 hPa	-90 to + 60 ^{o}C	0 % to Saturation
Resolution	0.1 hPa	0.1 ^{o}C	1 %
Response time	< 0.4s (1000 hPa) < 1s (100 hPa) < 2.5s (10 hPa)	< 0.5s (1000 hPa, +20 ^{o}C) < 20s (1000 hPa, -40 ^{o}C)	
Accuracy	± 1 hPa (1080-100 hPa) ± 0.6 hPa (100-3 hPa)	± 0.5 ^{o}C (Full range$^{\$}$)	± 5 % (Full range$^{\$}$) ± 2 % change near saturation

$^{\$}$*within 2-sigma confidence level and this includes repeatability, long term stability, effects due to measurement conditions, effects due to measurement electronics with temperature > -60 ^{o}C for RH and < 35 ^{o}C for pressure.*

Radiosonde also includes a GPS unit which is used to calculate wind speed and wind direction during the flight. Rubber balloon (350 gm) from Totex is used and filled with Helium gas for ~15 minutes at 15 psi pressure in a specially designed hub. The ascent rate of balloons is about 5 m/s and generally balloon burst altitude is around 20-25 km. Duration of complete flight (ascent only) is 1-1.5 hours. These balloons with radiosonde were launched four times in a day and some variability in the launch time was mainly due to constraints of flight permissions from the Air Traffic/Navigation Controllers of this region (Pantnagar and Bareilly). More details on this are provided in chapters 5 and 6.

2.3 Satellite Data

In-situ observations, surface as well as balloon borne provide information on smaller scales, therefore to study over a greater region, space borne sensors are used. The majority of satellites used in atmospheric measurements are flying at low altitude (about 700 km) polar orbits which have orbital period of about 90-100 min and they provide complete global coverage in 2-3 days. Here in this thesis, we use the space-borne observations from five sensors namely Moderate Resolution Imaging Spectroradiometer, Advanced Along Track Scanning Radiometer, Tropical Rainfall Measuring Mission, Ozone Monitoring Instrument, and Atmospheric Infra-Red Sounder. These sensors basically measure the Earth's upwelling radiance and then desired parameters are retrieved. The radiances are calibrated using the information about the geophysical fields and satellite viewing geometry. The calibrated radiances are processed using a set of robust algorithms to retrieve the information about the trace gases and meteorological parameters. The geographical coverage of the satellites depends upon the orbit and the orientation of the instrument with respect to the orbital plane.

2.3.1 Moderate Resolution Imaging Spectroradiometer (MODIS)

Fire Counts: MODIS instrument onboard Terra and Aqua (EOS satellites) retrieved active fire locations are used to study spatio-temporal variations in the biomass burning activity. MODIS collection 5, Level 2 (combined Aqua and Terra) global monthly fire product mcd14ml at 1 km resolution, provides information about the geographic location of fire and its intensity [*Giglio,*2010]. The MODIS fire detection algorithm uses the strong mid-infrared (IR) emissions from the fires

[*Dozier,* 1981; *Matson and Dozier,* 1981] and is based on the brightness temperatures derived from MODIS at 4 and 11 µm channels. The channels at 12 µm, 0.65 µm, 0.86 µm and 2.1 µm are used to eliminate false detections due to cloud masking, sun glint and other bright surfaces and the target pixels are classified into one of the following classes: missing data, cloud, water, non-fire, fire and unknown. Level 2 fire products allows to bin fire counts spatially and temporally; however, they might contain some biases as it does not provide any information on cloud cover and missing data [*Giglio,*2010]. The retrieval algorithm classifies fire pixels in three categories; low confidence (0-30 %), nominal confidence (30-80 %) and high confidence (> 80 %). This confidence limit allows rejection of false fires. The detailed description of the principle can be found in *Giglio et al.* [2003] and *Justice et al.,* [2006].

Fire Radiative Power (FRP): MODIS-retrieved fire location data also include "Fire Radiative Power (FRP)", which is related to the rate at which fuel is being consumed and provides information on measured radiant heat output of fires. The FRP (MW) is calculated by an empirical relation [*Kaufman et al.,* 1998] and is defined in equation (2.10):

$$\mathrm{FRP} = (4.34 \times 10^{-19}\mathrm{MWK^{-8}km^{-2}})(\mathrm{T_4^8} - \mathrm{T_4'^8})\mathrm{Apix} \qquad \textbf{[2.10]}$$

Where $T_4$is the 4 µm brightness temperature, T_4' is the mean 4 µm brightness temperature of the non-fire background, and $Apix$ is the total pixel area (km^2). More information on data products can be obtained from MODIS collection 5 active fire product user's guide version 2.4 [*Giglio,*2010].

Aerosol Optical Depth (AOD): MODIS collection 5 level 3 daily aerosol data MOD_08_D3 at 1 x 1 deg horizontal resolution are used to study fire induced changes in the aerosol burden. The algorithm calculates the column aerosol loading at 0.55 μm over the surfaces that appear "dark" (have lower reflectance values in visible and short wave infra-red region of the electromagnetic spectrum) and provide contrast relative to brighter aerosols [*Levy et al.,* 2007]. The algorithm uses three wavelength channels in shortwave-infrared (SWIR) region namely 0.47 and 0.65 μm in the visible and 2.12 μm in the IR region along with a few other wavelength bands to mask out clouds, deserts, and snow-ice surfaces. The pixels are first screened for clouds, snow-ice and inland water bodies via NDVI tests. The remaining pixels are tested for their brightness (2.12 μm). The brightest 50% and the darkest 20% pixels are removed and reflectance in remaining pixels is used to determine the AOD. Further details of the retrieval algorithm can be found in *Levy et al.,* [2007] and MODIS algorithm theoretical basis document [*Justice et al.,* 2006].

2.3.2 Advanced Along Track Scanning Radiometer (AATSR)

Global fire maps provided by the European Space Agency's (ESA) AATSR onboard ESA satellite were also compared with MODIS fire location retrievals to obtain consensus between the two products. Such a comparison is essential because some of the previous studies have used AATSR fire retrievals [e.g., *Ghude et al. 2013*] to study variations in fire activity over South Asia while others have used MODIS fire retrievals (e.g. *Kumar et al.,* [2011]). The AATSR retrievals are based on detection of the surface radiances in 4 bands (1.6, 3.7, 11.0 and 12.0 μm). The radiance at 3.7 μm during the night time is used to detect hotspot if its brightness

temperature exceeds 312 K (algorithm-1). The algorithm is limited by cloud presence, atmospheric effects etc. and underestimates hotspot number but its nighttime detection enables no contamination in signal due to sun (false fire signal). Further details of AATSR algorithm can be seen elsewhere [*Arino et al.*, 2011].

2.3.3 Tropical Rainfall Measuring Mission (TRMM)

The TRMM based 3B42 version 7.0 (TRMM 3B42v7), 3 hourly rainfall product is used to examine link between the fire activity and rainfall over the study region. The algorithm is based on combined and rescaled microwave (9 channel Visible and Infrared Scanner) and IR (5-channel visible/IR radiometer) estimates of rainfall to give merged high quality IR precipitation and root mean square (rms) precipitation error estimates at a spatial resolution of $0.25^{o} \times 0.25^{o}$between 50^{o}N and 50^{o}S latitudes [*Huffman et al.*, 2007]. The 3B42 data products are used to calculate daily and monthly total rainfall over the study region.

2.3.4 Ozone Monitoring Instrument (OMI)

OMI onboard NASA's EOS Aura satellite is a nadir-viewing imaging spectrometer, that measures various gases such as ozone, NO_2 and aerosol properties etc. with daily global coverage (http://aura.gsfc.nasa.gov/instruments/omi.html).

Tropospheric column NO_2: The OMI level-3 daily tropospheric column amount NO_2 data product OMNO2d (cloud screened at 30%) at 0.25 x0.25 deg resolution is used in this study. This product is based on the measurements made by OMI in visible (VIS, 405-465nm) channels. The slant column amount NO_2 is calculated

from measured Earth's radiance and solar irradiance using differential absorption spectroscopy (DOAS) algorithm together with NO_2 cross-section measured at 220K. These are then corrected for cross-track biases of satellite and is related to vertical column density by the following relation,

$$S = \sum_i Si \approx \sum_i Ai\, Vi \qquad \textbf{[2.11]}$$

Where V_i is the vertical column NO_2 for each atmospheric layer and A_i is the differential Air-Mass Factor for corresponding layer. The A_i are calculated from the scattering weight and monthly mean climatologies of NO_2 vertical profiles (GMI-CTM simulations), further A_{trop} and A_{strat} (tropospheric and stratospheric Air Mass Factors) are separated using GOES-5 monthly tropopause pressures. Vertical tropospheric NO_2 column densities are calculated using the equation (2.12),

$$\text{Vtrop} = \frac{\text{S} - A_{strat} * V_{strat}}{A_{trop}} \qquad \textbf{[2.12]}$$

The global gridded tropospheric column NO_2 are then produced by screening above data for solar zenith angle, highly reflective and cloudy pixels and then calculating weighted average of remaining data. For detailed description of measurement principle refer *Bucsela et al.,* [2013].

Aerosol Index (AI): The aerosol index provides information about the type of aerosols (Torres et al. 1998). The coarser aerosols/clouds generally do not absorb UV radiation, while fine aerosols absorb ultra-violet (UV) radiation. We use OMI level-3 daily OMAEROe dataset at 0.25 x 0.25 deg resolution. The UV AI, AI_{388} is defined as:

$$AI_{388} = -100\, log\, \{[\frac{I_{\lambda 342.5}}{I_{\lambda 388}}]_{\text{meas}}\} + 100\, log\, \{[\frac{I_{\lambda 342.5\,(ALER)}}{I_{\lambda 388\,(ALER)}}]_{\text{calc}}\} \qquad \textbf{[2.13]}$$

Where $(I_{\lambda 342.5} \& I_{\lambda 388})_{meas}$ are measured radiances at 342.5 and 388 nm respectively, and $(I_{\lambda 342.5} \& I_{\lambda 388})_{calc}$ are calculated radiances at these wavelengths, A_{LER} is wavelength dependent lambert equivalent reflectivity. For further details, refer *Torres et al.,* [2002b].

2.3.5 Atmospheric Infrared Sounder (AIRS)

Atmospheric Infrared Sounder (AIRS) instrument onboard Aqua satellite is a part of NASA's EOS mission. AIRS was the first instrument that measured vertical profiles of temperature and water vapour in the atmosphere, further it also measures few trace gases and clouds. AIRS retrieval procedure uses the Earth's upwelling infrared radiance through the atmosphere. These infrared wavelengths are dispersed into several detectors that are sensitive to temperature and water vapor over a range of heights in the atmosphere. AIRS in total have 2378 detectors which greatly improves accuracy over last generation instruments. Here, AIRS level-3 daily standard physical retrieval datasets viz., CO volume mixing ratio profile, water vapour and relative humidity profile, tropopause pressure, height and temperature at $1^o x 1^o$ resolution (AIRX3STD v006, http://disc.sci.gsfc.nasa.gov/datacollection/AIRX3STD_V006.html) are used.

CO profile: AIRS CO retrieval exploits the cloud cleared radiances of CO in its 1st fundamental Vibrational-Rotational band (4.50-4.58 μm). The retrieval further uses an a priori profile based on monthly climatologies for both the Hemispheres that blend smoothly across the tropics. The maximum sensitivity of CO detection is at 500 hPa and algorithm is based on optimal estimation. The CO data profile has 24 levels between 1000-1 hPa.

2.4 Emission inventories

To examine uncertainties and variations in the current biomass burning emissions for South Asia, this study uses biomass burning emissions estimates of CO, NO_x and BC from two emission inventories: Global Fire Emission Database version3.1 (GFEDv3.1; 2003-2010) and MACC Global Fire Assimilation System, version 1.0 (GFASv1.0; 2003-2013). The GFEDv3.1 has a spatial resolution of $0.5^o \times 0.5^o$ and a temporal resolution of one month, whereas GFASv1.0 emissions have at $0.5^o \times 0.5^o$ spatial resolution and are provided daily.

2.4.1 GFED:

GFEDv3.1uses the classical bottom-top approach to calculate emissions using the following relation given by *Seiler and Crutzen* [1980];

$$M = A \times F \times E \qquad \textbf{[2.14]}$$

where M = quantity of matter burnt (kg); A = area burned (m^2); F = Fuel (matter) load or density (kg/m^2); and E = fractional burn efficiency or combustion completeness. The fuel loads and combustion completeness are derived using a biogeochemical model (CASA-Global Fire Emissions Database) and MODIS/Advanced Very High Resolution Radiometer (AVHRR) derived vegetation productivity and types every month. MODIS/TRMM-VIRS/Along-Track Scanning Radiometer (ATSR) derived burnt area are combined to estimate fire emissions at monthly temporal resolution from 1997-2010. The contribution from agricultural waste burning might have lower values in this inventory due to underestimation of burnt area by these fires [*van der Werf et al.,* 2010].

2.4.2 GFAS:

GFASv1.0 dataset is based on a top-down approach, which assimilates fire radiative power retrievals from MODIS (both Terra and Aqua) [*Kaiser et al.,* 2012]. The algorithm fills the observation gaps due to cloud cover and filter out the spurious signals from volcanoes, gas flares and industrial activities. The combustion rate is calculated with land cover-specific conversion factors. The updated emission factors for gases and aerosols are used to calculate daily global emissions from 2003 to the present. Details of the GFAS algorithm are described by *Kaiser et al.,* [2012].

2.5 Models used for this study

Atmospheric models have been developed to study the physical, chemical and biological processes in the global environment and to support the emissions-mitigation control policies. In fact, the models provide the only method to predict and evaluate the possible impacts of proposed emission reduction strategies. The trace gases present in atmosphere exhibit a large degree of spatial and temporal variability and the systematic and long-term measurements of these species is often difficult and expensive task to follow. In this regard, model also play an important role in providing some of the missing information, particularity over the least studied and inaccessible regions. The models also play a vital role in interpreting the field observations and identifying the key variables and processes. Depending upon the complexity, spatial dimensions and the computational requirements, there exists a variety of atmospheric models (Figure 2.10).

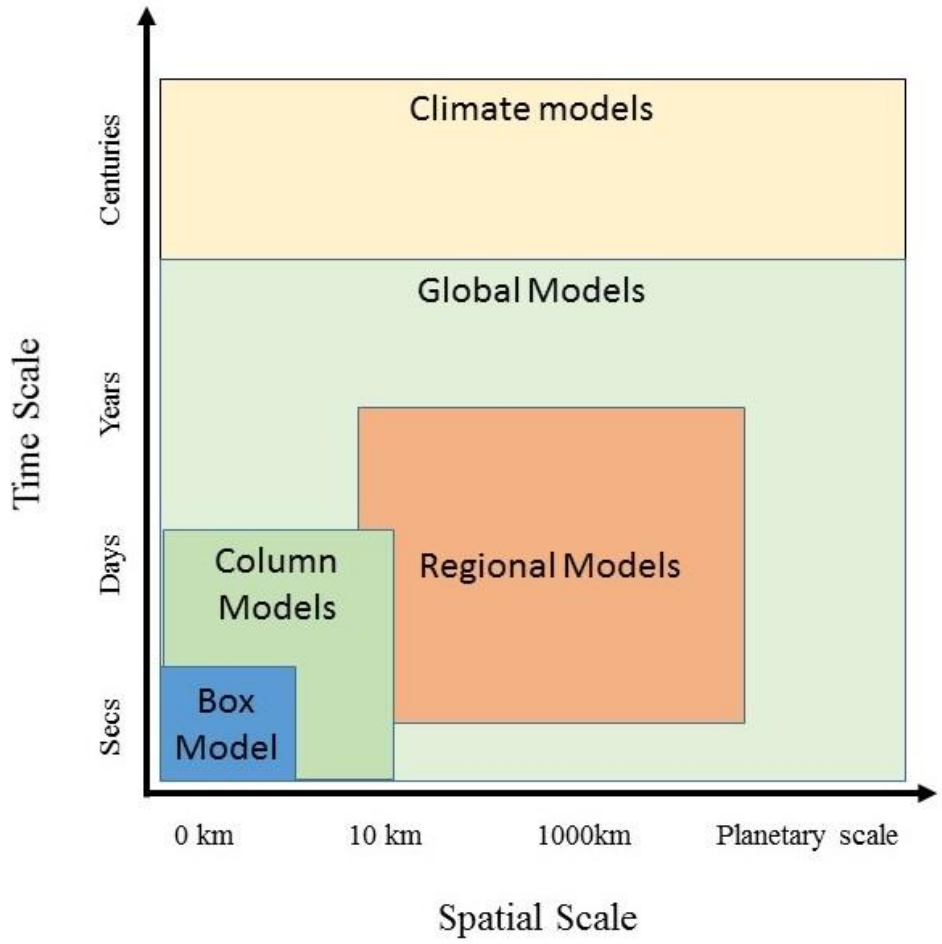

Figure 2.10: *Classification of different models based on their temporal and spatial scales.*

Generally, box models (zero-dimensional models) are used to study the detailed chemistry, meteorology or dynamics at a particular location or to follow an air parcel along its trajectory in the atmosphere but they do not have exchanges between the chemistry and transport [e.g. *Madronich,* 2006]. The column models (one-dimensional models) are used to study the vertical distribution, by treating atmosphere as a single vertical column and neglecting spatial variations [e.g. *Kasting and Singh,* 1986]. The three-dimensional models provide the most realistic representation of the Earth's atmosphere that includes exchanges along longitude, latitude and altitude [e.g. *Grell et al.,* 2005], however, these models can be

computationally expensive. The three dimensional models are further classified as global models (e.g., MOZART, MATCH etc.) and regional models (e.g., WRF-Chem, CMAQ, MM5), with the later having higher resolution and main focus on regional scale processes.

A model in general is a mathematical representation of physical laws that governs the Universe. They provide information on the evolution of atmospheric variables when sufficient boundary conditions are provided. Vilhelm Bjerknes in 1904 for the first time used a set of equations that governs the evolution of atmosphere. These equations include Newton's second law of motion (conservation of momentum), the continuity equation (conservation of mass), first law of thermodynamics (conservation of energy), ideal gas equation and conservation equation for water vapor.

$$\frac{d\vartheta}{dt} = -\frac{1}{\rho}\nabla p - \nabla\phi - 2\Omega \mathrm{x}\vartheta + F \qquad [\mathbf{2.15}]$$

$$\frac{\partial\rho}{\partial t} = -\nabla \cdot (\rho\vartheta) \qquad [\mathbf{2.16}]$$

$$\frac{dQ}{dt} = C_v \frac{dT}{dt} - \frac{1}{\rho}\frac{dp}{dt} \qquad [\mathbf{2.17}]$$

$$p = \rho RT \qquad [\mathbf{2.18}]$$

where, ϑ = (u,v,w), speeds along the three directions, p is the hydrostatic pressure, ρ is the volume, ϕ is the geopotential (effective gravity), Ω is the angular speed, F is friction term, T is temperature, Q is heat exchanged, C_v is the specific heat at constant volume, R is gas constant for dry air. In these equations temperature is replaced by potential temperature, which is defined as temperature acquired by a parcel if it is adiabatically brought from a pressure level p to a standard reference pressure (1000 hPa),

$$\theta = T\left(\frac{1000}{p(hPa)}\right)^{0.286} \qquad [\mathbf{2.19}]$$

These equations are then discretized to be solved numerically and with proper boundary conditions one can determine concentration of various species and determine meteorological variables. However, the major problem with these equations is their chaotic nature, due to which it is impossible to solve them exactly and small errors grows quickly with time. Even with the perfect input data and perfect model the present understanding limits the maximum time for accurate forecasts to be about 14 days. In this thesis two different types of models are used, a regional chemistry transport model (WRF-Chem) and a Lagrangian particle dispersion model (HYSPLIT).

2.5.1 Weather Research and Forecasting with Chemistry (WRF-Chem)

The Weather Research and Forecasting model also known as WRF [*Grell et al.,* 2005] is a fully compressible and non-hydrostatic model that can be coupled with Chemistry. This model is developed jointly by NOAA, NCAR, DOE/PNNL and other research institutes. The model contains several dynamical cores and allows the user to select among a number of different physical parameterizations to represent the processes that cannot be resolved by the model. The model is capable of simulating the spatial and temporal distribution of trace gases and aerosols simultaneously with meteorology and they use same transport scheme, same horizontal and vertical grids, same time steps and the same physics schemes for subgrid-scale transport [*Grell et al.,* 2005]. The online nature of the WRF-Chem model also allows for feedbacks between chemistry and meteorology. The major components of WRF-Chem modeling system are represented in Figure 2.11 and it includes (1) WRF Preprocessing System, (2) real data initialization and (3) the

WRF solver (ARW or NMM) including the chemistry. These components are described in the upcoming subsections.

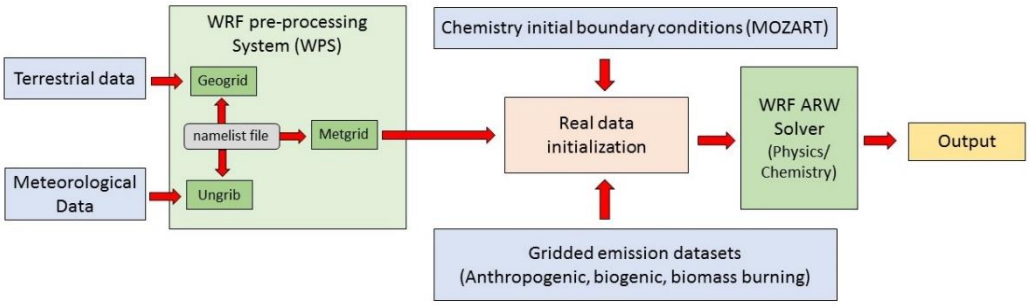

Figure 2.11: *Schematic representation of major components of the WRF-Chem Modeling System specific to this study. The light blue boxes represent the input datasets to the model and remaining boxes represent major components of the modeling system (Compiled from WRF user manual)*

2.5.1.1 The WRF Pre-processing System (WPS)

The WRF Preprocessing System (WPS) comprises of three components (Figure-2.11) whose collective role is to prepare the input data for the real data initialization program. These three components are called geogrid, ungrib and metgrid respectively and all of these uses a common input namelist file which specifies the type of solver (ARW or NMM), time period of simulation, location of model domain(s), resolution for input met data, type of projection, input and output file paths and format etc. The geogrid interpolates the static geographical data to the simulation domain(s); ungrib extracts meteorological data from the gridded binary (GRIB) formatted data files; and metgrid program combines the outputs of the geogrid and ungrib programs and horizontally interpolates the meteorological data

to the simulation domain. The vertical interpolation of meteorological fields to WRF eta levels is done by the "real" program.

For this study, WRF-Chem version 3.5.1 is used to simulate vertical distribution of ozone and meteorological parameters over Nainital region at 45 and 15 km resolution during 2011-2012. The model setup is centered at 27^{o}N, 83^{o}E, had 76, 130 grid points along east-west and 80, 94 grid points along north-south directions at 45 and 15 km resolution respectively. More details about this can be seen in chapter 6 and *Kumar et al.*, [2012a, b]. WRF-Chem version 3.6.1 is used to simulate distribution of surface ozone, CO and meteorological parameters at 9, 3 and 1 km spatial resolution over Kathmandu region during 2013.

In this setup simulation domain is defined on Mercator projection centered at 27.69^{o}N, 85.37^{o}E (Bode) with 320, 166, 232 grid points in east-west and 200, 133, 190 grid points in north-south at 9, 3 and 1 km resolution respectively. The setup had 57 vertical eta levels from the surface to 10 hPa and uses two different input terrestrial datasets viz., United States Geological Survey (USGS) and MODIS data set at different resolutions. The model is driven by input from two different meteorological data sets viz., National Center for Environmental Prediction's Final (FNL) meteorological reanalysis fields (http://rda.ucar.edu/datasets/ds083.2/) and European Center for Medium-Range Weather Forecast's (ECMWF) atmospheric operational model analyses and products derived from short-term forecasts (http://rda.ucar.edu/datasets/ds113.0/).

2.5.1.2 Input emission datasets

Anthropogenic emissions of CO, SO_2, NOx, non-methane volatile organic compound, PM10, PM2.5, and black carbon and organic carbon are taken from Emission Database for Global Atmospheric Research - Hemispheric Transport of Air Pollution (EDGAR-HTAP) v2 (http://edgar.jrc.ec.europa.eu/htap_v2/index.php?SECURE=123), which provides monthly and annual gridded emissions at 0.1^o deg. resolution based on year 2010. Fire emissions were provided to the model using the Fire Inventory from NCAR version 1 (FINNv1) [*Wiedinmyer et al.,* 2011], and biogenic emissions of trace species are calculated online using the Model of Emissions of Gases and Aerosols from Nature (MEGAN) [*Guenther et al.,* 2006]. Fire emissions are distributed vertically in the model following a plume-rise parameterization [*Freitas et al.,* 2007]. Spatially and temporally (6 hourly) varying chemical boundary conditions were provided by global model simulations from the Model for Ozone and related Chemical Tracers (MOZART-4) [*Emmons et al.,* 2010].

2.5.1.3 Model physics

The WRF-Chem model uses different physics options for microphysics, cumulus parameterization, planetary boundary layer parameterization, land-surface model and radiation. The two different types of schemes are used to explicitly resolve water vapor, clouds and precipitation processes. The single moment schemes predict only the number concentrations while double moment schemes predict not only the number concentration but also the mixing ratios of cloud, ice, snow, graupel and hail. The later one allows for a more robust treatment of the particle size distributions, which are very important for calculating the microphysical

process rates. Therefore, the double moment microphysical parameterization described by *Thompson et al*., [2004] has been used for the present study. The Kain-Fritsch cumulus parameterization scheme that utilizes a simple cloud model with moist updrafts and downdrafts including the effects of entrainment and relatively simple microphysics [*Kain,* 2004] has been used in the present study. The radiation scheme provides earth's radiation budget and it includes atmospheric heating due to various fluxes. The solar insolation (short-wave radiation) and terrestrial radiation (long-wave) radiation undergoes absorption, reflection and scattering in the atmosphere and at the surface. In the present model configuration, the rapid radiative transfer model (RRTM) [*Mlawer et al*., 1997] is used to simulate long-wave and short-wave radiation. The Noah land-surface model, developed jointly by NCAR and NCEP, has been used in the model set-up for this study. The Planetary boundary layer (PBL) scheme determine the flux profiles within the well-mixed boundary layer and the stable layer and thus provide atmospheric tendencies of temperature, moisture (including clouds) and horizontal momentum in the entire atmospheric column. Here, Yonsei University (YSU) scheme is used for the parameterization of the turbulence in the PBL and free atmosphere [*Hong, Noh and Dudhia*, 2006].

All of the processes indicated above are governed by various physical laws including Beer-Lambert's law, Stefan-Boltzmann law, Wien's displacement law, laws of thermodynamics, Clausius-Clapeyron equation etc. The Beer-Lambert's law is already discussed in section 2.2. Stefan-Boltzmann law describes the power radiated from a black body is directly proportional to the fourth power of its temperature. Wien's law states that the peak emission wavelength in the spectra

from an object is inversely proportional to its temperature. First law of thermodynamics is essentially, the principle of conservation of energy which states that the amount of heat energy supplied to a system (removed) is partly used in raising (decreasing) its internal energy and remaining is used in work done by (on) the system. The Clausius-Clapeyron equation is the application of laws of thermodynamics that allows us to estimate the vapor pressure of any fluid at another temperature, if the enthalpy of vaporization and vapor pressure is known at some temperature.

2.5.1.4 Model chemistry

The model uses MOZCART scheme which is based on Model for Ozone and Related Chemical Tracers version 4 (MOZART-4) gas phase chemistry [Emmons et al., 2010] linked to the Goddard Chemistry Aerosol Radiation and Transport (GOCART) aerosol scheme [*Chin et al.,* 2000]. The MOZART-4 chemistry mechanism includes 85 different gas-phase species and 12 bulk aerosol compounds with 157 gas-phase and 39 photolysis reactions. The GOCART aerosol scheme simulates five major tropospheric aerosol types including black carbon, organic carbon, sulfate, dust and sea-salt, assuming externally mixed aerosols. BC and OC aerosols in GOCART are considered to be present in hydrophobic and hydrophilic modes with a hydrophobic-to-hydrophilic conversion e-folding lifetime of 2.5 days. All primary OC and BC emissions are assumed to occur in hydrophobic mode. BC and OC are removed by dry deposition from both the hydrophobic and hydrophilic modes and by wet deposition from hydrophilic mode. Dust and sea-salt aerosols are removed by dry deposition and gravitational settling.

2.5.2 Back-air trajectories (HYSPLIT)

Back-air trajectory models serve an important tool to trace the sources of an air parcel and to understand the role of local and regional scale pollution in the variability of various trace species. In this study, Hybrid Single Particle Lagrangian Integrated Trajectory (HYSPLIT) model is used to simulate the back air trajectories of the air masses at the measurement sites in the Himalayan region. The model is driven by standard meteorological fields obtained from regional or global models. In this study, meteorological fields form Global Data Assimilation System (GDAS) at 1^{o} x 1^{o} spatial and 3-hour temporal resolution are used. These datasets include the gridded data of winds, temperature and other meteorological parameters at several pressure levels. The input data for topography and surface pressure are also provided as an input. HYSPLIT model can also be used to provide the variations in the meteorological parameters such as temperature, pressure, relative humidity, solar radiation and rainfall along the trajectories. More details of the back-air trajectory simulations using HYSPLIT model can be seen elsewhere [*Draxler and Rolph,* 2012; *Draxler et al*., 2012].

Chapter 3

Biomass Burning Over the Indian Subcontinent

Biomass burning emissions contribute to changes in the air quality, cloud properties, Earth's radiation budget [*Crutzen and Andreae,* 1990; *Galanter et al.*, 2000; *Duncan et al.*, 2003; *Kumar et al.,* 2010; *Bhardwaj et al.,* 2016] and thus affects the climate, particularly in the tropical and subtropical regions [*Seiler and Crutzen,* 1980; *Andreae et al.*, 1997]. Biomass burning has both anthropogenic and natural origins with fires used for cultivation shifting, deforestation and agricultural practices falling in the former category and those caused by lightning belonging to the later. However, anthropogenic sources are estimated to account for most (90%) of the biomass burning occurring on the planet [*Koppmann et al.,* 2005]. In addition to large perturbations in the budget of primary pollutants, trace species emitted by biomass burning can react and contribute to the formation of other secondary pollutants such as ozone and secondary aerosols. As a result, the impact of biomass burning on the regional distribution of trace species has been a focus of several studies in the past. These studies have focused mainly in Africa and South America [*Fishman et al.,* 1996, *Lindesay et al.,* 1996, *Blake et al.,* 1999], East Asia,

Southeast Asia and Australia [*Thompson et al.,* 2001; *Kondo et al.,* 2002; *Takegawa et al.,* 2003]. Among Asian regions, the highest amount of biomass is burnt in Southeast Asia (about 45 %) majority of which is in the form of forest fires, followed by East Asia (about 25 %) and South Asia (about 23 %) where crop residue burning is dominant [*Streets et al.,* 2003]. The investigation of biomass burning impacts on air pollution over the Indian subcontinent is limited, despite the fact that biomass burning in this region is expected to be a significant contributor to the budget of many trace species [*Galanter et al.,* 2000].

Apart from these implications, the few studies [*Venkatraman et al.,* 2006; *Kharol and Badrinath,* 2006; *Sharma et al.,* 2010; *Kumar et al.,* 2011; *Ghude et al.,* 2013; *Jena et al.,* 2014] done over the Indian region have provided valuable but only short-term (spatial and temporal) information about the role of biomass burning. Detailed investigation of long-term changes including the seasonal and interannual variability of the biomass burning activity over South Asia was still lacking. In light of the above conditions, this study was done with three objectives in mind: (i) characterization of long-term variations in biomass burning activity over different regions of South Asia using long-term (2003-2013) observations of fire locations from satellites, (ii) estimating uncertainty in the biomass burning emissions over South Asia using emission estimates available from the current state-of-the-art emission inventories derived using bottom-top and top-down approaches, and (iii) quantifying the differences in effects of biomass burning on the tropospheric pollution loading over the cropland and forest regions using satellite retrieved tropospheric column nitrogen dioxide (NO_2) and aerosol optical depth (AOD).

3.1 Study region

The interannual and seasonal variations in fire activity are studied over South Asia. To put our results in context of the Asian continent, fire activity in South Asia is also compared with two other major biomass burning regions of Asia, namely East Asia and Southeast Asia. The geographical boundaries of these regions considered here are shown in Figure 3.1.

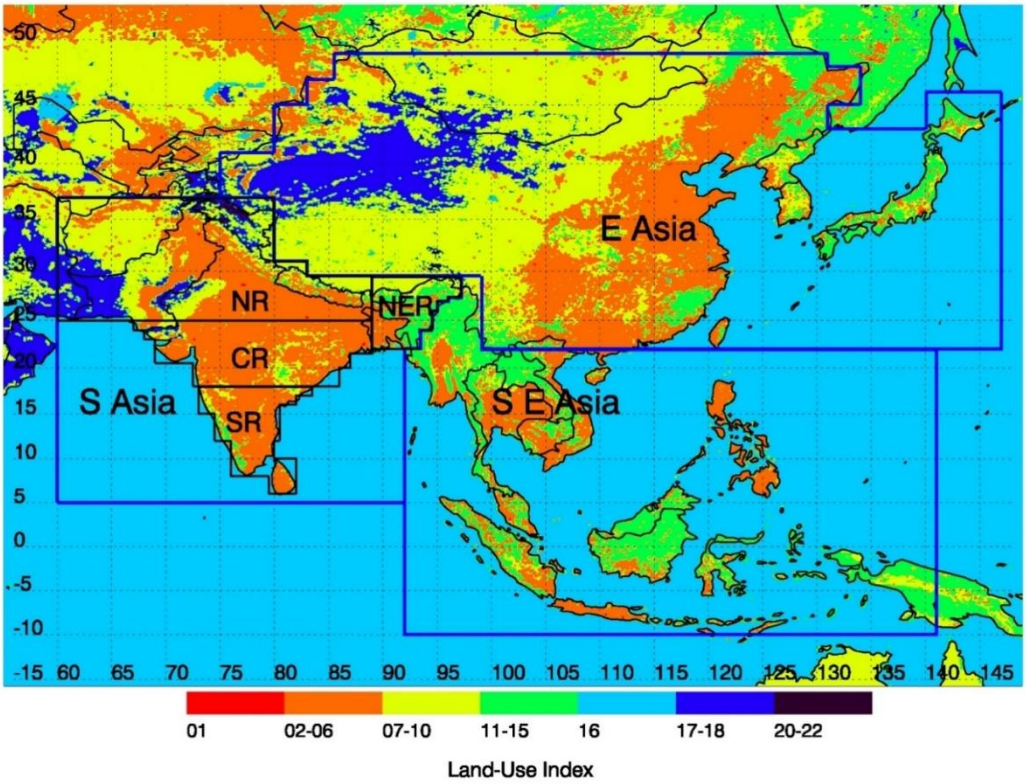

Figure 3.1: *Depiction of three Asian regions (enclosed by blue lines) namely; South Asia (S Asia), Southeast Asia (S E Asia) and East Asia (E Asia) those are used in the present study. South Asia is further subdivided into four regions shown by black lines; (NR) north region, (CR) central region, (SR) south region and (NER) northeast region. Spatial distributions of different landuse categories (USGS) are also shown in the background. (The details of these landuse indices are given in Table 3.1).*

Based on USGS landuse-land cover map, cropland and shrubland/grassland are the most common land cover types in South Asia (46% cropland, 32% shrubland/grassland) and East Asia (48% shrubland/grassland, 25% cropland) while Southeast Asian region is primarily covered by the forests (56%) and cropland (38%). Since this work focuses on South Asia, this region is further classified into four regions namely north (NR: 24^{o}N-35^{o}N, 70^{o}E-89^{o}E), northeast (NER: 22^{o}N-29^{o}N, 89^{o}E-97^{o}E), central (CR: 18^{o}N-24^{o}N, 68^{o}E-89^{o}E), and south (SR: 08^{o}N-18^{o}N, 73^{o}E-84^{o}E) for a detailed characterization of spatio-temporal variations in biomass burning activity (Figure 3.1). The northern region of South Asia includes Afghanistan, Pakistan, Nepal and the highly fertile Indo-Gangetic Plain where agricultural practices are widely conducted. This area is covered mostly by desert/shrubland/grassland (about 44%) followed by croplands (about 30%). Forests have the highest area in northeast region (about 45%), while the cropland are the dominant land-use type in the south (about 77%) and central (about 75%) regions, followed by the shrubland/grasslands (about 14% and 20%, respectively).

Table 3.1: *The land-use index and description of 24 different USGS land-use categories.*

Land-Use Index	Land Use Description
1	Urban and Built-up Land
2-6	Cropland (different types)
7-10	Grassland/Shrubland/Savanna
11-15	Forest (different types)
16	Water Bodies
17-18	Herbaceous/Wooden Wetlands
20-22	Tundra (different types)

3.2 Variations in biomass burning

In this section, we first discuss the seasonal variability of fire activity in South Asia as a whole and compare it to East and Southeast Asia (Figure 3.2). The MODIS level-2 fire data is classified in three categories; low confidence (0-30%), nominal confidence (30-80%) and high confidence (> 80%) data. This confidence limit allows rejection of false fires. Here, in this study data with high confidence (>80%) are used (unless otherwise stated). Figure 3.2 also shows differences between high confidence fires with all data.

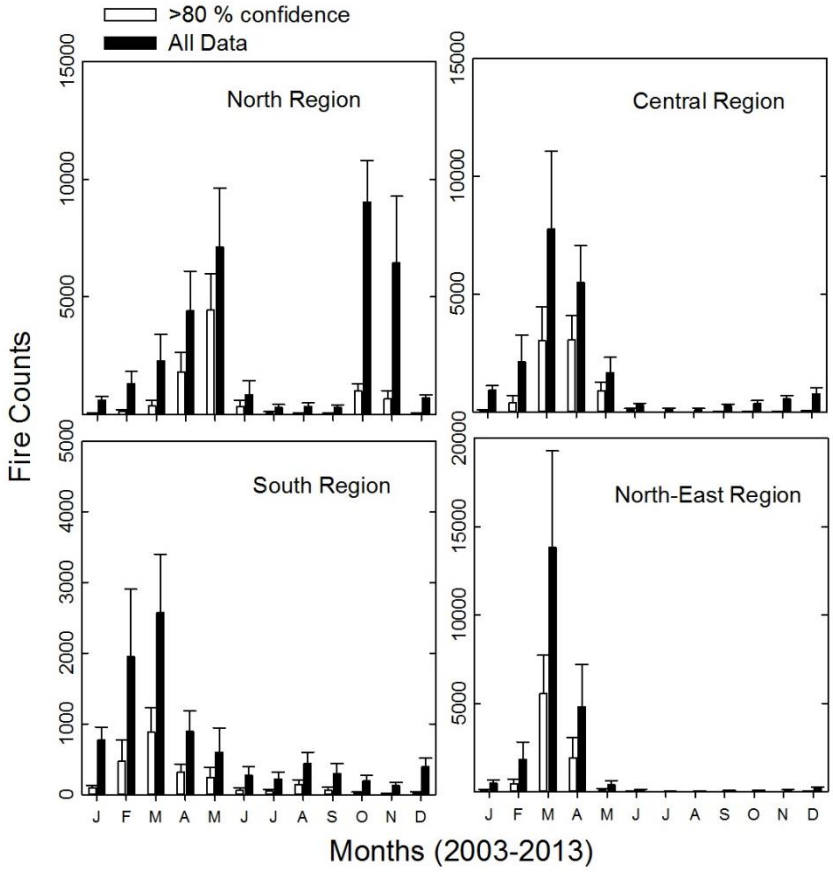

Figure 3.2: *Seasonal variations of MODIS fire counts over four regions in South Asia for 11 years (2003-2013). Fire counts having more than 80% detection confidence are shown in white colour and all fire data is shown in black colour. Black bars are one sigma deviations.*

Here, it is to be noted that the number of active fires detected is not necessarily directly proportional to the amount of biomass burnt [*Venkatraman et al.,* 2006], and thus this discussion is not meant to compare the amounts of trace species emitted in different Asian regions. The annual total fire counts in Southeast, South and East Asia are estimated in the range of 52200-96663, 24154-37827 and 11000-17089 respectively for the period of 2003-2013. These numbers suggest that fires over South Asia are more frequent or spread in wider region compared to East Asia but less frequent than Southeast Asia (Table 3.2).

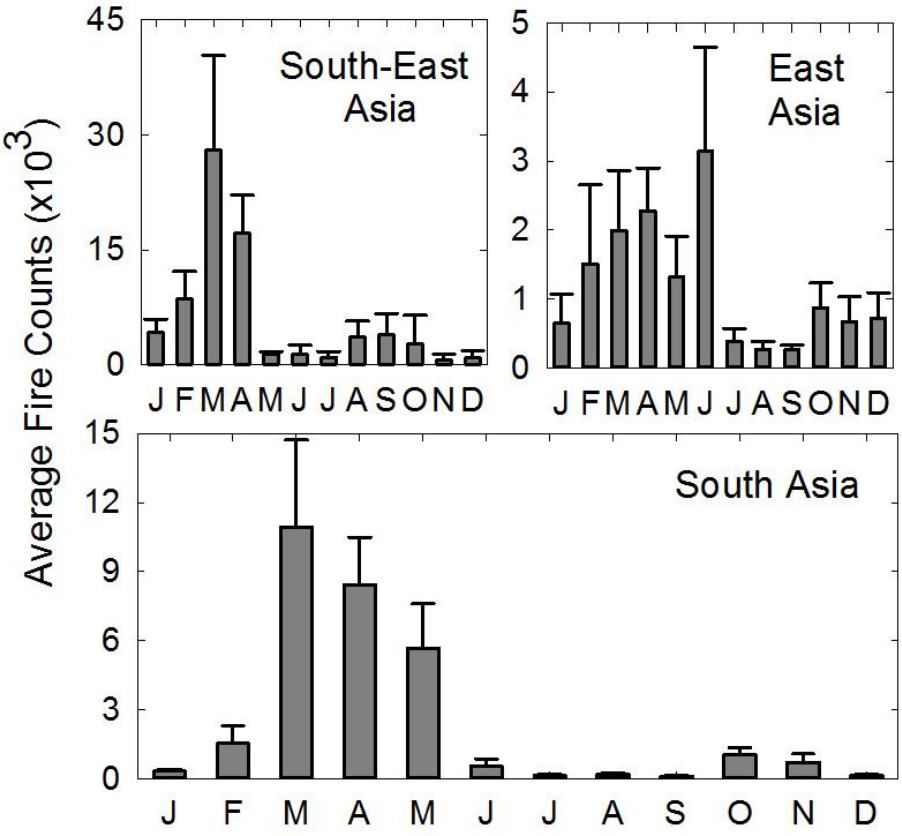

Figure 3.3: *Seasonal variations in MODIS fire counts over three Asian (Southeast Asia, South Asia and East Asia) regions for a period of 11 years (2003-2013). Vertical bars are one sigma standard deviations. Note that the y-axes have different scales.*

Table 3.2: *Average fire counts during four seasons over three Asian regions. The four seasons are Winter (DJF), Spring (MAM), Summer (JJA) and Autumn (SON). The values are mean ± 1 sigma of fire counts. Annual range of fire counts is also shown by minimum and maximum counts during 2003-2013.*

Asian Regions		South Asia	East Asia	Southeast Asia
Winter		2003 ± 799	2889 ± 1333	13889 + 4790
Spring		25042 ± 3731	5597 ± 944	46644 ± 10847
Summer		856 ± 383	3810 ± 1660	6040 ± 2916
Autumn		1867 ± 358	1810 ± 535	7349 ± 6693
Annual	Avg ± Std	29768 ± 4376	14107 ± 1842	73921 ± 14400
	Min - Max	24154 - 37827	11000 - 17089	52200 - 96663

Interannual variability is largest over Southeast Asia (85%) followed by over South Asia (57%) and East Asia (55%). The fire activity in all the three Asian regions shows distinct seasonal variation and peaks during spring/summer months. However, the duration and peak timing of fire activity differ among these three regions. Fire activity in Southeast Asia occurs during January-April, while the peak activity in South and East Asia occurs during February-May and January-June, respectively. The highest fire activity occurs in March over Southeast Asia (38%) and South Asia (37%) and in June over East Asia (22%). Some fire activity is also seen during autumn/winter in all three regions. The fire activity over East Asia occurs for a longer time period (January to June) than in South and Southeast Asia. Fire activities almost cease in all four regions during the monsoon period.

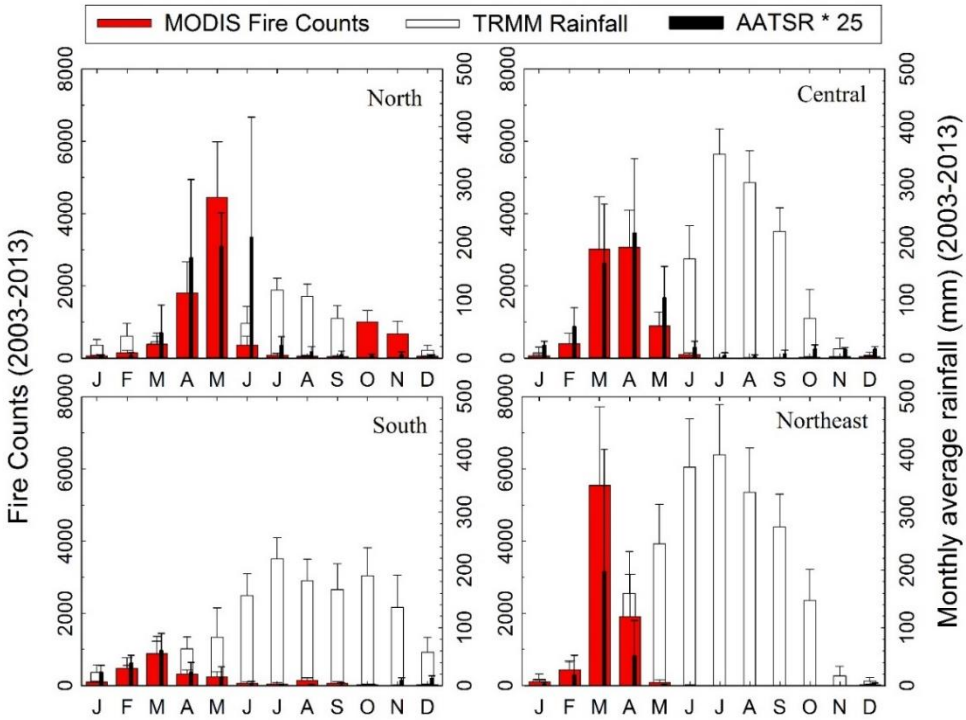

Figure 3.4: *Seasonal variations of monthly averaged MODIS fire counts, TRMM rainfall for 11 years (2003-2013) and AATSR fires counts for 9 years (2003-2011) over four South Asian regions (north, central, south and northeast). AATSR fires are scaled up 25 times. Vertical bars are one sigma standard deviation.*

The seasonal variations in MODIS fire counts over the four defined regions of South Asia (north, central, south and northeast) are shown in Figure 3.4 and are compared with AATSR retrieved fire counts. The seasonal variation of TRMM retrieved monthly average rainfall is also shown to help distinguish between the dry and wet periods over these regions. In South Asia, the annual total of fire counts is highest over the north (9093± 1626), followed by the northeast (8114 ± 1710), the central (7654 ± 2297) and are lowest over the south (2371 ± 552) region for the period of 2003-2013 (Table 3.2). This suggests that fire activity has lowest frequency in the south region, while it has similar frequency in the other three regions. Both MODIS and AATSR show large seasonal variability in fire activity

over the four South Asian regions, with the highest fire activity occurring during the dry period of March-May, and the lowest fire activity occurring during the wet period of June-September. The peak fire activity occurs in March (68%) over the northeast region, in March-April (79%) over the central region, in May (49%) over the north region, and in March (37%) over the south region.

Table 3.3: *Seasonal variations of fire counts (high confidence) over four South Asian regions. The four seasons are winter (DJF), spring (MAM), summer (JJA) and autumn (SON). The values are mean ± 1 sigma of fire counts.*

South Asian Regions		North Region	Central Region	South Region	Northeast Region
Winter		258 ± 90	517 ± 303	598 ± 301	565 ± 248
Spring		6638 ± 1497	6969 ± 2176	1435 ± 116	7532 ± 1580
Summer		492 ± 272	105 ± 49	250 ± 116	8 ± 11
Autumn		1705 ± 349	63 ± 20	88 ± 52	10 ± 8
Annual	Avg ± Std	9093 ± 1626	7654 ± 2297	2371 ± 552	8114 ± 1710
	Min – Max	6544 - 12474	4601 – 10651	1652 - 3280	5400 - 10827

AATSR fire count shows some differences when compared to the MODIS fire counts. AATSR retrievals show significant fire activity during June over the north region; this is not observed by the MODIS retrievals. MODIS retrievals show significant fire activity in October-November that is not seen in the AATSR retrievals. These differences between the satellite products can be attributed to differences in their detection algorithms and temperature thresholds (refer Chapter 2 for algorithm differences among the two satellites). The above detection criterion ensures that MODIS is more sensitive to smaller fires. Further, the AATSR retrievals are limited by the high level of omission due to cloud coverage, satellite

coverage and higher threshold value which can lead to under estimation of fires [*Arino et al.,* 2011].

To understand the long-term changes and interannual variability in fire activity over four regions of South Asia, we compared time series of annual total fire counts and rainfall. The annual average fire counts over South Asia are found to be increased by about 20% during 2008-2013 compared to those during 2003-2007. The contribution of fire counts from the north and central regions to the total fire counts in South Asia has increased from 45% (during 2003-2007) to about 69% (during 2008-2013) and thus making net enhancement by 24% from these two regions in South Asia [*Bhardwaj et al., 2016*]. Fire counts in north and central regions have increased by about 47% during 2008-2013 compared to 2003-2007 period. Fire counts in the southern region increased by about13%, while those in the northeast region decreased by about 17% between these periods.

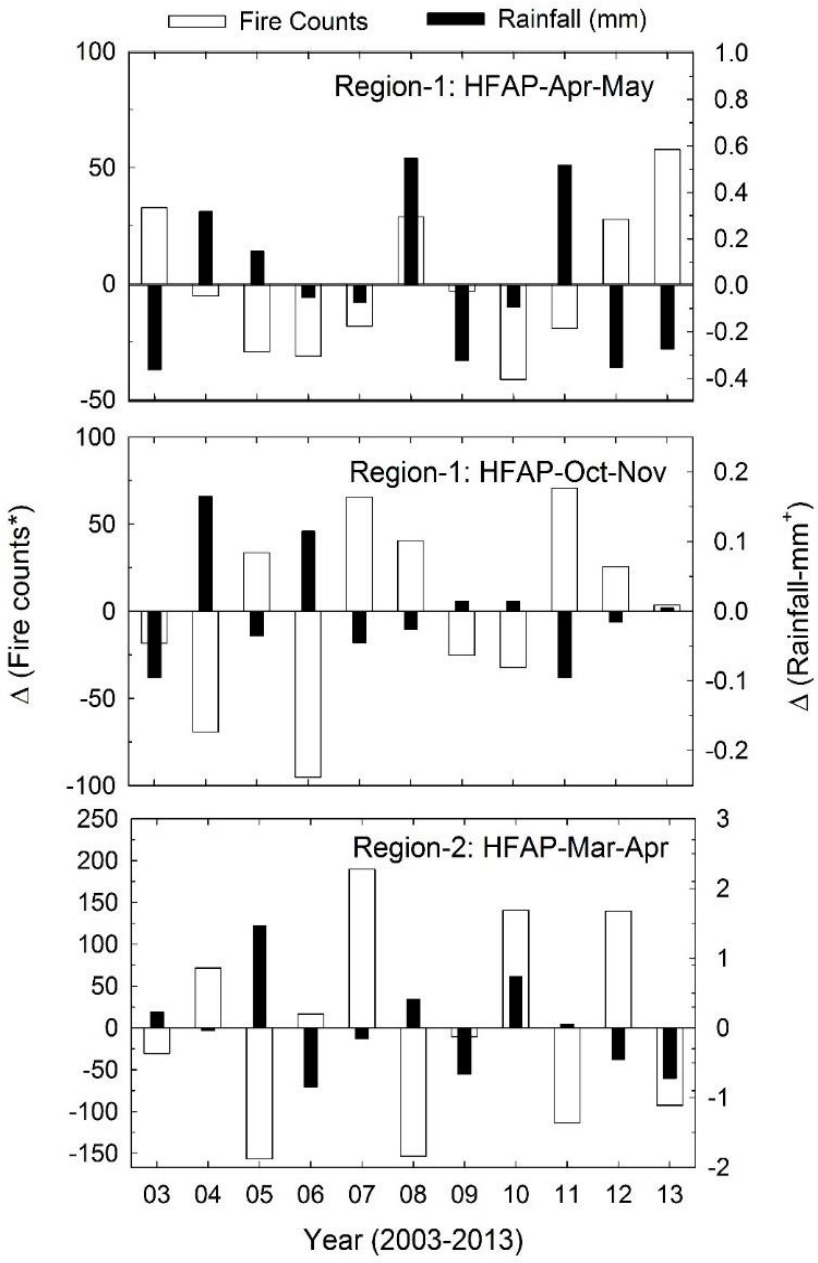

Figure 3.5: *Inter-annual variations in fire counts and rainfall deviations over cropland (region-1) in spring and autumn season and over forest region (Region-2) in spring during high fire activity periods.*

We feel that decrease in fire counts over northeast could be due to reduction in forest cover. Forest cover area in seven northeastern state in India is reducing by rate of about 110 sq. km per year but net reduction in area from 2003-2007 to 2008-

2013 is about 435 sq. km (data from https://fsi.nic.in). Analysis of the crop production data shows that the rice and wheat production over India has increased by about 15% from period 2003-2007to period 2008-2013.Agricultral land area has also increased by about 2.5 million ha from period 2003-2007 to period 2008-2013. The increase in the crop production and arable area might have some contribution to the increase in fire frequency over South Asia. The comparison of time series of annual total fire counts with annual total rainfall do not show any clear relationship between them suggesting that changes in fire activities could be of anthropogenic origin. However, a tendency of anti-correlation (Figure 3.5) between them is seen over a two smaller regions (cropland and forest regions, defined later in section 3.4) with an exception during 2003 and 2008.

To characterize the spatial variability of fire activity over the four defined regions in South Asia, we compared the variability of MODIS retrieved fire counts from February to June (peak fire months) during three years 2010-2012 (Figure 3.6).

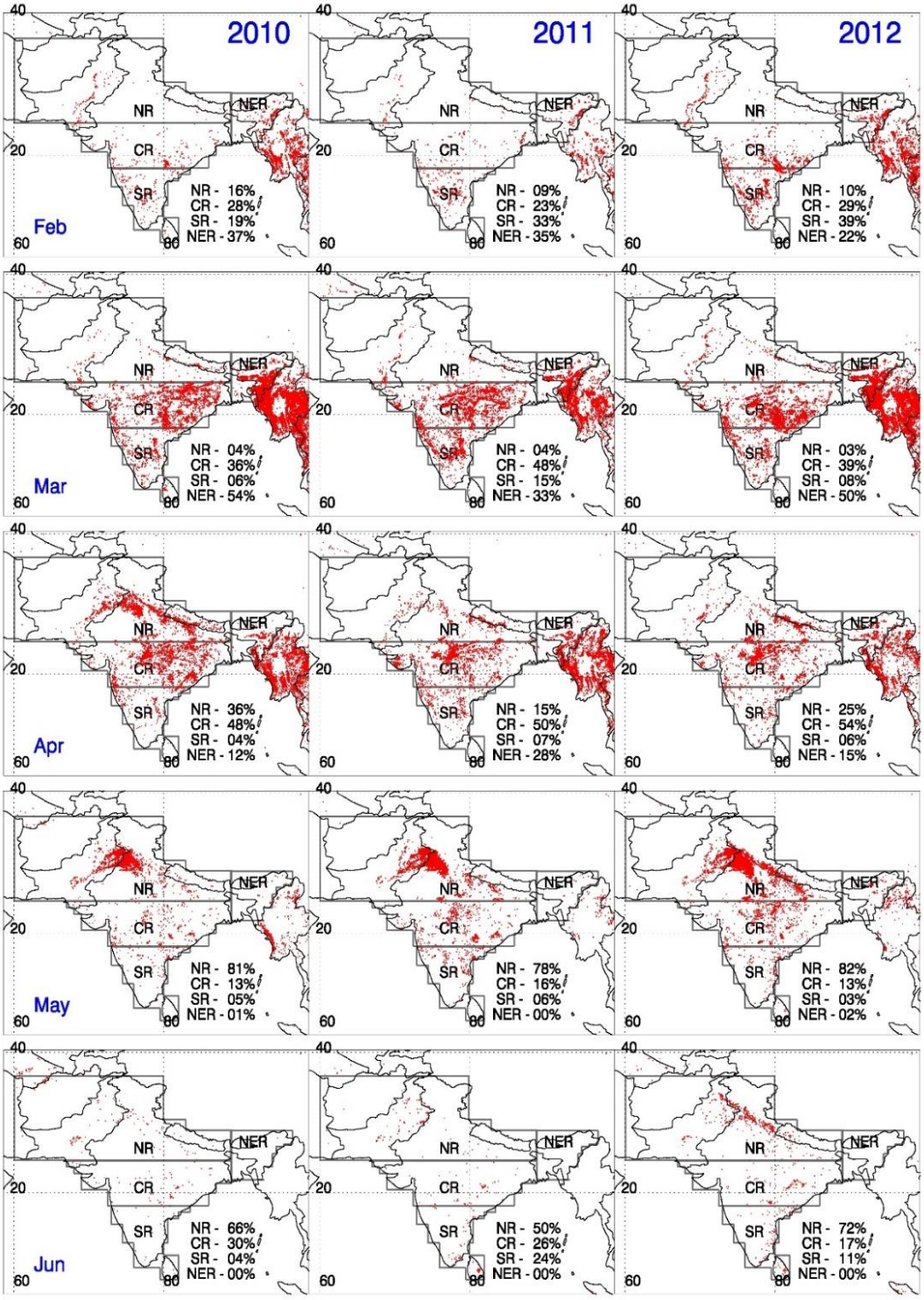

Figure 3.6: *Spatial distribution of MODIS fire counts over South Asia for five months (feb-Jun) during 2010-2012. Four regions north (NR), central (CR), south (SR) and northeast (NER) are also marked with grey color boundaries. The fire counts (percentage of total) are also mentioned for the the respective regions.*

These three years are shown only as an example and spatial distribution of fire activity during other years are also similar. Large spatial variability in fire activity over South Asia is clearly evident from Figure 3.6. Wide spread fire activity is observed during spring season with hot spots over central, northeastern states of India and Punjab region. The analysis of land use map (Figure 3.1) along with maps of satellite retrieved fire locations (Figure 3.6) shows that springtime peak in fire activity over north, central and south regions is dominated by the agricultural crop residue burning while that in the northeast region is dominated by the forest fires. The secondary peak observed over the north region during October-November is associated with the crop residue burning. The crop residue burning is a regular land clearing activity practiced in this region following the harvesting of wheat and paddy crops in April-May and October-November, respectively. These two seasons account for about 96% of the total annual fire counts, with 75% in the spring season and remaining in the months of October and November over the north region.

3.3 Uncertainty in biomass burning emissions over South Asia

Previous section highlighted the large spatial and temporal variability in biomass burning activity over South Asia. In this section, we address the variability and uncertainties associated with biomass burning emission estimates available from a top-down (GFAS) and a bottom-top (GFED) emission inventory. Here, we are using carbon monoxide (CO), nitrogen oxide (NO_x) and black carbon (BC) as representative of biomass burning emissions of trace gases and aerosols. As expected, the seasonal variations in biomass burning emissions from both the emission inventories are similar to those in fire count data in all the four regions. However, there are large differences in the magnitude between the two inventories

(Figure 3.7) and these differences are not spatially consistent [*Bhardwaj et al.*, 2016].

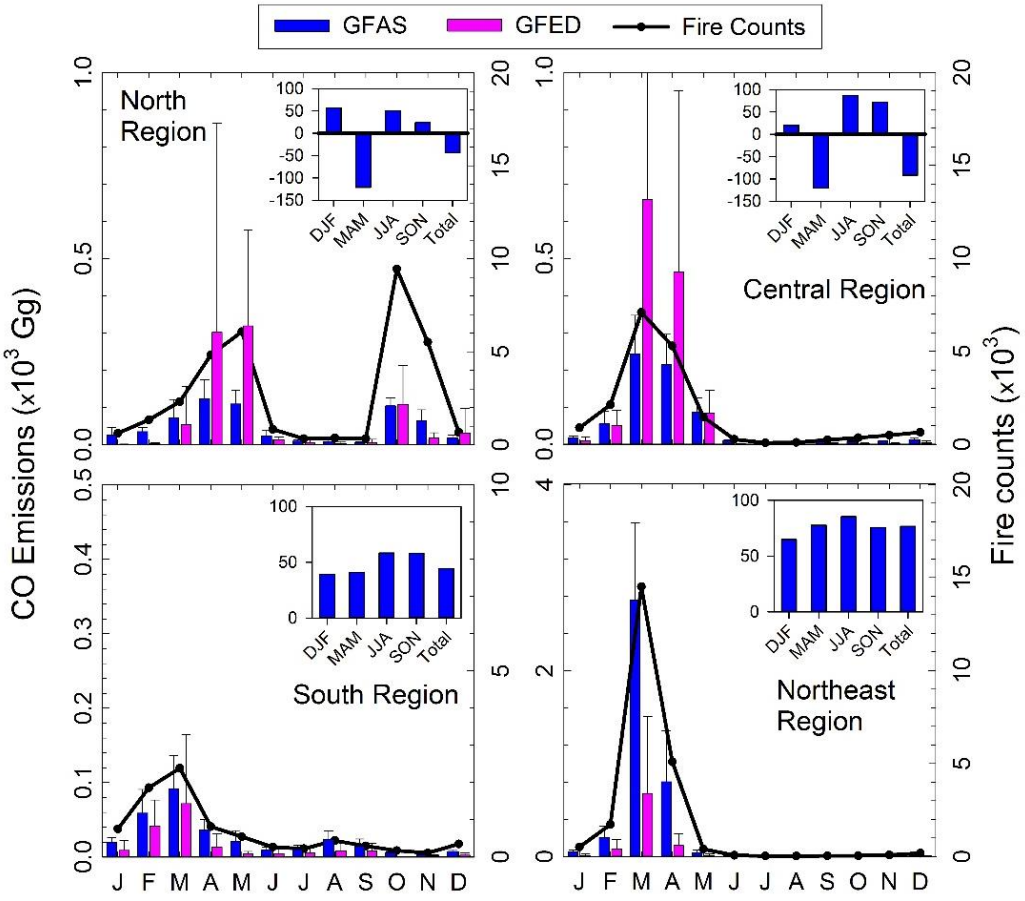

Figure 3.7: *Seasonal variations in CO from biomass burning emissions using GFAS v1.0 and GFED v3.1 emission inventories for eight years (2003-2010). CO emissions are in 10^3 Giga-grams (10^9 grams) per month. Over plotted is the seasonal variations fire counts without 80% confidence condition applied (also see Figure 3.2). Inset, figures are showing % deviation in GFAS emissions with respect to GFED emissions. Scales are different on y-axes among four regions.*

In South Asia, the annual average GFED CO emissions are higher over the north and central regions by about 43% and 92% than the GFAS CO emissions, respectively, while GFED CO emissions are lower by about 44% and 77% in the south and northeast regions, respectively. Overall, GFED CO emissions are lower compared to the GFAS CO emissions in all the seasons and over all the regions,

except during spring (March-May) in the north and central regions where GFAS is lower than GFED by about 121% (Table 3.3). Additionally, annual average CO emissions are largest (1280.7 ± 704.2 Gg/yr) over the central region in the GFED inventory, while CO emissions are largest (3875.9 ± 640.3 Gg/yr) over the northeast region in the GFAS inventory. *Venkatraman et al.,* [2006] also showed similar results with central India having the largest burned biomass among different regions of India. Analysis of annually-averaged NO_x and BC emissions from the GFED and GFAS emission inventories shows similar variations. The annual GFAS NO_x and BC emissions are lower by 45% and 51%over the north and 117% and 104%over central regions respectively than the GFED emissions. However, these are higher by about 41% and 44% in the south and 73% & 76% in northeast region, respectively.

Table 3.4: *Seasonal Variations in CO emissions (Gg) from GFAD and GFED emission inventories over four South Asian regions.*

S. Asia Regions	Emission Inventory	Winter	Spring	Summer	Autumn	Annual
North	GFAS	80.5 ± 25.2	306.4 ± 102.7	42.3 ± 16.6	175.4 ± 34.3	604.6 ± 106.6
	GFED	34.9 ± 64.8	676.7 ± 733.3	20.9 ± 15.6	133 ± 113	865.6 ± 717.2
Central	GFAS	84.1 ± 38.1	546.2 ± 176.2	15.9 ± 4.8	22.4 ± 4.2	668.6 ± 198.7
	GFED	67.3 ± 50.0	1205.0 ± 721.6	2.1 ± 1.6	6.3 ± 6.1	1280.7 ± 704.2
South	GFAS	86.0 ± 34.3	149.2 ± 45.0	41.9 ± 16.2	22.3 ± 8.9	299.4 ± 70.7
	GFED	52.5 ± 31.3	88.4 ± 88.3	17.5 ± 13.8	9.4 ± 11.7	167.7 ± 105.4
Northeast	GFAS	264.0 ± 119.7	3600.1 ± 581.7	5.7 ± 4.5	6.0 ± 2.7	3875.9 ± 640.3
	GFED	93.2 ± 120.3	810.0 ± 939.0	0.9 ± 1.1	1.5 ± 2.0	905.5 ± 1044.1

To further understand the differences in the emissions from different land cover types, specifically croplands and forests, we analyze the emissions from a smaller

region in the north-western Indo-Gangetic Plain (to represent fires in croplands) and a smaller region in northeast region and Burma (to represent fires in forests) in Figure 3.8.

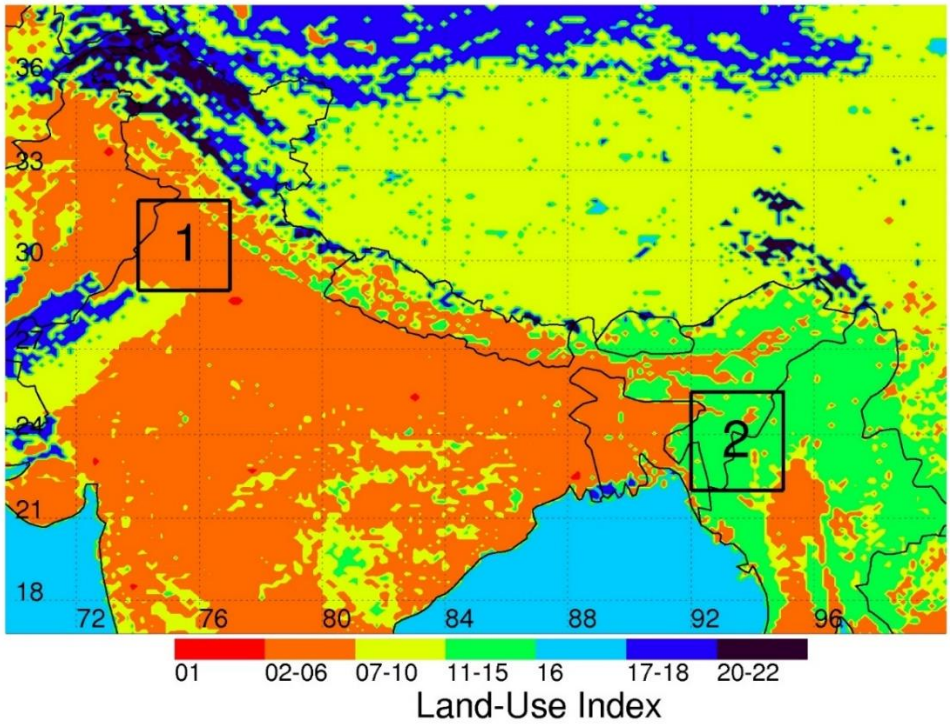

Figure 3.8: *The two regions representing two different types of land use. Region-1 is representative for cropland [(29, 32), (74, 77)] and Region-2 for forests [(22, 26), (92, 95)]. Please refer land use index table-3.1.*

Here we have used all MODIS fire count data (instead of high confidence fire data) as no such filter is used for other data products, further all datasets are first regridded to $1^{o}x1^{o}$ and then used for above two regions. The time series of daily MODIS retrieved fire radiative power (FRP) (2003-2013) in each of these regions is shown in Figure 3.9 along with the MODIS fire counts and NO_x and BC emissions from GFAS inventory. The annual average fire counts in the forest region are slightly more than those in the cropland region (19503 to 18403 fire counts), but the amount of both BC and NO_x emitted in forest region are about 17 and 13 times (17.28 Gg BC vs1.03GgBC and 70.10 Gg NO_x vs 5.53 Gg NO_x) higher compared to the

emissions from the cropland region.

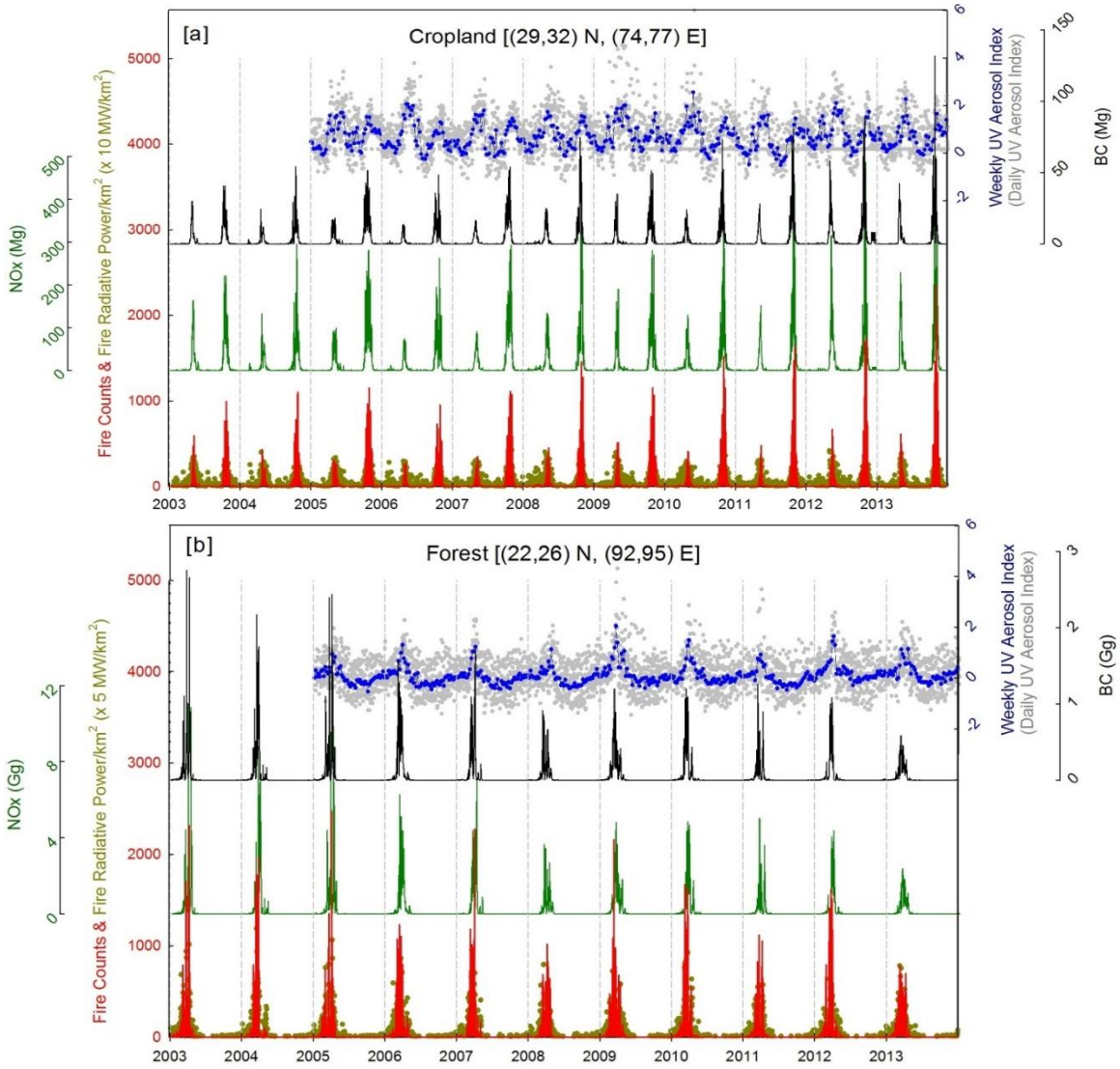

Figure 3.9: *Inter-year variations in MODIS fire counts, OMI daily and weekly uv-aerosol index fire radiative power (FRP), GFAS v1.0 NO_x biomass burning emissions and GFAS black carbon (BC) emissions over cropland [a] and forest [b] regions for 2003-2013. Positive uv-aerosol index means absorbing type of aerosols emitted from the study regions. FRP is in Mega-Watt/ km^2 (MW/km^2) and NO_x emissions are in Giga-grams (Gg).*

This is likely because of the fact that forests have much more biomass compared to croplands and thus more biomass can burn per fire detection in a forest region than

in a cropland. This is corroborated by much higher values of FRP in the forest region compared to those in the cropland region (Figure 3.9) as FRP values are directly proportional to the amount of biomass burned. The average BC and NO_x emissions for the period of 2003-2013are higher during October-November~ 66% (0.68 Tg of BC; 3.70 Gg of NO_x) as compared to April-May ~ 31% (0.31Tg of BC; 1.68 Gg of NO_x) over the cropland. To understand these differences, we found that average FRP values are lower (12.5 MW/pixel vs 14.1 MW/pixel) in October and November over the cropland region compared to April and May. However, fire counts in this period are much higher during October-November season than April-May period over the cropland region (13609 vs 4423 fire counts). Thus we feel that October-November fires are likely less intense and cooler compared to April-May fires and higher emissions in October-November over the cropland region could be due to smoldering form of combustion that takes place at the lower temperature.

3.4 Effect of biomass burning on tropospheric pollution

To examine the effect of biomass burning on the tropospheric pollution over the cropland region and forest region, we examined a time series of MODIS aerosol optical depth, OMI tropospheric column NO_2 and UV aerosol index over the cropland and forest regions. For this analysis, we classified satellite retrievals into the low and high fire activity periods following *Kumar et al.*, [2011]. To demark the low and high fire activity periods, the median of fire counts is calculated separately in April-May and October-November over the cropland and February-April over the forest region. High fire activity periods are those for which the three-day running mean of fire counts exceeds the respective medians, while remaining period prior to high fire activity period are termed as low fire activity periods. The

low fire activity periods are restricted to those prior to high fire periods.

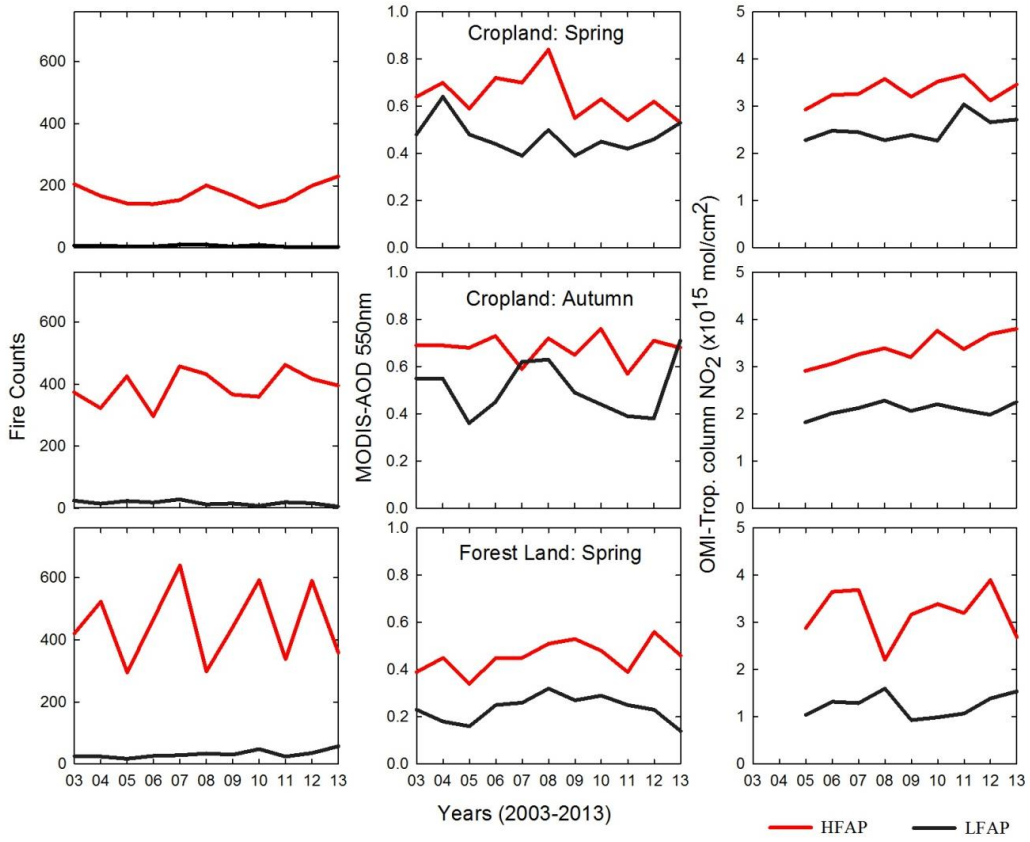

Figure 3.10: *Inter year variations in MODIS fire counts & AOD, and OMI tropospheric column NO_2 over the cropland and the forest during high fire activity period (HFAP) and low fire activity period (LFAP).*

Tropospheric column NO_2 and MODIS AOD show clear enhancements during the high fire activities period over both the cropland and forest regions when compared with their respective levels during low fire activity periods (Figure 3.10). The percentage increase in fire counts, MODIS AOD, OMI UV AI and tropospheric NO_2 during the high fire activity periods relative to the low fire activity periods are tabulated in Table 3.4. Similar to the results of the analysis of the GFAS emissions, the percentage increase in both the MODIS AOD and tropospheric column NO_2 are much higher over the forest (more than 100%) compared to the cropland (34-62%).

The aerosol indices also increase much more over the forest region (396%) than the cropland region (110-176%) indicating large increase in the abundance of absorbing aerosols from low fire activity to high fire activity periods. Larger increase over the forest region is consistent with higher BC emissions compared to the croplands.

Table 3.4: *Percentage increase in MODIS fire counts and AOD, OMI tropospheric column NO_2 and UV aerosol index (AI) over the cropland and forest regions during high fire activity period (HFAP) from low fire activity period in three seasons.*

Percentage increase	Cropland (Spring)	Cropland (Autumn)	Forest (Spring)
Fire Counts	3634 ± 2042	2908 ± 1932	1444± 500
MODIS AOD	38 ± 24	40 ± 34	103 ± 53
OMI NO2	34 ± 14	62 ± 12	168 ± 69
OMI UV AI	110 ± 66	176± 76	396 ± 305

3.5 Conclusions

The seasonal, interannual and long-term variations in biomass burning activity and related emissions are not well studied over South Asia. Here, active fire location retrievals from the Moderate Resolution Imaging Spectroradiometer (MODIS), the retrievals of aerosol optical depth (AOD) from MODIS Terra and tropospheric column NO_2 from Ozone Monitoring Instrument (OMI) are used to understand the effects of biomass burning on the tropospheric pollution loadings over South Asia during 2003-2013. Biomass burning emission estimates from Global Fire Emission Database (GFED) and Global Fire Assimilation System (GFAS) are also used to

quantify uncertainties and regional discrepancies in the emissions of CO, NO_x and BC due to biomass burning in South Asia. In the Asian continent, the frequency of fire activity is highest over Southeast Asia, followed by South Asia and East Asia. The biomass burning activity in South Asia shows a distinct seasonal cycle that peaks during February-May with some differences among four (north, central, northeast and south) regions in India. The annual biomass burning activity in north, central and south regions shows an increasing tendency, particularly after 2008, while a decrease is seen in northeast region during 2003-2013.The increase in fire counts over the north and central regions contributes 24% of the net enhancement in fire counts over South Asia. MODIS AOD and OMI tropospheric column NO2 retrievals are classified into high and low fire activity periods and show that biomass burning leads to significant enhancement in tropospheric pollution loading over both the cropland and forest regions. The enhancement is much higher (110-176 %) over the forest region compared to the cropland (34-62%) region.

Chapter 4

Ozone and Related Trace Gases Over the Himalayas and its Foothills

The Himalayan region is among the least studied parts in the world despite its known importance in influencing the lively-hood of living beings and agricultural systems. This is spread over a large region covering mainly Afghanistan, Bangladesh, Bhutan, China, India, Myanmar, Nepal and Pakistan and provides water to a billion people. However, the growing economies, industrialization and increasing population in the region are polluting this pristine environment and perturbing the regional climate. In this regard, the observations of trace gases become important in the Himalayan region. However, only a few surface measurements of ozone and related trace species were reported from the Indian region of the Himalayas, which showed influences of regional scale pollution and long range transport to the ozone levels at a high altitude site, Nainital [*Kumar et al.,* 2010; *Sarangi et al.,* 2014]. The Himalayan foothill have been shown to influence by the photochemistry and shows higher levels of ozone during spring season [*Ojha et al.,* 2012].

The urban centers surrounded by high mountains often face severe air pollution problems as these mountains act like a barrier for the horizontal ventilation of the pollutants and the upslope, downslope and valley winds govern the diurnal variations in air pollutants. These kinds of processes have been well studied over other parts of the world e.g., Mexico City [*de Foy et al.,* 2006; *Molina et al.,* 2007 etc.], Santiago de Chile [*Schmitz,* 2005; *Rappengluck et al.,* 2005] etc. and confirm such influences. The rapid unplanned urbanized center in the Kathmandu valley, which is surrounded by Himalayan ranges is an ideal natural laboratory to study such processes. The valley's population has increased by four times to 3 million in last 25 years. Further, to meet the demands of growing population in Kathmandu, during past two decades the total vehicle fleet increased by about 5 times [*Faiz et al.,* 2006]. The total fuel usage in the valley is about 50% of entire Nepal with coal, petrol, diesel kerosene and LPG usage being 40%, 66%, 35%, 50%, 55% respectively [*Pradhan et al.,* 2012]. Previous studies of ozone, CO, NO_x, VOCs and aerosols reported from this region have indicated the high values of these pollutants especially during winter and pre-monsoon period [*Pudaisanee et al.,* 2006; *Pandey and Prin,* 2009; *Putero et al.,* 2015, *Sarkar et al.,* 2016].

In light of above facts, Sustainable atmosphere for Kathmandu valley (SusKat) field campaign was initiated during December 2012 in the Kathmandu valley for about two months and later it was extended for few more months. In this campaign, several research groups from different countries participated and about 150 instruments were installed for measurements of aerosols, gases and meteorological parameters. The campaign had total 23 sites in the region with 1 being the supersite (Bode), 4 satellite sites (in the valley), 2 regional sites (Pokhara and Lumbini) and

other collaborating sites including Nainital and Pantnagar in India. Here, results from surface measurements of ozone and CO at Bode (supersite) and few Indian sites for a period of about 6 months from Jan 2013 to Jun 2013 are presented.

4.1 Observational sites

Kathmandu valley is an oval-shaped urban basin located in the central Himalayas between IGP and Tibetan Plateau (Figure 4.1). The valley is surrounded by mountain peaks with heights ranging from 2000-2800 m amsl and five mountain passes with altitude ranging from 1500-1550 m amsl.

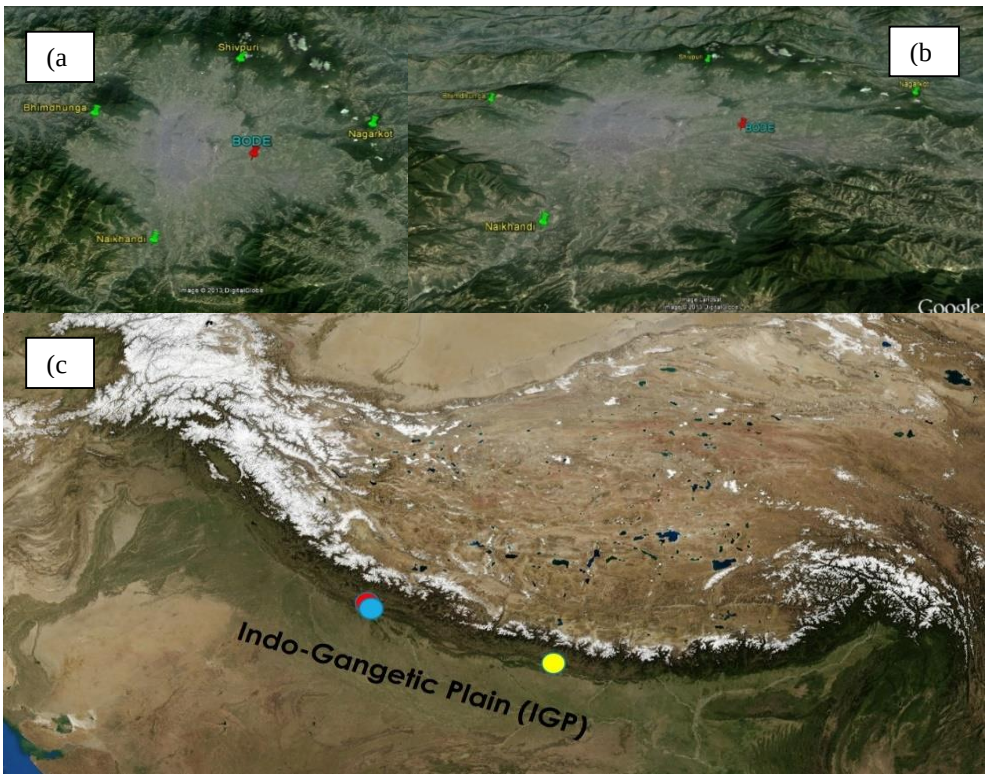

Figure 4.1: *(a), (b) Google Earth image of Kathmandu valley (zenith and edge on view) with the five measurement sites. (c) Location of Bode (yellow) together with other measurement sites in India (Nainital is shown in red, Pantnagar in blue).*

The flat base area of the Kathmandu valley is about 340 km^2 with mean elevation

about 1300m amsl. There is no river inlet into the Kathmandu valley, and only one narrow river outlet (Baghmati River) is in the southern side. The spatial extent of the valley is about 25 km in East-West and around 20 km in the North-South direction. The measurement sites which were planned in the valley are shown in Figure 4.1 and details about their locations are provided in Table 4.1. Here, measurements of ozone, CO and meteorological parameters at supersite Bode (85.39^{o}E, 27.68^{o}N, 1326 m amsl) are discussed. Observations from Nainital and Pantnagar are also used to analyze regional processes. The ozone and CO instruments were installed at third floor of a building in Bode (Figure 4.2).

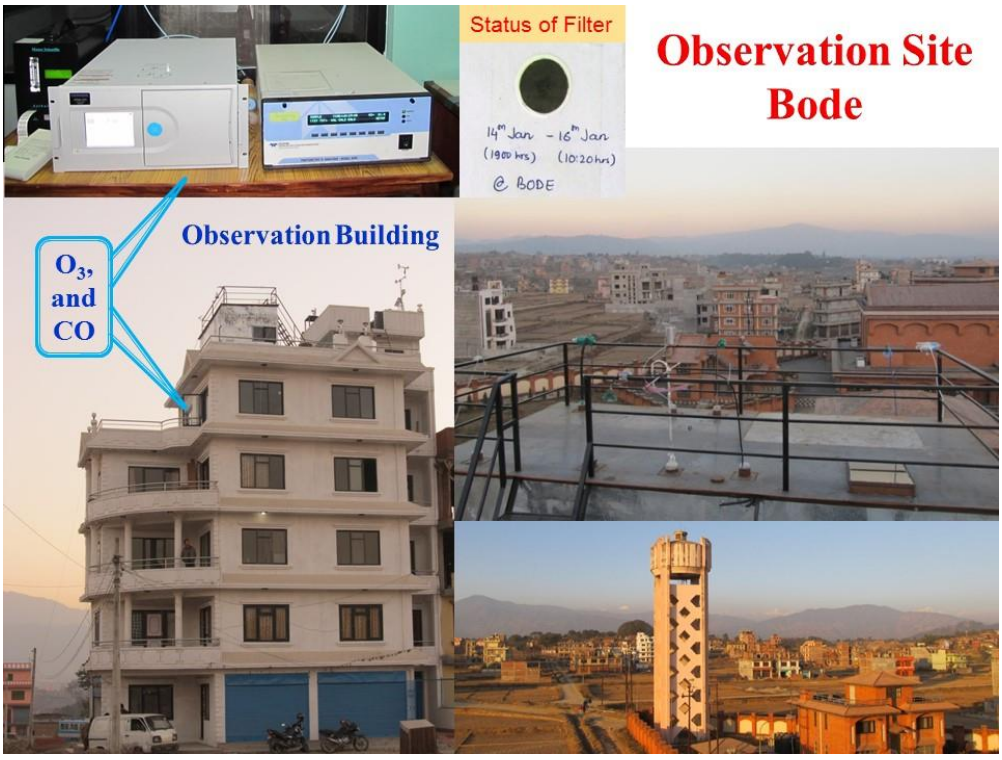

Figure 4.2: *The observation site Bode in the Kathmandu valley. (Left) the building where instrument setup was done, with status of filter after 2 days. (Right) View from the supersite Bode showing air-inlets from the top and the northern side.*

The sampling inlet for the instruments was placed at the top of the building and

Teflon TFE tubes were used for air intake. This site is downwind of the urban city center of the Kathmandu valley. Apart from the surface measurements made at Bode, simultaneous measurements of ozone, CO and meteorological parameters were also carried out at two Indian sites *viz.*, ARIES, Nainital; a high altitude site located on a mountain top (79.45 E, 29.36 N, 1958 m amsl) and Pantnagar; located in Himalayan foothills in IGP (79.5 E, 29.0 N, 231 m amsl) (Figure 4.1c).

4.2 General Meteorology

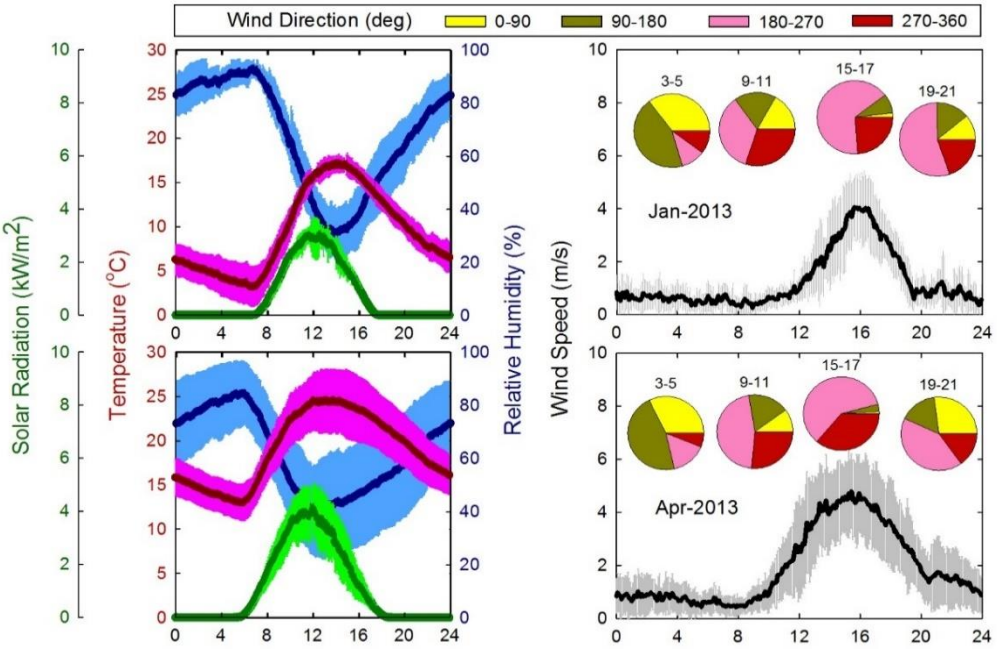

Figure 4.3: *Diurnal variations in temperature, solar radiation, relative humidity, wind speed and wind direction at Bode during January (upper panel) and April 2013 (bottom panel). These two months are taken as representative for winter and spring season respectively. (right) Wind directions during four time periods (3-5, 9-11, 15-17 and 19-21 hours) are shown as pie charts in wind speed plots.*

Diurnal variations in temperature, RH, solar radiation, wind speed and wind

direction during January and April are shown in Figure 4.3. The Kathmandu receives its 90% of rainfall during summer-monsoon months (June-September) when cleaner marine air flows over the valley. The remaining months are relatively dry with average temperatures ranging from 9 to 27^{o}C during spring-summer and 2-20^{o}C during winter months. The solar radiation peaks during May while RH showed higher levels during January. The high surface wind speed (4-5 m/s) mostly north or south-westerlies were observed during mid to late afternoon, which ceases to slow easterlies during night and early morning. The seasonal changes in wind direction during winter and spring is marginal, however during spring months relatively higher wind speeds are observed.

4.3 Diurnal variations

The monthly (January to June) averaged diurnal variations in ozone and CO at Bode are shown in Figure 4.4. As an example of hourly variations in ozone, CO, solar radiation, temperature, RH and wind speeds in a month, April 2013, are shown in Figure 4.5. The diurnal variations in ozone shows higher levels during daytime while those in CO are characterized by morning and evening peaks. The daytime build-up in ozone is consistently observed during all months, with relatively smaller increment during the month of June due to prevailing cloudy/rainy conditions. Such daytime increment in surface ozone is a typical feature of polluted sites and is associated with daytime photochemical production of ozone from its precursors in presence of sunlight [e.g *Kleinman et al.,* 1994]. Figure 4.5 also shows that changes in ozone levels are largely following the tendency of the changes in CO level, in general. Further, there has been decrease in solar radiation on 21 April, 2013 that is

leading to show lower levels in ozone and CO also, confirming the role of the photochemistry. The very low levels of ozone (sometimes below detection limit of 1 ppbv, during winter months) were observed during night-time and are likely due to titration of ozone by NO.

Just around sunrise, a dip in ozone levels was also observed which is suggested to be due to its reaction with NO and NO_2 (which are produced by photodissociation of NO_3 and N_2O_5 at sunrise). Similar dip in ozone is also reported from an urban site in India [*Lal et al.*, 2000]. At Bode, spring time higher levels of ozone with a broader peak can be attributed to the increase in incoming solar radiation and hence inducing the photochemical ozone production. In addition to photochemical production of ozone, the boundary layer evolution during morning hours also contribute to rapid increase in ozone levels, since ozone rich air aloft gets mixed with near surface ozone depleted air [*Rao et al.*, 2003] and thus increases the ozone levels.

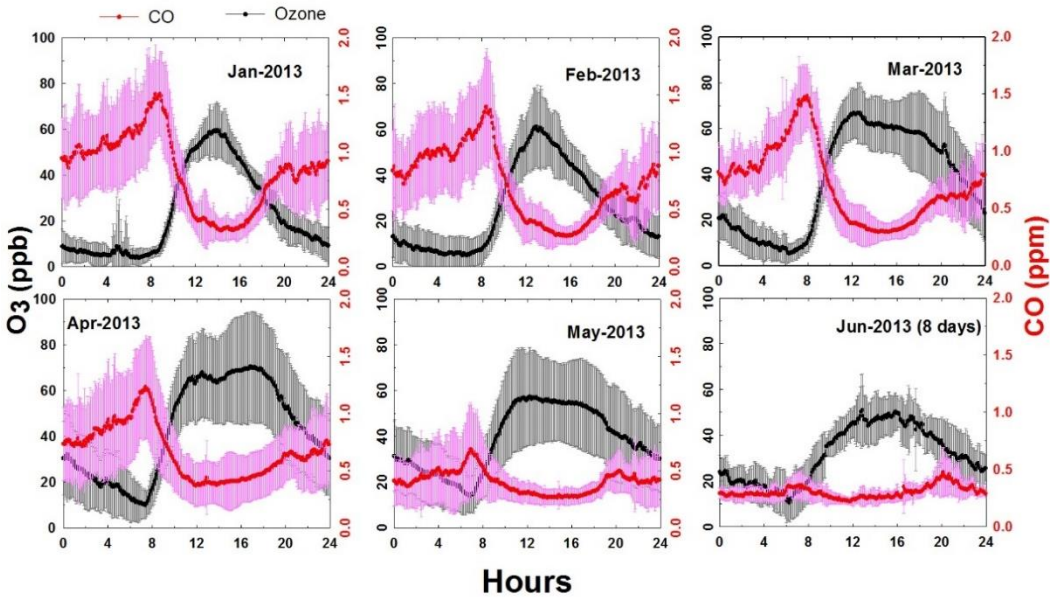

Figure 4.4: *Monthly variations in diurnal ozone and CO at Bode from January to June 2013.*

The diurnal variations in CO showed two peaks during morning and evening hours. Such twin peaks are commonly observed over polluted regions. The evening peak was relatively less prominent which could be due to high westerly winds blowing through the daytime across the valley which flushes out CO. These winds cease out during night time and due to overnight accumulation of CO, the highest levels (~2000 ppbv) were observed during morning time. After reaching its maximum, CO starts to decrease as the day progresses. This decrease can be attributed to the boundary layer evolution which dilutes the CO levels. The chemical loss of CO via reaction with OH radical can also contribute to this decrease. The monthly mean ozone and CO levels with maximum and minimum values are given in Table 4.1.

Table 4.1: *Monthly variations in ozone and CO over Bode during January-June 2013.*

Month	Ozone (ppbv)	Max/Min (ppbv)	Daytime average (11-17 hours)	CO (ppbv)	Max/Min (ppbv)
Jan	23.5 ± 19.9	87.1/1.4	49.8 ± 10.2	832 ± 422	2323/218
Feb	25.6 ± 20.4	94.5/1.2	49.9 ± 13.9	717 ± 397	2182/162
Mar	37.4 ± 24.3	105.9/1.2	61.8 ± 12.0	698 ± 364	2011/158
Apr	43.5 ± 26.6	116.2/1.4	67.0 ± 20.4	667 ± 372	1969/175
May	38.6 ± 21.4	111.1/1/9	55.1 ± 18.9	401 ± 213	1656/146
Jun	31.1 ± 14.6	68.4/1.7	46.5 ± 8.5	303 ± 85	676/166

An event of very high ozone levels (>100 ppbv) was observed in the early morning time on 25 Jan 2013. This was also associated with simultaneous reductions in CO and RH. This event could be due to downward transport of ozone rich air mass from higher altitudes. It has been discussed in chapter 1 that such events are common

during winter or early spring.

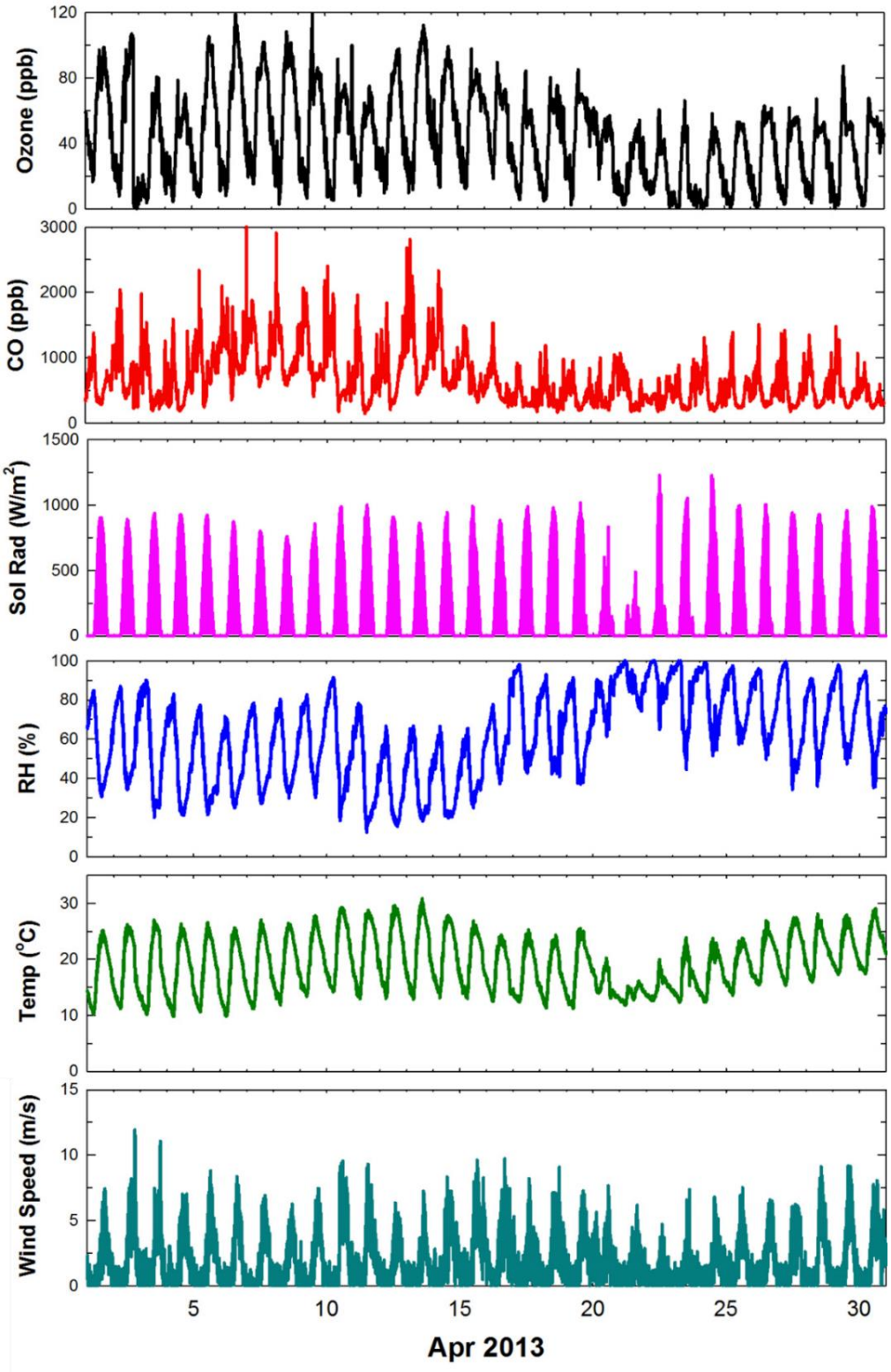

Figure 4.5: *Hourly variations in ozone, CO, solar radiation, temperature, RH and wind speed during April 2013 at Bode.*

4.4 Seasonal variations and correlation between ozone and CO

Generally, ozone photochemical production dominates during the daytime and higher daytime levels of ozone are observed over urban or rural regions. Some of the precursors (e.g. CO) react with OH radicals and show noontime lowest levels. Therefore, over urban and rural regions, generally it is expected that ozone and CO will have contrasting variations. Additionally, CO has rather longer life time of 1-2 months, when compared with other urban pollutants and hence it is also utilized as a tracer. Figure 4.6 shows correlated variations in ozone and CO. Highest negative correlation is seen in winter period (r^2=0.82 in January and r^2=0.71 in February) and this negative correlation reduces gradually with lowest value in May (r^2=0.12). Hourly average CO level shows a systematic decrease from its level of about 2100 ppbv in January to about 600 ppbv in June (Figure 4.5), while ozone shows opposite tendency.

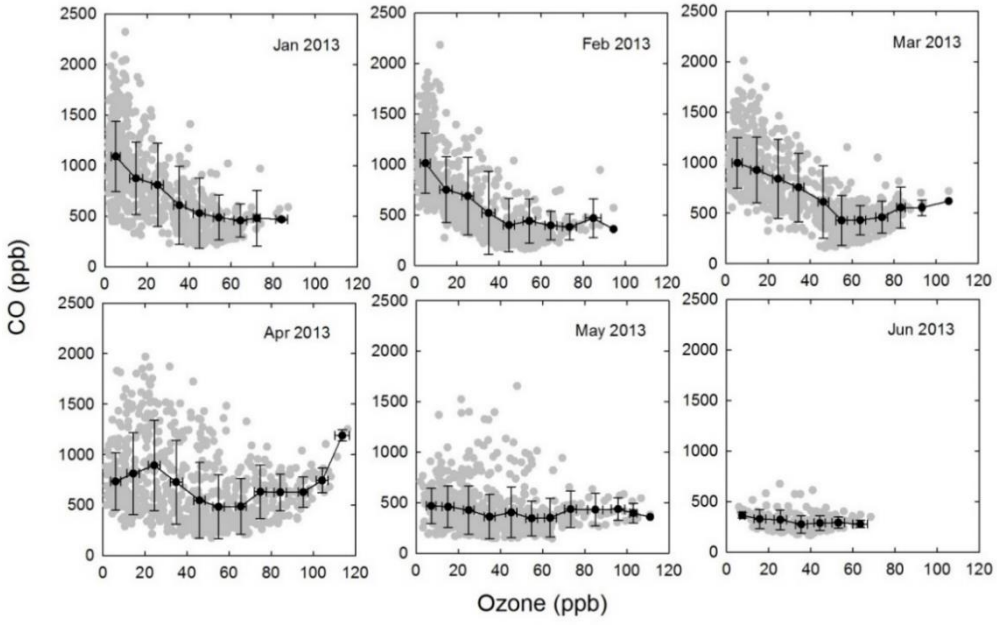

Figure 4.6: *Correlation between ozone and CO from January 2013 to June 2013 at Bode. Grey circle are hourly average data and black filled circles are 10 ppbv binned averaged with respect to ozone. Spread is one sigma value.*

Figure 4.7 shows daily variations in ozone and CO during 0300-0500 hours, 0730-0830 hours, 1300-1500 hours, and 2200-2300 hours. It is considered that 0300-0500 hours and 2200-2300 hours would provide information when photochemistry is not much active, while 1300-1500 hours can be used to understand the behavior during intense phase of photochemistry and the boundary is well evolved. The boundary layer just start evolving during 0730-0830 hours and air mass close to surface begins to mix with air at higher heights.

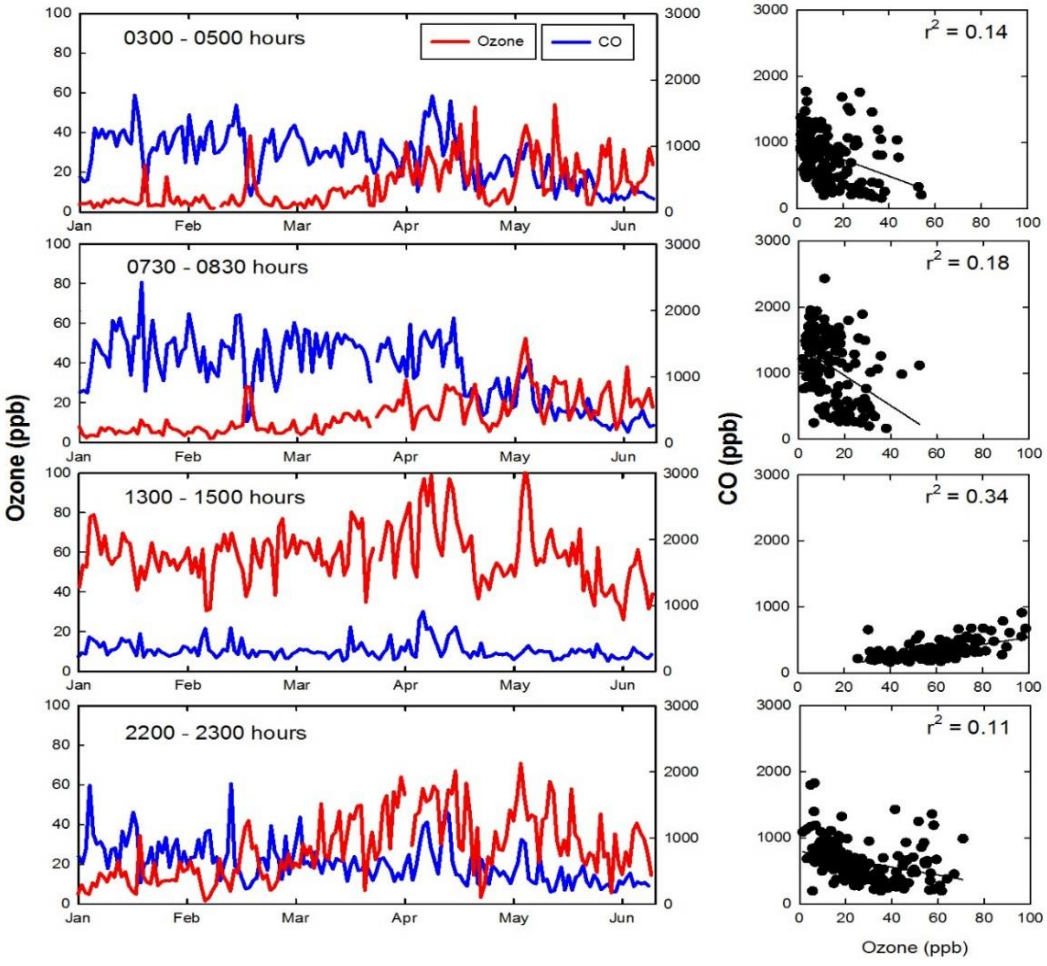

Figure 4.7: *Variations in ozone and CO during four-time periods at Bode. (right) Correlation between them is also shown.*

In general, CO levels show a decrease from January to June during 0300-0500

hours, 0730-0830 hours, and 2200-2300 hours, while CO levels do not show significant changes during 1300-1500 hours. In-contrast, ozone levels are increasing from January to May/June during all periods.

Major source of ozone in the troposphere is photochemistry among its precursors, including CO, and its lifetime is few days in lower troposphere. Noontime ozone levels are observed to be maximum about 80 ppbv during January, February and March, while ozone is observed to be up to about 102 ppbv during April and May. The noontime ozone level comes down to about 40 ppbv in June. Increase in ozone (on moving from January to May) is rather more during nighttime or early morning hours, when photochemistry is not very active. This suggests toward the enhancement in the background ozone levels. Night time (2200-2300 hours) values might have more influences of the daytime air mass when compare to the early morning hours. Hence, probably, average ozone values during early morning periods (13-14 ppbv) would represent background ozone levels (Table 4.2).

Figure 4.7 also shows correlation between ozone and CO. Week negative correlation is seen during early morning (0300-0500 and 0730-0830 hours) or night hours (2200-2300 hours), while a slight positive correlation is seen during noon period (1300-1500 hours). Generally, high altitude [*Kaji et al.,* 1998; *Tsutsumi and Matsueda,* 2000; *Naja et al.,* 2003; *Sarangi et al.,* 2014] and cleaner site (e.g. Island sites) [*Pochanart et al.,* 1999] show a positive correlation between ozone and CO. It is observed that CO average values during early morning hours are higher than those night hours (Table 4.2). It was suggested by *Pandey and Prinn,* [2009] that the morning higher CO values could be due to recirculation of pollutants emitted

the night before. The Boundary layer is well mixed and wind speed is higher and generally it is westerly during noontime. This will reduce the direct sampling of air-mass from its immediate emission sources. Therefore, probably CO mixing ratio (325.4 ± 98.3 ppbv) during 1300-1500 hours (Table 4.2) could be considered as background levels for the Bode region.

Table 4.2: *Average (avg), standard deviation (std), maximum (max), minimum (min) and daily counts of ozone and CO values and* r^2 *values during four time periods.*

Time period		0300-0500 hr	0730-0830 hr	1300-1500 hr	2200-2300 hr
Ozone	Avg	13.1	13.9	58.9	27.8
	Std	1.2	1.7	10.0	4.7
	Max	54.0	52.5	102.4	70.8
	Min	1.8	2.0	25.9	1.4
	Counts	158	158	158	158
CO	Avg	833.8	1103.2	325.4	626.1
	Std	292.6	380.3	98.3	304.6
	Max	1770.0	2430.0	910.0	1820.0
	Min	150.0	160.0	160.0	190.0
	Counts	159	158	159	158
R^2		0.14	0.18	0.34	0.11

In general, the CO levels decreases from winter to spring whereas, an increase in ozone levels was observed. The average CO levels in the morning are higher during winter months (January and February) than in late spring season. The use of biofuels and biomass burning is more in winter to keep warm. This leads to higher emission of CO that gets accumulated overnight resulting in higher CO levels. During spring months, the abundance of solar radiation induces the photo oxidation

of CO via OH. The ozone level however, shows a broader peak in spring with slightly higher (~62 ppbv) values when compared with its levels during winter (~54 ppbv) noontime. Apart from the local photochemical production, the regional air pollution can also influence the levels of ozone at Bode. One example of regional scale pollution influencing ozone and CO levels at Bode and IGP will be discussed in section 4.6.

4.5 Intercomparision with the Indian sites

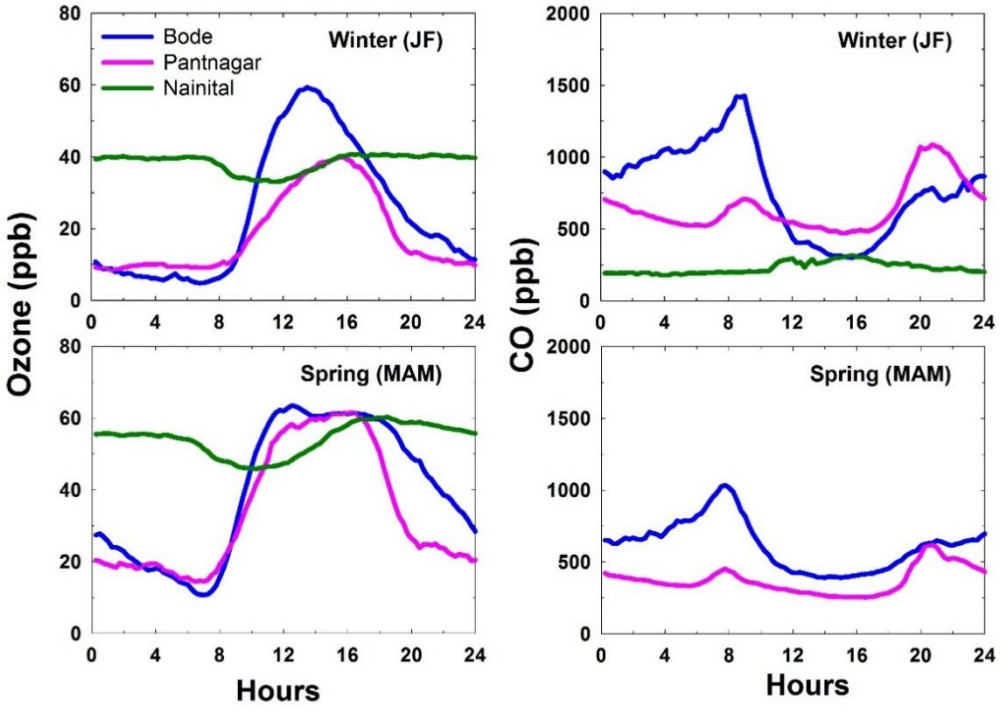

Figure 4.8: *Seasonal variations in diurnally averaged ozone and CO at Bode, Pantnagar and Nainital. During spring season CO measurements were not available*

Here, simultaneous observation of ozone and CO made at Nainital and Pantnagar are discussed (Figure 4.8). The diurnal pattern in ozone and CO are similar at Bode

and Pantnagar however, different variations are observed at Nainital, which, being a relatively remote and high altitude site do not show any daytime buildup or nighttime losses in ozone. The levels of these gases, however, are different with Bode showing higher values than Pantnagar in both the seasons. The amplitude in ozone is somewhat higher during winter when compared to spring.

Shorter duration of solar heating during winter leads to weaker dynamical processes including convective mixing of pollutants, which in turn confines the pollutants near to the surface. Additionally, the Kathmandu valley is isolated inside the Himalayas and the only way for pollutants to reach here is either via upslope flow of polluted air masses through the mountain valleys, or arrival of polluted regional air masses from the air aloft. Thus, the wintertime higher levels of ozone and CO at Bode are likely not influenced by the IGP pollution. Further similar trapping of pollutants during winter season are also reported by previous studies done over this region [*Panday and Prin,* 2009]. However, intense heating and stronger convective mixing could induce the IGP outflow to influence this valley region during spring. One event of regional scale pollution influencing levels of ozone and CO at Bode is discussed in section 4.6.

The rate of change of ozone during morning and evening hours can be used as an indicator of chemical environment (rural or urban) over a site [*Naja and Lal.*, 2002]. The distributions at an urban site is nearly symmetric during morning and evening, however, it is asymmetric with slower changes occurring during evening time at a rural site. Ozone production is strongly dependent on amount of precursor gases and available sunlight. On the contrary, evening time ozone loss depends mainly

upon its titration with NO, apart from surface deposition.

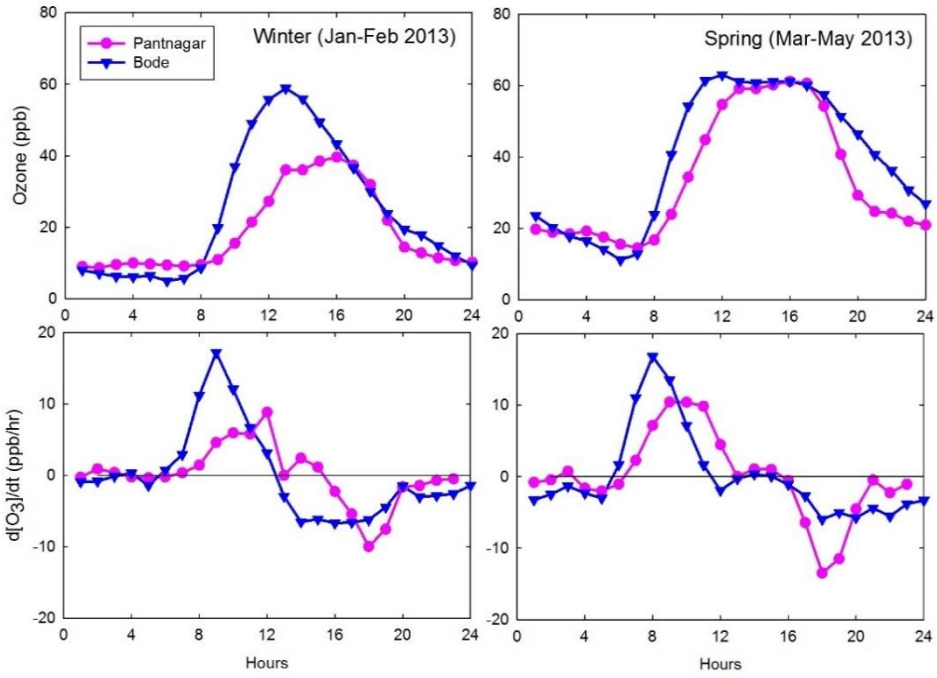

Figure 4.9: *(Top panel) Diurnal variation in ozone during winter and spring 2013 at Bode (blue) and Pantnagar (Pink). (Bottom panel) Diurnal varition in rate of change in ozone during the same period.*

Wintertime rate of ozone increase in morning hours is much higher at Bode (about 17 ppbv/hour), when compare to Pantnagar (about 9 ppbv/hour) (Figure 4.9). This suggests a rapid ozone buildup at Bode than at Pantnagar. During the spring, ozone decrease rate is lower at Bode (5-6 ppbv/hour) when compare to the decrease rate at Pantnagar (about 14 ppbv/hour). This suggests rather slower ozone loss at Bode via NO titration, indicating somewhat rural environment in Bode during spring. Additionally, faster westerly winds flush the pollutants away from the valley every day, the rate of ozone destruction during evening time is slower, however due to overnight accumulation of precursor gases in nocturnal boundary layer, the next morning ozone levels again builds up. Therefore, slower decrease rate in evening

time ozone and lower value of CO during spring, confirms somewhat lesser contribution of local pollutions in spring ozone enhancement in the valley. Regional contribution in this regards cannot be ruled out.

4.6 Influences of springtime northern Indian biomass burning

Every year northern Indian biomass burning emits large quantities of trace gases and aerosols and significantly affect regional distribution of these trace species [*Kumar et al.*, 2010; *Bhardwaj et al.*, 2016].

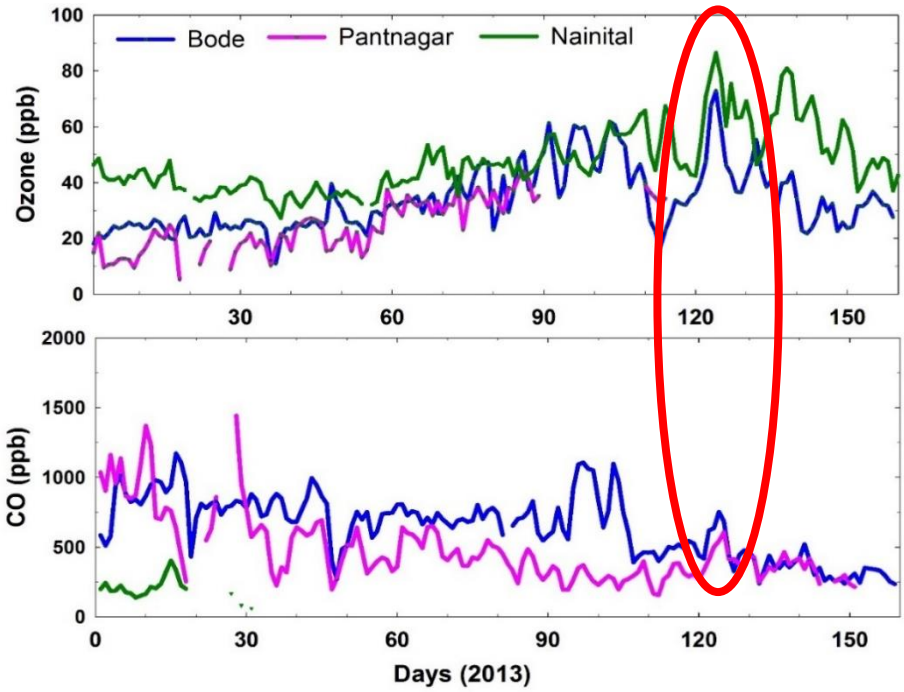

Figure 4.10: *Time series of ozone and CO observations over the three sites viz., Bode, Nainital and Pantnagar. Red oval indicates the enhancement during first week of May.*

During the first week of May, simultaneous increase in ozone and CO levels are observed at Bode, Pantnagar and Nainital (Figure 4.10). The global model

(MOZART) simulations also showed about two-fold increase CO levels at 992 hPa. OMI tropospheric column NO_2 also showed enhancement but with somewhat lesser in magnitude (Figure 4.11).

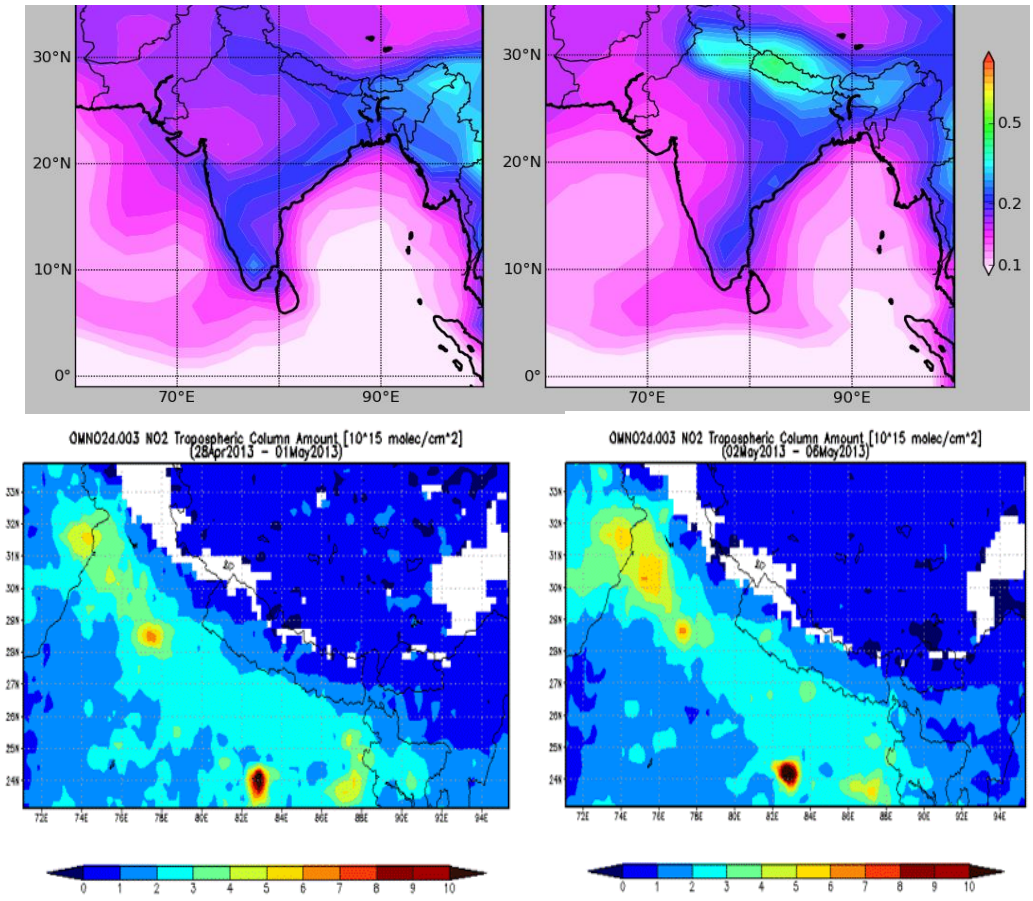

Figure 4.11: *(Top panel) MOZART CO during (left) 1 May and (right) 4 May 2013 at 992 hPa. (lower panel) OMI tropospheric column NO_2 during these two days.*

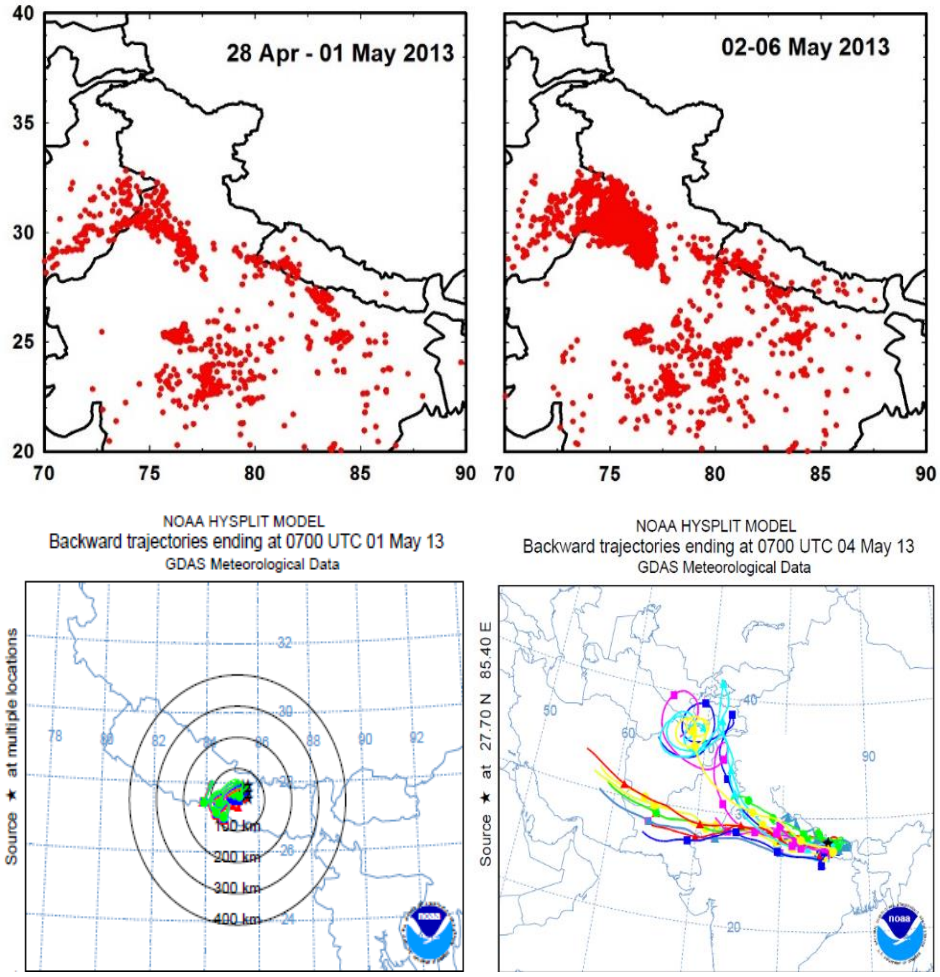

Figure 4.12: *(top Panel) MODIS fire counts (left) before (28 Apr – 1 May) and (right) during (2-6 May) the event period. (lower panel) Back-air trajectories at Bode on 1 and 4 May, 2013.*

MODIS derived fire location showed 256% increment in fire counts over the Punjab region in IGP during 2-6 May, 2013 when compared with few days prior (28 Apr – 1 May, 2013) (Figure 4.12). Further, HYSPLIT backward trajectory analysis shows that the air masses arriving at Bode were circulating over Nepal region (left panel Figure 4.12) before the event day. However, during the high fire period the air

masses were coming from the active fire region to Bode. The balloon borne ozone profiles from Nainital also confirmed significant enhancement in ozone in the lower troposphere as observed in balloon borne observations made on 9 May, 2013 when compared with ozone profile on 1 May, 2013 (Figure 4.13). Ozone levels are higher by 15.9 ppbv in 2-4 km region and 13.7 ppbv in 4-6 km region. Such events are generally observed during spring season, when influences of regionally polluted air masses could travel to long distances.

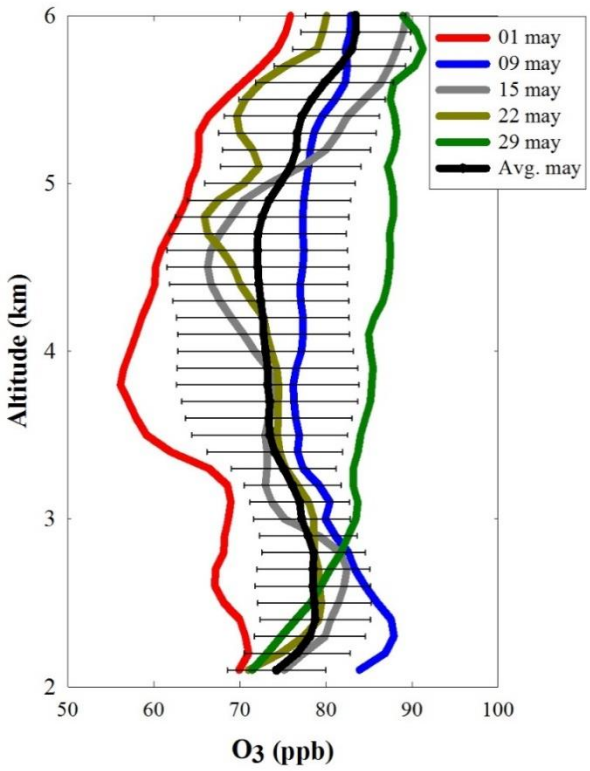

Figure 4.13: *Vertical ozone distribution at Nainital in lower troposphere (2-6 km) during May 2013.*

4.7 WRF-Chem simulations

The high resolution WRF-Chem simulations were used to compare and analyze observed variability in meteorological parameters, ozone and CO. The detailed

model setup is already discussed in chapter 2. The model run was conducted using a three domain set up with grid spacing of 9, 3, 1 km, respectively (Figure 4.14).

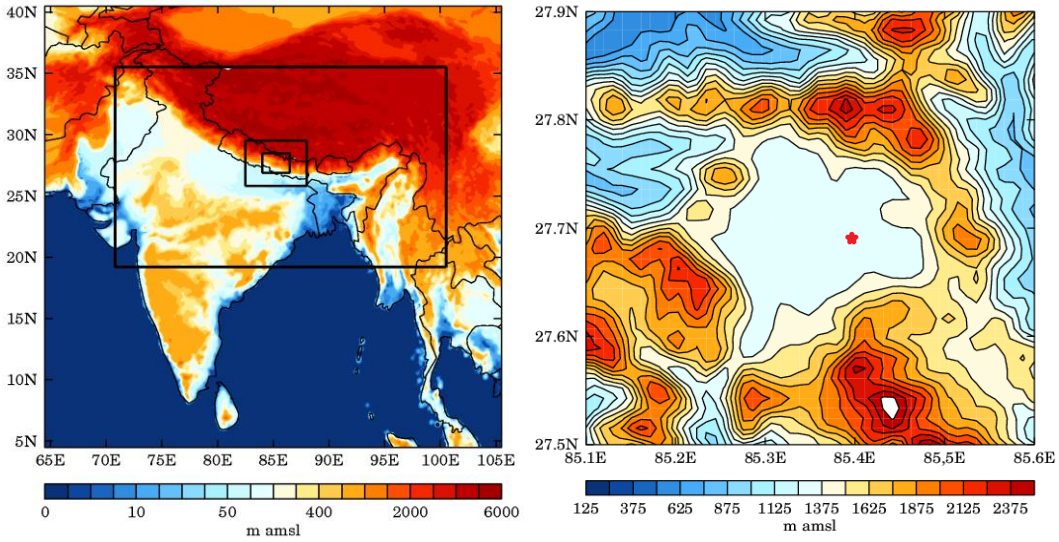

Figure 4.14: *Three nested domain configuration of WRF-Chem is shown with three nested black boxes. (left) Parent domain is 9 km and remaining inner domains are 3 and 1km respectively. (right) The topography map of the Kathmandu valley at 1 km resolution with Bode represented as red star.*

Orography of the Kathmandu valley was not sufficiently resolved in 9 km resolution model run. Hence, 3 km resolution is used for meteorology and chemistry variables. The higher resolution improved diurnal variations. Model simulated wind speeds and wind direction showed better agreement with observations, when compared with temperature and RH. Differences in wind speed are less than 1 m/s during entire day at 3 km resolution model run (Figure 4.15). Model simulated temperature and RH showed improvements in 3 km run during daytime when compared with 9 km. But diurnal amplitude does not improve in case of temperature and RH.

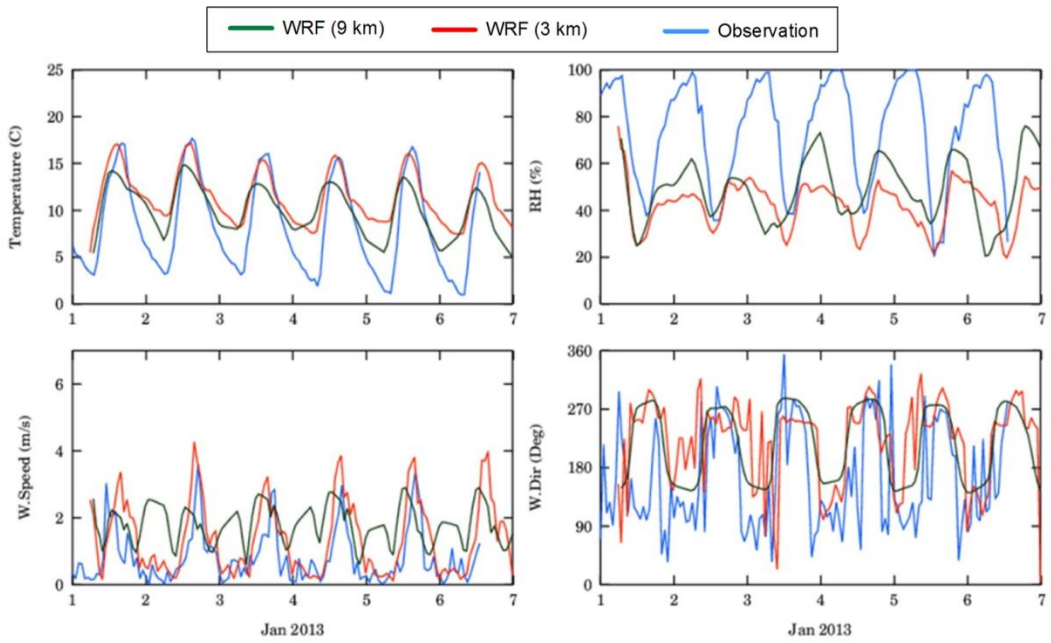

Figure 4.15: *Comparison of observed meteorological parameters (temperature, RH, wind speed and wind direction) with WRF-Chem model simulations at 9 and 3 km resolution at Bode.*

The daytime (11-16 hour) temperature shows very small (~1^{o}C) differences between WRF model and observational data, however large difference (4-8^{o}C) are seen during the night time. Similar differences in relative humidity (RH) are also observed with daytime differences of about 10% but greater differences (40-60%) during nighttime (Figure 4.15). There was dense fog during early morning hours in January that is leading to show very high RH (about 95%) and model setup was unable to simulate fog in the valley.

Figure 4.16 shows comparison between observed and model values of ozone and CO during daytime (1100-1600 hours). Model is over predicting ozone, while it is under predicting CO values. Modeled (3 km) ozone values are higher by 4 ppbv to 32 ppbv than the observations. While, modeled (3 km) CO values are as low as 173

ppbv. The reason for this much difference in ozone could be due to less NO levels in the model as compared to levels reported by previous studies in the valley [*Yu et al.,* 2009]. Nitric oxide (NO) leads to the ozone loss in evening and night time thereby reducing its levels and then during daytime it aids in ozone production via VOCs and CO in the sunlight.

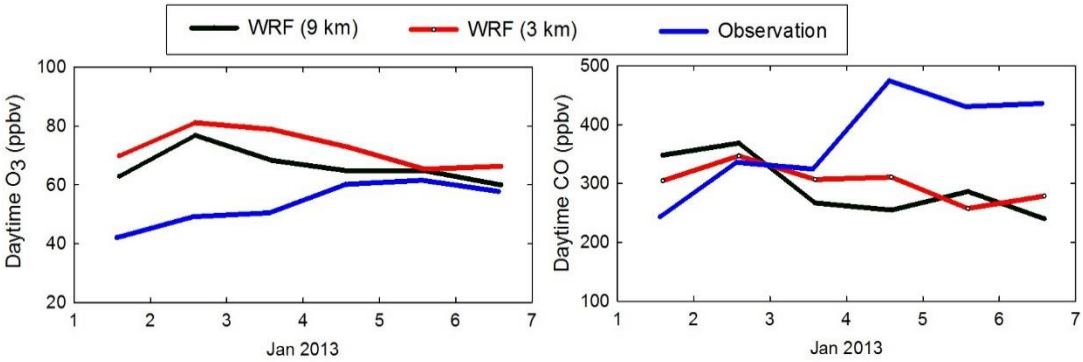

Figure 4.16: *Daily variations in ozone and CO between WRF-Chem at 9 and 3 km resolution and observations during daytime (11:00-16:00 hours).*

To improve the model setup, changes are made that includes, (1) increasing vertical resolution in the lower troposphere with three levels in night-time boundary layer, (2) using newer MODIS land use/land cover data. Over supersite Bode the improvements made in model setup had very small impact. However, the variations of these parameters over a mountain site Nagarkot (1898m amsl, east of Bode) were in good agreement (Figure 4.17), where the differences in temperature and RH are lesser than 2^{o}C and 15% even during nighttime.

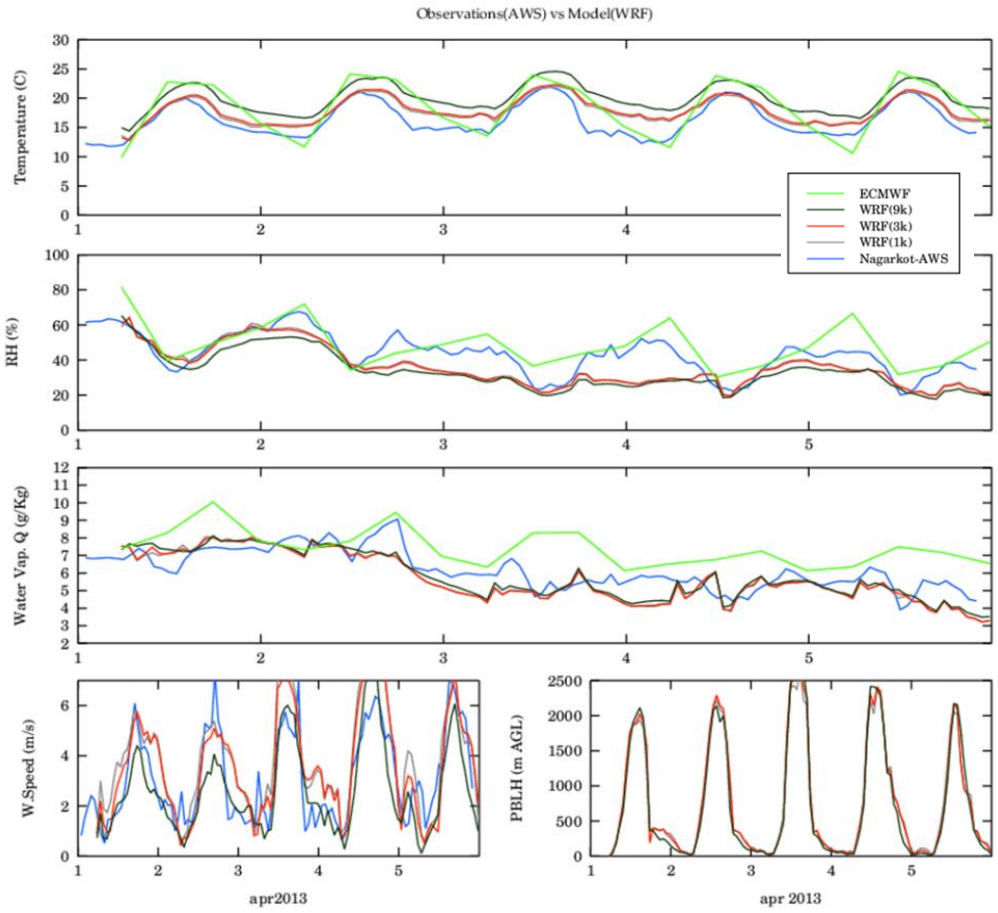

Figure 4.17*: The diurnal variations in meteorological parameters from WRF-Chem at 9, 3 and 1 km resolution at Nagarkot (1898m amsl) during 1-5 April 2013. ECMWF meteorological data is also shown.*

Overall model is able to capture the daytime levels of CO and meteorological parameters however a strong positive bias is observed in ozone. There is a need for further improvement in model setup and various physics schemes should be tested to further tune the model for complex topography. Further there is a need for high resolution input emission inventory over the region.

4.8 Conclusions

Simultaneous surface measurements of ozone, CO and meteorological parameters were made at Bode, Pantnagar and Nainital. The diurnal variations at Bode were typical of a polluted site with sharp day time build-up in ozone and CO having higher levels during morning and evening hours. The average early morning CO levels were higher during winter than spring. However, daytime ozone levels were slightly higher during spring when compared with those during winter. CO levels and its diurnal amplitude are higher at Bode as compare those at Pantnagar, particularly in winter. These higher levels at Bode are suggested to be due to local sources during winter season with some contributions from regional pollution during spring season. Simultaneous enhancement in ozone and CO are observed at Bode, Pantnagar and Nainital during a regional pollution event in the first week of May 2013. These enhancements are influenced by the biomass burning. WRF-Chem simulations showed large night time variations in meteorological parameters at Bode. The daytime differences in temperature and RH between model and observations are ~1^{o}C and 10% respectively. Model was able to capture winds very well. Modeled ozone is somewhat overestimating while it is underestimating CO values. There is scope for further improvement in model, particularly with high resolution of emission inventories. Different land use schemes needs to be tested and applied over this region of complex topography.

Chapter 5

Balloon Borne Observations of Ozone Over Nainital

Apart from the surface based observations, it is also important to observe the vertical distribution of trace gases. As mentioned in chapter 1, the downward transport of ozone from stratosphere is one of the major contributing factor to the springtime maximum of surface ozone observed at a number of sites, particularly mountain site across the globe [e.g. *Oltmans,* 1981; *Levy et al.,* 1985; *Logan,* 1985; *Cristofanelli et al.,* 2010]. Generally, intrusion of stratospheric air occurs mainly at extratropical latitude and associated with tropopause folding events near the jet streams [*Danielsen,* 1968]. The annual ozone transported from stratosphere to troposphere can be estimated using measurements of conserved tracers or by general circulation models but there is quite uncertainty in this.

Heating at the surface induces the vertical lifting and mixing of trace gases. Such vertical lifting of trace gases from the boundary layer to the free troposphere in the

warm air ahead of the cold fronts further induces it and known as frontal lifting. This process plays an important role in exporting the Asian air-mass to western Pacific [e.g. *Bey et al.,* 2001] and also in transporting from Northern America [*Milne et al.,* 2000]. Additionally, ozone radiative forcing at higher altitude, e.g. the tropical troposphere is much higher (0.4 W m^{-2}) [*Portmann et al.,* 1997]. Therefore, it is important to observe vertical profiles of trace gases to better understand the downward transport, vertical lifting and warming at higher altitudes.

The vertical observations of ozone using balloon borne sensors are severely limited over the Indian subcontinent. Several satellite based observations have indicated large spatial variability in tropospheric column ozone distribution over the Indian subcontinent with highest levels across IGP region [*Fishman et al.,* 2003]. The observations of vertical ozone distribution in India were initiated in 1960s by Indian Meteorological Department (IMD) using Indian ozonesondes [*Sreedharan,* 1968] and these data were also used to estimate the ozone trends [*Saraf and Beig,* 2004]. These IMD observations were made using Indian version of electrochemical sensors (Brewer-Mast type having single cell), designed by IMD and some concerns were raised about these sensors [e.g. *Logan,* 1999]. Over the globe, balloon-borne ozone observations were initiated in 1960s or 1970s and electrochemical concentration cell (ECC) type [*Komhyr,* 1969] of sensor is used at several places. Japanese group also developed their own version of ECC type ozonesonde.

Apart from ozone observations made by IMD, vertical distribution of ozone is also observed over Ahmedabad [*Srivastava et al.,* 2012, *Lal et al.,* 2013, 2014], over the

Indian Ocean [*Srivastava et al.,* 2011] and IGP [*Gupta et al.,* 2007] using ECC sonde, supplied by Environmental Scientific (EN-SCI), USA. The vertical ozone measurements of ozone over the Himalayan region was also initiated from Nainital and one year of observations were reported by *Ojha et al.,* [2014]. However, all these measurements were for a limited time period with no continuous and long term observations. These measurements of vertical distribution of ozone and meteorological parameters are essential to understand the role of various processes controlling the ozone distribution over this region. Further this data can be used to validate satellite based datasets over this region.

5.1 Vertical distribution over Nainital

In light of above, extended observations of vertical ozone distribution and meteorological parameters were made from ARIES, Nainital (79.45^{o}E, 29.37^{o}N, 1958 m amsl) and five years (2011-2015) of analysis are presented here. Since the site is away from any major anthropogenic emission sources it is considered as a better regional representative site in the northern Indian region [e.g. *Kumar et al.,* 2010; *Kumar et al.,* 2011]. The site is surrounded by sharply peaking mountains in the north and east directions while low altitude mountains (altitudes < 1000 m) are located in the south and west. The Nainital city is about 2 km northward of this site and there are no major industrial activities in the city. The city is sparsely populated with nearby cities, Haldwani, Kashipur and Rudrapur about 20 to 40 km away. These cities have some small-scale industries. Further this site is north of highly polluted IGP region. Since its initiation, so far total 203 flights are conducted. Out of these, radiosonde had problem during five flights and ozonesonde had problem

during eight flights. Hence, radiosonde data are used from 198 flights and ozonesonde data are used from 195. Detailed monthly and interannual information about these launches are provided in Table 5.1. These launches also include one flight conducted at Pantnagar site on 13 April 2011. The location of balloon launch was relocated to the ST Radar site within ARIES campus in February 2015.

Table-5.1: *Number of the successful balloon launches from ARIES in different months during 2011-2015. More details of each flight are listed in Annexure-I.*

	2011	2012	2013	2014	2015	Monthly Total
Jan	2	2	5	5	2	16
Feb	3	4	4	2	1	14
Mar	3	4	4	4	2*	17
Apr	4	4	4	4	2	18
May	6	8	5	5	1	25
Jun	4	4	3	3	2	16
Jul	3	1	5	3	1	13
Aug	5	2	4	3	1	15
Sep	4	2	4	2	0	12
Oct	4	5	5	3	1*	18
Nov	5	4	4	2	2	17
Dec	3	3	4	2*	5	17
Annual Total	48	45	51	38	21	198

** Denotes successful flight but no ozone data*

Efforts are made to keep balloon launch time at about 1200 hour IST. However, it

varies (Figure 5.1) due to clearance permission from local air traffic controller. In general, the launch time has been within a time window of about three hours around 1200 hour. The details about the experimental setup including ozonesonde and radiosonde is described in chapter 2. The raw data obtained from PV7 post processing software is first filtered using 2-sigma filter from mean value and then is averaged to 100 m binned data, which are used for further analysis.

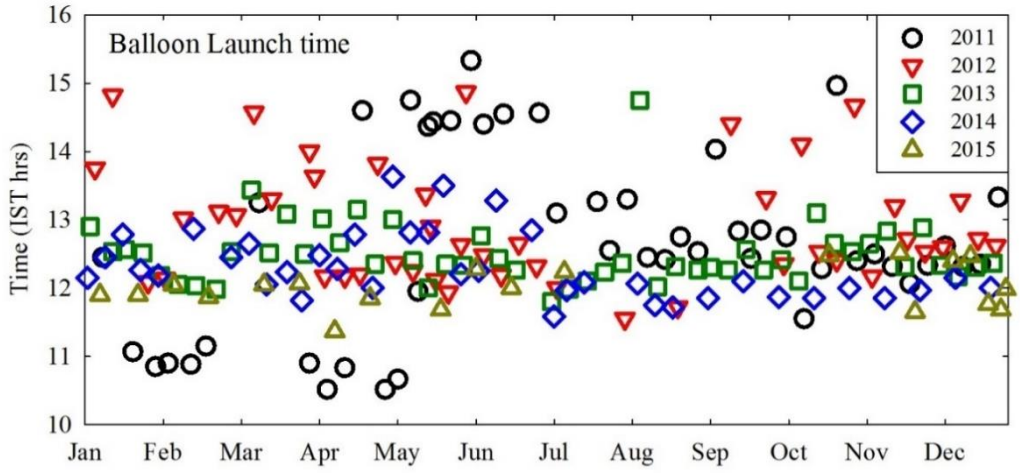

Figure 5.1: *Launch time for all balloon flights conducted from Manora Peak during 2011-2015.*

5.2 Variations in the meteorological parameters

The synoptic winds over this region are shown using back air trajectories, those indicate a distinct seasonal cycle (Figure 5.2). The air masses circulate over the northern Indian region during spring and autumn seasons prior to reaching the site. However, the monsoon circulation brings cleaner marine air masses during summer season and westerly and northwesterly winds prevail during winter season.

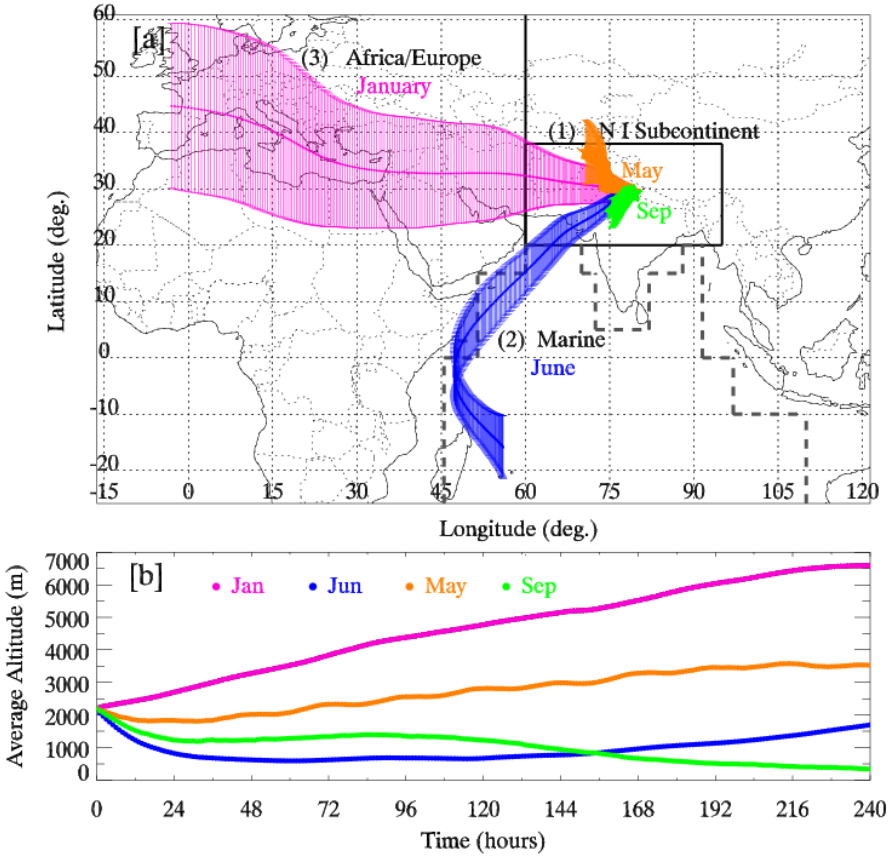

Figure 5.2: *[a] Most probable back-air trajectories (10 days) at Nainital showing influence of westerly winds during winter (January) and southwesterly during summer/monsoon (June). Late spring (May) and early autumn (September) are the changeover periods and the winds mostly circulate over the Indian Subcontinent. Panel [b] shows average altitudes at which these trajectories have been traveling. (Adapted from Kumar et al., 2010).*

Maximum solar radiation is observed during spring season with lowest levels in winter months. The relative humidity and rainfall is maximum during monsoon months of June-September. The detailed discussion about general meteorology and the synoptic winds over this region can be seen elsewhere [e.g., Kumar *et al.*, 2010; *Ojha et al.*, 2014]. The next subsection describes vertical distribution of meteorological parameters over Himalayan region.

5.2.1 Temperature and relative humidity

Radiosonde observations are used to obtain vertical profiles of temperature and relative humidity. The monthly variations in temperature profile during years 2011-2015 are shown in the Figure 5.3.

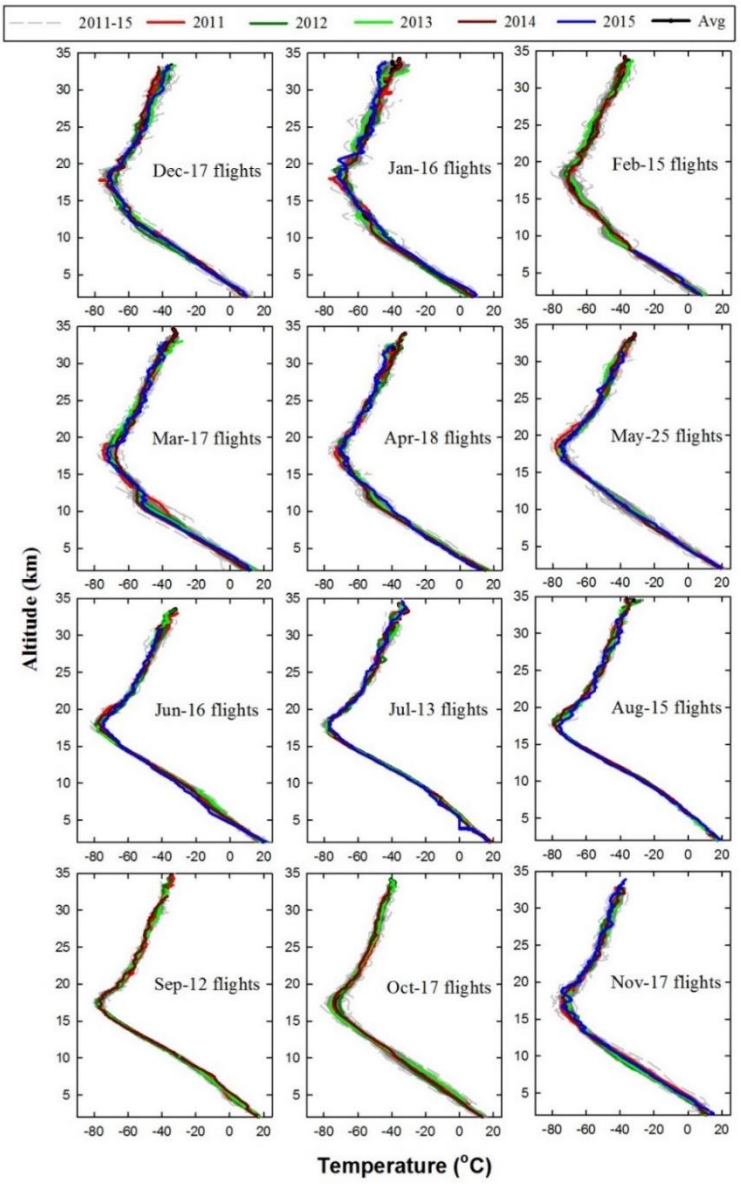

Figure 5.3: *Monthly variations in vertical distribution of temperature during years 2011-2015. Average profile for five years (2011-2015) is shown by black color and its one sigma variation is shown by filled grey color. Color lines are average profiles for individual year and dashed grey lines are for individual flight. Winter, spring, summer-monsoon and autumn seasons are represented by Dec-Jan-Feb, Mar-Apr-May, Jun-Jul-Aug and Sep-Oct-Nov, respectively.*

The near surface temperature (2.5 km amsl) is highest during the summer-monsoon season (15.7 ± 1.5 ^{o}C) with June being the warmest month (16.5 ± 1.9 ^{o}C). The lowest temperatures were observed during winter season (5.6 ± 3.1 ^{o}C), with February being the coldest (4.5 ± 3.2 ^{o}C). However, the maximum variability (1σ value expressed as percentage) observed during winter season is the highest (55%) as compared to spring (34%), summer (10%) and autumn (25%) seasons. The seasonal variation of temperature at 10 km altitude is also similar to that near surface, however the maximum and minimum temperatures were observed during months of July (-25.1 ± 1.0 ^{o}C) and January (-45.8 ± 4.2 ^{o}C) respectively.

The temperature variations at 15 and 20 km peaks at different months than lower and middle troposphere. The maximum temperatures at 15 and 20 km are observed during the months of April (-61.9 ± 3.1 ^{o}C) and December (-64.2 ± 2.0 ^{o}C), respectively. The minimum temperatures observed at these altitudes were in November (-67.2 ± 2.6 ^{o}C) and May (-69.4 ± 3.6 ^{o}C) respectively. The temperature profiles observed during winter and early spring showed inversions in middle troposphere which could be attributed to presence of multiple tropopause. The tropopause break events and downward transport of ozone rich air from stratosphere is also more during these periods. These features were observed almost every year and some of the cases of downward transport are discussed in section 5.4. The monthly vertical profiles of relative humidity (RH) during the years 2011-2015 are shown in the Figure 5.4.

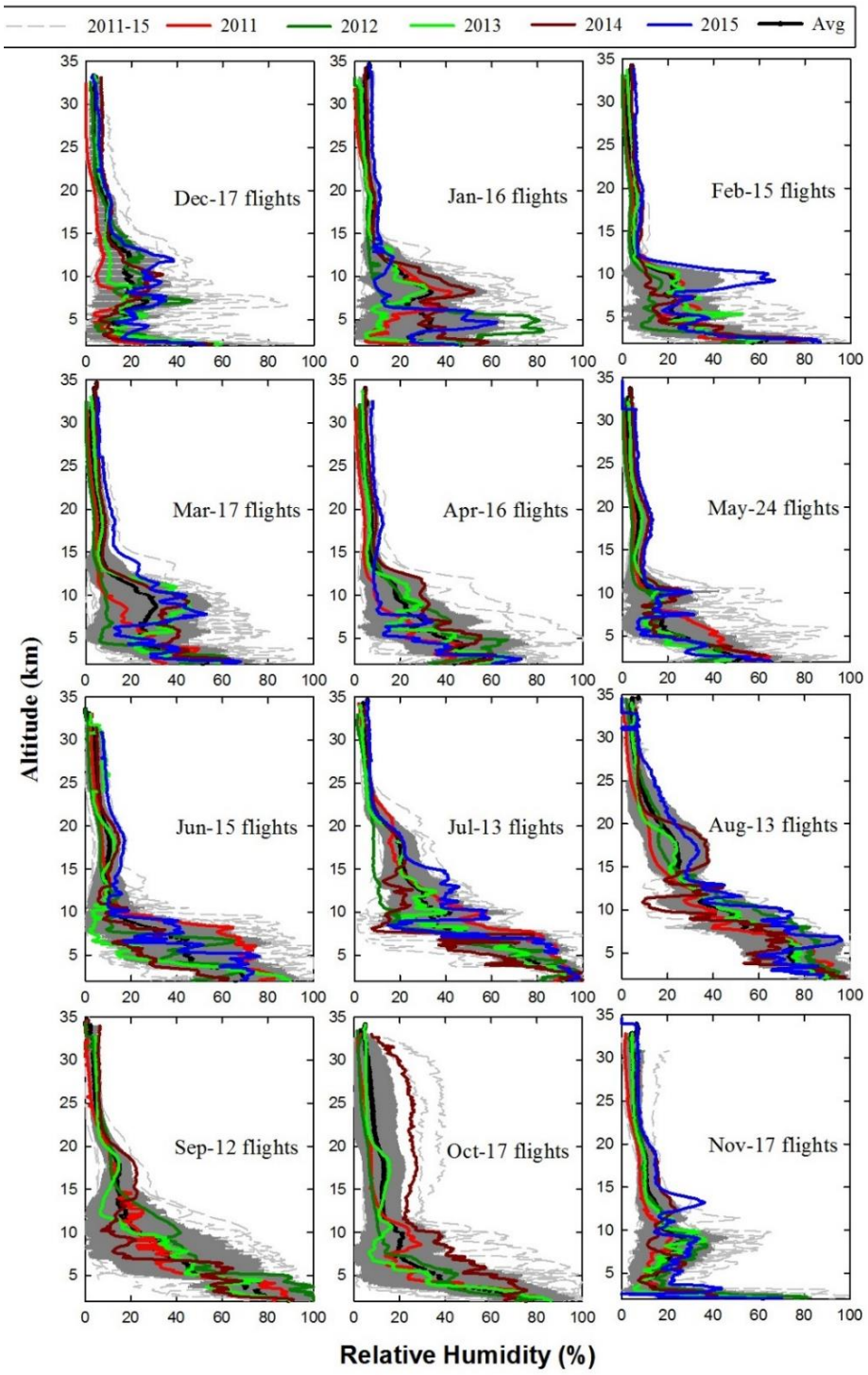

Figure 5.4: *Monthly variations in vertical distribution of relative humidity (RH) during years 2011-2015. Average profile for five years (2011-2015) is shown by black colour and its one sigma variation is shown by filled grey colour. Colour lines are average profiles for individual year and dashed grey lines are for individual flight. Winter, spring, summer-monsoon and autumn seasons are represented by Dec-Jan-Feb, Mar-Apr-May, Jun-Jul-Aug and Sep-Oct-Nov, respectively.*

Apart from seasonal variations in RH, large variations were also observed during each flights. The near surface RH was maximum during summer-monsoon season (84.0 ± 17.9 %) with highest levels observed during July (93.6 ± 6.8 %). The minimum RH was observed during winter season (41.5 ± 27.6 %) with December being the driest (30.0 ± 22.0 %) month. Similar to temperature variations, the maximum variability is observed during winter season (67%). The maximum RH (>80%) during the late summer-monsoon (July-September) indicates the prevailing monsoon circulation over this region. .

5.2.2 Wind speed and direction

The monthly vertical profiles of wind speed observed during 2011-2015 are shown in Figure 5.5. The wind speeds are strongest in the middle tropospheric region during all seasons except in monsoon period (late June-early September). The near surface winds are strongest during spring season (6.0 ± 3.0 m/s) with highest speeds in month of May (7.3 ± 2.6 m/s) and weakest during autumn season (4.2 ± 3.5 m/s) with slowest winds in month of October (3.1 ± 2.5 m/s). In contrast to the lower troposphere, winds are highest during winter (62.6 ± 14.5 m/s) in the middle troposphere (12 km amsl) with wind speeds reaching up to about 94 m/s during month of February, while it is slowest during summer-monsoon season (12.9 ± 8.0 m/s). The strong winds present in the middle-upper troposphere region are observed every year during winter months. These high wind speeds are suggested to be due to sub-tropical jet stream passing over this region during this season. These stronger winds could transport pollutants from far regions to the pristine Himalayas.

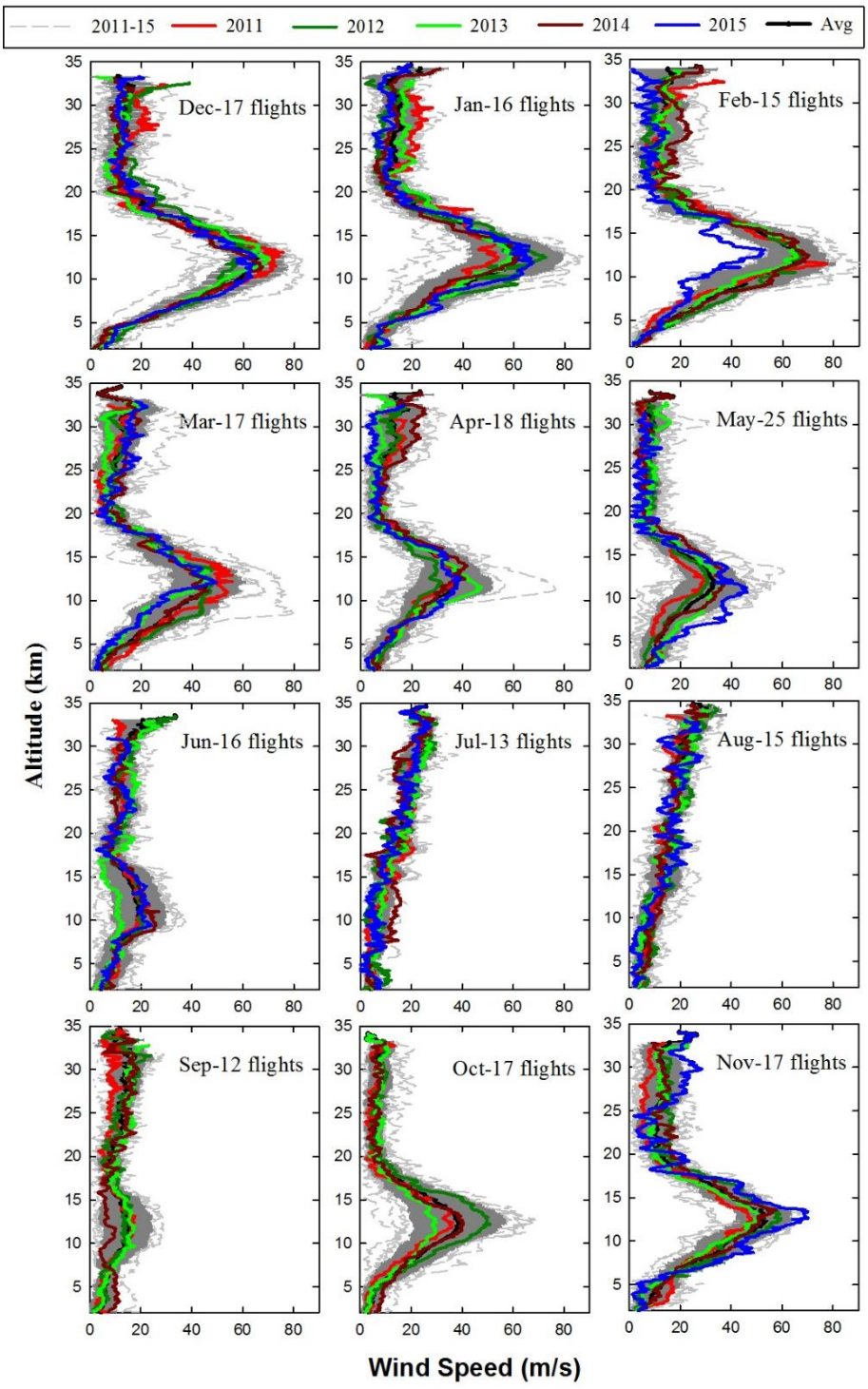

Figure 5.5: *Monthly variations in vertical distribution of wind speed during years 2011-2015. Average profile for five years (2011-2015) is shown by black colour and its one sigma variation is shown by filled grey colour. Colour lines are average profiles for individual year and dashed grey lines are for individual flight. Winter, spring, summer-monsoon and autumn seasons are represented by Dec-Jan-Feb, Mar-Apr-May, Jun-Jul-Aug and Sep-Oct-Nov, respectively.*

Apart from high wind speeds during winter season the presence of other dynamical processes such as multiple tropopause/stratosphere troposphere exchange processes are also observed over this region and are discussed in the subsequent section.

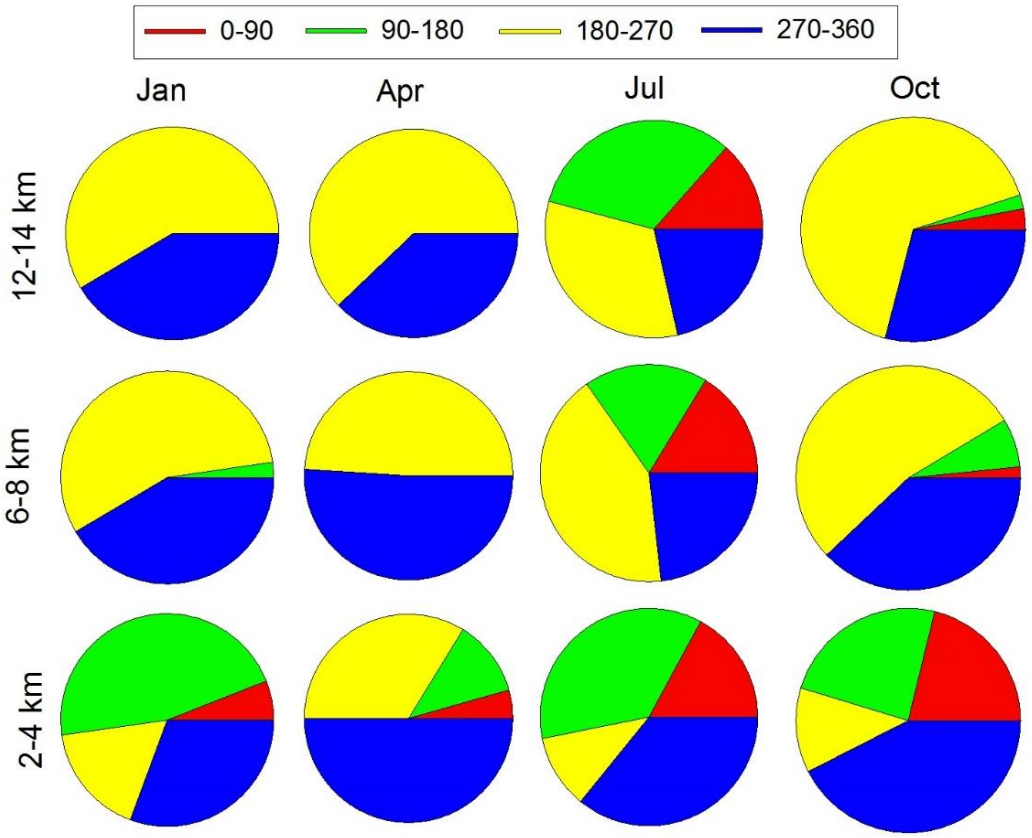

Figure 5.6: *The mean seasonal variations in wind direction at 3 different altitude levels in the troposphere as the percentage occurrences in four quadrants (0-90, 90-180, 180-270, 270-360) during year 2011-2015. Here January, April, July and October are considered as seasonal representative for winter (DJF), spring (MAM), summer-monsoon (JJA) and autumn (SON), respectively.*

The wind direction at three altitude levels (2-4 km, 6-8 km and 12-14 km) are shown (Figure 5.6) as percentage occurrences in four quadrants during 2011-2015. The winds are primarily north westerly (42-50%) during April (spring) and October (autumn), however they are mainly south easterly (36-46%) during January (winter) and July (summer-monsoon) in the lower troposphere (2-4 km). On the contrary, at higher altitudes (6-8 km and 12-14km) the majority of winds are south westerly (32-66%) followed by north westerly (21-51%) in all the seasons. The only exception being summer season when the south easterly (18-32%) winds also prevail over this region.

5.3 Vertical distribution of ozone

Vertical distribution of ozone during twelve months in years 2011-2015 period is shown in Figure 5.7. In general, the maximum variability in the lower troposphere are observed during spring and summer-monsoon seasons whereas, at higher levels (8-18 km) maximum variability is in winter and spring. The near surface ozone shows highest levels during spring season in the month of May (90.6 ± 13.2 ppbv) with August (38.7 ± 8.7 ppbv) in the summer monsoon period having the lowest ozone levels (Figure 5.8). However, the summer-monsoon season shows highest variability of 44% (1-sigma expressed as percentage) and minimum variability is in winter (~11%).

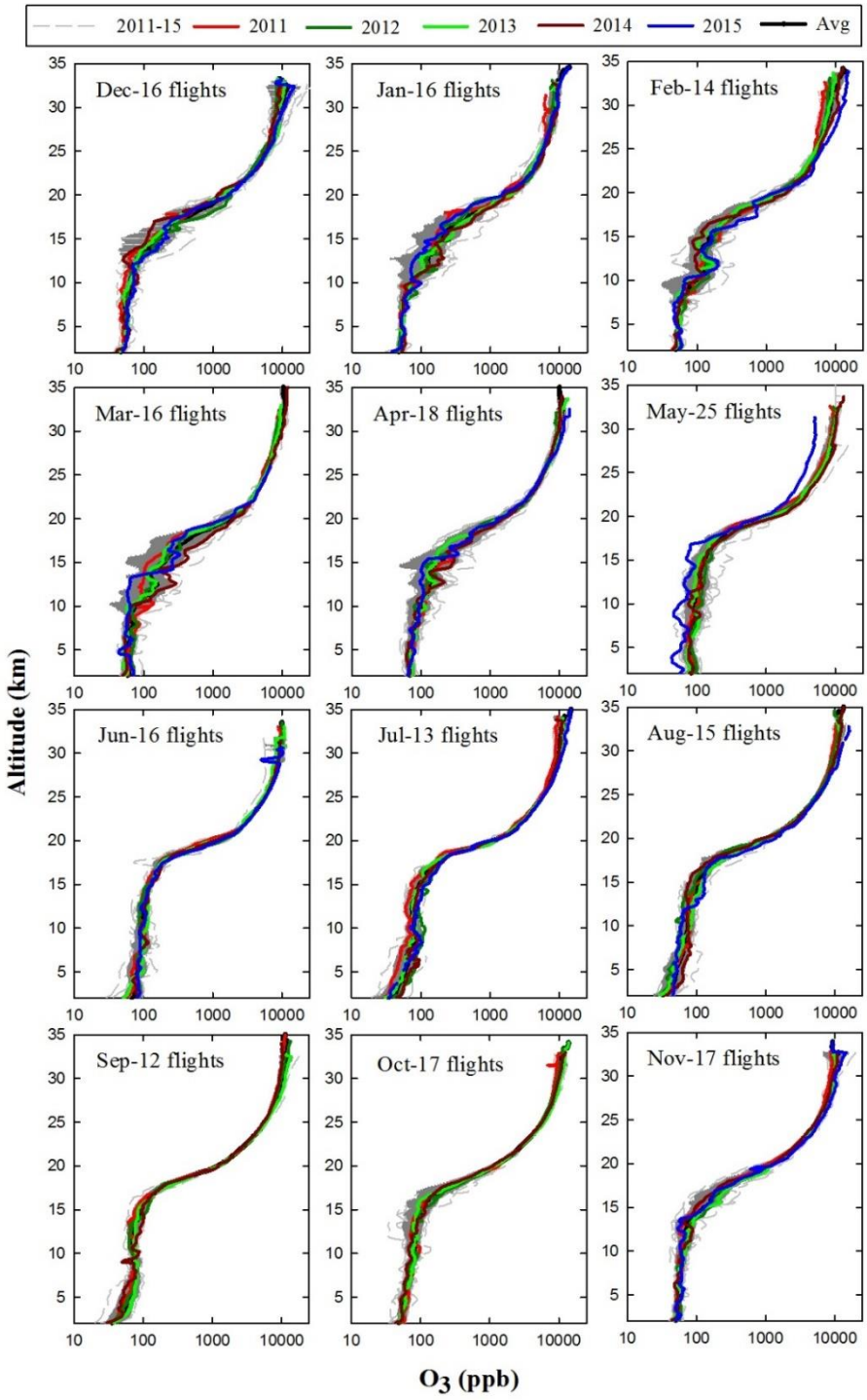

Figure 5.7: *Monthly variations in vertical distribution of ozone during years 2011-2015. Average profile for five years (2011-2015) is shown by black colour and its one sigma variation is shown by filled grey colour. Colour lines are average profiles for individual year and dashed grey lines are for individual flight. Winter, spring, summer-monsoon and autumn seasons are represented by Dec-Jan-Feb, Mar-Apr-May, Jun-Jul-Aug and Sep-Oct-Nov, respectively.*

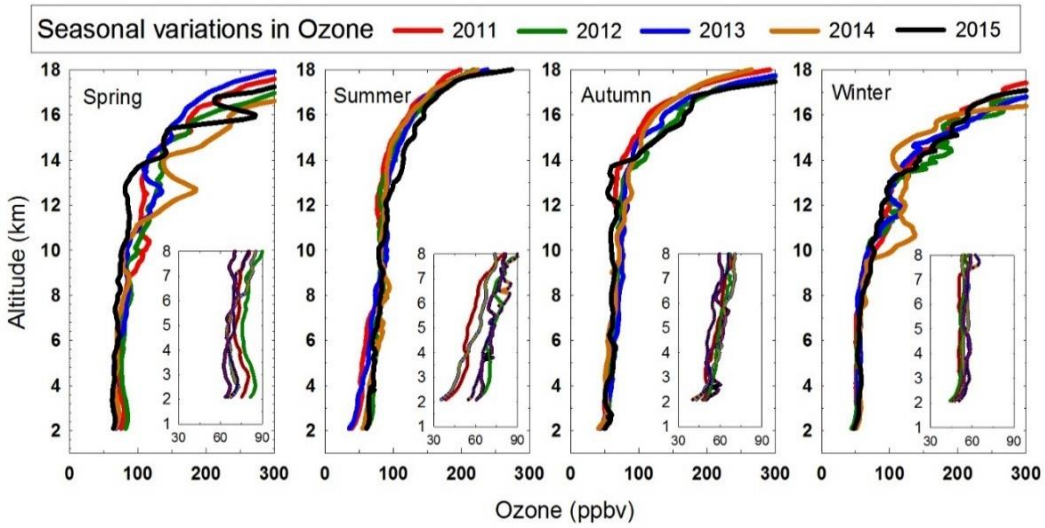

Figure 5.8: *Seasonal variations in tropospheric ozone from surface to 18 km for the years 2011-2015 using ozonesonde observations over Nainital. The figure in inset shows the vertical ozone distribution from surface to 8 km.*

In the middle troposphere (~10 km amsl), the highest variability (54%) is observed during winter season, with the lowest (20%) in autumn season. The average ozone value is maximum (95.0 ± 35.0 ppbv) in winter at this altitude. The average ozone values in rest of three seasons are 83.4 ± 44.7 ppbv, 86.7 ± 20.4 ppbv and 73.8 ± 15.0 ppbv during spring, summer-monsoon and autumn respectively. These variations in ozone levels again changes as we move to 15 km altitude region, where ozone variability is highest in spring season (57%) and lowest in summer (21%) season. The average ozone value is maximum in winter (168.7 ± 61.9 ppbv), and followed by in spring (164.5 ± 94.3 ppbv), summer-monsoon (108.4 ± 22.5 ppbv) and autumn (106.3 ± 35.7 ppbv). Here, average ozone is somewhat similar in winter and spring.

To further investigate the interannual changes and trend in ozone levels, the data is

divided into six layers, each of 2 km height from surface to 14 km amsl (Figure 5.9 and Table 5.3). The seasonal variations of ozone in the lower troposphere (2-4 km and 4-6 km) shows highest levels during spring (~ 100 ppbv in May) with a secondary peak in autumn. Lowest ozone levels are observed during summer-monsoon (~ 30 ppbv in July) period. The ozone seasonal variations in the lower troposphere are also consistent with the previous surface [*Kumar et al.,* 2010] and balloon based observations [*Ojha et al.,* 2014] of ozone at Nainital. It has been observed that air masses generally circulate over northern India and do not move faster. Solar radiation is intense and biomass burning is also active during spring. Thereby, availability of precursor gases and intense photochemistry induces ozone production. The role of spring time biomass burning on ozone distribution will be discussed in next section.

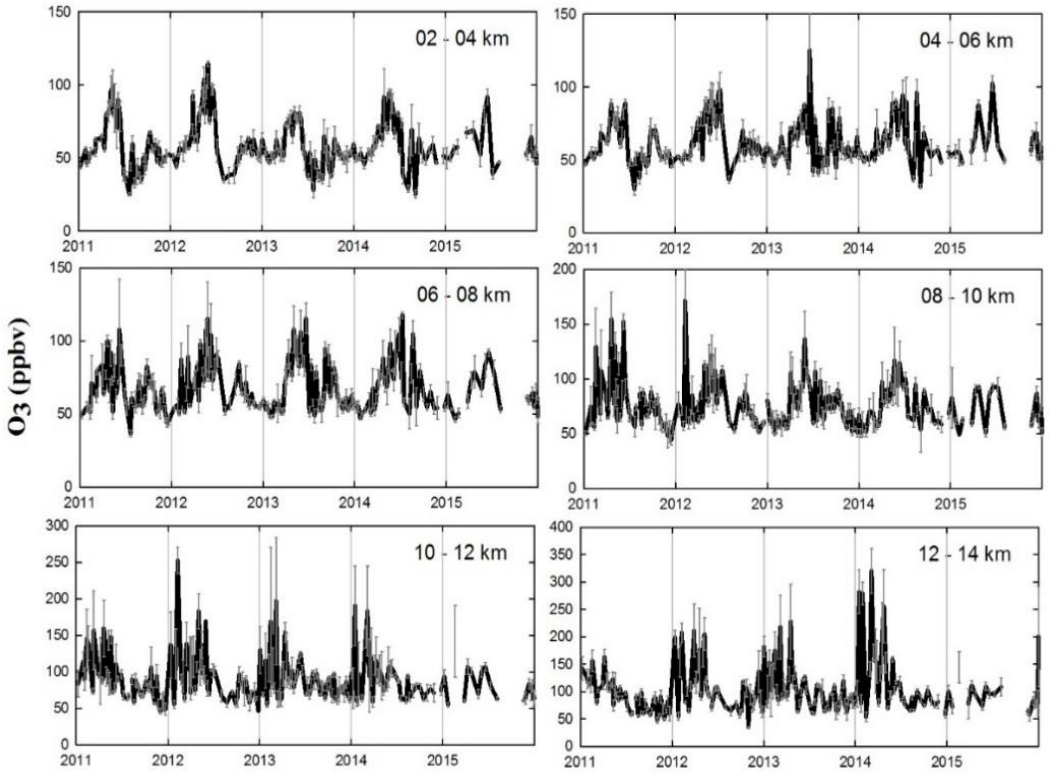

Figure 5.9: *Time series of ozone concentration at different levels in the troposphere during 2011-2015.*

The reduction in the lower tropospheric ozone levels during summer-monsoon period are associated with the arrival of cleaner marine air masses over this region. Further, during this period the prevailing cloudy and/or rainy conditions suppress the ozone production through photochemistry. The ozone seasonality at higher altitudes is not as pronounced compared to the lower troposphere. Contribution of regional emissions is rather small and dynamical processes like tropopause folds and stratosphere-troposphere exchange processes play an important role in the middle-upper troposphere. The five-year long ozone observations show a decreasing trend of about 1.6 ppbv per year and about 2.5 ppbv per year in 2-4 km and 8-12 km regions. However, a positive trend of 3.2 ppbv per year is observed in the upper troposphere (12-14km). Very small positive trend of (0.2 ppbv per year) is observed in the middle troposphere (4-8km).

Table 5.3: *Seasonal ozone variations from 2-18 km at 2 km bins during 2011-2015.*

		DJF	MAM	JJA	SON
2-4km	2011	50.3± 4.3	76.8± 15.9	49.7± 20.4	50.8± 8.3
	2012	52.7± 5.6	82± 18.2	68.3± 24.4	54.8± 7.7
	2013	52.9± 5.9	68.8± 11.6	46.2± 13.9	52.7± 10.3
	2014	51.4± 4.8	69.2± 15	61.7± 19.6	50.3± 12.6
	Avg	52.4±5.8	73.9±16.3	55.5±21.4	52.3±9.6
	2015	53.9± 7	64.1± 9	64.8± 22.3	53.2± 4.1
4-6km	2011	51.4± 4.6	71.7± 9.8	55.4± 16.2	58.2± 9.5
	2012	52.5± 3.8	76.7± 13.8	73± 22.8	59.8± 7.4
	2013	55.6± 6.7	66.8± 12.3	61.5± 24.7	62± 13.2
	2014	53± 3.9	68.4± 13.5	72± 21.2	53.2± 11.6
	2015	55.5± 7	66.3± 14.6	71.3± 21.2	61.2± 5.8
	Avg	53.8±5.8	70.9±13.3	64.6±22.5	59.0±10.9
6-8km	2011	52.8± 10.9	75.2± 14.9	67.5± 22	64.6± 10.3
	2012	59.6± 12.2	82.3± 19	78.7± 20.4	65.6± 10
	2013	55± 6	80.8± 20.2	70.2± 20	69.3± 13.6

	2014	54.1± 4.9	73.2± 15.2	82.8± 22	61.5± 11
	2015	56.5± 8.2	69.5± 10.5	77.5± 15.7	60± 2.6
	Avg	55.6±8.9	77.5±17.7	73.9±21.5	65.5±11.6
8-10 km	2011	66.3± 30.6	93.8± 32.3	82.9± 25.5	67.8± 13.8
	2012	79.3± 43.8	88.6± 23.5	84.3± 21.2	70.5± 13.9
	2013	60.7± 10.5	83.7± 26	83.1± 19.2	74.6± 11.1
	2014	62.3± 13.7	81.5± 21.5	86.7± 19.1	67± 14.9
	2015	69.8± 16	73.6± 19	81.7± 15.9	61.9± 5.3
	Avg	67.0±25.8	86.1±26.1	83.9±21.0	70.0±13.4
10-12km	2011	93.6± 39.9	107.1± 38.2	80.6± 17.4	73.3± 18.4
	2012	114.1± 64.4	109.7± 35.7	82± 18.7	72.5± 16.7
	2013	93.6± 47.6	101.9± 47.3	89.9± 19	77.4± 12.7
	2014	103.9± 54	104.3± 43.3	85.2± 17.7	73.9± 9.4
	2015	82± 33.7	84.7± 21.1	88.4± 17.7	62.6± 7
	Avg	97.0±50.0	104.4±40.5	85.1±18.5	74.0±15.1
12-14 km	2011	110.3± 36	108.8± 23.6	82.3± 17.5	67.9± 15.9
	2012	123.2± 57.9	130.4± 50.2	87.2± 17.8	81.6± 25.6
	2013	108.8± 40.1	119.9± 52.4	93.4± 24.3	82.1± 19.6
	2014	135± 88.8	156.3± 76	89.5± 19	86.5± 12.8
	2015	110.2± 59.6	90.9± 24.1	103.4± 12.2	61.4± 10.4
	Avg	116.9±58.7	126.3±55.7	89.7±20.5	77.8±20.5
14-16 km	2011	173.4±70.4	153.6±69.5	103.4±24.0	95.6±37.3
	2012	183.0±74.5	160.0±69.7	112.7±19.5	130.3±44.5
	2013	176.8±125.2	143.3±47.1	115.1±26.5	110.7±57.6
	2014	152.2±60.0	205.4±161.4	105.6±27.9	107.5±15.5
	2015	180.7±120.6	167.3±111.5	127.6±13.7	132.8±27.4
	Avg	173.7±98.6	165.6±100.4	110.9±25.2	111.2±45.1
16-18km	2011	285.6±155.5	251.4±153.1	155.6±37.1	181.3±77.7
	2012	375.7±229.6	306.6±169.9	167.2±33.7	227.9±97.3
	2013	346.7±231.5	220.6±88.0	167.8±70.1	219.3±127.3
	2014	387.4±219.0	390.3±256.9	165.2±40.1	179.4±48.9
	2015	314.3±162.2	293.1±202.4	181.4±38.5	245.7±88.8
	Avg	345.2±210.7	292.5±189.2	165.3±49.2	205.4±98.7

5.4 Influences of biomass burning

Biomass burning emits a large quantities of ozone precursor gases and thus play an important role in the ozone chemistry in the troposphere. The spring time emissions from northern Indian biomass burning is found to increase the surface levels of ozone and precursor gases over the Himalayan region [*Kumar et al.,* 2011]. The emissions from biomass burning also reaches to the higher heights and perturbed the natural environments there, including changes in the levels of ozone and other gases. Such studies, covering higher altitude regions and using different years of observations, are severely lacking in the Indian subcontinent. In view of this, five years of vertical ozone distribution data are analyzed to understand the influence of biomass burning over the Himalayan region. Fire count data from MODIS are also used in this study.

To study the seasonal variations in biomass burning over northern Indian subcontinent (70 to 90 E and 25 to 35 N) combined MODIS fire counts data for 2011-2015 has been used. The biomass burning activity generally peaks during spring (May) and autumn (November) over this region and it varies from one year to another [*Bhardwaj et al.,* 2016]. The majority of spring time biomass burning over northern Indian subcontinent are due to crop residue burning and some contributions from forest fires in Himalayan region [*Kumar et al.,* 2010, *Bhardwaj et al.,* 2016]. To investigate the role of this biomass burning on the vertical ozone distribution, more numbers of balloon flights were also conducted in May during years 2011-2013.

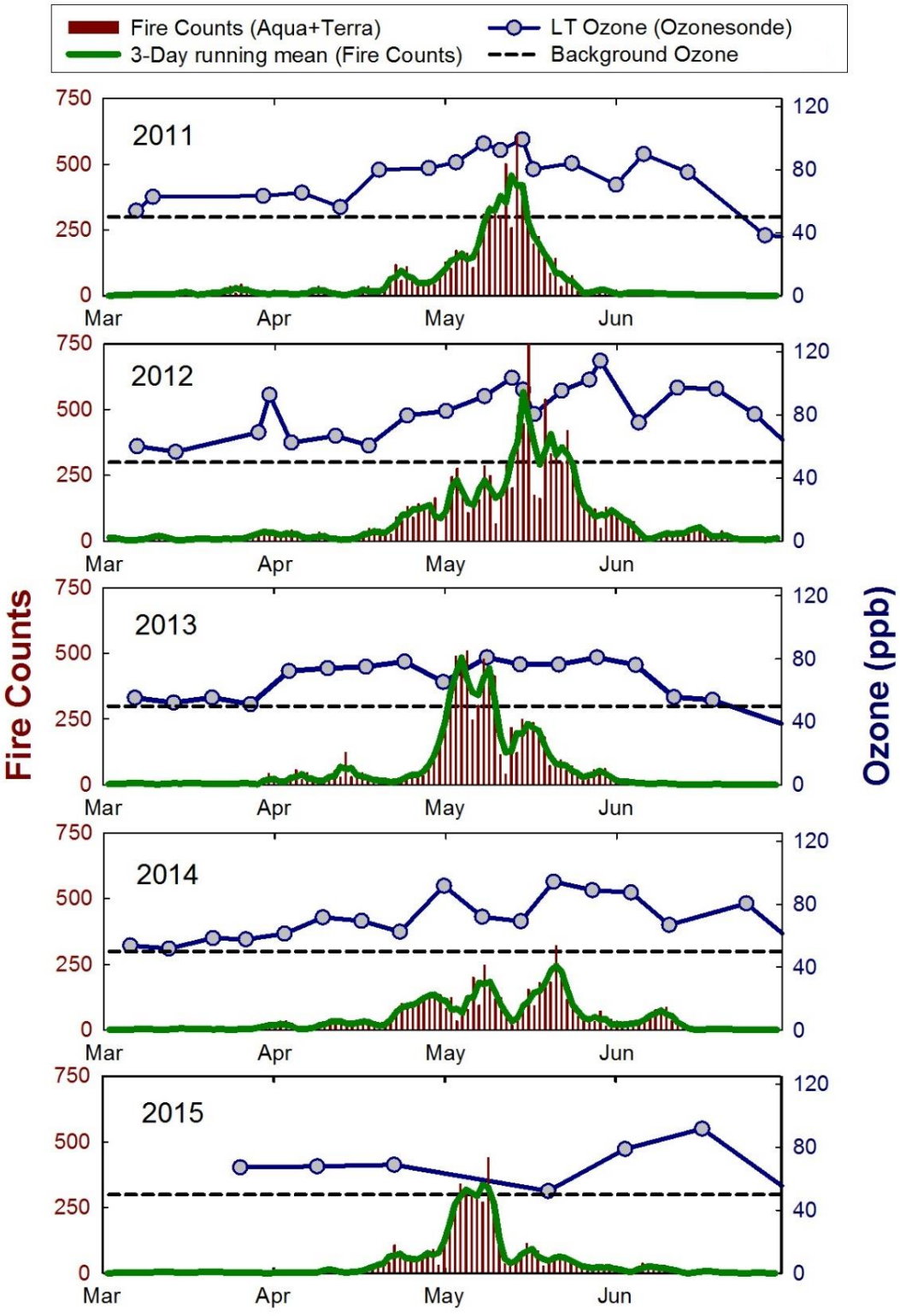

Figure 5.10: *Variations in daily MODIS fire counts, three-day running mean of fire counts and lower tropopheric ozone (2-4 km). Dashed line is surface ozone background levels during March-June months as defined by Kumar et al., [2010].*

Classification of high and low fire activity periods: The daily time series of MODIS fire counts with its 3-day running mean and lower tropospheric ozone levels (2-4 km) from March to June in five years (2011-2015) are shown in Figure 5.10. Dashed line in the figure, shows surface ozone background levels during this period as defined by *Kumar et al.,* [2010]. This time series of fire counts is used to calculate median fire counts between 15 April and 15 June for each year. If the three-day running mean (from April 1 to June 30 of every year) of fire counts is higher than the respective median of the year, the period is classified as the High Fire Activity Period (HFAP) whereas, if it is lesser, than the period is Low Fire Activity Period (LFAP). The enhancement in the lower tropospheric ozone levels during high fire activity periods is seen during four years, except during year 2015 when lesser number of flights were conducted (Figure 5.10).

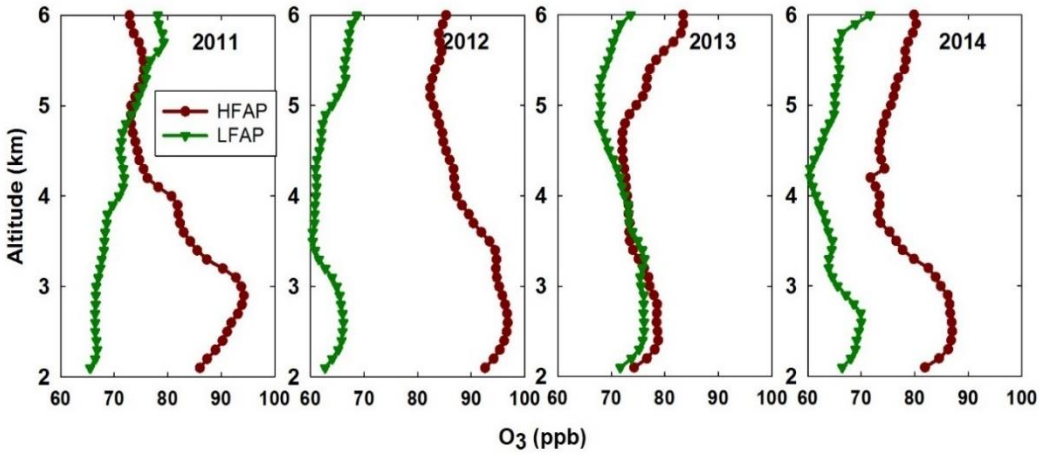

Figure 5.11: *Vertical ozone distribution in high and low fire activity periods during years 2011-2014.*

Vertical (surface to 6 km) ozone distribution during HFAP and LFAP is shown in Figure 5.11. The enhancement in vertical ozone levels during HFAP is consistent with years and only exception was 2013, where LFAP ozone levels were also higher

due to which the difference is minimal.

The mixing depth over nearby plain regions generally reaches 3-4 km during month of May [*Ojha et al.,* 2012] which allows the pollutants to get mixed during daytime. Further mixing at higher heights may influence the distribution of the near surface fire emissions in the lower troposphere (LT). The influence reduces at higher heights, except in year 2013. The maximum enhancement in the ozone levels is observed in 2-4 km region with average HFAP ozone levels of 89 ± 14 ppbv as compared with the LFAP ozone levels of 66 ± 7 ppbv (Table 5.3). The ozone level during HFAP is maximum (94 ± 13 ppbv) during 2012, which was due to wide spread biomass burning activity as compared to other years.

Table 5.3: *The HFAP and LFAP ozone levels during year 2011, 2012 and 2014.*

	HFAP O_3 (ppbv)	LFAP O_3 (ppbv)
LT (2-4 km)		
year_2011	88 ± 13	67 ± 10
year_2012	94 ± 13	63 ± 5
year_2014	81 ± 15	66 ± 6
Average (2011-2014)	89 ± 14	66 ± 7
LT (2-6 km)		
year_2011	81 ± 12	71 ± 11
year_2012	89 ± 13	64 ± 10
year_2014	79 ± 14	65 ± 6
Average (2011-2014)	84 ± 13	67 ± 10

The average ozone enhancement during these biomass burning is about 23 ppbv in 2-4 km altitude with levels ranging from 15 to 31 ppbv. The enhancement is lesser in 4-6 km region. *Kumar et al.,* [2010] have estimated the enhancement in surface ozone of about 19 ppbv during 2007-2009. This analysis highlights the importance of studies on influences of northern Indian subcontinent biomass burning even at higher altitude regions, apart from its role at surface.

5.5 Influences of downward transport: stratosphere-troposphere exchange

Stratosphere-Troposphere Exchange (STE) is a dynamical process in which ozone and other atmospheric constituents are mixed and transported across the tropopause. The troposphere and stratosphere can be characterized by difference in their atmospheric stability, ozone and water vapour mixing ratio etc., however they are coupled dynamically, radiatively and chemically. Several studies in the past have shown that STE and related processes can play an important role in the vertical distribution of ozone [*Levy et al.,* 1985; *Holton and Lelieveld,* 1996; *Cristofanelli et al.,* 2003; *Marcy et al.,* 2004]. There is still a large uncertainty in the tropospheric ozone budget on part of downward ozone transport from the stratosphere to troposphere as discussed in chapter 1. The downward ozone transport, in general affects the ozone distribution in middle-upper part of the troposphere. One of the tracer methods using potential vorticity maps to identify STE process will be used in this work and is discussed further in detail.

The isentropes are the lines of constant potential temperature and fluid parcels in the atmosphere tends to follow these lines. The isentropes bounding troposphere and stratosphere in tropics is at about 100hPa (380 K). The exchange of air across tropopause occurs if these isentropes cross the tropopause or if there are vertical turbulent motions *[Shapiro.,* 1980, *Hoskins et al.,* 1985; *Holton.,* 1995]. The tropopause can also be defined dynamically based on its "potential vorticity (PV)" which is defined as -

$$PV = - g (\varsigma_{\Theta} + f) \partial\Theta/\partial P \qquad [5.1]$$

Where g is the acceleration due to gravity, ς_{Θ} is component of the curl of wind vector normal to isentropic surface, f is Coriolis parameter, Θ is potential temperature and P is the atmospheric pressure. If contributions from diabatic and turbulent processes are neglected, the PV of an air parcel is conserved along its path. The extratropical tropopause is generally at around 2 potential vorticity unit or PVU (1 PVU = 10^{-6} K m^2/Kg/sec) and the PV of the stratosphere is about 1-2 magnitude higher than the troposphere [*Beekmann et al.,* 1994]. Due to this difference, the higher values of PV in the troposphere indicates the intrusion (downward transport) of air masses from stratosphere.

Further, this downward transport is also characterized by higher values of ozone since stratospheric ozone levels are also about two orders higher than that of the troposphere. These are short term events and for timescales greater than months, the exchange across tropopause is governed by Brewer-Dobson circulation. The detailed description of the use of PV maps to characterize STE and in general STE

process can be found elsewhere [*Hoskins et al.,* 1985; *Holton et al.,* 1995; *Mohanakumar, K.,* 2008]. A few attempts in the past were made to understand role of STE over the Indian subcontinent [*Mandal et al.,* 1998; *Ganguly and Tzanis,* 2011]. In general, the tropopause folding events and influences of STE over this region (including Indian Ocean and Tibetan plateau) are more frequent during winter and early spring seasons [*Zachariasse et al.,* 2000; *Cristofanelli et al.,* 2010; *Chen et al.,* 2011]. The highest PV is also observed during winter and early spring months over Nainital region and the detailed seasonal variations in PV is discussed in *Ojha, N.,* [2013]. Apart from increase in PV and ozone levels the arrival of stratospheric air in troposphere can also be indicated by reduction in RH levels and CO mixing ratios [*Stohl et al.,* 2000; *Trickl et al.,* 2010].

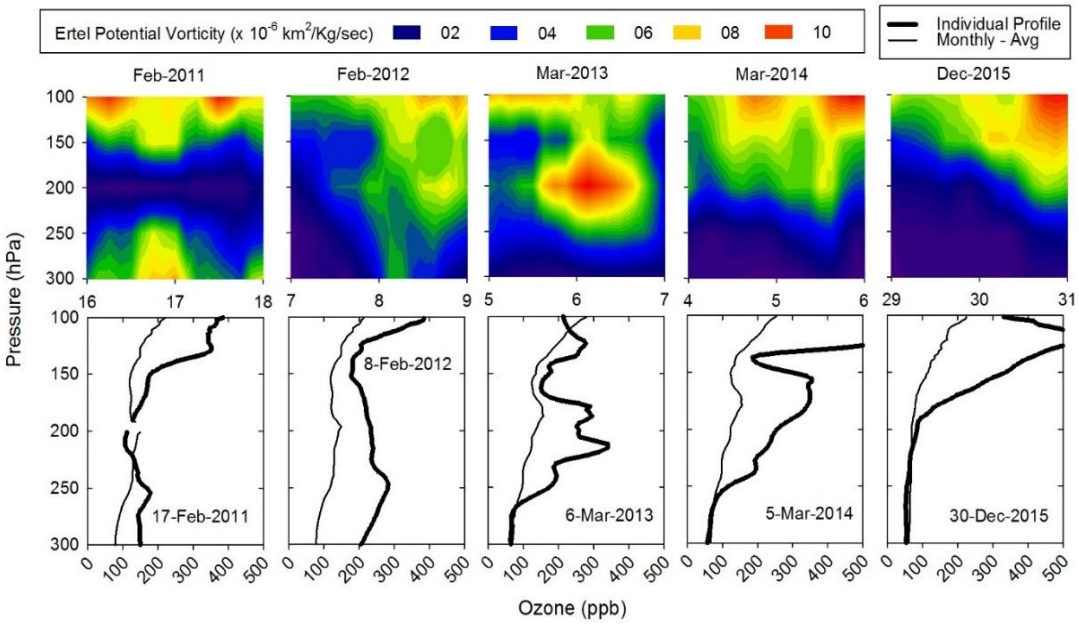

Figure 5.12: *Vertical (300-100 hPa) ozone profiles during five cases of downward ozone transport. Month mean ozone profiles are also shown for the comparison. Potential vorticity before, during and after the event period is also shown.*

In the present work, five cases (17 February, 2011; 8 February 2012; 6 March 2013; 5 March 2014; 30 December 2015) of downward transport of ozone rich air from stratosphere were identified during 2011-2015. All these five events indicated the elevated levels of ozone in the middle-upper troposphere. Figure 5.12 shows the vertical (300-100 hPa) ozone distribution during five days when downward ozone transport was marked. Monthly mean distribution and PV contours (300-100 hPa) before, during and after the event period is also shown.

The increases in ozone levels are 1.7 - 2.9 times from the monthly mean levels during these events. However, no such increase is observed at lower altitudes (2-6 km). The corresponding increase in PV levels was 1.4 to 3.6 times. In general, the PV during the all events was much higher than the threshold value of 1.6 PVU suggested by *Cristofanelli et al.,* [2006]. To further investigate these events, AIRS retrieved CO and RH data are also used. CO and RH data are not available during 5 March 2014 and 30 December 2015. Percentage change in ozone, CO and RH is also estimated (Table 5.5) at five altitudes (between 300-100 hPa).

It is observed that ozone enhancement is maximum at around 300 hPa during year 2011 (92%) and year 2012 (157%). During year 2013, enhancement (95%) is at around 200 hPa while it is further high up at around 150 hPa during year 2014 (147%) and year 2015 (191%). These altitudinal differences in ozone enhancement are also supported by higher values of PV at those altitudes (Figure 5.12). Reduction in CO and RH levels is also observed during these periods, suggesting that these enhancements in ozone levels are due to downward transport. Further the spatial

distribution of PV over northern India during the event day and one day prior to the event are shown in Figure 5.13. PV values are found to be higher over a larger region on the day of the events when compare to the one-day prior of the respective event. Hence, enhancement in ozone and PV while reduction in CO and RH confirm that the occurrence of stratospheric intrusions during five identified days over this region.

Table 5.5 : *Percentage change (with respect to monthly mean) in ozone, CO and RH during the events. CO and RH data was not not available during 5 March, 2014 and 30 December 2015.*

years	P (hPa)	300	250	200	150	100
2011	Ozone	92	41	-25	45	74
	CO	-7	-3	0	2.5	2
	RH	-70	-57	12	69	26
2012	Ozone	157	138	65	48	76
	CO	-7	-8	-8	-6	-3
	RH	-78	-87	-86	-75	-55
2013	Ozone	-6	82	95	28	-24
	CO	-2	-1	0	1	1
	RH	-14	-42	-42	-43	-42
2014	Ozone	-14	34	107	147	141
	CO	--	--	--	--	--
	RH	--	--	--	--	--
2015	Ozone	-12	-16	19	191	47
	CO	--	--	--	--	--
	RH	--	--	--	--	--

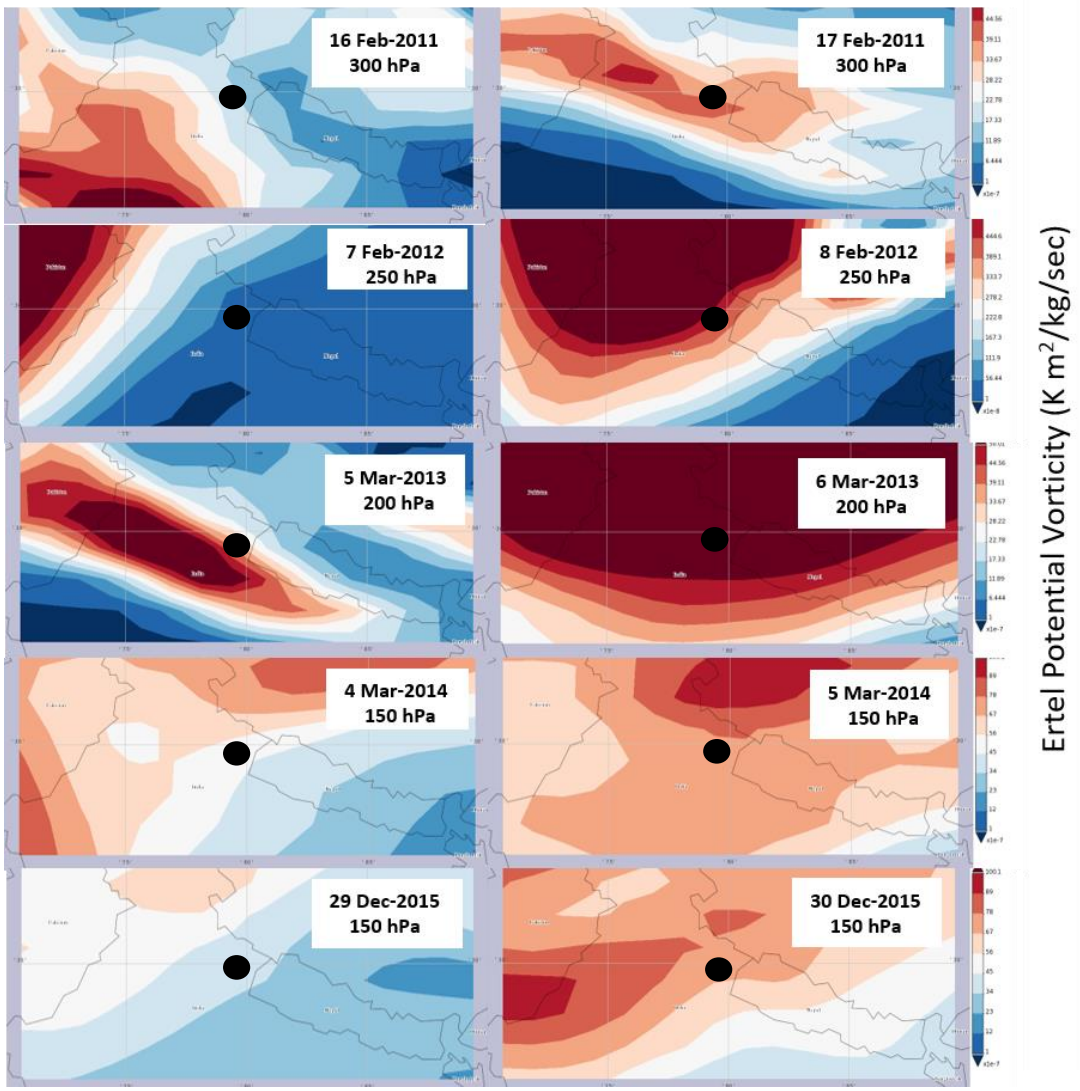

Figure 5.12: *PV contour maps (MERRA reanalysis) over northern Indian region at various pressure levels during five STE events in 2011-2015. PV maps in right panels are on the days of event and PV maps on day before the event are shown in the left panel.*

5.6 Conclusions

The balloon borne observations of ozone and meteorological parameters are made at Nainital during 2011-2015. The near surface temperature was highest during the month of June (16.5 ± 1.9^{o}C) and February being the coldest (4.5 ± 3.2^{o}C) month. However maximum variations are also observed during winter months. The RH is

observed to be maximum during summer-monsoon in the lower troposphere. The high wind speed at 10-14 km indicated the presence of southwesterly subtropical jet stream. These south-westerly jets reached highest speeds of up to ~94 m/s. Ozone levels in the lower troposphere showed prominent seasonality with highest levels during May (~100 ppbv) and lowest during summer-monsoon period. These seasonal variations are also consistent with the previous studies performed over this region. The spring time enhancement in the lower tropospheric ozone levels was mainly due to northern Indian biomass burning. Estimated enhancement in ozone ranges from 15 ppbv to 31 ppbv with average value of about 23 ppbv in the lower troposphere region. Occurrence of downward ozone transport from stratosphere to troposphere is identified during five events when enhancement in ozone and PV while reduction in CO and RH are shown. Estimated increase in ozone is found to be as high as 191% during year 2015.

Chapter 6

Vertical Profiling of Meteorological Parameters During RAWEX-GVAX Campaign

Dynamical, physical and chemical processes those are controlling different meteorological systems, including monsoon systems, are poorly understood over the Indian subcontinent [*Moorthy at al.*, 2001; *Satheesh et al.*, 2008]. Monsoon system, over Asia, is one of the largest regional climate phenomena and has major influence on the regional atmospheric composition. The Asian monsoon circulation provides an effective pathway for pollution from South Asia to enter the tropical tropopause layer [*Feuglistaler et al.*, 2009] and the stratosphere [*Randal et al.*, 2010] and thereby influencing radiation budget, chemical composition and air-quality over wide region. Coupling between the stratosphere and troposphere

through chemical, radiative and dynamical processes play an important role in climate change and this becomes more critical in tropical regions where determination of the tropopause shows greatest deviation [*Reichler et al.,* 2003]. It has also been shown that stratosphere-to-troposphere exchange (STE) is pronounced and persistence along the subtropical jet stream [*Trickl et al.,* 2011]. Further, the Himalayas in the north modifies the atmospheric circulation by acting acts as a physical barrier to air-flow. These interact with the upper tropospheric subtropical jet stream during the winter [*Moore et al.,* 2004] and amplifies the summer monsoon circulation by blocking the moist southerly flow from the Indian Ocean, the Arabian Sea and the Bay of Bengal [*Kennett and Toumi,* 2005]. The Himalayas are also the source of several rivers including three of the world's largest rivers, the Indus, Ganges and Brahmaputra that supply water to more than a billion people living in the downstream areas. In addition to the meteorology, the Himalayas also affect the global atmospheric composition by transporting key trace gases and aerosols in the upper troposphere and lower troposphere during the monsoon season [*Randel et al.,* 2010]. The accumulation of absorbing aerosols over the southern slopes of Himalayas are also suggested to affect the Indian summer monsoon system [*Lau et al.,* 2010]. However, meteorology and dynamical aspects including the transport pathways in this region remain poorly understood and poorly quantified and the Asian tropical troposphere is also least studied and insufficient observations are available for this region.

Considering the importance of this region and to understand meteorological and chemical characteristics of the Himalayan region, an extensive field study RAWEX-GVAX (Regional Aerosols Warming Experiment - Ganges Valley Aerosol

Experiment**)** was planned jointly between DOE (USA), IISc (India), DST (India) and ISRO (India). During the campaign, observations of wide range of parameters like physical and optical properties of aerosols, meteorological parameters, boundary layer evolution are made using the first ARM (Atmospheric Radiation Measurement) Mobile Facility (AMF-1) for a 10-month campaign at ARIES, Nainital (29.4°N, 79.5°E; 1950 m amsl). Scientific objectives of the campaign and studies on aerosols properties are presented in the special section of a journal current science [*Vol. 111, No. 01, 10 July* 2016]. Here, this work presents results obtained from high frequency balloon-borne observations of meteorological parameters. The main objective of this work was to assess the variabilities in winds and tropopause and biases in reanalysis/satellite data. Note that this study will complement the ongoing efforts of the Indian Meteorological Department (IMD), who is operating surface meteorological stations at several Himalayan sites (Srinagar, Shimla, Dehradun, Gangtok and Itanagar) along with upper-air observations at Jammu. During this campaign for the first time balloon-borne observations of meteorological parameters with four launches in a day are made continuously for about ten-month period during 2011-2012.

6.1 Observation site and experimental setup

During RAWEX-GVAX campaign balloon-borne radiosonde observations were carried out in the premises of ARIES, Nainital. The site and its meteorological features are discussed in earlier chapters. Weather balloons were launched four times (0000, 0600, 1200 and 1800 GMT or 0530, 1130, 1730, and 2330 IST) every day and total 1069 flights were conducted during June 2011-March 2012. Figure 6.1(a) indicates variations in the balloon launch time during four times in a day

during June 2011 - March 2012. Some variability in the launch time was mainly due to constraints of flight permissions from the Air Traffic/Navigation Controllers of this region (Pantnagar and Bareilly). These times represents the local conditions of early morning, daytime, evening time and nighttime leading to study meteorological conditions during these periods.

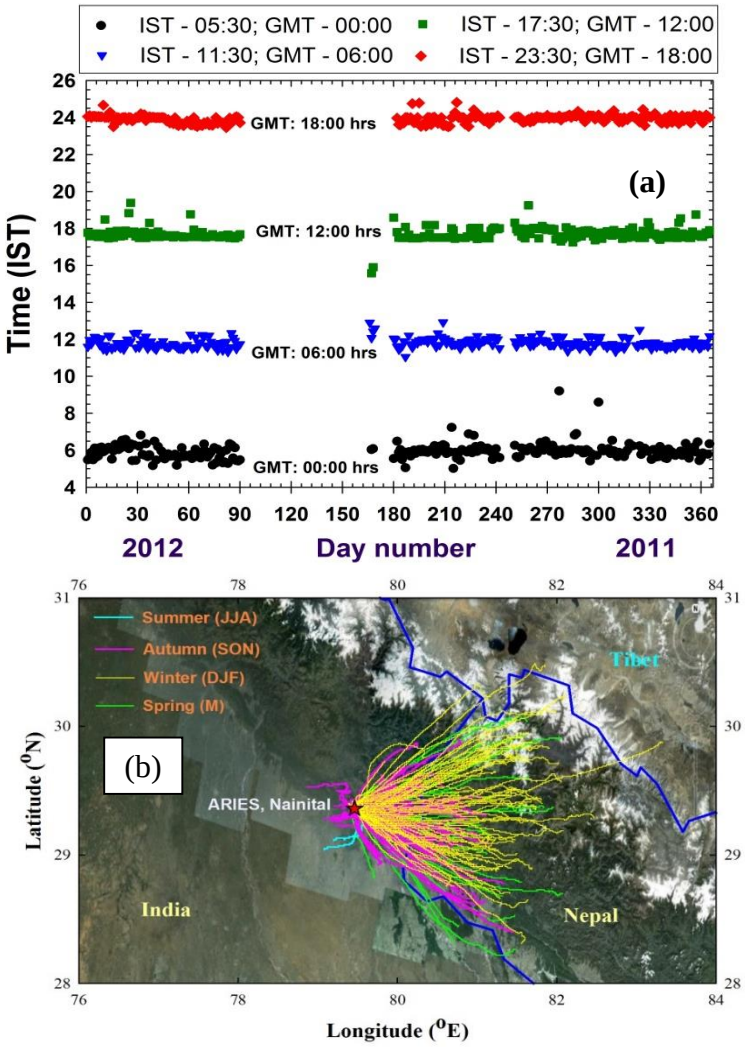

Figure 6.1: *(a) Upper panel shows variations in the balloon launch time during four times in a day during June 2011 - March 2012. (b) Lower panel shows location of the observation site (ARIES, Nainital, 29.4N, 79.5E, 1958 m amsl) and path of all the balloons flown during RAWEX-GVAX field campaign.*

In this study we are using 1061 successful flights (Table 6.1) and discarding 8 flights those were not successful above 5 km. Few test flights were carried out during May 2011 and fully operational flights were started from 1st June, 2011. Figure 6.1 (b) shows the latitude-longitude distribution of all 1061 balloons those were flown from ARIES, Nainital. It can be seen that majority of the balloons drifted to the East. This pattern dominates at higher altitude and in winter/spring.

Table 6.1: *Number of successful balloon flights from 1st June 2011 to 31st March 2012. Total 1069 flights were carried out and 8 flights did not cross altitude beyond 5 km and were discarded from further analysis this making total 1061 flights during 10-month period.*

Flight Time/Months	0530 hrs	1130 hrs	1730 hrs	2330 hrs	Daily Total
Jun	3	6	3	0	12
Jul	31	29	30	28	118
Aug	29	30	27	26	112
Sep	28	30	30	30	118
Oct	25	30	31	31	117
Nov	26	30	29	29	114
Dec	29	30	31	30	120
Jan	30	30	31	31	122
Feb	26	27	29	30	112
Mar	30	30	28	28	116
Total	257	272	269	263	1061

6.2 Inter-comparison with i-Met radiosonde

Apart from radiosonde from Vaisala (RS92-SGP), radiosonde from i-Met (iMet-1-RSB 403 MHZ GPS) were also flown together during five occasions (7 Feb, 29 Feb, 7 Mar, 14 Mar, and 29 Mar) in year 2012 to inter-compare both these types of sensors. Data from both the sensors are averaged in the bin of 100 m resolution. These average temperature, relative humidity and wind speed profiles shows a good agreement with square of correlation coefficient of 0.95-0.99 (Figure 6.2). During all five days, temperature profiles show r^2 of 0.99 and average iMet temperature is higher by 0.3. RH and wind speed also show a good correlation with 0.95-0.99 and 0.98-0.99, respectively [*Naja et al.*, 2016]. These parameters are observed to be slightly higher by iMet (RH by 4.9 and wind speed by 0.21).

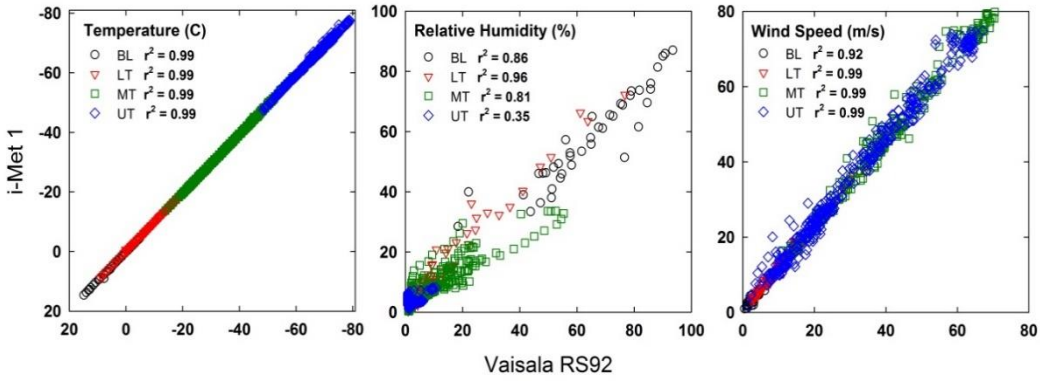

Figure 6.2: *Comparison between Vaisala and i-Met observations of temperature, relative humidity and wind speed during five intercomparison flights on 7 Feb, 29 Feb, 7 Mar, 14 Mar and 29 Mar, 2015. Data are classified in the BL (up to 3km), LT (3-6 km), MT (6-12 km) and UT (12-18 km) regions.*

6.3 Variations in the meteorological parameters

Variations in observed pressure, temperature, relative humidity and wind speed at

1130 IST from June 2011 to March 2012 are shown up to 20 km altitude (Figure 6.3). As expected, pressure decreases exponentially with increasing altitude. Temperature is highest during summer-monsoon (~15 C) and lowest during winter (~6 C) near the surface.

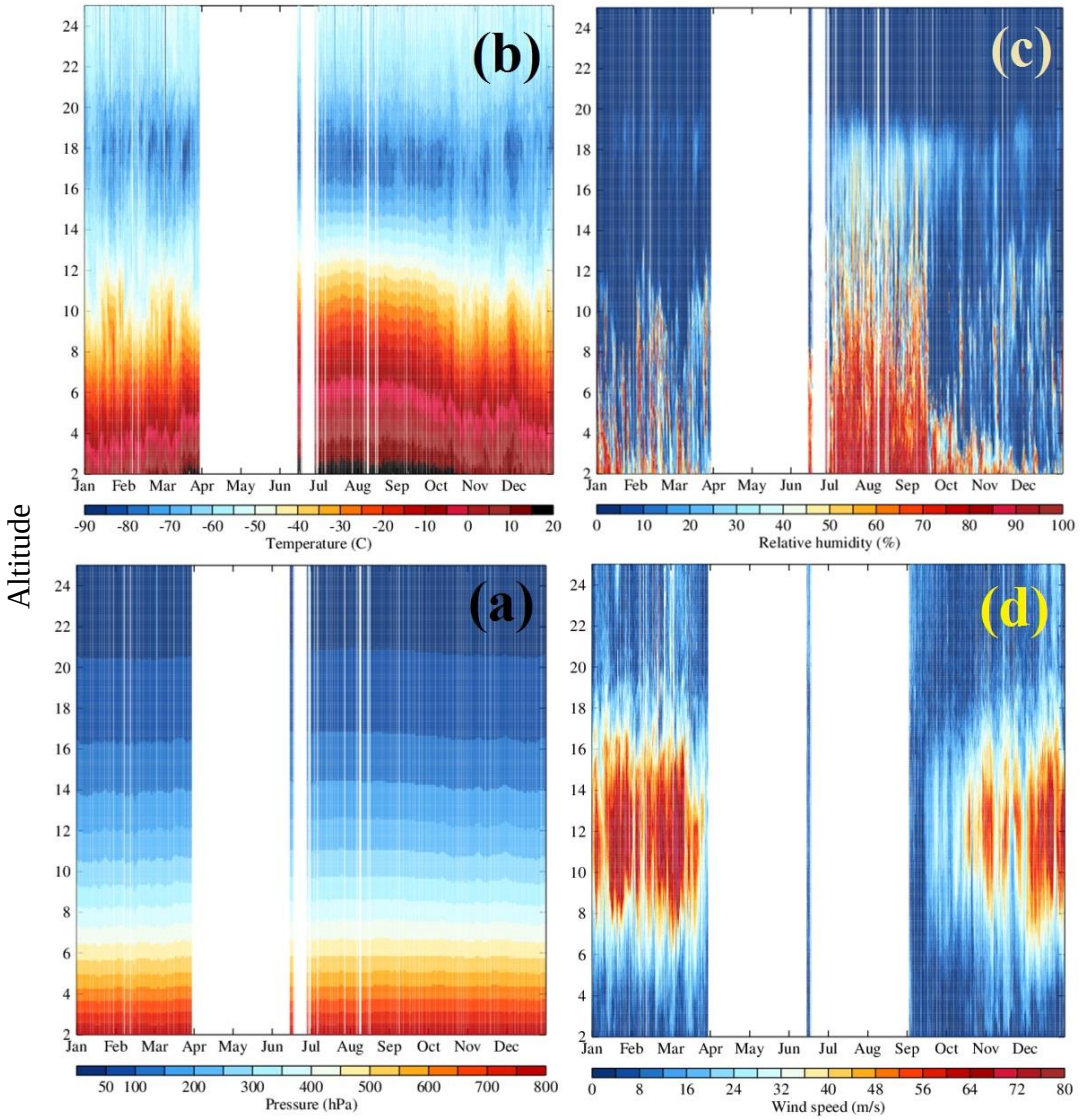

Figure 6.3: *Contour maps showing altitude variations in daily balloon-borne observations of (a) pressure, (b) temperature, (c) relative humidity, (d) wind speed during June 2011 – March 2012 at 1130 IST at ARIES, Nainital.*

The variability in near surface temperature is lower during summer-monsoon than other seasons. Temperature in the lower-middle troposphere show somewhat

similar seasonal variation to that near the surface. However, the variations are different in the upper troposphere, where the maximum temperature is seen during winter. Temperature also showed greater variability near the tropopause (~18 km) region in winter. Relative humidity (RH) profiles show very large variabilities over this region (Figure 6.3c). Near surface RH values are highest during summer-monsoon and dominance of dry air is seen during winter. Prevalence of the cloudy-rainy conditions leads to the RH maximum during summer-monsoon.

Wind speed shows a prominent vertical profile with strongest winds in the middle troposphere in all the seasons except summer-monsoon. Wind observations could not be collected during June-August due to a technical problem. Near surface wind speed is stronger during spring/autumn and weaker during winter. While, in the lower to upper tropospheric altitudes, the wind speeds are strongest during the winter and weakest during the summer-monsoon. The peak wind speeds in seasonally averaged profiles were strongest (~ 70 m s^{-1} at 11.5 km) during winter and moderately higher during spring (~ 40 m s^{-1} at 12 km) and autumn (36 m s^{-1} at 12.1 km). During the summer-monsoon, the wind speed does not show a clear maximum in the profile and winds were moderately stronger in the middle-upper troposphere (~ 14 m s^{-1}).

The presence of very strong winds (40-80 m s^{-1}) in middle-upper troposphere, observed more frequently during winter and occasionally during spring and autumn, is suggested to be associated with the prevailing subtropical jets. These stronger winds could bring pollution from upwind to above the Himalayas, while, emissions uplifted from this region could be transported downwind on faster timescales. This

also indicates stronger dynamical processes in middle-upper troposphere particularly during winter, which is consistent with the suggested possibility of the wintertime multiple tropopause. Additionally, RH values are much lower in middle-upper troposphere during winter. These aspects will be discussed in more detail later.

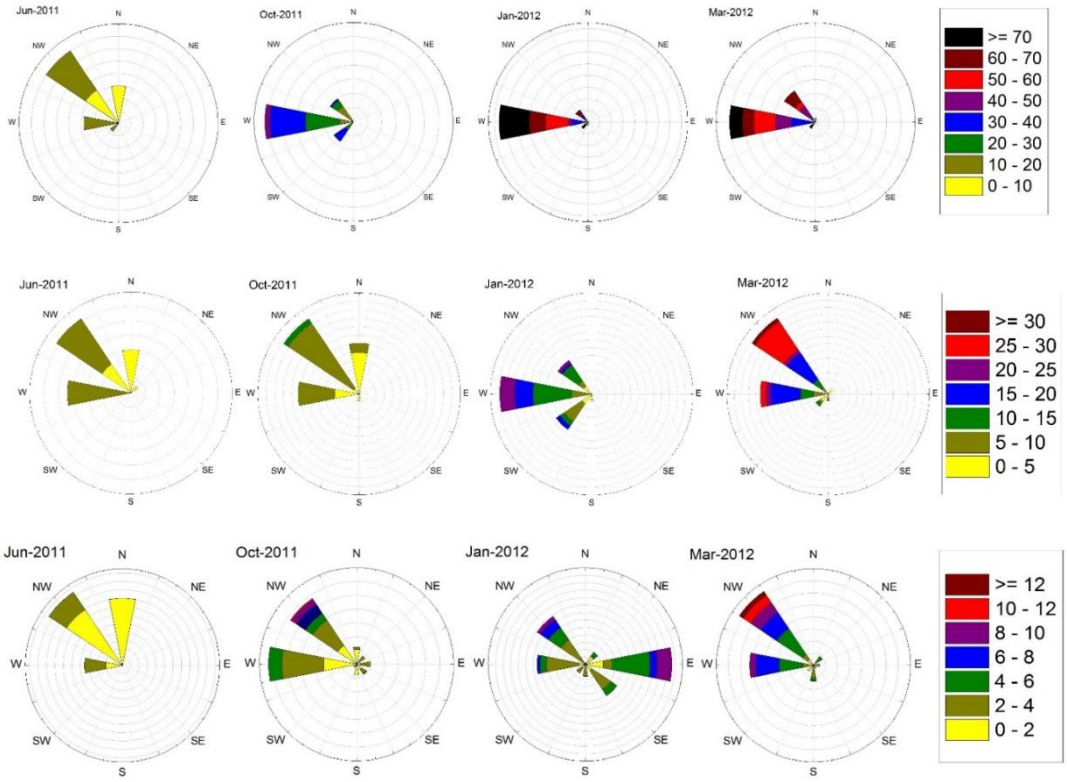

Figure 6.4: *Wind rose plots at 2 km, 5 km and 10 km (bottom to top) altitude during June 2011, October 2011, January 2012, March 2012 at ARIES, Nainital.*

The monthly variations in the wind direction at different altitudes over the central Himalayas are shown (Figure 6.4) in the form of percentage occurrences in four wind direction bands of 90 degrees. The dominance of westerly winds is clearly visible (62-77% in the 2-4 km) during winter and spring in the lower troposphere. The maximum contribution during summer-monsoon is from the easterly winds (42%) in 2-4 km range [*Ojha et al.*, 2014]. The westerly winds also contribute

significantly during summer-monsoon in 4-6 km (~36%). The variations in the wind directions are different in higher altitudes (8-12 km), where, the contributions from all the directions other than westerly are very less (0-8%) in all the seasons, except summer-monsoon.

6.4 Simulations with WRF model

Observed temperature, RH and wind speed profiles are also compared with WRF simulated profiles during summer-monsoon (July 2011) and winter (January 2012) (Figure 6.5). Wind observations were not available in July and hence shown for September. In this study weather research and forecasting (WRF) model version 3.4.1 is used, the model setup consists of two nested domains (45 and 15 km) defined on Mercator projection. The parent domain at 45 km horizontal resolution is defined from 10-40^{o}N, 66-100^{o}E in north-south & east-west directions respectively and nested domain at 1 5km resolution was over 21-34^{o}N, 70-90^{o}E region. The model consists of 51 vertical levels from the surface to 10 hPa (~ 30 km) and simulations were done for a period of 10 months from June 2011 to March 2012. The different physics options were adapted from earlier work [*Kumar et al.*, 2012a, 2014]. The static geographical data were used from United States Geological Survey (USGS) and processed using WRF preprocessing system (WPS). The boundary conditions for the meteorological fields were obtained from National Center for Environmental Predictions (NCEP) Final Analysis (FNL) data at 6-hour temporal resolution and 1^{o} x 1^{o} spatial resolution.

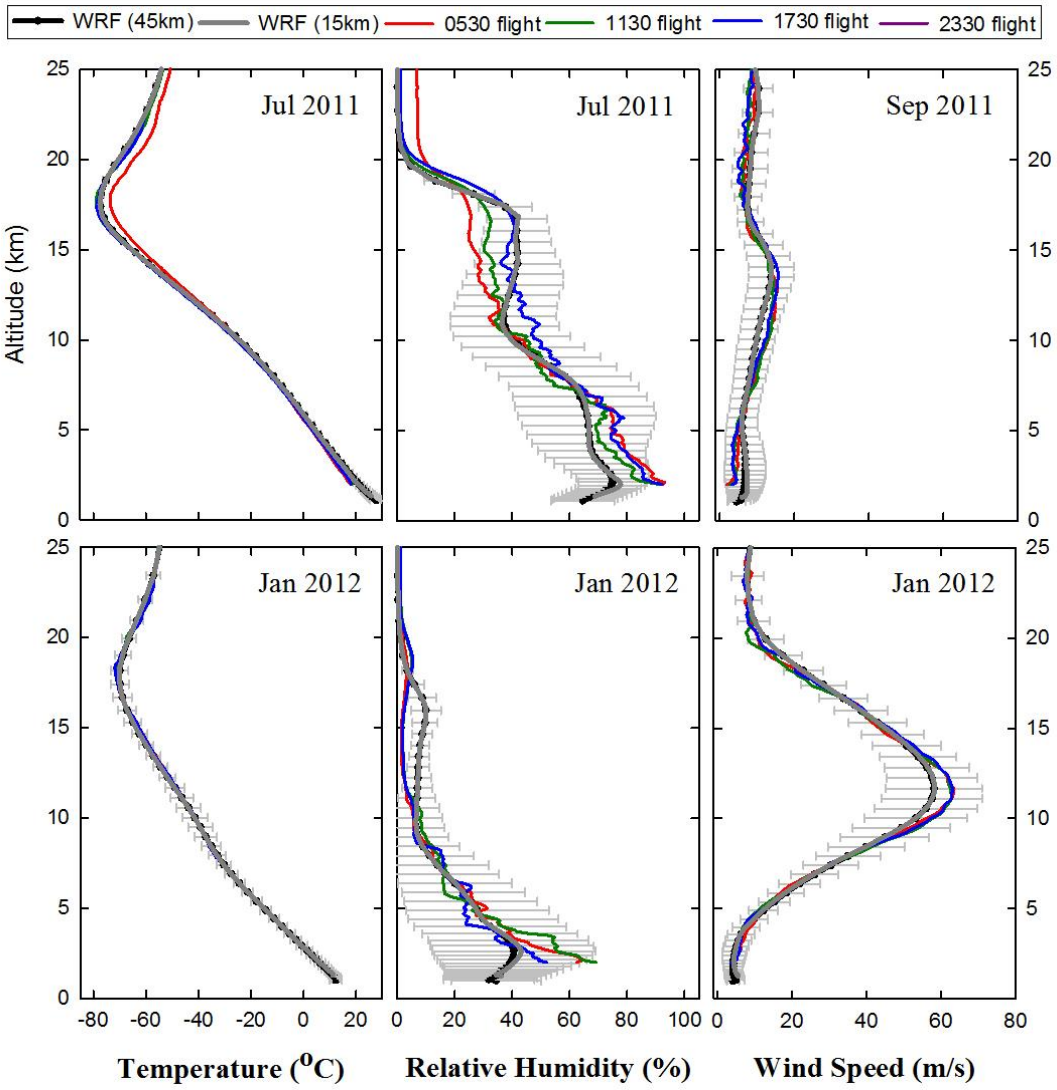

Figure 6.5: *Vertical distribution of temperature, relative humidity and wind speed from radiosonde observations and WRF model simulations during winter (January 2012) and summer-monsoon (July 2011). Wind speed is not available for July and shown for September 2011.*

Model simulated temperature, RH and wind speed profiles are in reasonable well agreement with the observations. Temperature profiles show almost no difference to ± 2.2 C in January 2012 and -2.1 C to 6.5 C in July 2011 in different altitude regions (Table 6.2). RH shows somewhat more differences, particularly in lower troposphere and middle-to-upper troposphere. Observation and model both agree

reasonable well and showed strong winds around 9-13 km with very high values in winter. This confirms presence of the sub-tropical jet stream in this region and period. Model simulated wind speed is lower by about 5 m/s in 9-13 km region during winter when compared with the observations.

Table 6.2: *Differences (radiosonde - model) between observed temperature, RH and wind speed and model simulated data for five altitude regions. Negative values are indicative that model values are higher than the observed value and vice-versa. Percentage differences are shown in the brackets.*

Altitude region	Temperature Difference (%)		RH Difference (%)		Wind Speed Difference (%)	
	Jan-12	Jul-11	Jan-12	Jul-11	Jan-12	Sep-11
02-05 km	-2.2 (40)	-2.8 (-25)	3.8 (9)	9.3 (12)	0.9 (14)	-2.9 (-69)
05-10 km	-0.5 (1.7)	0.2 (-2)	0.3 (2)	3.4 (6)	1.4 (4)	0.6 (7)
10-15 km	0.8 (-1)	1.8 (-4)	-4.4 (-139)	-2.5 (-7)	3.1 (5)	1.5 (11)
15-20 km	-0.8 (1)	1.6 (-2)	-3.4 (-104)	-2.4 (-9)	-4.8 (-19)	-1.0 (-13)
20-25 km	2.2 (-4)	2.5 (-4)	0.9 (62)	3.1 (85)	-1.1 (-13)	-1.9 (-24)

6.5 Seasonal variations in wind speed near sub-tropical jet

Seasonal variations in wind speed from radiosonde data are further studied in the region of sub-tropical jet i.e. 250 hPa and compared with 100 hPa and 500 hPa regions (Figure 6.6). Maximum speed is observed during winter (57.9±13.6 m/s) and minimum during summer-monsoon (12.7±7.5 m/s). Variability in wind speed is seen to be greater during January with speed as-high-as about 84 m/s and lowest is about 2 m/s during September [*Naja et al.,* 2016]. Wind speed follows nearly similar monthly variations at higher altitude (100 hPa) and lower altitude (500 hPa)

regions.

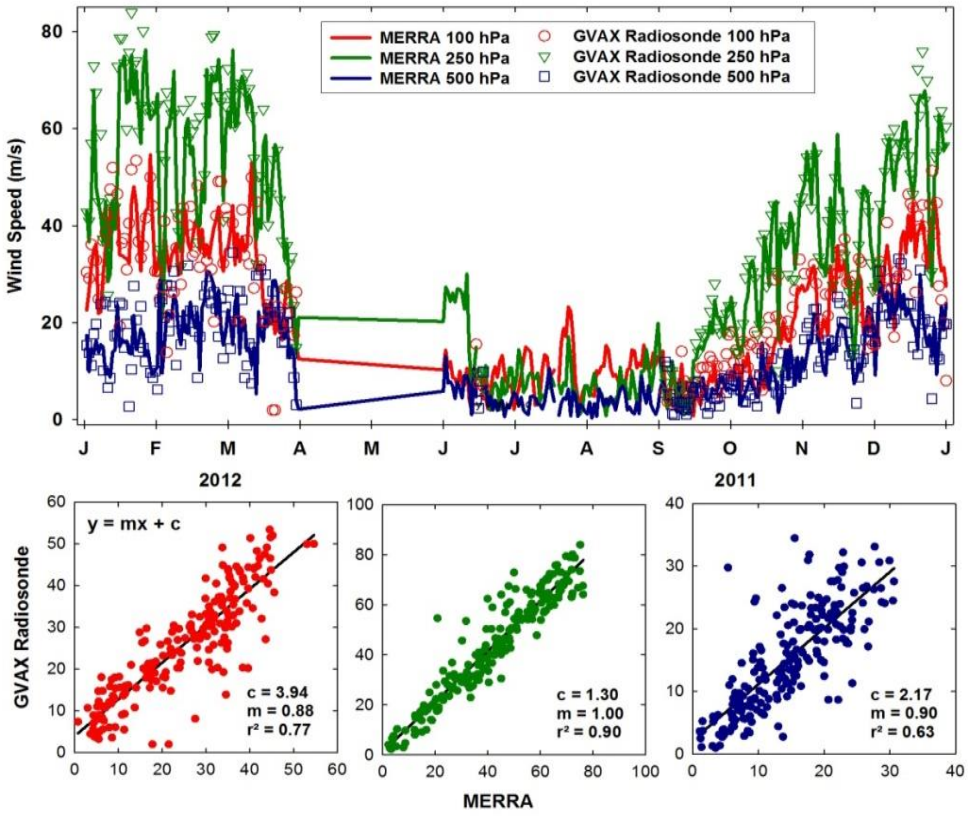

Figure 6.6: *Monthly variations in observed wind speed and MERRA wind speed at peak altitude of sub-tropical jet i.e. 250 hPa and also at 100 hPa and 500 hPa. Correlation between them is also shown in the three altitude regions.*

Figure 6.6 also shows seasonal variations in wind speed derived from Modern Era Retrospective-Analysis for Research and Application (MERRA) and these found to be in reasonable agreement with the observed winds at all three altitudes. Wintertime average MERRA winds (54.3±13.4 m/s) is more-or-less similar to the those of observed winds from radiosonde at 250 hPa (Table 6.3). Such similarity is also seen between MERRA (35.2±7.0 m/s) and radiosonde winds (35.1±9.7 m/s) at 100 hPa and also at 500 hPa (18.9±5.7 m/s and 19.4±6.8 m/s). Correlation between MERRA and radiosonde winds are positive (r^2 = 0.9) at 250 hPa. This correlation is slightly lower at 100 hPa (0.77) and 500 hPa (0.63).

Table 6.3: *Average wind speed from radiosonde and MERRA at the three pressure levels.*

Pressure Levels (hPa)	DJF		JJAS	
	MERRA	Radiosonde	MERRA	Radiosonde
100	35.2 ± 7.0	35.1 ± 9.7	9.0 ± 4.1	8.5 ± 3.7
250	54.3 ± 13.4	57.9 ± 13.6	10.3 ± 7.1	12.7 ± 7.5
500	18.9 ± 5.7	19.4 ± 6.8	4.5 ± 2.6	5.1 ± 2.8

6.6 Biases in AIRS retrieved temperature profiles

Temperature profiles from the Atmospheric Infrared Sounder (AIRS) are found to be more-or-less in agreement, in terms of altitude variations, with the average temperature profiles of radiosonde (Figure 6.7). Correlation between radiosonde and AIRS temperatures are positive ($r^2 \sim 0.9$). However, AIRS data show a negative bias (AIRS temperature lower than radiosonde temperature) of about 5^{o}C in the lower troposphere region. This bias is mainly from lower altitude region (Figure 6.8), except in summer, when this bias is seen at higher altitude also. Both the data set showed a lowest temperature in winter and highest temperature in summer-monsoon in the lower troposphere.

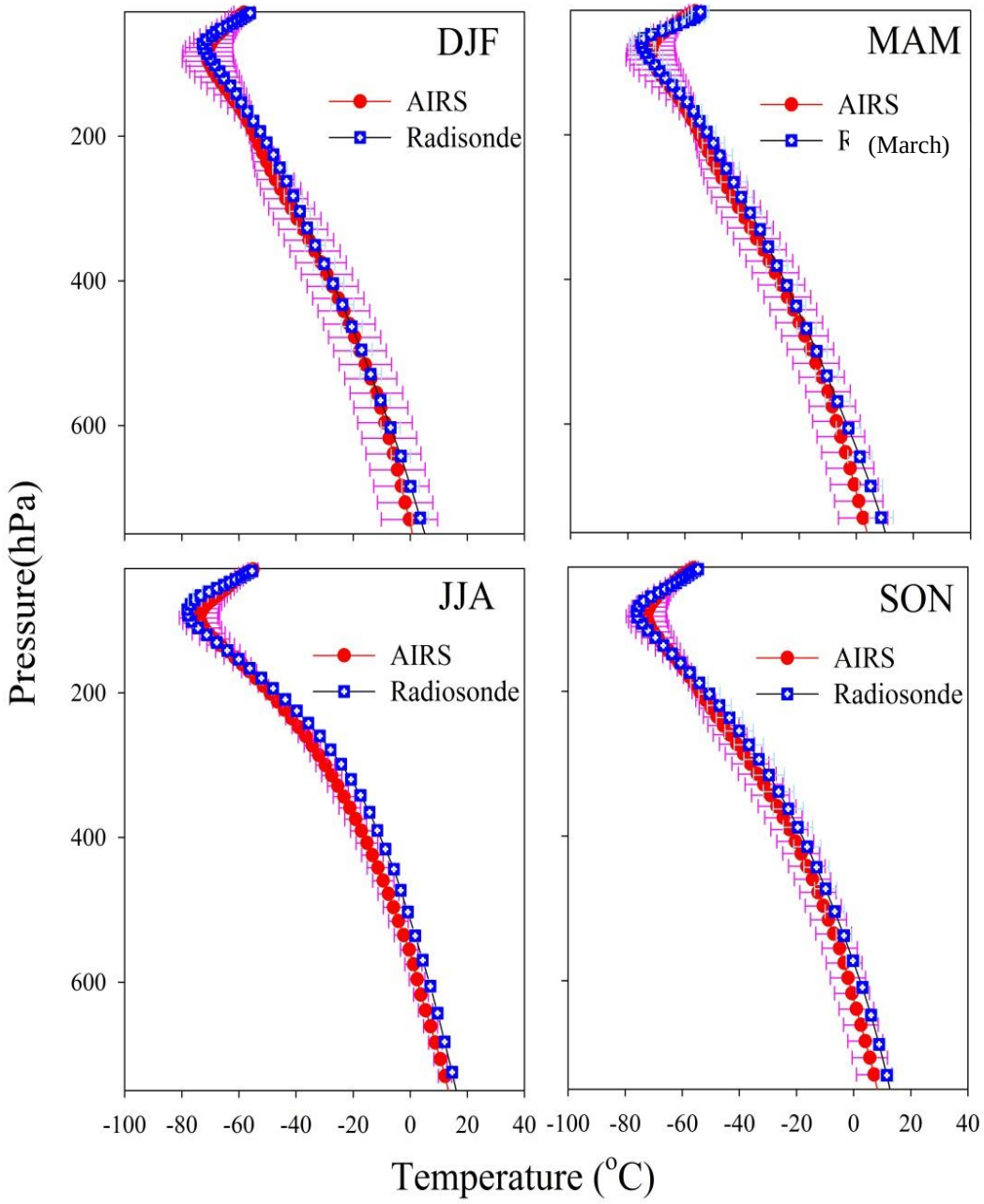

Figure 6.7: *Seasonal average temperature profiles from radiosonde and AIRS. Radiosonde observations are available only during March in spring.*

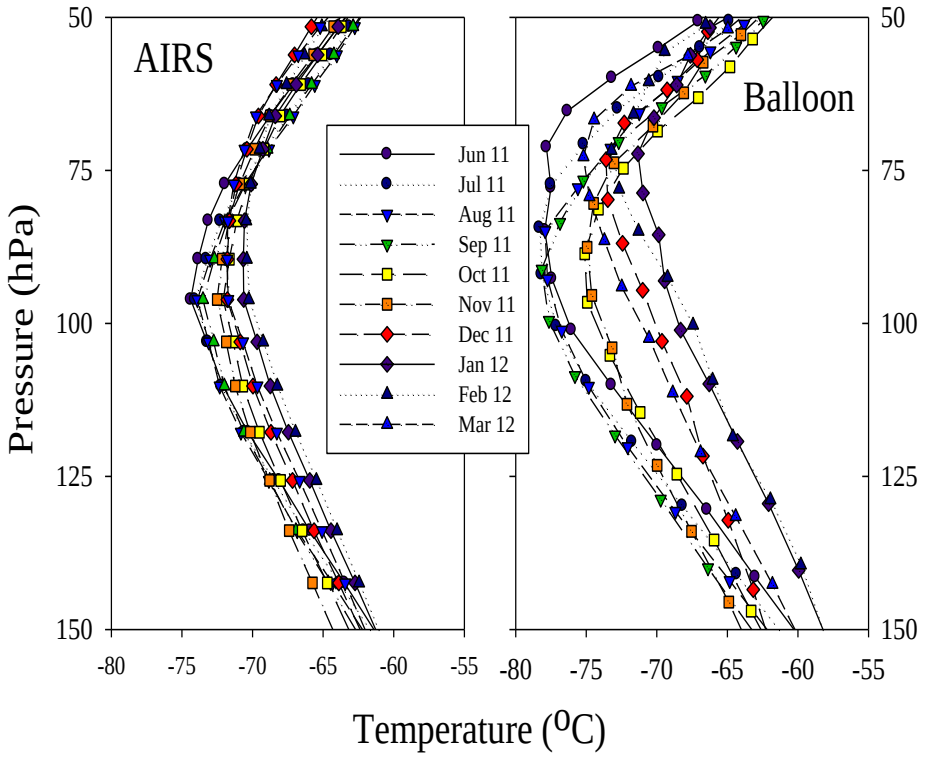

Figure 6.8: *Radiosonde monthly average temperature (°C) profile and data retrieved from AIRS over the central Himalayas in the (a) lower troposphere (600-800 hPa) and (b) upper troposphere-lower stratosphere region (150-50 hPa) from June 2011 to March 2012.*

Figure 6.8 also shows detailed information in the temperature variations from radiosonde data and AIRS data in the tropopause region. In general, monthly variations in both the data set are similar, however month-to-month variations are greater in case of radiosonde data. It is to be noted that the AIRS temperature shows positive bias in the tropopause temperature, in contrast to the lower troposphere region where AIRS temperature show negative biases in the lower altitude region (Figure 6.8) [*Naja et al.,* 2016]. Additionally, tropopause altitude is somewhat higher in case of radiosonde. This will be discussed further in the next section.

6.7 Seasonal variations in the tropopause

Seasonal variations in the tropopause pressure, temperature and height, estimated from radiosonde observations (1130 IST) are shown in figure 6.9. The tropopause height is 16-17 km with tropopause pressure of about 100 hPa and tropopause temperature of about 200 K. Tropopause pressure is calculated using WMO's criteria for determination of tropopause. According to this, the lowest level at which the lapse rate decreases to 2 deg K per kilometer or less, provided also the average lapse rate between this level and all higher levels within 2 kilometers does not exceed 2 deg K. We have further discarded profiles having tropopause height lesser than 12 km and this has led to removal of 62 profiles.

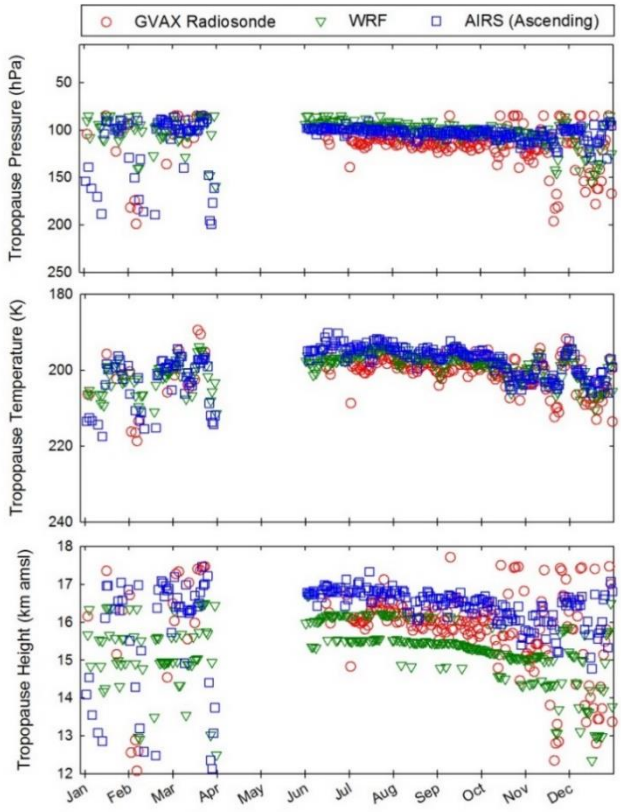

Figure 6.9: *Seasonal variations in the estimated tropopause pressure, temperature and height from radiosonde observations. Estimations from WRF model results and space-borne (AIRS) sensors are also shown.*

The tropopause height and the tropopause temperature are defined corresponding to the determined tropopause pressure. These are also estimated from WRF model results and AIRS using the same definition. Tropopause shows greater variability during winter and early spring, while it is almost stable in summer-monsoon and early autumn [*Naja et al.,* 2016]. Greater variations during winter are mainly due to double tropopause and tropopause break [*Kumar et al.,* 2012a]. The tropopause height shown to have greater deviation ~30-40 hPa in subtropics than in tropics ~10-20 hPa [*Fueglistaler et al.,* 2009].

6.8 Conclusions

This results obtained from high frequency (4 launches per day) balloon-borne observations of meteorological parameters (pressure, temperature, relative humidity, wind speed and wind direction) during RAWEX-GVAX are shown. These observations show wind speed as high as 84 m/s near the subtropical jet. It is shown that reanalysis wind speeds are in better agreement at 250 hPa (altitude of subtropical jet) than those at 100 hPa or 500 hPa. These observations also indicate that Atmospheric Infrared Sounder (AIRS) temperature profiles are negatively biased in the lower altitude region, while they are positively biased near tropopause. WRF simulated results are able to capture variations in temperature, humidity and wind speed profile reasonable well. WRF and AIRS derived tropopause height, tropopause pressure, tropopause temperature also show agreement with radiosonde estimates.

Chapter 7

Summary and Future Perspectives

Present thesis is aimed to understand the underlying processes and fill the gaps through surface based and balloon-borne observations of ozone and related trace gases, analysis of data from space-borne sensors and modeling over the densely populated Indian subcontinent, which is also highly polluted and one of the least studied regions in the world. In this thesis, results from two extensive field campaigns conducted in the Himalayan region viz., SusKat and RAWEX-GVAX are discussed. Apart from these measurements, a satellite based study of biomass burning over the Indian subcontinent, and balloon borne measurements of ozone and met parameters over Nainital are also discussed. The results from these studies has been presented in the chapters 3, 4, 5 and 6 and here, a summary of above studies and their conclusions are discussed in the following subsections.

7.1 Biomass burning over the Indian subcontinent

The impact of biomass burning on the regional distribution of trace gases has been a focus of several studies in the past, however such studies were mostly done over the USA, southeast Asian and Africa. The impacts of biomass burning on regional air quality and budgets of various trace gases is not very well understood over the Indian subcontinent. In this regard, the seasonal, inter-annual and long-term variability of the fire activity over this region, using more than a decade long record (2003-2013) of active fire locations retrieved by MODIS are studied. The uncertainty in biomass burning emissions over South Asia is estimated using different emission inventories. In addition, MODIS retrieved aerosol optical depth and OMI retrieved tropospheric column NO_2 are also used to examine the effects of biomass burning on tropospheric pollution loadings in the cropland and forest regions.

The biomass burning activity in South Asia is observed to be less frequent than Southeast Asia but more frequent than East Asia. Interannual variability is seen to be largest over Southeast Asia (85%) followed by South Asia and East Asia. However, the burning season is longer (January to June) over East Asia compared to South and Southeast Asia (February-May). Within South Asia (Indian subcontinent), the fire activity shows large spatial and temporal variations. Among the four defined regions in the subcontinent, the frequency of fire activity is lowest in the south region and is more-or-less similar over the north, central and northeast regions. The fire activity in Indian subcontinent shows a distinct seasonal cycle with maximum during February-May in both the MODIS and AATSR retrievals but with

some differences in levels. The peak fire activity show large variability among different regions in South Asia like the northeast region shows peak fire in March, over the central region in March-April, over the north region in May and over the south region in March. A secondary peak in fire counts over north region, mainly cover by cropland is due to smoldering form of combustion that takes place at the lower temperature.

Fire counts are observed to be greater (20%) over South Asia during 2008-2013 than those during 2003-2007. This increase is driven mostly (24%) by increase of fire in the north and central regions of South Asia. Uncertainties in CO, NOx and BC emissions from biomass burning estimates in GFED and GFAS are quantified over the defined four regions of South Asia. The CO emissions are estimated to be about 121% higher in case of GFED when compared with those of GFAS over the cropland regions (north and central regions) in spring. On the other hand, CO emissions in GFED are lower (44-77%) over south and northeast region. NO_x also show nearly similar differences between the two inventories. MODIS AOD and OMI tropospheric column NO_2 retrievals are segregated in high and low fire activity periods. The comparison of AOD and NO_2 retrievals between the low and high fire activity periods showed that the biomass burning significantly enhances tropospheric pollution over both the cropland and forest regions. However, the percentage increase in the forest (110-176 %) is estimated to be much higher than the cropland region (34-62 %).

7.2 Ozone and related trace gases over Himalayas and its foothills

The Himalayan region is among the least studied parts in the world, despite its known importance. Only, a few studies of surface measurements of ozone and related trace gases were reported from its Indian region [*Kumar et al.,* 2010; *Ojha et al.,* 2012; *Sarangi et al.,* 2014]. Few observations are also made in Nepal [e.g. *Pandey and Prinn,* 2009], however there has been lack of systematic and simultaneous observations of ozone and its precursors. In light of above facts, Sustainable atmosphere for Kathmandu valley (SusKat) field campaign was initiated during December 2012 in the Kathmandu valley for about two months and later it was extended for few more months. Here, this study presents results from surface measurements of ozone and CO at Bode in the Kathmandu valley and Indian sites *viz.,* Nainital and Pantnagar for a period of about 6 months from Jan 2013 to Jun 2013.

The Kathmandu valley receives its 90% of the rainfall during monsoon months (Jun-Sep) and the solar radiation peaks during spring season. The high surface wind speed (4-5 m/s) mostly north or south-westerlies were observed during mid to late afternoon, which ceases to slow easterlies during night and early morning in the valley. The diurnal variations in ozone and CO shows higher levels of ozone during daytime, and morning/evening peaks in CO. This daytime build-up in ozone is consistent during all months, with relatively smaller increment during the month of June due to prevailing cloudy or rainy conditions. Such daytime increment in surface ozone is due to its photochemical production from precursors in presence of sunlight [*Kleinman et al.,* 1994]. The very low nighttime levels of ozone were

also observed during winter season, which can be attributed to titration and surface deposition of ozone. The diurnal variations in CO showed two peaks during morning and evening hours and such distribution is common to a polluted site. The evening peak was relatively less prominent which might be due to fast westerly winds blowing across the valley during daytime that flushes out CO. On the contrary, the winds cease out during nighttime and due to overnight accumulation of CO, the highest levels were observed during morning time. After reaching its maximum levels during morning time (up to 3000 ppbv in winter months), the levels decrease as day progresses. This decrease can be attributed to the boundary layer evolution which dilutes the CO levels and is further decreased due to its reaction with OH radical.

The correlations between ozone and CO indicate highest negative correlation in winter period (r^2=0.82 in January and r^2=0.71 in February) and this negative correlation reduces gradually with lowest value in May (r^2=0.12). Hourly average CO level also shows a systematic decrease from its level of about 2100 ppbv in January to about 600 ppbv in June, while ozone shows opposite tendency. The weaker negative correlation is observed during early morning (0300-0500 and 0730-0830 hours) or night hours (2200-2300 hours), while a slight positive correlation is seen during noon period (1300-1500 hours). This analysis suggests that the background ozone value could be 13-14 ppbv and background CO value could be about 325 ppbv.

It is shown that ozone and CO levels are higher at Bode than those at one of the IGP site (Pantnagar) in the Himalayan foothill, particularly in winter. The rate of change of ozone during morning and evening hours are different at Bode, with faster ozone increase rate in day (about 17 ppbv/hour) but slower ozone decrease rate (5-6 ppbv/hour) in the evening. This is suggesting Bode as a rural site. The slower decrease rate in evening time ozone and lower value of CO during spring, confirms somewhat lesser contribution of local pollutions in spring ozone enhancement in the valley. Regional contribution in this regards cannot be ruled out.

Simultaneous increase in ozone and CO levels were observed at Bode, Pantnagar and Nainital during the first week of May. The MOZART simulations also indicated about two-fold increase in near-surface CO levels. During the same period, the MODIS derived fire location showed 256% increment over the Punjab region in IGP which could emit large amounts of precursor gases. Further, during the event, the air masses arriving at Nainital, Pantnagar and Bode were coming from Punjab region. The balloon borne ozone profiles from Nainital also confirmed the significant enhancement in ozone (~16 ppbv) in lower troposphere between the balloon flights on 9 and 1 May 2013. Such events are mainly observed during spring season, when influences of regionally polluted air masses from the IGP region are observed over measurement sites in the Himalayan region.

The high resolution WRF-Chem simulations were also used to study observed variability in meteorological parameters, ozone and CO during SusKat campaign.

The differences in daytime (1100-1600 hours) temperature between WRF model observations are found to be less (~1^{o}C), however large variations (4-8^{o}C) were seen during the night time. Similar differences in relative humidity (RH) were also observed with lesser daytime differences. Further the differences in wind speeds are lower (< 1m/s) and wind directions were also in good agreement. The model setup is modified while increasing eta levels and using higher spatial resolution results. This has shown improvement in results over a mountain site Nagarkot, where the differences in temperature and RH are lesser than 2 ^{o}C and 15% even during nighttime, respectively. Modeled ozone is somewhat overestimating while it is underestimating CO values. Nevertheless, further improvement is needed, particularly with high resolution of emission inventories. Different land use schemes need to be tested and applied over this region of complex topography.

7.3 Balloon borne observations of ozone over Nainital

Different satellite based observations have indicated large spatial variability in tropospheric column ozone distribution over the Indian subcontinent with highest levels across IGP region [*Fishman et al.,* 2003]. However, there is lack of observational support to verify this. The previous balloon borne measurements were mainly focused over the western India [*Srivastava et al.,* 2012, *Lal et al.,* 2014, 2015] and the Indian Ocean region [*Srivastava et al.,* 2011]. Over IGP, limited measurements were performed during a campaign [*Gupta et al.,* 2007]. In light of this, observations of ozone vertical distribution were initiated from Nainital. These observations were initiated in year 2011, which are further extended till year 2015 during this work. This thesis presents complete long-term observations during

2011-2015 period. Total 203 flights were conducted and data from 198 flights are using for meteorological parameters and 195 flights are used for ozone.

The ozone vertical distribution shows strong seasonality over this region with near surface ozone showing highest levels during May (90.6 ± 13.2 ppbv) and lowest during August (38.7 ± 8.7 ppbv). However, during summer monsoon period the highest variability is observed which could be due to highly variable meteorological conditions (including change in wind direction from north-westerly to south-easterly) during that period. The highest variability, in the middle troposphere, is observed during winter season (54%) and the lowest in autumn (20%) season. The maximum variations during winter season can be attributed to various dynamical processes, since that period coincides with the strongest wind speeds and presence of multiple tropopause and tropopause break events. These variations in ozone levels again changes as we move to higher altitudes, where ozone variations are highest in spring season (57%) and lowest in summer (21%) season. The five-year long ozone observations show a decreasing trend of about 1.6 ppbv and about 2.5 ppbv in 2-4 and 8-12 km, however a positive trend of about 3.2 ppbv is observed in the 12-14 km region. Very small positive trend of (0.2 ppbv) is observed in the 4-8 km region.

The northern Indian biomass burning is shown to enhance the ozone levels with in first 2 km with average ozone levels of 89 ± 14 ppbv as compared to 66 ± 7 ppbv during high fire and low fire periods. The interannual variations in these fire

induced enhancement is also observed with highest ozone levels (94 ± 13 ppbv) during 2012. The average enhancement during 2011-2014 in 2-4 km altitude range is estimated to be about 23.6 ppbv, with levels ranging from 15.4 to 30.5 ppbv. At higher altitudes (4-6 km) however, relatively less enhancement was observed. Apart from biomass burning, the dynamical processes such as stratosphere- troposphere exchange also influences the vertical ozone distribution. Here five cases of downward transport of ozone rich air from stratosphere were observed during 2011-2015. All of these events indicated the elevated levels of ozone (1.7-2.9 times the monthly mean) in upper-middle troposphere during the event. The corresponding increase in PV levels were 1.4 to 3.6 times. In general, the PV during the all events were much higher than the threshold value of 1.6 PVU. In these events, the increase in ozone and PV levels are also accompanied by decrease in CO and RH levels which strongly suggests that these enhancements in ozone levels are due to downward transport from stratosphere.

7.4 Vertical profiling of meteorological parameters during RAWEX-GVAX campaign

The vertical measurements of meteorological parameters are essential to understand the meteorological characteristics of a region and dynamical processes occurring in the troposphere. In light of this, high frequency balloon borne observations of meteorological parameters were made during an extensive field campaign, RAWEX-GVAX (Regional Aerosols Warming Experiment - Ganges Valley Aerosol Experiment) at Nainital. During the campaign period of about 10 months (June 2011 to March 2012) daily four balloons were launched. These observations

show high wind speed (up to ~84 m/s) in the middle troposphere near the subtropical jets. The reanalysis wind speeds from MERRA were in better agreement at 250 hPa (altitude of subtropical jet) than those at 100 hPa or 500 hPa. These observations also showed that the AIRS temperature profiles are negatively biased in the lower altitude region, while they are positively biased near tropopause. WRF simulated results are able to capture variations in temperature, humidity and wind speed profile reasonable well. WRF and AIRS derived tropopause height, tropopause pressure, tropopause temperature also show agreement with radiosonde estimates.

7.5 Future Scope

Observation of surface ozone, precursor gases and meteorological parameters are made at different sites during this thesis. Further, balloon borne observations of ozone and meteorological parameters were also made. These observations showed some of the underlying processes that influence the levels of ozone and related trace gases in these regions. Further the vertical measurements are used to show influences of various regional scale processes such as northern Indian biomass burning and stratosphere troposphere exchange on vertical distribution of ozone. The satellite based study of biomass burning provided the variabilities in biomass burning over this region and discrepancies associated with their budgets using various emission inventory datasets. High resolution WRF-chem model set up was performed and tested over the northern Indian region. In continuation of these studies a number of interesting prospects that can be further investigated are :

- More efforts are required to understand role of biomass burning induced changes in the atmospheric composition leading to change in the air quality, monsoonal rainfall and regional climate over this part of the world. Such efforts would require an integration of the simultaneous observations of different trace species (including biomass tracers), analysis of satellite data and chemical transport models, which is generally lacking in this region.
- During the SusKat observations, it was realized that the collocated measurements of ozone, CO, NOx, VOCs, OH radical, formaldehyde N_2O_5, HNO_3, PAN, boundary layer height, meteorological parameters and estimation of fluxes are essential to understand the ozone chemistry in a particular region. Further the vertical profiling of meteorological parameters and some of the gases would provide in-depth information on the transport of air masses. Emphasis need to be given on understanding of the nighttime chemistry over this region.
- The discrepancies between the model and observation results over Indian subcontinent can be mainly attributed to large uncertainties in the input emission datasets. To improve these emission inventories, inverse models should be used to assimilate satellite and ground based datasets over this region. Further, these simulations should be used to quantify the impacts of uncertainties in the emission estimates on the budgets of tropospheric ozone and related gases in this region. To further improve the model output, tuning in model setup is also required, which includes testing of various land surface models etc.

Bibliography

Adams R. M., B. H. Hurd, S. Lenhart and N. Leary (1998), Effects of global climate change on agriculture: an interpretative review, Clim. Res., 11,19 – 30.

Ahmad S. S. and N. Aziz (2013), Spatial and temporal analysis of ground level ozone and nitrogen dioxide concentration across the twin cities of Pakistan, Environmental Monitoring and Assessment, 185, 3133–3147.

Akimoto, H. (2003), Global air quality and pollution, Science, 302, 1716-1719, doi: 10.1126/science.1092666.

Andreae M. O. and P. J. Crutzen (1997), Atmospheric Aerosols: Biogeochemical Sources and Role in atmospheric chemistry, Science, doi:10.1126/science.276.5315.1052.

Andreae M. O. and P. Merlet (2001), Emission of trace gases and aerosols from biomass burning, Global Biogeochem. Cycles, doi:10.1029/2000GB001382

Arino O., S. Casadio and D. Serpe (2011), Global night-time fire season timing and fire count trends using the ATSR instrument series, Remote Sensing of Environment, doi:10.1016/j.rse.2011.05.025.

Ashmore, M. R (2005), Assessing the future global impacts of ozone on vegetation, Plant Cell Environ., 28, 949– 964.

Asnani, G. C. (2005), Climatology of the tropics, in Tropical Meteorology-1, 100-204, Pune, India.

Attmannspacher, W., and H. Du¨tsch (1970), International Ozone Sonde Intercomparison at the Observatory of Hohenpeissenberg, Rep. 120, Dtsch. Wetterdienstes, Offenbach, Germany.

Avnery, S., D. L. Mauzerall, J. Liu and L. W. Horowitz (2011a), Global crop yield reductions due to surface ozone exposure: 1. Year 2000 crop production losses and economic damage, Atmos. Environ., doi:10.1016/j.atmosenv.2010.11.045.

Avnery, S., D. L. Mauzerall, J. Liu and L. W. Horowitz (2011b), Global crop yield

reductions due to surface ozone exposure: 2. Year 2030 potential crop production losses and economic damage under two scenarios of O_3 pollution, Atmos. Environ., doi:10.1016/j.atmosenv.2011.01.002.

Badrinath, K. V. S., A. R. Sharma, S. K. Kharol and V. K. Prasad (2009), Variations in CO, O3 and black carbon aerosol mass concentrations associated with planetary boundary layer (PBL) over tropical urban environment in India, J. Atmos. Chem., 62, 73-86.

Barnes, R. A., A. R. Bandy and A. L. Torres (1985), Electrochemical concentration cell ozonesonde accuracy and precision, J. Geophys. Res., 90, 7881– 7887.

Beekmann, M., G. Ancellet and G. Megie (1994), Climatology of tropospheric ozone in southern Europe and its relation with potential vorticity, J. Geophys. Res., 99, 12841–12853.

Beig, G., N. Saraf and S. K. Peshin (2002), Evidence of Pinatubo volcanic eruption on the distribution of ozone over the tropical Indian region, J. Geophys. Res., 107, 4674, doi: 10.1029/2002JD002337.

Beig, G. and G. P. Brasseur (2006), Influence of anthropogenic emissions on tropospheric ozone and its precursors over the Indian tropical region during a monsoon, Geophys. Res. Lett., 33, L07808, doi: 10.1029/2005GL024949.

Beig, G. and K. Ali (2006), Behavior of boundary layer ozone and its precursors over a great alluvial plain of the world: Indo-Gangetic Plains, Geophys. Res. Lett., 33, L24813, doi: 10.1029/2006GL028352.

Bhardwaj P., M. Naja, R. Kumar and H. C. Chandola (2015), Seasonal, interannual and long term variabilities in biomass burning activity over South Asia, Environ. Science and Pollution research, doi:10.1007/s11356-015-5629-6.

Bhuyan P. K., C. Bharali, B. Pathak and G. Kalita (2014), The role of precursor gases and meteorology on temporal evolution of O_3 at a tropical location in northeast India, Environmental Science and Pollution Research, 21 , 6696–6713.

Blake N. J., D. R. Blake, S. O. W. Wingenter (1999), Influence of southern hemispheric biomass burning on midtropospheric distributions of nonmethane hydrocarbons and selected halocarbons over the remote South Pacific, J. Geophys. Res, doi:10.1029/1999JD900067.

Bojkov, D. R. (1988), Ozone changes at the surface and in the free troposphere, in Tropospheric Ozone: Regional and Global Scale Interactions, edited by I. S.

A. Isaksen, 83-96, D. Reidel, Dordrecht, Netherlands.

Bonasoni, P., P. Laj, A. Marinoni, M. Sprenger, F. Angelini, J. Arduini, U.Bonafe, F.Calzolari, T. Colombo, S. Decesari, C. Di Biagio, A. G. di Sarra, F.Evangelisti, R. Duchi, M. C. Facchini, S. Fuzzi, G. P. Gobbi, M. Maione, A. Panday, F., Roccato, K.Sellegri, H. Venzac, G.P. Verza, P. Villani, E. Vuillermoz and P. Cristofanelli (2010), Atmospheric Brown Clouds in the Himalayas: first two years of continuous observations at the Nepal-Climate Observatory at Pyramid (5079 m), Atmos. Chem. Phys. Discuss., 10, 4823–4885, doi:10.5194/acpd- 10-4823-2010.

Bousquet, P. (2005), Two decades of OH variability as inferred by an inversion of atmospheric transport and chemistry of methyl chloroform, Atmos. Chem. Phys., 5, 1679–1731.

Boyd, I. S., G. E. Bodeker, B. J. Connor, D. P. J. Swart and E. J. Brinksma (1998), An assessment of ECC ozonesondes operated using 1% and 0.5% KI cathode solutions at Lauder, New Zealand, Geophys. Res. Lett., 25, 2409–2412.

Brasseur, G. P., J. J. Orlando and G. S. Tyndall (1999), Atmospheric Chemistry and Global Change, 209-234, Oxford University Press, New York.

Brentsen, T. I., S. A. Isaksen, W. Wang and X. Liang (1996), Impacts of increased anthropogenic emissions in Asia on tropospheric ozone and climate, Tellus, 48B, 13-32.

Brewer, A.W. and J. G. Milford (1960), The Oxford-Kew Ozone Sonde, Proc. Roy. Soc. London, Ser. A, 470–495.

Bucsela E. J., N. A., KrotkovE. A. Celarier and et al (2013), A new stratospheric and tropospheric NO_2 retrieval algorithm for nadir-viewing satellite instruments: applications to OMI, Atmos Meas Tech. doi:10.5194/amt-6-2607-2013.

Chameides, W. L. and J. C. G. Walker (1973), A photochemical theory of tropospheric ozone, J. Geophys. Res., 78, 8751 – 8760.

Chand, D., K. S. Modh, M. Naja, S. Venkataramani and S. Lal (2001), Latitudinal trends in O_3, CO, CH4 and SF_6 over the Indian Ocean during the IFP INDOEX-1999 ship cruise. Current Science, 80, 100 – 104.

Chand, D., S. Lal and M. Naja (2003), Variations of ozone in the marine boundary layer over the Arabian Sea and the Indian Ocean during the 1998 and 1999 INDOEX campaigns, J. Geophys. Res., 108, 4190,

doi:10.1029/2001JD001589.

Chen, X. L., Y. M. Ma, H. Kelder, Z. Su and K. Yang (2011), On the behavior of the tropopause folding events over the Tibetan Plateau, Atmos. Chem. Phys., 11, 5113–5122.

Chen, Y.-H. and R. G. Prinn (2006), Estimation of atmospheric methane emissions between 1996 and 2001 using a three-dimensional global chemical transport model, J. Geophys. Res., 111, D10307, doi:10.1029/2005JD006058.

Chin, M., R. B. Rood, S. -J. Lin, J. -F. Müller and A. M. Thompson (2000), Atmospheric sulfur cycle simulated in the global model GOCART: Model description and global properties, J. Geophys. Res., 105(D20), 24671–24687, doi:10.1029/2000JD900384.

Chuwah C., T. van Noije, D. P. van Vuuren, E. Stehfest, W. Hazeleger (2015), Global impacts of surface ozone changes on crop yields and land use, Atmospheric Environment, 106, 11 – 23, doi:10.1016/j.atmosenv.2015.01.062.

Claude, H., R. Hartmannsgruber and U. Köhler (1987), Measurement of atmospheric profiles using the Brewer-Mast sonde, WMO Rep. 17, Global Ozone Res. and Monit. Proj., World Meteorol. Org., Geneva.

Cooper, O. R., D. D. Parrish, A. Stohl, M. Trainer, P. Nédélec, V. Thouret, J. P. Cammas, S. J. Oltmans, B. J. Johnson, D. Tarasick, T. Leblanc, I. S. McDermid, D. Jaffe, D., R. Gao, J. Stith, T. Ryerson, K. Aikin, K., T. Campos, A. Weinheimer. and A. Avery (2010), Increasing springtime ozone mixing ratios in the free troposphere over western North America, Nature, 463, 344-348, doi: 10.1038/nature08708.

Cristofanelli, P. *and et al. (*2003*),* Stratosphere-to-troposphere transport: A model and method evaluation, J. Geophys. Res., 108, *8525*, *doi:*10.1029/2002JD002600, D12.

Cristofanelli, P., P. Bonasoni, L. Tositti, U. Bonafe, F. Calzolari, F. Evangelisti, S. Sandrini and A. Stohl (2006), A 6-year analysis of stratospheric intrusions and their influence on ozone at Mt. Cimone (2165 m above sea level), J. Geophys. Res., 111, D03306, doi:10.1029/2005JD006553.

Cristofanelli, P. and et al. (2010), Tropospheric ozone variations at the Nepal Climate Observatory-Pyramid (Himalayas, 5079 m a.s.l.) and influence of deep stratospheric intrusion events, Atmos. Chem. and Phys., 10, 6537-6549.

Crutzen P. J. and M. O. Andreae (1990), Biomass burning in the tropics: impact on atmospheric chemistry and biogeochemical cycles, Science, doi:10.1126/science.250.4988.1669.

Crutzen, P. J. (1973), A discussion of the chemistry of some minor constituents in the stratosphere and troposphere, Pure Appl. Geo-Phys., 106-108, 1385-1399.

Crutzen, P. J. (1995), Ozone in the troposphere, in composition, Chemistry and Climate of the Atmosphere, edited by H. B. Singh, 349 – 393.

Daniel, J. S. and S. Solomon (1988), On the climate forcing of carbon monoxide, J. Geophys. Res., 103, 13,249 – 13,260.

Danielsen, E. F. (1968), Stratosphere-troposphere exchange based on radioactivity, ozone, and potential vorticity, J. Atmos. Sci, 25, 502-518.

Dave, J. V. (1957), Studies on twilight and atmospheric ozone, Ph. D. Thesis, pp.III.1-III.29, Gujarat University at Ahmedabad, India.

Davies, T.D. and E. Schuepbach (1994), Episodes of high ozone concentrations at the earth's surface resulting from transport down from the upper troposphere/lower stratosphere: a review and case studies, Atmos. Environ,. *28*, 53-68.

De, N. S., S. Sen and D. K. Chakrabarty (2009), Surface ozone and its precursors at two sites in the northeast coast of India, Indian Journal of Radio & Space Physics, 38, 86-97.

de Foy, B., J.R. Varela, L.T. Molina and M.J. Molina (2006), Rapid ventilation of the Mexico City basin and regional fate of the urban plume. Atmospheric Chemistry and Physics, 6, 2321-2335.

Denman, K. L., G. Brasseur, A. Chidthaisong, P. Ciais, P. M. Cox, R. E. Dickinson, D. Hauglustaine, C. Heinze, E. Holland, D. Jacob, U. Lohmann, S. Ramachandran, P. L. da Silva Dias, S. C. Wofsy and X. Zhang (2007), Couplings Between Changes in the Climate System and Biogeochemistry. In: Climate Change 2007: The Physical Science Basis. Contribution of Working Group I to the Fourth Assessment Report of the Intergovernmental Panel on Climate Change [Solomon, S., D. Qin, M. Manning, Z. Chen, M. Marquis, K.B. Averyt, M.Tignor and H.L. Miller (eds.)]. Cambridge University Press, Cambridge, United Kingdom and New York, NY, USA.

Dentener, F., D. Stevenson, K. Ellingsen, T. van Noije, M. Schultz, M. Amann, C. Atherton, N. Bell, D. Bergmann, I. Bey, L. Bouwman, T. Butler, J. Cofala, B.

Collins, J. Drevet, R. Doherty, B. Eickhout, H. Eskes, A. Fiore, M. Gauss, D. Hauglustaine, L. Horowitz, I.S.A. Isaksen, B. Josse, M. Lawrence, M. Krol, J.F. Lamarque, V. Montanaro, J.F. Müller, V.H. Peuch, G. Pitari, J. Pyle, S. Rast, J. Rodriguez, M. Sanderson, N.H. Savage, D. Shindell, S. Strahan, S. Szopa, K. Sudo, R. Van Dingenen, O. Wild, and G. Zeng (2006), The global atmospheric environment for the next generation, Environ. Sci. Technol., 40, 3586-3594, doi:10.1021/es0523845.

Derwent, R. G., P. G. Simmonds, S. Seuring and C. Dimmer (1998), Observation and interpretation of the seasonal cycles in the surface concentrations of ozone and carbon monoxide at Mace Head, Ireland from 1990 to 1994, Atmos. Environ., 32, 145-157.

Deshler, T. and et al. (2008), Atmospheric comparison of electrochemical cell ozonesondes from different manufacturers, and with different cathode solution strengths: The Balloon Experiment on Standards for Ozonesondes, J. Geophys. Res., 113, D04307, doi:10.1029/2007JD008975.

Desqueyroux, H., J. C. Pujet, M. Prosper, F. Squinazi and I. Momas (2002), Short-term Effects of low-level air pollution on respiratory health of adults suffering from moderate to severe asthma, Environ. Res. 89, 29-37.

Dibb, J. E., L. D. Macker, R. C. Finkel, J. R. Southon, M. W. Caffee, L. A. Barrie (1994), Estimation of the stratospheric input to the Arctic troposphere: 7Be and 10Be in aerosols at Alert, Canada, J. Geophys. Res., 99, 12855-12864.

Diouri, M. and et al. (1998), Size distributions of aerosols over NE Morocco and Particulate matter in wet deposition over central Europe, J. Aerosol Sci., 29, S197-S198.

Dozier J., (1981) A method for satellite identification of surface temperature fields of subpixel resolution, Remote Sensing of Environment, doi: 10.1016/0034-4257(81)90021-3.

Draxler, R. R. and G. D. Rolph (*2012), HYSPLIT (HYbrid Single-Particle Lagrangian Integrated Trajectory) Model access via NOAA ARL READY Website (*http://ready.arl.noaa.gov/HYSPLIT.php*), NOAA Air Resources Laboratory, Silver Spring, MD.*

Dumka, U. C., S. K. Satheesh, P. Pant, P. Hegde and K. K. Moorthy (2006), Surface changes in solar irradiance due to aerosols over central Himalayas, Geophys. Res. Lett., 33, L20809, doi: 10.1029/2006GL027814.

Duncan B. N., R. V. Martin, A. C. Staudt, R. Yevich and J. A. Logan (2003), Interannual and seasonal variability of biomass burning emissions constrained by satellite observations, J. Geophys. Res. doi:10.1029/2002JD002378.

Duncan, B. N., J. A. Logan, I. Bey, I. A. Megretskaia, R. M. Yantosca, P. C. Novelli, N. B. Jones and C. P. Rinsland (2007), Global budget of CO, 1988–1997: Source estimates and validation with a global model, J. Geophys. Res., 112, D22301, doi:10.1029/2007JD008459.

Ehhalt, D. H., J. W. Drummond (1982), in *Chemistry of the Unpolluted and Polluted Troposphere*, ed. by H.W. Georgii, W. Jaeschke. NATO ASI Series C 96, 219–251.

Ehhalt, D.H. (1999), Gas phase chemistry of the troposphere. In: Global Aspects of Atmospheric Chemistry, Vol. 6 [Baumgaertel, H., W. Gruenbein, and F. Hensel (eds.)]. Springer Verlag, Darmstadt, pp. 21–110.

Emmons, L. K., S. Walters, P. G. Hess, J. F. Lamarque, G. G. Pfister, D. Fillmore, C. Granier, A. Guenther, D. Kinnison, T. Laepple, J. Orlando, X. Tie, G. Tyndall, C. Wiedinmyer, S. L. Baughcum and S. Kloster (2010), Description and evaluation of the Model for Ozone and Related chemical Tracers, version 4 (MOZART-4), Geosci. Model Dev., 3, 43–67, doi:10.5194/gmd-3-43-2010.

Engardt, M. (2008), Modelling of near-surface ozone over South Asia, J. Atmos. Chem., 59, 61–80, doi:10.1007/s10874-008-9096-z.

Faiz, S., B. B. Ale and R. K. Nagarkoti (2006), The role of inspection and maintenance in controlling vehicular emissions in Kathmandu Valley, Nepal, Atmos. Environ., 40, 5967–5975, doi:10.1016/j.atmosenv.2005.11.064.

Fishman J, J. M. Hoell Jr,R. D. Bendura, R. J. McNeal, V. W. J. H. Kirchhoff (1996), NASA GTE TRACE-A experiment (September–October 1992): Overview, J. Geophys. Res., doi:10.1029/96JD00123.

Fishman J., A. E. Wozniak and J. K. Creilson (2003), Global distribution of tropospheric ozone from satellite measurements using the empirically corrected tropospheric ozone residual technique: Identification of the regional aspects of air pollution, Atmos. Chem. and Phys., 3, 893 – 907.

Forster, P., V. Ramaswamy, P. Artaxo, T. Berntsen, R. Betts, D. W. Fahey, J. Haywood, J. Lean, D.C. Lowe, G. Myhre, J. Nganga, R. Prinn, G. Raga, M. Schulz and R. Van Dorland (2007), Changes in Atmospheric Constituents and

in Radiative Forcing. In: Climate Change 2007: The Physical Science Basis. Contribution of Working Group I to the Fourth Assessment Report of the Intergovernmental Panel on Climate Change [Solomon, S., D. Qin, M. Manning, Z. Chen, M. Marquis, K.B. Averyt, M.Tignor and H.L. Miller (eds.)], Cambridge University Press, Cambridge, United Kingdom and New York, NY, USA.

Freitas, S. R., Longo, K. M., Chatfield, R., Latham, D., Silva Dias, M. A. F., Andreae, M. O., Prins, E., Santos, J. C., Gielow, R., and Carvalho Jr., J. A.: Including the sub-grid scale plume rise of vegetation fires in low resolution atmospheric transport models, Atmos. Chem. Phys., 7, 3385–3398, doi:10.5194/acp-7-3385-2011.

Fueglistaler, S., A. E. Dessler, T. J. Dunkerton, I. Folkins, Q. Fu, and P. W. Mote (2009), Tropical tropopause layer, Rev. Geophys., 47, RG1004, doi:10.1029/2008RG000267.

Fujimoto T., Takahiro S., Katsue N., Tatsumi N., Masanori S., Yoshihiro K., Seiji M., Kazuaki A., Toru S. (2004), Further evaluation and improvements of Japanese KC-Ozonesonde through JOSIE-2000, Quadrennial Ozone Symposium 2004, extended abstracts, 224.

Gadhavi, H. and A. Jayaraman (2006), Airborne lidar study of the vertical distribution of aerosols over Hyderabad, an urban site in central India, and its implication for radiative forcing calculations, Ann. Geophys., 24, 1–10.

Galanter M., H. Levy II, G. R. Carmichael (2000), Impacts of biomass burning on tropospheric CO, NOx, and O_3. J. Geophys Res. doi:10.1029/1999JD901113.

Ganguly, D., A. Jayaraman, T. A. Rajesh and H. Gadhavi (2006), Wintertime aerosol properties during foggy and nonfoggy days over urban center Delhi and their implications for shortwave radiative forcing, J. Geophys. Res., 111, D15217, doi: 10.1029/2005JD007029.

Ganguly N. D. and T. Chris (2011), Study of Stratosphere-Troposphere exchange events of ozone in India and Greece using ozonesonde ascents, Meteorol. Appl., 18, 467 – 474.

Gaur, A., S. N. Tripathi, V. P. Kanawade, V. Tare and S. P. Shukla (2014), Four-year measurements of trace gases (SO_2, NO_x, CO, and O_3) at an urban location, Kanpur, in Northern India, J. Atmos. Chem., 71, 283–301, doi:10.1007/s10874-014-9295-8.

Gauss, M. and et al. (2006), Radiative forcing since preindustrial times due to ozone changes in the troposphere and the lower stratosphere, Atmos. Chem. and Phys., 6, 575–599.

Ghude, S. D., S. Fadnavis, G. Beig, S. D. Polade and R. J. van der A (2008b), Detection of surface emissions hot spots, trends, and seasonal cycle from satellite-retrieved NO_2 over India, J. Geophys. Res., 113, D20305, doi: 10.1029/2007JD009615.

Ghude, S. D., D. M. Lal, G. Beig, R. J. van der A and D. Sable (2010), Rain-Induced Soil NO_x Emissions from India During the Onset of the Summer Monsoon: A Satellite Perspective, J. Geophys. Res., 115, D16304, doi: 10.1029/2009JD013367.

Ghude S. D., S. H. Kulkarni, C. Jena, G. G. Pfister, G. Beig, S. Fadnavis, A. R. J. van der (2013), Application of satellite observations for identifying regions of dominant sources of nitrogen oxides over the Indian Subcontinent, J. Geophys. Res. Atmos., doi:10.1029/2012JD017811.

Ghude, S. D., C. Jena, D. M. Chate, G. Beig, G. G. Pfister, R. Kumar and V. Ramanathan (2014), Reductions in India's crop yield due to ozone, Geophys. Res. Lett., 41, 5685–5691, doi:10.1002/2014GL060930.

Giglio L., J. Descloitres, C. O. Justice, Y. Kaufman (2003), An enhanced contextual fire detection algorithm for MODIS, Remote Sensing of Environment, doi:10.1016/S0034-4257(03)00184-6.

Giglio L. (2010), MODIS Collection 5 Active Fire Product User's Guide Version-2.4
http://www.fao.org/fileadmin/templates/gfims/docs/MODIS_Fire_Users_Guide_2.4.pdf.

Girach I.A. and P. R. Nair (2014), Carbon monoxide over Indian region as observed by MOPITT, Atmos. Env., 599 – 609, doi./10.1016/j.atmosenv.2014.10.019.

Gregory, G. L., H. E. Fuelberg, S. F. Longmore, B. E. Anderson, J. E. Collins, and D. R. Blake.(1996), Chemical characteristics of tropospheric air over the tropical south Atlantic Ocean: Relationship to trajectory history, J. Geophys. Res., 101 (D19), 23 957–23 972.

Grell, G. A., S. E. Peckham, S. A. McKeen, R. Schmitz and G. Frost (2005), Fully coupled ''online'' chemistry within the WRF model, Atmos. Environ., 39, 6957– 6975.

Guenther, A., T. Karl, P. Harley, C. Wiedinmyer, P. I. Palmer and C. Geron (2006), Estimates of global terrestrial isoprene emissions using MEGAN (Model of Emissions of Gases and Aerosols from Nature), Atmos. Chem. and Phys., 6, 3181–3210, doi:10.5194/acp-6-3181-2006.

Gupta, S., S. Lal, S. Venkataramani, T. A. Rajesh and Y. B. Acharya (2007), Variability in the vertical distribution of ozone over a subtropical site in India during a winter month, J. Atmos Sol-Terr Phys (UK), 69, 1502.

Haagen-Smit, A. J. (1952), Chemistry and physiology of Los Angeles smog, Ind. Eng. Chem., 44(6), 1342–1346, doi:10.1021/ie50510a045.

Haq Z-ul, S. T., and A. Muhammad(2015), Tropospheric NO_2 Trends over South Asia during the Last Decade (2004–2014) Using OMI Data, Advances in Meteorology, vol. 2015, Article ID 959284, page 18 , doi:10.1155/2015/959284.

Heard, D. E. (2006), Analytical Techniques for Atmospheric Measurement, Blackwell Publishing, ISBN-13: 978–1–4051–2357–0.

Hegde, P. and et al. (2007), South Asian dust episode in June 2006: Aerosol observations in the central Himalayas, Geophys. Res. Lett., 34, L23802, doi: 10.1029/2007GL030692.

Holland, M. and et al. (2006), Development of a framework for probabilistic assessment of the economic losses caused by ozone damages to crops in Europe, Part of the UNECE International Cooperative Programme on Vegetation, Contact Report EPG, 1/3/205. CEH Project No: C02309NEW, page 49.

Hollaway, M. J., S. R. Arnold, A. J. Challinor and L. D. Emberson (2012), Intercontinental trans-boundary contributions to ozone-induced crop yield losses in the Northern Hemisphere, Biogeosciences, 9, 271–292.

Holloway, T., H. Levy II and P. Kasibhatla (2000), Global distribution of carbon monoxide, J. Geophys. Res., 105(D10), 12123–12147, doi:10.1029/1999JD901173.

Holton, J. R. and et al. (1995), Stratosphere-troposphere exchange, Rev. Geophys., 33 (4), doi: 10.1029/95RG02097.

Holton, J. R. and J. Lelieveld (1996), Stratosphere–troposphere exchange and its role in the budget of tropospheric ozone. Clouds, Chemistry and Climate, P. J. Crutzen and V. Ramanathan, Eds., NATO ASI Series, 35, Springer-Verlag,

173–190.

Hong S., Y. Noh and J. Dudhia (2006), A new vertical diffusion package with an explicit treatment of entrainment processes, Mon. Weather Rev., 134 (9) , 2318–2341.

Hoskins, B. J., M. E. McIntyre and A. W. Robertson (1985), On the use and significance of isentropic potential vorticity maps, Quart. J. Roy. Meteorol. Soc., 111, 877 – 946. [also see corrigendum etc. (1987), 113, 402-404,].

Huffman G. J., R. F. Adler, D. T. Bolvin (2007), The TRMM Multi-satellite Precipitation Analysis: Quasi-Global, Multi-Year, Combined-Sensor Precipitation Estimates at Fine Scale. J. Hydrometeor, 8, 38-55.

IPCC(2013), Climate Change 2013: The Physical Science Basis. Contribution of Working Group I to the Fifth Assessment Report of the Intergovernmental Panel on Climate Change [Stocker, T. F., D. Qin, G.-K. Plattner, M. Tignor, S. K. Allen, J. Boschung, A. Nauels, Y. Xia, V. Bex and P. M. Midgley (eds.)]. Cambridge University Press, Cambridge, United Kingdom and New York, NY, USA, 1535, doi:10.1017/CBO9781107415324.

Jacob, D. J., J.A. Logan and P. P. Murti (1999), Effect of rising Asian emissions on surface ozone in the United States, Geophys. Res. Lett., 26, 2175-2178.

Jain, S. L., B. C. Arya, A. Kumar, S. D. Ghude and P. S. Kulkarni (2005), Observational study of surface ozone at New Delhi, India, International Journal of Remote Sensing, 26(16), 3515 – 3524.

Jayaraman, A., H. Gadhavi, D. Ganguly, A. Misra, S. Ramachandran and T. Rajesh (2006), Spatial variation in aerosol characteristics and regional radiative forcing over India: Measurements and modeling of 2004 road campaign experiment, Atmos. Environ., 40, 6504 – 6515.

Jena C, S. D. Ghude, G. G. Pfister andet al. (2014), Influence of springtime biomass burning in South Asia on regional ozone (O_3): A model based case study, doi:10.1016/j.atmosenv.2014.10.027.

Jenkins, G. S., J.-H., Ryu, A. Thompson, and J. Witte (2003), Linking horizontal and vertical transports of biomass fire emissions to the Tropical Atlantic Ozone Paradox during the Northern Hemisphere winter season: 1999, J. Geophys. Res., doi.10.1029/JD2002003297.

Junge, C. E. (1962), Global ozone budget and exchange between stratosphere and troposphere. Tellus, 14, 363–377. doi: 10.1111/j.2153-3490.1962.tb01349.x.

Just J., C. Segala, F. Sahraoui, G. Priol, A. Grimfeld and F. Neukirch (2002), Short-term health effects of particulate and photochemical air pollution in asthmatic children, Eur. Respir. J., 20(4), 899-906.

Justice C. O., L. Giglio, S. Korontzi and et al. (2002), The MODIS fire products, Remote Sensing of Environment, doi:10.1016/S0034-4257(02)00076-7.

Justice C., L. Giglio, L. Boschetti, D. Roy, I. Csiszar, J. Morisette and Y. Kaufman (2006), Algorithm Technical Background Document, MODIS FIRE PRODUCTS, (Version 2.3, 1 October 2006).

Kain, J. S. (2004), The Kain-Fritsch convective parameterization: An update, J. Appl. Meteorol., 43(25), 170–181.

Kaiser J. W., A. Heil, M. O. Andreae (2012), Biomass burning emissions estimated with a global fire assimilation system based on observed fire radiative power, Biogeosciences, doi:10.5194/bg-9-527-2012.

Kajii, Y., K. Someno, H. Tanimoto, J., Hirokawa, H., Akimoto, T., Katsuno, J., Kawara (1998), Evidence for the seasonal variation of photochemical activities of tropospheric ozone: long term observation of ozone and CO at Mt. Happo, Japan, Geophysical Research Letters, 25, 3505–3508.

Kar, J. and et al. (2010), Wintertime pollution over the Eastern Indo-Gangetic Plains as observed from MOPITT, CALIPSO and tropospheric ozone residual data, Atmos. Chem. and Phys., 10, 12273-12283.

Kasting, J. F. and H. B. Singh (1986), Nonmethane hydrocarbons in the troposphere: Impact on the odd hydrogen and odd nitrogen chemistry, Journal of Geophysical Research, 91, doi: 10.1029/JD080i012p13239. issn: 0148-0227.

Kaufman Y. J., C. O. Justice, L. P. Flynn and et al. (1998), Potential global fire monitoring from EOS-MODIS, J Geophys Res., doi:10.1029/98JD01644.

Kennedy, I. M. (2007), The health effects of combustion-generated aerosols, Proceedings of the Combustion Institute, 31 (2), 2757-2770.

Kennett, E. J. and Toumi, R. (2005), Himalayan rainfall and vorticity generation within the Indian summer monsoon, Geophys. Res. Lett., 32 (4), art–L04802.

Kerr, J. B., H. Fast, C. T. McElroy, S. J. Oltmans, J. A. Lathrop, E. Kyro, A. Paukkunen, H. Claude, U. Kohler, C. R. Sreedharan, T. Takao and Y., Tsukagoshi (1994), The 1991 WMO International Ozonesonde Intercomparison at Vanscoy, Canada, Atm. Ocean, 32, 685-716.

Khalil M. A. K. and R. A. Rasmussen (1990), Constraints on the Global Sources of Methane and an Analysis of Recent Budgets. Tellus, 42B, 229-236.

Khalil M. A. K., R. A. Rasmussen and R. Gunawardena (1993), Atmospheric Methyl Bromide: Trends and Global Mass Balance, J. Geophys. Res., 98, 2887-2896.

Kharol S. K. and K. V. S. Badarinath (2006), Impact of biomass burning on aerosol properties over tropical urban region of Hyderabad, India.Geophys Res Lett. doi:10.1029/2006GL026759.

Khemani, L. T., G. A. Momin, P. S. P. Rao, R. Vijayakumar and P. D. Safai (1995), Study of surface ozone behavior at urban and forested sites in India, Atmos. Environ., 29, 2021 – 2024.

Kleinman, L. (1994), Ozone formation at a rural site in the southern United State, J. Geophys. Res., 99, 3469-3482, doi: 10.1029/93JD02991.

Kobayashi, J. and Y. Toyama (1966), On various methods of measuring the vertical distribution of atmospheric ozone (III)—Carbon iodide type chemical ozonesonde, Pap. Meteorol. Geophys., 17, 113– 126.

Komhyr. W. D. (1969), Electrochemical concentration cells for gas analysis, Ann. Geoph., 25, 203-210.

Komhyr, W. D., S. J. Oltmans, A. N. Chopra, P. R. Franchois (1985), Performance characteristics of high-altitude ECC ozonesondes, Atmospheric Ozone, C. S. Zerefos, A. Ghazi, 499–503.

Komhyr, W. D. (1986), Operations handbook-Ozone measurements to 40-km altitude with model 4A electrochemical concentration cell (ECC) ozonesondes (used with 1680 MHz radiosondes) NOAA Tech. Memo. ERL ARL-149, 49Air Resour. Lab., Boulder, Colorado.

Komhyr, W. D., R. A. Barnes, G. B. Brothers, J. A. Lathrop and D. P. Opperman (1995), Electrochemical concentration cell ozonesonde performance evaluation during STOIC 1989, J. Geophys. Res., 100 (D5), 9231–9244.

Kondo Y., M. Ko, M. Koike, S. Kawakami, T. Ogawa (2002), Preface to Special Section on Biomass Burning and Lightning Experiment (BIBLE), J Geophys Res., doi:10.1029/2002JD002401.

Koppmann R., K.von Czapiewski, J. S. Reid (2005), A review of biomass burning emissions, part I: gaseous emissions of carbon monoxide, methane, volatile organic compounds, and nitrogen containing compounds, Atmos Chem Phys

Discuss., doi:10.5194/acpd-5-10455-2005.

Koppmann R. (2007), Volatile Organic Compounds in the Atmosphere, Wiley-Blackwell, ISBN: 978-1-4051-3115-5.

Krol, M., and J. Lelieveld (2003), Can the variability in tropospheric OH be deduced from measurements of 1,1,1-trichloroethane (methyl chloroform)?, J. Geophys. Res., 108(D3), 4125, doi: 10.1029/2002JD002423.

Kumar, R., M. Naja, S. Venkataramani and O. Wild (2010), Variations in surface ozone at Nainital, a high altitude site in the Central Himalayas, J. Geophys. Res., 115, D16302, doi: 10.1029/2009JD013715.

Kumar, R., M. Naja, S. K. Satheesh, N. Ojha, H. Joshi, T. Sarangi, P. Pant, U. C. Dumka, P. Hegde and S. Venkataramani (2011), Influences of the springtime northern Indian biomass burning over the central Himalayas, J. Geophys. Res., 116, D19302, doi: 10.1029/2010JD015509.

Kumar, R., M. Naja, G. G. Pfister, M. C. Barth and G. P. Brasseur (2012a), Simulations over South Asia using the Weather Research and Forecasting model with Chemistry (WRF-Chem): set-up and meteorological evaluation, Geosci. Model Dev., 5, 321-343, doi: 10.5194/gmd-5-321-343-2012.

Kumar, R., M. Naja, G. G. Pfister, M. C. Barth, C. Wiedinmyer and G. P. Brasseur (2012b), Simulations over South Asia using the Weather Research and Forecasting model with Chemistry (WRF-Chem): chemistry evaluation and initial results, Geosci. Model Dev., 5, 619 – 648, doi: 10.5194/gmd-5-619-2012.

Kumar, R., M. Naja, G. G. Pfister, M. C. Barth and G. P. Brasseur (2013), Source attribution of carbon monoxide in India and surrounding regions during wintertime, J. Geophys. Res. Atmos., 118, 1981–1995, doi:10.1002/jgrd.50134.

Kumar, R., M. C. Barth, S. Madronich, M. Naja, G. R. Carmichael, G. G. Pfister, C. Knote, G. P. Brasseur, N. Ojha and T. Sarangi (2014), Effects of dust aerosols on tropospheric chemistry during a typical pre-monsoon season dust storm in northern India, Atmos. Chem. and Phys., 14, 6813-6834, doi:10.5194/acp-14-6813-2014.

Lal, S., M. Naja and A. Jayaraman (1998), Ozone in the marine boundary layer over the tropical Indian Ocean, J. Geophys. Res., 103, 18907–18917.

Lal, S., M. Naja and B. H. Subbaraya (2000), Seasonal variations in surface ozone

and its precursors over an urban site in India, Atmos. Environ., 34, 2713-2724, doi: 10.1016/S1352-2310(99)00510-5.

Lal, S. and M. G. Lawrence (2001), Elevated mixing ratios of surface ozone over the Arabian Sea, Geophys. Res. Lett., 28(8), 1487-1490.

Lal, S. (2007), Trace gases over the Indian region, Indian Journal of Radio & Space Physics, 36, 556-570.

Lal, S., S. Venkataramani, S. Srivastava, S. Gupta, C. Mallik, M. Naja, T. Sarangi, Y. B. Acharya and X. Liu (2013), Transport effects on the vertical distribution of tropospheric ozone over the tropical marine regions surrounding India, J. Geophys. Res. Atmos., 118, 1513–1524, doi:10.1002/jgrd.50180.

Lal, S., S. Venkataramani, N. Chandra, O. R. Cooper, J. Brioude and M. Naja (2014), Transport effects on the vertical distribution of tropospheric ozone over western India, J. Geophys. Res. Atmos., 119, 10,012–10,026, doi:10.1002/2014JD021854.

Lamarque, J.-F., J. T. Kiehl, P. G. Hess, W. D. Collins, L. K. Emmons, P. Ginoux, C. Luo and X. X. Tie (2005b), Response of a coupled chemistry climate model to changes in aerosol emissions: Global impact on the hydrological cycle and the tropospheric burdens of OH, ozone, and NO_x, Geophys. Res. Lett., 32, L16809, doi:10.1029/2005GL023419.

Langford, A.O., K.C. Aikin, C.S. Eubank and E.J. Williams (2009), Stratospheric contribution to high surface ozone in Colorado during springtime, Geophys. Res. Lett., 36, L12801, doi: 10.1029/2009GL038367.

Lau, W. K. M. and K. M. Kim (2010), Fingerprinting the impacts of aerosols on long-term trends of the Indian summer monsoon region rainfall, Geophys. Res. Lett., 37, L16705, doi: 10.1029/2010GL043255.

Lawrence, M. G. and J. Lelieveld (2010), Atmospheric pollutant outflow from southern Asia: a review, Atmos. Chem. and Phys, 10, 11017 – 11096.

Lee, D. S., I. Kohler, E. Grobler, F. Rohrer, R. Sausen, L. Gallardo Klenner, J. G. J. Olivier, F. J. Dentener and A. F. Bouwman (1997), Estimations of global NO_x emissions and their uncertainties, Atmos. Environ., 31, 1735-1749.

Lelieveld, J. (2001), The Indian Ocean Experiment: Widespread Air Pollution from South and Southeast Asia, Science, 291, 1031-1036.

Lelieveld, J., C. Barlas, D. Giannadaki and A. Pozzer (2012), Model calculated global, regional and megacity premature mortality due to air pollution,

Atmos. Chem. and Phys., 13, 7023-7037, doi:10.5194/acp-13-7023-2013.

Levy, H. II (1971), Normal Atmosphere: large radical and formaldehyde concentrations predicted, Science, 173, 141-143.

Levy, H. II, J. D. Mahlman, W. J. Moxim and S. C. Liu (1985), Tropospheric ozone: The role of transport, J. Geophys. Res., 90, 3753-3772.

Levy, R. C., L. A. Remer, S. Mattoo, E. F. Vermote and Y. J. Kaufman (2007), Second-generation operational algorithm: Retrieval of aerosol properties over land from inversion of Moderate Resolution Imaging Spectroradiometer spectral reflectance, J. Geophys. Res., 112, D13211, doi:10.1029/2006JD007811.

Lindesay J. A., M. O. Andreae, J. G. Goldammer and et al. (1996), International geosphere-biosphere programme/international global atmospheric chemistry SAFARI-92 field experiment: Background and overview, J Geophys Res., doi:10.1029/96JD01512.

Liu, H. and et al. (2003), Transport pathways for Asian pollution outflow over the Pacific: Interannual and seasonal variations, J. Geophys. Res., 108 (D20), 8786, doi: 10.1029/2002JD003102.

Logan, J. A., M. J. Prather, S. C. Wofsy and M. B. McElroy (1981), Tropospheric chemistry: A global perspective, J. Geophys. Res., 86, 7210 – 7255.

Logan, J. A. (1983), Nitrogen oxides in the troposphere: Global and regional budgets, J. Geophys. Res., 88, 10785-10807.

Logan, J. A. (1985), Tropospheric ozone: Seasonal behavior, trend and anthropogenic influences, J. Geophys. Res., 90 (D6), 10463-10482.

Logan, J. A. (1999), An analysis of ozonesonde data for the troposphere: Recommendations for testing 3-D models and development of a gridded climatology for tropospheric ozone, J. Geophys. Res., 104 (D13), 16,115-16,149.

Logan, J. A. and et al. (2012), Changes in ozone over Europe: Analysis of ozone measurements from sondes, regular aircraft (MOZAIC) and alpine surface sites, J. Geophys. Res, 117, D09301, doi: 10.1029/2011JD016952.

Madronich, S. (2006), Chemical evolution of gaseous air pollutants down-wind of tropical megacities: Mexico City Case Study, Atmos. Environ., 40, 6012 – 6018.

Mandal, T. K., J. Y. N. Cho, P. B. Rao, A. R. Jain, S. K. Peshin, S. K. Srivastava,

A. K. Bohra *and* A. P. Mitra *(*1998*),* Stratosphere-troposphere ozone exchange observed with the Indian MST radar and a simultaneous balloon-borne ozonesonde, Radio Sci., 33*(*4*),* 861–893, *doi:*10.1029/97RS03553.

Mandal, T.K., D. Kley, H.G.J Smit, S. K. Srivastav, S. K. Peshin and A. P. Mitra (1999), vertical distribution of ozone over the Indian Ocean (15N-15S) during the First Field Phase INDOEX-1998, Current Science, 76, 938-943.

Marcy, T. P., D. W. Fahey, R. S. Gau, P. J. Popp, E. C. Richard, T. L. Thompson, K. H. Rosenlof, E. A. Ray, R. J. Salawitch, C. S. Atherton, D. J. Bergmann, B. A. Ridley, A. J. Winheimer, M. L. E. M. Weinstock and M. J. Mahoney (2004), Quantifying Stratospheric Ozone in upper troposphere with in situ measurements of HCl, Science.

Marenco, A., H. Gouget, P. Nédélec, J. Pagés and F. Karcher (1994), Evidence of a long-term increase in tropospheric ozone from Pic du Midi data series: Consequences: Positive radiative forcing, J. of Geophy. Res., 99, doi: 10.1029/94JD00021. ISSN: 0148-0227.

Matson M. and J. Dozier (1981) Identification of subresolution high temperature sources using a thermal IR sensor. Photogrammetric Engineering and Remote Sensing, 47(9), 1311-1318.

Matsuda, K. and et al. (2005), Ozone dry deposition above a tropical forest in the dry season in northern Thailand, Atmos. Environ., 39 (14), 2571-2577.

Mickley, L. J., P. P. Murti, D. J. Jacob, J. A. Logan, D. M. Koch and D. Rind (1999), Radiative forcing from tropospheric ozone calculated with a unified chemistry climate model, J. Geophys. Res., 104, 30153 - 130172.

Middleton J. T., J. B. Jr Kendrick and H. W. Schwalm (1950), Injury to herbaceous plants by smog or air pollution, Plant Dis Rep, 34, 245–252.

Mikaloff Fletcher, S. E., P. P. Tans, J. B. Miller and M. Heimann (2004a), CH_4 sources estimated from atmospheric observations of CH_4 and its $^{13}C/^{12}C$ ratios: 1. Inverse modeling of source processes, Global Biogeochem. Cycles, 18, GB4004, doi:10.1029/2004GB002223.

Miller, B.R. and et al. (1998), Atmospheric trend and lifetime of chlorodifluoromethane (HCFC-22) and the global tropospheric OH concentration, J. Geophys. Res., 103(D11), 13237–13248, doi: 10.1029/98JD00771.

Milne, P. J. and et al. (2000), Nonmethane hydrocarbon mixing ratios in continental

outflow air from eastern North America: Export of ozone precursors to Bermuda, J. Geophys. Res., 105, 9981-9990.

Mitra, A. P. (1999), INDOEX (India): Introductory note, Curr. Sci., 80, 3-6.

Mittal, M. L., P. G. Hess, S. L. Jain, B. C. Arya and C. Sharma (2007), Surface ozone in the Indian region, Atmos. Environ., 41, 6572-6584.

Mlawer, E. J., S. J. Taubman, P. D. Brown, M. J. Iacono and S. A. Clough (1997), Radiative transfer for inhomogeneous atmospheres: RRTM, a validated correlated-k model for the longwave, J. of Geophy. Res., 102, doi: 10.1029/97JD00237. ISSN: 0148-0227.

Mohanakumar K. (2008), Stratosphere troposphere interactions: an introduction. Springer, Heidelberg, 416.

Molina, L. T., C. E. Kolb, B. de Foy, B. K. Lamb, W. H. Brune, J. L. Jimenez, R. Ramos-Villegas, J. Sarmiento, V. H. Paramo- Figueroa, B. Cardenas, V. Gutierrez-Avedoy and M. J. Molina (2007), Air quality in North America's most populous city – overview of the MCMA-2003 campaign, Atmos. Chem. and Phys., 7, 2447–2473, doi:10.5194/acp-7-2447-2007.

Moore, G. W. K. (2004) Mount Everest snow plume: A case study. Geophys. Res. Lett., 31 (22), art–L22102.

Moorthy, K. K. (2001), Aerosol optical depths over peninsular India and adjoining oceans during the INDOEX campaigns: spatial, temporal, and spectral characteristics, J. Geophys. Res., 106, D22, 28539-28554, doi:10.1029/2001JD900169.

Moorthy, K. K., S. S. Babu and S. K. Satheesh (2003), Aerosol spectral optical depths over the Bay of Bengal: Role of transport, Geophys. Res. Lett., 30(5), 1249, doi:10.1029/2002GL016520.

Moorthy, K. K. and et al. (2004), Altitude profiles of aerosol BC, derived from aircraft measurements over an inland urban location in India, Geophys. Res. Lett., 31, L22103, doi: 10.1029/2004GL021336.

Moorthy, K. K., S. K. Satheesh and S. S. Babu (2006), ICARB: An integrated campaign for Aerosols, gases and radiation budget over India, Proc. of SPIE, 6408, doi: 10.1117/12.696110.

Müller, J. -F. (1992), Geographical distribution and seasonal variation of surface emissions and deposition velocities of atmospheric trace gases, J. Geophys. Res., 97(D4), 3787–3804, doi:10.1029/91JD02757.

Müller, J.-F. and T. Stavrakou (2005), Inversion of CO and NOx emissions using the adjoint of the IMAGES model, Atmos. Chem. and Phys., 5, 1157-1186, doi:10.5194/acp-5-1157-2005.

Nair, P. R. and et al. (2002), Temporal variations in surface ozone at Thumba (8.6°N, 77°E): A tropical coastal site in India, Atmos. Environ., 36, 603–610, doi:10.1016/S1352-2310(01)00527-1.

Naja, M. and S. Lal (1996), Changes in surface ozone amount and its diurnal and seasonal patterns, from 1954-55 to 1991-93 measured at Ahmedabad (23 N), India, Geophys. Res. Lett, 231(1), 81-84, doi: 10.1029/95GL03589.

Naja, M. (1997), Tropospheric Chemistry in the Tropics, Ph. D. Thesis, Gujarat Univ., Ahmedabad, India.

Naja, M., S. Lal, S. Venkataramani, K. S. Modh and D. Chand (1999), Variabilities in O3, NO, CO and CH4 over the Indian Ocean during winter season. Current Science, 76, 101-107.

Naja, M. and S. Lal (2002), Surface ozone and precursor gases at Gadanki (13.5^{o} N, 79.2^{o} E), tropical rural site in India, J. Geophys. Res., 107(D14), doi: 10.1029/2001JD000357.

Naja, M., H. Akimoto and J. Staehelin (2003a), Ozone in background and photochemically aged air over central Europe: Analysis of long-term ozonesonde data from Hohenpeissenberg and Payrene, J. Geophys. Res., 108(D2), 4063, doi: 10.1029/2002JD002477.

Naja, M., S. Lal and D. Chand (2003b), Diurnal and seasonal variabilities in surface ozone at a high altitude site Mt Abu (24.6o N, 72.7o E, 1680 m asl) in India, Atmos. Environ., 37, 4205-4215.

Naja, M., D. Chand, L. Sahu and S. Lal (2004), Trace gases over marine regions around India, Indian Journal of Marine Sciences, 33(1), 95-106.

Naja M., P. Bhardwaj, N. Singh, P. Kumar, R. Kumar, R. Sagar, S. K. Satheesh, K. Krishna Moorthy, V. R. Kotamarthi (2016), High frequency vertical profiling of meteorological parameters using AMF1 facility during RAWEX-GVAX at ARIES, Nainital, Current Science, 111(1).

National ambient air quality Standards (NAAQS) at website on 2-11-08. http://cpcb.nic.in/oldwebsite/Environmental%20Standards/default_Environment_standards.html.

Nishanth, T., N. Ojha, M. K. Satheesh Kumar and M. Naja (2011), Influence of

solar eclipse of 15 January 2010 on surface ozone, Atmos. Environ., 45, 1752 – 1758.

O'Doherty, S., D. M. Cunnold, A. Manning, B. R. Miller, R. H. J. Wang, P. B. Krummel, P. J. Fraser, P. G. Simmonds, A. McCulloch, R. F. Weiss, P. Salameh, L. W. Porter, R .G. Prinn, J. Huang, G. Sturrock, D. Ryall, R. G. Derwent and S. A. Montzka (2004), Rapid growth of hydrofluorocarbon 134a and hydrochlorofluorocarbons 141b, 142b, and 22 from Advanced Global Atmospheric Gases Experiment (AGAGE) observations at Cape Grim, Tasmania, and Mace Head, Ireland, J. Geophys. Res., 109, D06310, doi: 10.1029/2003JD004277.

Ohara, T., H. Akimoto, J. Kurokawa, N. Horii, K. Yamaji, X. Yan and T. Hayasaka (2007), An Asian emission inventory of anthropogenic emission sources for the period 1980–2020, Atmos. Chem. and Phys., **7**(16), 4419–4444, doi:10.5194/acp-7-4419-2007.

Ojha, N., M. Naja, K. P. Singh, T. Sarangi, R. Kumar, S. Lal, M. G. Lawrence, T. M. Butler and H. C. Chandola (2012), Variabilities in ozone at a semi-urban site in the Indo-Gangetic Plain region: Association with the meteorology and regional processes, J. Geophys. Res., 117, D20301, doi: 10.1029/2012JD017716.

Ojha, N., (2013), Syudy of ozone and other trace gases distribution in the lower troposphere, Ph. D. Thesis, Kumaun Univ., Nainital, India.

Ojha N., M. Naja, T. Sarangi, R. Kumar, P. Bhardwaj, S. Lal, S. Venkataramani, R. Sagar, A. Kumar and H.C. Chandola (2014), On the processes influencing the vertical distribution of ozone over the central Himalayas: Analysis of yearlong ozonesonde observations, Atmospheric Environment, 88, 201 – 211, doi: 10.1016/j.atmosenv.2014.01.031.

Oltmans, S. J. (1981), Surface ozone measurements in clean air, J. Geophys. Res., 86, 1174-1180.

Oltmans, S., A. S. Lefohn, H. E. Scheel, J. M. Harris, H. Levy II, I. E. Galbally, E.-G. Brunke, C. P. Meyer, J. A. Lathrop, B. J. Johnson, D. S. Shadwick, E. Cuevas, F. J. Schmidlin, D. W. Tarasick, H. Claude, J. B. Kerr, O. Uchino, V. Mohnen (1998), Trends of ozone in the troposphere, Geophys. Res. Lett., 25, 139–142, doi:10.1029/97GL03505.

Pacyna, J. M. and T.E. Graedel (1995), Atmospheric emissions inventories: status

and prospects. Annual Review of Energy and the Environment 20, 265e300.

Panday, A. K. and Prinn R. G. (2009), The diurnal cycle of air pollution in the Kathmandu Valley, Nepal: Observations, J. Geophys. Res., 114, D09305, doi:10.1029/2008JD009777.

Parrish, D. D., D. B. Millet and A. H. Goldstein (2009), Increasing ozone in marine boundary layer inflow at the west coasts of North America and Europe, Atmos. Chem. and Phys., 9, 1303-1323.

Pfister, G. G. and et al. (2010), Variability of springtime transpacific pollution transport during 2000-2006: the INTEX-B mission in the context of precious years, Atmos. Chem. and Phys., 10, 1345 – 1359.

Pfister, G. G., et al. (2010), Variability of springtime transpacific pollution transport during 2000-2006: the INTEX-B mission in the context of precious years, Atmos. Chem. & Phys., 10, 1345-1359.

Pio, C. A., M. S. Feliciano, A. T. Vermeulen and E. C. Sousa (1999), Seasonal variability of ozone dry deposition under southern European climate conditions, in Portugal, Atmos. Environ., 34 (2), 195-205.

Pitts, B. J. F. and J. N. Pitts (2000), Chemistry of the Upper and Lower Atmosphere: Theory, Experiments and Applications, Academic Press, 24-28, Oval Road, London, UK.

Pochanart, P., J. Hirokawa, Y. Kajii, H. Akimoto and M. Nakao (1999), The influence of regional scale anthropogenic activity in northeast Asia on seasonal variations of surface ozone and carbon monoxide observed at Oki, Japan, J. of Geophy. Res., 104, 3621–3631.

Pochanart, P., J. Kreasuwun, P. Sukasem, W. Geeratithadaniyom, M. S. Tabucanon, J. Hirokawa, Y. Kajii and H. Akimoto (2001), Tropical tropospheric ozone observed in Thailand, Atmos. Environ., 35, 2657–2668.

Portmann, R. W. and et al. (1997), Radiative forcing of the earth's climate system due to tropical tropospheric ozone production, J. Geophys. Res., 102, 9409-9417.

Pradhan, B. B., P. M. Dangol, R. M. Bhaunju, S. Pradhan (2012), Rapid urban assessment of air quality for Kathmandu, Nepal: Summary. Kathmandu: ICIMOD.

Prather, M. J., C. D. Holmes and J. Hsu (2012), Reactive greenhouse gas scenarios: Systematic exploration of uncertainties and the role of atmospheric

chemistry, Geophys. Res. Lett., 39, L09803.

Prinn, R.G. and et al. (2001), Evidence for substantial variations of atmospheric hydroxyl radicals in the past two decades. Science, 292, 1882–1888.

Prospero, J. M., R. A. Glaccum and R. T. Nees (1981), Atmospheric transport of soil dust from Africa to South America, Nature, 289, 570 – 572.

Pudasainee, D., B. Sapkota, M. L. Shrestha, A. Kaga, A. Kondo and Y. Inoue (2006), Ground level ozone concentrations and its association with NO_x and meteorological parameters in Kathmandu Valley, Nepal, Atmos. Environ., 40, 8081–8087, doi:10.1016/j.atmosenv.2006.07.011.

Pudasainee, D., B. Sapkota, A. Bhatnagar, S. H. Kim and Y. C. Seo (2010), Influence of weekdays, weekends and bandhas on surface ozone in Kathmandu valley, Atmos. Res., 95, 150–156.

Putero, D., P. Cristofanelli, A. Marinoni, B. Adhikary, R. Duchi, S. D. Shrestha, G. P. Verza, T. C. Landi, F. Calzolari, M. Busetto, G. Agrillo, F. Biancofiore, P. Di Carlo, A. K. Panday, M. Rupakheti and P. Bonasoni (2015), Seasonal variation of ozone and black carbon observed at Paknajol, an urban site in the Kathmandu Valley, Nepal, Atmos. Chem. and Phys., 15, 13957–13971, doi:10.5194/acp-15-13957-2015.

Ramachandran, S., R. Rengarajan, A. Jayaraman, M. M. Sarin and S. K. Das (2006), Aerosol radiative forcing during clear, hazy and foggy conditions over a continental polluted location in north India, J. Geophys. Res., 111, D20214, doi: 10.1029/2006JD007142.

Ramanathan, K. R. (1956), Atmospheric ozone and the general circulation of the atmosphere, Sci. Proc. International Association of Meteorology, IUGG 10th Central Assembly, Rome, 3-24.

Ramanathan, V., R. J. Cicerone, H. B. Singh and J. T. Kiehl (1985), Trace gas trends and their potential role in climate change, J. Geophys. Res., 90, 5547-5566.

Ramanathan, V., P. J. Crutzen, J. T. Kiehl and D. Rosenfeld (2001), Aerosols, climate and the hydrological cycle, Science, 292, 2119-2124.

Randel W. J., M. Park, L. Emmons, D. Kinnison, P. Bernath, K. A. Walker, C. Boone and H. Pumphrey (2010), Asian Monsoon Transport of Pollution to the Stratosphere, Science, 328(5978), 611-613 doi: 10.1126/science.1182274.

Rao, S. T., Ku, Jia-Yeaong., S. Berman, K. Zhang and H. Mao (2003), Summertime

characteristics of the atmospheric boundary layer and relationships to ozone levels over the eastern United States, Pure Appl. Geophys., 160, 21-55.

Rappenglück, B., R. Schmitz, M. Bauerfeind, F. Cereceda-Balic, D. von Baer, H. Jorquera, Y. Silva, Y. and P. Oyola (2005), An urban photochemistry study in Santiago de Chile, Atmos. Environ., 39, 2913–2931, doi:10.1016/j.atmosenv.2004.12.049.

Rasheed, A., V. P. Aneja, A. Aiyyer, and U. Rafique (2014), Measurements and analysis of air quality in Islamabad, Pakistan, Earth's Future, 2, doi:10.1002/2013EF000174.

Reddy, K. K., M. Naja, N. Ojha, P. Mahesh and S. Lal (2012), Influences of the Boundary Layer Evolution on Surface Ozone Variations at a Tropical Rural Site in India, Journal of Earth System Science, 121 (4), 911-922.

Reddy, R. R. and et al. (2008), Measurements of surface ozone at semi-arid site Anantapur (14.62^{o} N, 77.65^{o} E, 331 m asl) in India, J. Atmos. Chem., 59, 47-59, doi: 10.1007/s10874-008-9094-1.

Regener, E. (1949), Ozonschicht und atmospharische turbulenz, Ber. Dsch. Wetterdienstes, 11, 45-57.

Reichler, T., M. Dameris and R. Sausen (2003), Determining the tropopause height from gridded data, Geophy. Res. Lett., 30, doi:10.1029/2003GL018240.

Reiner, T., et al. (2001), Chemical characterization of pollution layers over the tropical Indian Ocean: Signatures of emissions from biomass and fossil fuel burning, J. Geophys. Res., 106 (D22), 28497-28510. Rengarajan et al., 2007

Roy, S. D., G. Beig, and S. D. Ghude (2009): Exposure-plant response of ambient ozone over the tropical Indian region, Atmos. Chem. and Phys., 9, 5253-5260, doi:10.5194/acp-9-5253-2009.

Russell, J. M. III, L. L. Gordley, J. H. Park, S. R. Drayson, W. D. Hesketh, R. J. Cicerone, A. F. Tuck, J. E. Frederick, J. E. Harries, and P. J. Crutzen (1993), The halogen occultation experiment, J. Geophys. Res., 98, 10777-10797.

Sahu, L. K. (2004), Ozone and Related Gases in the Lower Atmosphere, Ph. D. Thesis, Mohan Lal Sukhadia University, Udaipur, India.

Sahu, L.K. and Lal, S. (2006b), Distributions of C2eC5 NMHCs and related trace gases at a tropical urban site in India. Atmospheric Environment 40, 880-891.

Sahu, L. K., S. Lal and S. Venkataramani (2011), Seasonality in the latitudinal distributions of NMHCs over Bay of Bengal, Atmos. Environ., 45(14), 2356–

2366.

Saraf, N, G. Beig and M. Schultz (2003), Tropospheric distribution of ozone and precursors over the tropical Indian Ocean, J. Geophys. Res., 108, 4636, doi: 10.1029/2003JD003521.

Saraf, N. and G. Beig (2004), Long-term trends in tropospheric ozone over the Indian tropical region, Geophys. Res. Lett., 31 (L05101), doi: 10.1029/2003GL018516.

Sarangi T. (2014), Variabilities in Surface Ozone and Precursors at Nainital, Ph.D. Thesis, Kumaun University, Nainital.

Sarangi, T., M. Naja, N. Ojha, R. Kumar, S. Lal, S. Venkataramani, S., A. Kumar, R. Sagar, R. and H. C. Chandola (2014), First simultaneous measurements of ozone, CO, and NO_y at a high-altitude regional representative site in the central Himalayas, J. Geophys. Res. Atmos., 119, 1592–1611, doi:10.1002/2013JD020631.

Sarangi, T., M. Naja, S. Lal, S. Venkataramani, P. Bhardwaj, N. Ojha, R. Kumar and H. C. Chandola (2016), First observations of light non-methane hydrocarbons (C2-C5) over a high altitude site in the central Himalayas, Atmospheric Environment, doi: 10.1016/j.atmosenv.2015.10.024.

Sarkar, C., V. Sinha, V. Kumar, M. Rupakheti, A. Panday, K. S. Mahata, D. Rupakheti, B. Kathayat and M. G. Lawrence (2016), Overview of VOC emissions and chemistry from PTR-TOF-MS measurements during the SusKat-ABC campaign: high acetaldehyde, isoprene and isocyanic acid in wintertime air of the Kathmandu Valley, Atmos. Chem. Phys., 16, 3979-4003, doi:10.5194/acp-16-3979-2016.

Satheesh, S. K. and V. Ramanathan (2000), Large differences in tropical aerosol forcing at the top of the atmosphere and Earth's surface, Nature, 405, 60-63.

Satheesh, S. K., K. K. Moorthy, S. S. Babu, V. Vinoj and C. B. S. Dutt (2008), Climate implications of large warming by elevated aerosol over India, Geophys. Res. Lett. 35, L19809. doi:10.1029/2008GL034944.

Saunders, S. M., M. E. Jenkin,R. G. Derwent and M. J. Pilling(2003), Protocol for the development of the Master Chemical Mechanism, MCM v3 (Part A): tropospheric degradation of non-aromatic volatile organic compounds, Atmos. Chem. Phys., 3, 161-180, doi:10.5194/acp-3-161-2003.

Schmitz, R. (2005), Modelling of air pollution dispersion in Santiago de Chile,

Atmos. Environ., 39, 2035–2047, doi:10.1016/j.atmosenv.2004.12.033.

Schwarzkopf, M. D. and V. Ramaswamy (1993), Radiative forcing due to ozone in the 1980s: Dependence on altitude of ozone change, Geophys. Res. Lett., 20(3), 205–208, doi:10.1029/93GL00209.

Sehmel G. A. (1980), Particle and gas dry deposition: A review, Atmos. Environ., 14, 983-1011.

Seiler W. and P. J. Crutzen (1980), Estimates of gross and net fluxes of carbon between the biosphere and atmosphere from biomass burning, Climatic Change, 2(3), 207-247.

Seiler, W. and R. Conrad (1987), Contribution of tropical ecosystems to the global budgets of trace gases, especially CH_4, H_2, CO and N_2O, in The Geophysiology of Amazonia: Vegetation and Climate Interactions, edited by R. E. Dickerson, 33 – 62, John Wiley, Hoboken, N. J.

Seinfeld, J. H. and S. N. Pandis (2006), Atmospheric Chemistry and Physics: From Air Pollution to Climate Change, A Wiley-Interscience Publication, New Jersy.

Shapiro, M. A. (1980), Turbulent Mixing within Tropopause Folds as a Mechanism for the Exchange of Chemical Constituents between the Stratosphere and Troposphere, J. Atmos. Sci., 37, 994–1004.

Sharma A. R, S. K. Kharol , K. V. S. Badarinath , D. Singh (2010), Impact of agriculture crop residue burning on atmospheric aerosol loading–a study over Punjab State, India, Ann Geophys, doi:10.5194/angeo-28-367-2010

Sharma, U. K., Y. Kajii, and H. Akimoto (2000) Characterization of NMHCs in downtown urban center Kathmandu and rural site Nagarkot in Nepal, Atmos. Environ., 34, 3297–3307, doi:10.1016/S1352-2310(99)00485-9.

Sikder H. A. (2013), Mohammed Nasiruddin, Jeeranut Suthawaree, Shungo Kato, Yoshizumi Kajii, Long term observation of surface O_3 and its precursors in Dhaka, Bangladesh, Atmos. Research, 122, 2013, 378–390, doi:10.1016/j.atmosres.2012.09.011.

Singla, V., A. Satsangi, T. Pachauri, A. Lakhani and K. M. Kumari (2011), Ozone formation and destruction at a suburban site in North Central region of India, Atmos. Res., 101(1–2), 373–385, doi:10.1016/j.atmosres.2011.03.011.

Sinha, B., K. Singh Sangwan, Y. Maurya, V. Kumar, C. Sarkar, B. P. Chandra and V. Sinha (2015), Assessment of crop yield losses in Punjab and Haryana using

2 years of continuous in situ ozone measurements, Atmos. Chem. Phys., 15(16), 9555–9576, doi:10.5194/acp-15-9555-2015.

Smit, H. G. J. and et al. (2007), Assessment of the performance of ECC-ozonesondes under quasi-flight conditions in the environmental simulation chamber: Insights from the Juelich Ozone Sonde Intercomparison Experiment (JOSIE), J. Geophys. Res., 112, D19306, doi: 10.1029/2006JD007308.

Sreedharan, C. R. and V. S. Tiwari (1971), The use of Brewer 'bubbler' as a continuous surface ozone sensor, J. Phys. E. Sci. Inst., 4, 706-707.

Sreedharan, C. R. (1968), An Indian electrochemical ozonesonde, Journal of Physics E Sci, Inst. Sr 2 (1), 995–997.

Srivastava S., S. Lal, S. Venkataramani, S. Gupta and Y. B. Acharya (2011), Vertical distribution of ozone in the lower troposphere over the Bay of Bengal and the Arabian sea during ICARB-2006: Effects of continental outflow, J. Geophys. Res., 116, D13301, doi:10.1029/2010JD015298.

Srivastava, S., S. Lal, M. Naja, S. Venkataramani and S. Gupta (2012), Influence of regional pollution and long range transport over western India: Analysis of ozonesonde data, Atmos. Environ., 47, 174-182, ISSN 1352-2310, 10.1016/j.atmosenv.2011.11.018.

Stevenson, D.S. and et al. (2006), Multi-model ensemble of present-day and near-future tropospheric ozone, J. Geophys. Res., 111, D8301, doi:10.1029/2005JD006338.

Stohl, A., N. Spichtinger-Rakowsky, P. Bonasoni, H. Feldmann, M. Memmesheimer, H. E. Scheel, T. Trickl and S. Hübener (2000), The influence of stratospheric intrusions on alpine ozone concentrations, Atmos. Environ, 34, 1323-1354.

Streets D. G, Yarber K. F, Woo J. H and G. R. Carmichael (2003), Biomass burning in Asia: Annual and seasonal estimates and atmospheric emissions, Glob Biogeochem Cycles, doi:10.1029/2003GB002040.

Streets, D. G. and S. T. Waldhoff (2000), Present and future emissions of air pollutants in China: SO_2, NO_x and CO, Atmos. Environ., 34, 363–374.

Surendran, D. E. and et al. (2015), Air quality simulation over South Asia using Hemispheric Transport of Air Pollution version-2 (HTAP-v2) emission inventory and Model for Ozone and Related chemical Tracers (MOZART-4),

Atmos. Environ., in press, doi: 10.1016/j.atmosenv.2015.08.023.

Takegawa N, Y, Kondo, M. Ko and et al. (2003), Photochemical production of O_3 in biomass burning plumes in the boundary layer over northern Australia, Geophys Res Lett, doi:10.1029/2003GL017017.

Tanimoto, H., T. Ohara and I. Uno (2009), Asian anthropogenic emissions and decadal trends in springtime tropospheric ozone over Japan: 1998-2007, Geophys. Res. Lett., 36, L23802, doi: 10.1029/2009GL041382.

Thompson A. M., A. M. Thompson and J. C. Witte (2001), Tropical Tropospheric Ozone and Biomass Burning, Science, doi:10.1126/science.291.5511.2128.

Thompson, A. M., J. O. Samuel, W. T. David,, G. Peter von der, G.J. S. Herman and C. W. Jacquelyn (2011), Strategic ozone sounding networks: Review of design and accomplishments, Atmos. Environ, 45, 2145-2163.

Thompson, G., R. M. Rasmussen and K. Manning (2004), Explicit forecasts of winter precipitation using an improved bulk microphysics scheme. Part I: Description and sensitivity analysis, Mon. Wea. Rev., 132, 519–542.

Thurston G.D. and I. Kazuhiko (2001), Epidemiological studies of acute ozone exposures and mortality, Journal of Exposure Analysis and Environmental Epidemiology, 11, 286–294. 10.1038/sj.jea.7500169.

Torres O., R. Decae, J. P. Veefkind, G. de Leeuw(2002b), OMI aerosol retrieval algorithm, in OMI Algorithm Theoretical Basis Document: Clouds, Aerosols, and Surface UV Irradiance, 3(2),http://eospso.gsfc.nasa.gov/ eos_homepage/for_scientists/atbd/docs/OMI/ATBD-OMI-03.pdf, 47 – 71.

Torres, A. L. (1981), ECC ozonesonde performance at high altitudes: Pump efficiency, NASA Tech. Memo, TM 93290, 10.

Trenberth, K. E., J. T. Fasullo and J. Kiehl (2009), Earth's global energy budget, Bull, Amer. Meteor. Soc., 90, 311–323.

Trickl, T., N. Bärtsch-Ritter, H. Eisele, M. Furger, R. R. Mücke, M. Sprenger and A. Stohl (2011), High-ozone layers in the middle and upper troposphere above Central Europe: potential import from the stratosphere along the subtropical jet stream, Atmos. Chem. Phys., 11, 9343-9366, doi:10.5194/acp-11-9343-2011.

Tripathi, S. N. and et al. (2006), Measurements of atmospheric parameters during Indian Space Research Organization Geosphere Biosphere Program Land Campaign II at a typical location in Ganga basin: 1 Physical and optical

properties, J. Geophys. Res., 111, D23209, doi: 10.1029/2006JD007278.

Tsutsumi, Y., Y. Igarashi, Y. Zaizen and Y. Makino (1998), Case studies of tropospheric ozone events observed at the summit of Mount Fuji, J. Geophys. Res., 103, 16935-16951.

Tsutsumi, Y. and H.Matsueda (2000), Relationship of ozone and CO at the summit of Mt. Fuji (35.35_N, 138.73_E, 3776m above sea level) in summer 1997, Atmospheric Environment, 34, 553–561.

Van der Werf G. R., J. T. Randerson, L. Giglio and et al. (2010), Global fire emissions and the contribution of deforestation, savanna, forest, agricultural, and peat fires, Atmos Chem Physics, doi:10.5194/acp-10-11707-2010.

Vaughan, G. (1988), Stratosphere-troposphere exchange of ozone, in tropospheric Ozone, Isaksen ISA (ed.) D Reidel: Dordrecht, The Netherlands, 125-135.

Venkataraman C., G. Habib, D. Kadamba and et al. (2006), Emissions from open biomass burning in India: Integrating the inventory approach with high-resolution Moderate Resolution Imaging Spectroradiometer (MODIS) active-fire and land cover data, Global Biogeochem. Cycles, doi:10.1029/2005GB002547.

Volz, A. and D. Kley (1988), Evaluation of the Montsouris series of ozone measurements made in the nineteenth century, Nature, 332, 240-242, doi:10.1038/332240a0.

Voulgarakis, A. and D. T. Shindell (2010), Constraining the sensitivity of regional climate with the use of historical observations, J. Clim., 23, 6068–6073.

Walcek, C. J., R. A. Brost and J. S. Chang (1986), SO_2, sulfate and HNO_3 deposition velocities computed using regional landuse and meteorological data, Atmos. Environ., 20, 949-964.

Wang, X. and D. L. Mauzerall (2004), Characterizing distributions of surface ozone and its impact on grain production in China, Japan and South Korea: 1990 and 2020, Atmos. Environ., 38, 4383-4402.

Wesley, M. L. and B. B. Hicks (1977), Some factors that affect the deposition rates of sulfur dioxide and similar gases on vegetation, J. Air Pollut. Control Ass., 27, 1110-1116.

Wiedinmyer, C., S. K. Akagi, R. J. Yokelson, L. K. Emmons, J. A. Al- Saadi, J. J. Orlando and A. J. Soja (2011), The Fire Inventory from NCAR (FINN): a high resolution global model to estimate the emissions from open burning,

Geosci. Model Dev., 4, 625–641, doi: 10.5194/gmd-4-625-2011.

Wuebbles D. J. and K. Hayhoe (2002), Atmospheric methane and global change, Earth-Science Reviews, 57(3–4), 177–210, doi:10.1016/S0012-8252(01)00062-9.

Yu, Y., B. Galle, A. Panday, E. Hodson, R. Prinn and S. Wang (2009), Observations of high rates of NO2-HONO conversion in the nocturnal atmospheric boundary layer in Kathmandu, Nepal, Atmos. Chem. Phys., 9, 6401-6415, doi:10.5194/acp-9-6401-2009.

Zachariasse, M., O. F. J.van Velthoven, Smit, J. Lelieveld, T. K. Mandal and H. Kelder (2000), Influence of stratosphere troposphere exchange on tropospheric ozone over the tropical Indian Ocean during the winter monsoon, J. Geophys. Res., 105, 15 403–15 416.

Zhang, L., D. J. Jacob, K. F. Boersma, D. A. Jaffe, J. R. Olson, K. W. Bowman, J. R. Worden, A. M. Thompson, M. A. Avery, R. C. Cohen, J. E. Dibb, F. M. Flock, H. E. Fuelberg, L. G. Huey, W. W. McMillan, H. B. Singh and A. J. Weinheimer (2008), Transpacific transport of ozone pollution and the effect of recent Asian emission increases on air quality in North America: an integrated analysis using satellite, aircraft, ozonesonde, and surface observations, Atmos. Chem. Phys., 8, 6117-6136, doi:10.5194/acp-8-6117-2008.

Annexure I: *Details of all (total 203) ozonesonde and radiosonde launches with their launch date, time, serial numbers of radiosonde & ozonesonde, sensor background current and flow rate. Note that radiosonde serial number starts with S and ozonesonde serial number starts with 2Z.*

Date (dd-mon-yr)	Time (HH:MM)	Radiosonde (Sxxxxx)	Ozonesonde (2Zxxxxx)	Bkg current (µA)	Flow Rate (sec/100ml)
7-Jan-11	12:27	12542	9172	0.08	29.1
19-Jan-11	11:04	12553	9180	0.02	28.3
28-Jan-11	10:51	12174	9173	0.02	29.4
2-Feb-11	10:54	12551	9188	0.02	29.4
11-Feb-11	10:53	12162	9174	0.01	28.5
17-Feb-11	11:09	12550	9176	0.02	29.4
7-Mar-11	16:05	6671	9141	0	28.6
10-Mar-11	13:15	12549	9177	0.02	29.3
30-Mar-11	10:54	9274	9171	0	29
6-Apr-11	10:31	12540	9186	0.02	28.4
13-Apr-11	10:50	12539	9194	0.02	28.2
20-Apr-11	14:36	12534	9179	0.01	28.2
29-Apr-11	10:31	8760	9178	0.02	28.4
4-May-11	10:40	12176	9182	0.02	28.2
9-May-11	14:45	12170	9181	0.02	27.8
12-May-11	11:57	4093	9175	0.02	27.9
16-May-11	14:22	2533	9193	0.02	28.2
18-May-11	14:26	4033	9185	0.02	28.2
25-May-11	14:27	3137	9169	0.01	28.2
2-Jun-11	15:20	6660	9135	0.03	28.5
7-Jun-11	14:24	4323	9187	0.01	27.7
15-Jun-11	14:33	7127	9138	0.02	28.8
29-Jun-11	14:34	6284	9190	0.02	28.5
6-Jul-11	13:06	6582	9140	0.02	27.6
22-Jul-11	13:16	7211	9191	0.04	28
27-Jul-11	12:33	3326	9---	0.02	28.2
3-Aug-11	13:18	6641	9189	0.02	29.5
11-Aug-11	12:27	12536	9192	0.02	28.8
18-Aug-11	12:25	12546	9139	0.02	28.4
24-Aug-11	12:45	12545	9184	0.01	28.5
31-Aug-11	12:32	16154	9183	0.02	28.2
7-Sep-11	14:02	16375	9166	0.02	28.5
16-Sep-11	12:50	16391	9164	0.02	27.8
21-Sep-11	12:26	16371	9195	0.03	28.8
25-Sep-11	12:51	16167	9142	0.02	28.7
5-Oct-11	12:45	16166	10267	0.02	28.6
12-Oct-11	11:33	16374	10265	0.02	28.8

19-Oct-11	12:17	16367	10273	0.02	29.4
25-Oct-11	14:58	7062	10271	0.02	28.8
2-Nov-11	12:24	12535	10272	0.02	29.1
9-Nov-11	12:30	16366	10278	0.01	28.5
16-Nov-11	12:19	14641	10269	0.02	29.2
23-Nov-11	12:04	16361	10268	0.01	28.5
30-Nov-11	12:20	16365	10259	0.01	29.3
7-Dec-11	12:37	16368	10262	0.03	28.3
14-Dec-11	12:19	16395	10263	0.02	28.5
21-Dec-11	12:21	16178	10260	0.02	28.8
28-Dec-11	13:20	16364	10257	0.02	28.9
4-Jan-12	13:45	16362	10256	0.01	28.7
11-Jan-12	14:49	16376	10261	0.02	28.8
25-Jan-12	12:05	14819	10264	0.01	28.7
1-Feb-12	12:08	16369	10274	0.02	28.4
8-Feb-12	13:01	16176	10258	0.02	28.3
22-Feb-12	13:07	16394	10275	0.02	27.8
29-Feb-12	13:04	14781	10280	0.02	27.9
7-Mar-12	14:34	14779	10270	0.02	28.7
14-Mar-12	13:18	14780	10277	0.02	29.1
29-Mar-12	14:00	16379	9156	0.04	28.2
31-Mar-12	13:38	14767	9157	0.04	27.6
4-Apr-12	12:10	16380	9155	0.02	27.7
12-Apr-12	12:10	12543	10304	0.03	28.9
18-Apr-12	12:12	12217	9144	0.02	28.9
25-Apr-12	13:49	12544	9145	0.02	27.5
2-May-12	12:22	14791	9162	0.02	28.6
9-May-12	12:15	14783	9161	0.02	27.7
14-May-12	13:22	14800	10303	0.05	28.6
16-May-12	12:54	16372	9150	0.05	28.4
18-May-12	12:07	16363	9154	0.03	27.7
23-May-12	11:56	6275	9158	0.05	28.5
28-May-12	12:38	14764	9165	0.04	28.3
30-May-12	14:52	16370	10276	0.05	28.5
6-Jun-12	12:29	16399	9149	0.03	28.1
13-Jun-12	12:11	16387	10279	0.01	28.8
20-Jun-12	12:39	16384	9146	0.02	29.1
27-Jun-12	12:19	16396	9151	0.03	29.1
5-Jul-12	12:00	16392	9148	0.02	28.5
1-Aug-12	11:33	14756	10298	0.04	29.4
22-Aug-12	11:43	16385	9147	0.03	29.2
12-Sep-12	14:24	16382	9153	0.05	29.5
26-Sep-12	13:19	16388	9163	0.05	29.6
3-Oct-12	12:21	16170	10291	0.03	28.8
10-Oct-12	14:06	16393	10281	0.05	28.8

17-Oct-12	12:32	16397	10288	0.05	28.2
24-Oct-12	12:24	12224	10283	0.03	28.5
31-Oct-12	14:40	12552	10289	0.02	28.8
7-Nov-12	12:10	12173	10286	0.01	28.1
16-Nov-12	13:12	16386	10284	0.02	29.4
21-Nov-12	12:43	14212	9159	0.02	28.4
28-Nov-12	12:32	14213	9152	0.03	28.5
5-Dec-12	12:36	14214	10294	0.01	27.1
12-Dec-12	13:17	14216	10299	0.02	27.8
19-Dec-12	12:43	14217	10293	0.03	28.2
26-Dec-12	12:37	14155	10290	0.03	28.5
2-Jan-13	12:54	14219	10292	0.06	28.8
11-Jan-13	12:32	14870	23159	0.03	28.9
16-Jan-13	12:34	14220	23152	0.07	27.5
23-Jan-13	12:31	14073	23193	0.02	29
30-Jan-13	12:11	14462	23158	0.04	27.7
6-Feb-13	12:03	14780	23149	0.05	27.8
13-Feb-13	12:02	14165	23150	0.08	26.7
21-Feb-13	11:59	14058	23153	0.02	29.3
27-Feb-13	12:32	13686	23140	0.03	27.8
6-Mar-13	13:26	14057	23155	0.04	28.6
13-Mar-13	12:31	14168	23161	0.03	27.8
20-Mar-13	13:05	12498	23157	0.03	28.5
27-Mar-13	12:30	12451	23144	0.03	28.4
3-Apr-13	13:01	12453	23146	0.02	29.1
10-Apr-13	12:40	12300	23194	0.03	29.4
17-Apr-13	13:09	12497	23143	0.02	28.2
24-Apr-13	12:21	12452	23151	0.02	28
1-May-13	13:00	12467	23142	0.02	28.7
9-May-13	12:24	12468	23154	0.01	28.4
15-May-13	12:00		23195	0.01	28.3
22-May-13	12:21	12455	23147	0.01	29.2
29-May-13	12:20	14915	23148	0.01	28
5-Jun-13	12:46	14805	23160	0.03	28.4
12-Jun-13	12:26	14768	23141	0.02	28.8
19-Jun-13	12:16	14917	23250	0.03	28.7
3-Jul-13	11:48	14767	23145	0.02	28.7
10-Jul-13	11:59	14804	23203	0.03	29.6
17-Jul-13	12:06	14918	23199	0.02	29.2
24-Jul-13	12:14	12337	23156	0.02	28.8
31-Jul-13	12:22	14901	23200	0.02	29.5
7-Aug-13	14:45	14150	23208	0.02	29.3
14-Aug-13	12:01	14806	23249	0.03	29.8
21-Aug-13	12:19	14903	23197	0.03	28.6

30-Aug-13	12:16	14807	23204	0.04	29
4-Sep-13	12:18	14151	23213	0.04	28.9
11-Sep-13	12:16	14667	23216	0.03	29.5
18-Sep-13	12:34	14501	23210	0.03	28.9
25-Sep-13	12:16	12303	10296	0.04	28
2-Oct-13	12:25	12440	10297	0.03	28.3
9-Oct-13	12:06	14166	9160	0.05	29
16-Oct-13	13:06	14913	10282	0.04	28.2
23-Oct-13	12:39	14170	10301	0.03	29
30-Oct-13	12:32	14911	10302	0.03	29
6-Nov-13	12:39	14920	10295	0.03	27.6
13-Nov-13	12:50	14916	9167	0.02	28
20-Nov-13	12:19	12469	10285	0.03	28.5
27-Nov-13	12:53	14910	25195	0.03	28
4-Dec-13	12:20	14919	25196	0.03	28
11-Dec-13	12:10	14167	23214	0.02	29
18-Dec-13	12:18	14056	25194	0.02	29
25-Dec-13	12:22	18458	10300	0.03	28
1-Jan-14	12:09	18459	23209	0.03	29.7
8-Jan-14	12:27	18565	23211	0.04	27.8
15-Jan-14	12:47	18418	23207	0.03	29
22-Jan-14	12:16	18417	23212	0.02	28.3
29-Jan-14	12:11	18421	23206	0.02	29.2
12-Feb-14	12:52	18620	23202	0.02	29.4
27-Feb-14	12:27	20001	23221	0.02	28.2
5-Mar-14	12:39	19465	23218	0.02	28.7
12-Mar-14	12:03	19409	23217	0.02	28.7
20-Mar-14	12:14	19988	23201	0.03	28.7
26-Mar-14	11:49	19999	23205	0.02	29.1
2-Apr-14	12:29	18435	23196	0.02	27.8
9-Apr-14	12:17	19996	23198	0.03	28.4
16-Apr-14	12:47	19357	25091	0.04	27.1
23-Apr-14	12:00	18420	25092	0.02	28.5
1-May-14	13:38	19973	25094	0.02	28.3
8-May-14	12:49	19989	25093	0.04	28.4
15-May-14	12:49	19470	25095	0.03	27.1
21-May-14	13:30	19972	26233	0.02	27.9
28-May-14	12:12	19969	26227	0.02	28.9
4-Jun-14	12:15	19358	25730	0.02	28.5
11-Jun-14	13:17	19467	26217	0.04	28.1
25-Jun-14	12:51	19991	26232	0.02	28.8
4-Jul-14	11:35	19994	26205	0.02	29.8
9-Jul-14	11:58	19373	26214	0.02	28.2
16-Jul-14	12:05	19469	26222	0.02	29.7
6-Aug-14	12:04	19383	24352	0.05	26.9

13-Aug-14	11:45	19401	26218	0.02	28.7
20-Aug-14	11:43	19372	26211	0.03	28.7
3-Sep-14	11:51	19993	26219	0.03	28.8
17-Sep-14	12:06	18415	26220	0.05	28.1
1-Oct-14	11:52	19990	26226	0.04	28
15-Oct-14	11:51	19992	24353	0.03	27.7
29-Oct-14	12:00	17873	26228	0.03	28.5
12-Nov-14	11:51	19377	26221	0.03	29
26-Nov-14	11:58	19474	26209	0.02	28.7
10-Dec-14	12:09	19985	26231	0.04	27.5
24-Dec-14	12:00	19984	26212	0.02	28.5
6-Jan-15	11:54	19462	26230	0.03	28.5
21-Jan-15	11:54	19997	26215	0.02	27.5
4-Feb-15	12:03	19981	26216	0.01	29.5
18-Feb-15	11:52	19837	26198	0.03	29.5
11-Mar-15	12:03	18048	26210	0.02	28.8
25-Mar-15	12:04	18422	26225	0.04	29.1
8-Apr-15	11:22	19468	26224	0.02	29.3
22-Apr-15	11:51	19848	26213	0.03	29.35
20-May-15	11:41	19987	26039	0.02	28.35
3-Jun-15	12:17	19406	26196	0.03	28.6
17-Jun-15	12:00	19385	26203	0.02	28.6
8-Jul-15	12:14	19986	26204	0.02	29.1
3-Aug-15	17:59	19983	26201	0.03	29.6
21-Oct-15	12:29	12477	26192	0.02	29.3
18-Nov-15	12:31	12475	26190	0.01	28.6
24-Nov-15	11:39	19378	26200	0.01	29.4
9-Dec-15	12:24	37627	26199	0.02	28.9
16-Dec-15	12:28	12479	26197	0.02	28.7
23-Dec-15	11:46	12476	26195	0.03	29
28-Dec-15	11:41	37615	26207	0.02	29
30-Dec-15	11:59	37615	26208	0.02	29